Revisiting crop root system ideotypes for water uptake

New tools and models



Félicien Meunier

Tuesday 26th September, 2017

Thèse présentée en vue de l'obtention du titre de docteur en sciences agronomiques et ingénierie biologique

Earth and Life Institute
Université catholique de Louvain

Thesis examining board

Supervisor:	Prof. Mathieu Javaux
President of the jury:	Prof. Marnik Vanclooster
Members of the jury:	Prof. Xavier Draye
	Prof. Paolo D'Odorico
	Prof. François Tardieu
	Prof. Jan Vanderborght

Credits

The four years of this PhD were funded by the Fonds National de la Rechercher Scientifique. Félicien Meunier is grateful to this organization for its confidence and financial support.

Aknowledgements

Ecrire des remerciements, c'est sans doute comme regarder dans un rétroviseur qui permettrait d'observer tout le chemin parcouru au cours d'une aventure malgré les faux pas et les tortuosités du chemin et y apercevoir tous ceux et celles qui, d'une façon ou d'une autre, ont fait partie du voyage.

SHORT CONTENTS

Introduction and objectives **1**

Water flow in Plants **37**

Hydraulic Phenes **153**

Plant and their environment **259**

Conclusion and outlooks **317**

TABLE OF CONTENTS

Introduction and objectives

1 Introduction **5**

1.1 Water flow in the soil-plant-atmosphere continuum . . 7

1.2 The root system is a highly regulated biophysical system 9

1.2.1 Root systems ideotypes and local phenes 12

1.2.2 Macroscopic parameters 14

1.3 The environment as an heterogeneous medium 16

1.3.1 Coincidence and colocation between root and soil . 16

1.3.2 The transpiration demand 19

1.4 Modeling can help to understand the root water uptake 20

1.5 Methods to investigate root water uptake dynamics . 21

1.6 Conclusive remarks 24

2 Objectives **25**

2.1 General objectives 25

2.2 Methodological developments 30

2.3 Research assumptions 34

Water flow in Plants

3 Water flow resolution **41**

3.1 Introduction 42

3.2 Theory 46
3.2.1 Existing approaches for modeling water flow . . . 46
3.2.2 Development of exact solutions 52
3.2.3 Summary of all solutions and assumptions 54

3.3 Material and Methods 55
3.3.1 Discretization error in static conditions 56
3.3.2 Propagation of errors in coupled models 57

3.4 Results 59
3.4.1 Discretization error in static conditions 59
3.4.2 Propagation of errors in coupled models 63

3.5 Conclusion 68

3.6 Appendices 69

4 From micro-traits to macro-parameters 77

4.1 Introduction 78

4.2 Theory 82
4.2.1 Water flow equation in a single root 82
4.2.2 General solutions of root water flow 83
4.2.3 Derivation of macroscopic root hydraulic properties 84
4.2.4 Resolution of the root water flow equation 86
4.2.5 Properties of an ageing root 88
4.2.6 Root System with laterals 89

4.3 Model illustration 91
4.3.1 Comparison between uniform and heterogeneous roots 91
4.3.2 Inverse modeling of root hydraulic properties . . . 93
4.3.3 Root in a heterogeneous soil 94
4.3.4 Optimal geometric properties 95
4.3.5 Root water uptake strategy 96
4.3.6 Sensitivity of a mature root system to hydraulic phenes 97

4.4 Results . . . 98
4.4.1 Comparison between uniform and heterogeneous roots 98
4.4.2 Inverse modeling of root hydraulic properties . . . 101
4.4.3 Root in a heterogeneous soil . . . 104
4.4.4 Optimal geometric properties . . . 105
4.4.5 Root water uptake strategy . . . 107
4.4.6 Sensitivity of a mature root system to hydraulic phenes 107

4.5 Conclusion . . . 110

4.6 Appendices . . . 112

5 Maize hydraulic architecture 125

5.1 Introduction . . . 127

5.2 Theory: towards a complete RSHA analytical model . 129
5.2.1 Analytical estimate of root system architecture . . 131
5.2.2 Analytical estimate of macrosocpic parameters . . 133
5.2.3 Analytical estimate of macroscopic geometric factors 133

5.3 Material and methods . . . 134
5.3.1 MARSHAL: a online tool to generate RSHA . . . 134
5.3.2 Model cross-validation . . . 138
5.3.3 Model applications . . . 140

5.4 Results . . . 142
5.4.1 Model cross-validation . . . 142
5.4.2 Model applications . . . 143

5.5 Conclusive remarks . . . 149

Hydraulic Phenes

6 Inverse modelling of water uptake 157

6.1 Introduction . . . 158

6.2 Material and methods 161

6.3 Hydraulic tree model 163
6.3.1 Modelling approach 165
6.3.2 Scenarios 167
6.3.3 Sensitivity analysis and parameter uncertainty . . 168

6.4 Results 169

6.5 Conclusive remarks 175

7 Inverse modelling of root conductances 181

7.1 Introduction 182

7.2 Material and Methods 184
7.2.1 Soil and plant material 184
7.2.2 Root pressure probe 185
7.2.3 Total root conductance 186
7.2.4 Axial conductance 187
7.2.5 Junction root-shoot conductance 189
7.2.6 Optimization scheme 189

7.3 Results 190
7.3.1 Example of pressure probe experiment 190
7.3.2 Conductance results and fits 190
7.3.3 Goodness of fit 194

7.4 Discussion 196

7.5 Conclusion 203

7.6 Appendix 204

8 Inverse modelling of water content 207

8.1 Introduction 208

8.2 Model description 211
8.2.1 Water flow 211

8.2.2 Boundary conditions 212

8.3 Application : Use of R-SWMS for hypothesis testing . 213
8.3.1 Material and methods 213
8.3.2 Representing experimental results 217
8.3.3 Hypothesis testing 220

8.4 Conclusion 224

9 Inverse modelling of isotope profiles 227

9.1 Introduction 228

9.2 Material and Methods 231
9.2.1 Experimental setup 231
9.2.2 Isotopic analysis 233
9.2.3 Modelling 233
9.2.4 Model-data comparison 237

9.3 Results 242
9.3.1 Experimental results 242
9.3.2 Modeling results 244

9.4 Discussion 250

9.5 Conclusion 253

9.6 Appendices 255

Plant and their environment

10 Root water uptake performance in silico 263

10.1 Introduction 264

10.2 Material and Methods 267
10.2.1 Root architecture modelling 267
10.2.2 Root water uptake and soil water flow modelling . 267

10.2.3 Simulation scenarios 271

10.3 Results 277
10.3.1 Influence of root system architecture 277
10.3.2 Influence of root hydraulic properties 282

10.4 Discussion 286

10.5 Conclusion 290

11 Towards crop quantitative eco-ideotypes 293

11.1 Introduction 294

11.2 Water flow model 297

11.3 Material and Methods 299
11.3.1 Plant water uptake and performance 299
11.3.2 Defining groups of phene states 300

11.4 Results 305
11.4.1 Defining groups of phene states 305

11.5 Discussion 313

11.6 Conclusion 314

Conclusion and outlooks

12 Conclusion and outlooks 321

12.1 General conclusion 321

12.2 Thesis summary 323
12.2.1 General objectives 323
12.2.2 Methodological developments 328

12.3 Perspectives 334

General bibliography **347**

LIST OF FIGURES

1.1 Water flow in the plant 8
1.2 Soil-Root System schematics 10
1.3 RWU location as predicted by R-SWMS 18

2.1 Workflow of the second part of the Ph.D. 26
2.2 General objectives of the Ph.D. 27
2.3 Methodological developments of the Ph.D. 31

3.1 Schematic of the water flow resolution in root systems 49
3.2 Finite-difference model error on plant transpiration . . 60
3.3 Comparison of the methods in terms of time 61
3.4 Variability of conductance *vs* numerical error 62
3.5 Segment size effect on local and total water uptake . . 63
3.6 Simulated water dynamics for different segment sizes . 64
3.7 Source of error in a maize mature root system 66

4.1 Maize conductivity observations 81
4.2 Schematic of a zoned root 84
4.3 Flowchart of the water flow equation resolution 88
4.4 Conductivity distributions used for comparison 92
4.5 Solutions of the root water flow equation 98
4.6 Macroscopic parameter solution 100
4.7 Model solution for a lateral root 101
4.8 Macroscopic parameters for a maize lateral root 102
4.9 Hydraulic properties of the maize brace roots 103
4.10 Root perfomances in a coupled soil-root model 105
4.11 Root conductance as a function of root radius 106
4.12 Growth *vs* development root strategies 108
4.13 Sensitivity analysis of a mature maize root system . . 109

5.1 Maize hydraulic and architectural parameters 130
5.2 Root growth parameters of the RootBox model 134
5.3 MARSHAL online application details 138

5.4 Analytical *vs* numerical approaches 139
5.5 Impact of standard deviation on accuracy 142
5.6 Model cross validation 143
5.7 Maize root length density profile fitting 145
5.8 Range of conductances observed and simulated 146
5.9 Sensitivity analysis of root system conductance 147
5.10 Sensitivity analysis of root water uptake depth 148
5.11 Sensitivity analysis of volumes 149
5.12 Regression of macroscopic parameters on local phenes 150

6.1 Schematic diagram of a lupine root system 162
6.2 Profile of hydraulic conductivities 170
6.3 Measured and simulated radial fluxes 171
6.4 Radial flux and xylem potential distribution 172
6.5 Profile of water uptake and xylem water potential . . 173
6.6 Sensitivity analysis of the model parameters 174
6.7 Root water uptake as a function of root length 177

7.1 Schematics of the root system of maize and lupine . . 183
7.2 Principle of the conductance measurements 188
7.3 Example of root conductance measurement 191
7.4 Hydraulic properties of the maize root types 192
7.5 Hydraulic properties of the lateral roots of lupine . . . 193
7.6 Junction conductance measurements 194
7.7 Overall goodness of fit 196
7.8 Root water uptake location in the different root types. 197
7.9 Comparison of the root radial conductivities 199
7.10 Comparison of the root axial conductance 200
7.11 Comparison of the relative water uptake 201

8.1 Methodology used to decrypt water flow 215
8.2 Inputs for R-SWMS simulations 216
8.3 Cumulative transpiration measured by weight loss . . 217
8.4 Experimental and simulated WC distributions 218
8.5 Modeled *vs* measured soil water content 220
8.6 Outputs available in RSWMS 221
8.7 WC change and integrated sink term 222

8.8 Scenarios tested with R-SWMS 223
8.9 Comparisons of the 4 considered scenarios 225

9.1 Soil macro-rhizobox experimental setup 232
9.2 Root model schematics 236
9.3 Model optimization scheme 241
9.4 Water retention curve 242
9.5 Experimental results 243
9.6 Root length density observations 245
9.7 Best model fit 246
9.8 Root-rhizosphere model sensitivity analysis 247
9.9 Best fit equivalent isotopic composition 249
9.10 Water release location and intensity 250

10.1 Phenotype architectures 272
10.2 Soil hydraulic properties 275
10.3 Water content distribution after 6.5 days of uptake . . 278
10.4 Transpiration dynamics of the phenotypes 279
10.5 Phenotype performance 280
10.6 Profiles of root water uptake 281
10.7 Impact of root conductivity on plant transpiration . . 284
10.8 Reduction of the actual to potential transpiration . . . 285

11.1 Local phenes impact on the transpiration 306
11.2 Macroscopic root system parametric space 307
11.3 Instantaneous cumulative transpiration 309
11.4 Water content profiles at 70 days 310
11.5 Macroscopic phenes impact on the transpiration . . . 311
11.6 Soil potential distribution after 80 days 312
11.7 Perspective of model validation 314
11.8 PCA of the macroscopic parameters 315

12.1 Leaf-root coupled model performance 335
12.2 Scenarios of CO_2 concentration changes 336
12.3 Water change distribution after 7 days 338
12.4 Intercropping positive impact on transpiration 341
12.5 Flowchart of a large-scale forecast model 342
12.6 European soil map 343

12.7 Potential evapotranspiration in Europe 344
12.8 Precipitation in Europe 344

LIST OF TABLES

3.1 Summary of all root water flow resolutions 55
3.2 Relative differences between model state variables . . 67

4.1 Local hydraulic property distribution 86
4.2 Linearly independent functions f_1 and f_2 87
4.3 Local hydraulic property function parameter 87

7.1 Summary of the considered scenarios for fitting 190
7.2 Best fit for the axial conductance profile 195
7.3 Best fit for the radial conductivity profile 195

9.1 Soil and reservoir hydraulic parameters 238

10.1 Root architectural parameters for the phenotypes 1-3 273
10.2 Averaged root statistics 273
10.3 Parameter values for Mualem-Van Genuchten 276
10.4 Root system efficiencies 283

11.1 Weather statistical data for the European locations . . 303
11.2 Soil hydraulic properties by horizon 304
11.3 Macroscopic parameters of the different categories . . 308

PART I

INTRODUCTION AND OBJECTIVES

In the very first section of this manuscript, we shortly introduce the context, the objectives, our research questions and the assumptions we made for the study

Like the plant changes its leaves and keeps intact its roots, change your opinions and keep to your principles

Victor Hugo

INTRODUCTION 1

This chapter is a modified version of a scientific article published as:

> Lobet G., Couvreur V., Meunier F., Javaux M. and Draye X. Plant water uptake in drying soils. Plant Physiology, 2014, 164 (4) 1619-1627

Food security is one of the greatest challenges humanity will face in the 21st century for at least three reasons (Daily et al. 1998). First, the ever growing world population that is expected to exceed 9 billion people by 2050 (Godfray et al. 2010) is requiring more food while nowadays approximately 805 million people remain chronically undernourished (FAO 2014). Second, limited arable land surface and freshwater resources essential for food production constrain indefinite expansion of cropped and irrigated surfaces. Finally, climate change will more than probably affect in the future the quality and quantity of food produced globally if food production systems do not become more resilient (Haile et al. 2017; Mach 2017).

While crop production is hoped to increase by 70% in the forthcoming 40 years to meet the global population demand (FAO 2009), almost 100% of land area suitable for rainfed crop production is today already used for agriculture in South Asia, most of Africa and Europe (Fischer et al. 2000). It is then most likely that the future food production increase will rely on intensive and/or innovative agricultural systems where careful agricultural management practices and high-yield crop genotypes will play an important role. In any case, understanding the plant mechanisms to grow and develop in a heterogeneous changing environment would be of great benefit in the quest for more efficient food production systems.

In this context, it is known for decades that plants are tremendous water consumers (Jensen 1968). Even though only a tiny fraction of water taken up by plants is truly consumed in their metabolism, water is, by far, their most absorbed resource. This is due to the plant mechanism of production of new assimilates that requires carbon assimilation from the atmosphere and, as a consequence, stomatal aperture and water transfer into the air (Lawlor and Cornic 2002). Almost half of the global freshwater passes annually through the rhizosphere, the small volume of soil directly influenced by plant roots (Sposito 2013). Almost 70% of the terrestrial precipitation is returned back to the atmosphere through evapotranspiration, which, for crops only, represents around 7.6×10^{15} liters of water worldwide (Oki and Kanae 2006). The equivalent volume of the lake Victoria is lost three times each year because of cropland evapotranspiration. Regarding the water supply, almost 90% of the human freshwater consumption is already allocated to agricultural production (Döll and Siebert 2002) and the water scarcity is expected to worsen in many regions of the globe, due to climate change, with more frequent and more intense droughts (Pachauri et al. 2015). Therefore, drought in agriculture has become the most significant abiotic stress and maintaining yield under dry conditions is one of the major challenges of plant breeding (Cattivelli et al. 2008).

However existing studies suggest that current crop water consumption often exceeds theoretical requirements. It has been the core-concept of strategic programs aspiring to produce more food with reduced water consumption despite the fact that breeding for crop more efficient in terms of water use often led to negative results (Blum 2005). In any case, Gregory et al. (2005) stresses that a more detailed consideration of the dynamics of water fluxes in the soil-plant-atmosphere system is needed. When water deficit occurs, it may lead to dramatic yield reductions because of the plant dependence on water to prevent excessive leaf heating, to ensure long-distance nutrient transport and, as already mentionned, to capture carbon dioxide from the atmosphere (Farooq et al. 2009). Some critical development stages are particularly important for the yield determination, such as flowering (Hall et al. 1971). Then if the actual plant transpiration is decreased as compared to the potential transpiration, which is determined by atmospheric demand and leaf properties, yield is likely to be considerably reduced.

1.1 Water flow in the soil-plant-atmosphere continuum

The fundamental mechanism of water flow in plants has been described for many years (Steudle 2001). Briefly, the diffusion of vapor through stomata leads to the evaporation of water from the surface of inner leaf tissues and an increase of tension in the xylem that propagates, *in fine* to each root following the cohesion-tension principle. Where this tension is higher than the tension in the surrounding soil (in absolute value), it induces an inflow of water from the rhizosphere following paths of lowest soil hydraulic resistance. How far plants are able to sustain their leaf water demand is therefore largely dependent on the hydraulic properties of the soil-root system. The water trajectory from the soil to the atmosphere is schematically illustrated in figure 1.1 together with orders of magnitude of observed water potential along its way.

Water supply is ensured by plant root system where uptake is unevenly shared among root segments. Indeed, individual segments differ by their axial and radial hydraulic conductivities and by the conductance of the lowest conductance paths that links them to the shoot base. These properties, encapsulated in the concept of root hydraulic architecture (i.e. the combination of the root system topology, root segments positions in space and root hydraulic property distributions), have a large impact on the hydraulic conductance of the root system and, together with the soil hydraulic status, on the distribution of water capture among individual root segments. Consequently, sites of higher uptake occur throughout the root zone and contribute to the heterogeneous spatial distribution of the plant available soil water (Doussan et al. 2006). For a given root under homogeneous soil conditions, these preferential sites are predicted a few centimeters from the root tip, where protoxylem and xylem elements are conductive and hydrophobic structures are lacking. This statement is however still controversial (Peterson et al. 1993), depends on root type and probably on external conditions as well. It was recently confirmed experimentally by neutron radiography experiments for example that root water uptake of lupine lateral roots occurs more in proximal regions (Zarebanadkouki et al. 2013). In the present text, the regions (close to root tips) will be

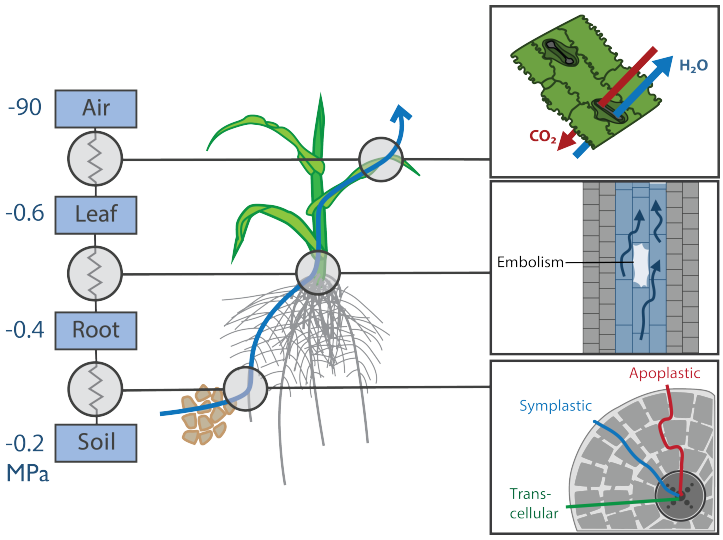


Figure 1.1: Water flow in the plant. A. Water flow in the plant is a passive process driven by water potential differences and regulated by hydraulic conductivities between the compartments of the system (soil-root-shoot-atmosphere). B. Axial water flow is influenced by the anatomy of the xylem pipes (size, number, presence of pits) and the occurrence of cavitation event (embolism of xylem elements). C. Radial water flow is influenced, on the long term, by the radial anatomy of the root such as the number of cell layers and the presence of hydrophobic layers (endodermis and exodermis). On a short term, the radial flow is influenced by the expression and localization of water channels called aquaporins.

consistently referred to as the distal regions, as opposed to proximal regions (closer to root collar). Main location of root water uptake will be continuously discussed throughout the manuscript.

In next sections, more insights on the different compartments of the soil-plant-atmosphere continuum that play alternately or simulatenously a key role for crop transpiration and plant water status are given. The plant is a living organism that can be seen as a regulated biophysical system (section 1.2) while, from an agricultural point of view, soil and meteorological conditions are external factors that mainly depend on the location on Earth (section 1.3).

1.2 The root system is a highly regulated biophysical system

Although all root segments are somehow connected to the plant stem, the negative water potential that develops at their surface as a result of the xylem tension is not necessarily uniform. Indeed, individual root segments are not equally conductive to water, both radially and axially, and the paths that link them to the shoot base are unique. On the one side, from the root surface to the xylem vessels, water flows radially following paths of lowest hydraulic resistance using apoplastic, symplastic and cell-to-cell pathways (see figure 1.1). This radial water inflow into the root, described as a composite transport, can be characterized at the root segment level by a radial hydraulic conductance, which has been shown to be variable between species (Bramley et al. 2009; Knipfer et al. 2011) and even ecotypes (Sutka et al. 2011). On the other side, the axial flow along the xylem is characterized by the axial conductance of successive root segments and may be affected by many processes such as embolism. The complete hydraulic structure of the root system, comprising its topology and the size and hydraulic properties of its constituting segments, forms, as mentionned earlier, its root hydraulic architecture. It can be seen as a regulated biophysical system and can be represented, thanks to the Ohm analogy, as an electrical network with each root segment having a radial and an axial conductance (Doussan et al. 1998a), see Figure 1.2.

The tissular organization of root segments is a long-term determinant of their radial conductivity. This includes the number and anatomy of cell layers between the root surface and the xylem (Yang et al. 2012), and the presence of hydrophobic casparian strips at the endodermis and exodermis (Enstone et al. 2002). The formation of hydrophobic structures has been shown to be influenced by the growing medium (Hachez et al. 2006) and be triggered by drought conditions (Enstone et al. 2002; Vandeleur et al. 2009). As the tissular organization is established permanently, this implies that the radial conductivity, partially determined by cell organization, reflects the root segment history (its development, in relation with its environment). Beyond these structural features, the root radial conductivity is also controlled on a shorter term by the regu-

lation of water channels (i.e. aquaporins) (Cochard et al. 2007; Hachez et al. 2012). Presence of functional aquaporins in cell membranes highly facilitates the passive flow of water and has been shown to contribute to 20 to 80% of the radial water inflow into the root (Javot et al. 2003; Maurel and Chrispeels 2001), although this contribution varies between species (Bramley et al. 2009). Aquaporin regulation is achieved through their expression intensity (Hachez et al. 2012), subcellular localization (Li et al. 2011) or through the gating of the aquaporin pore (gating) (Boursiac et al. 2008). In maize, aquaporins have been shown to be preferentially localized in the endodermis and exodermis (Hachez et al. 2006), see again Figure 1.1.

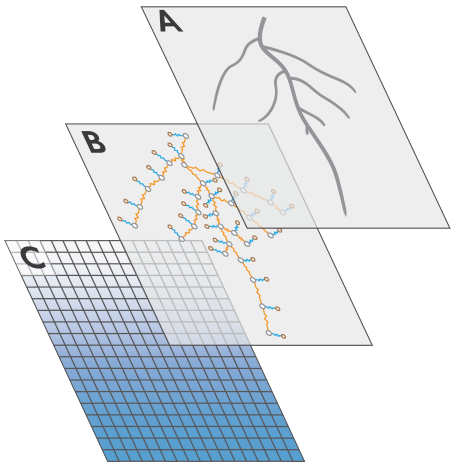


Figure 1.2: Properties of the soil-root system. A. Spatial geometry of the root system. B. Root hydraulic architecture is the integration of axial (orange lines) and radial (blue lines) hydraulic resistances of individual root segments (grey circles) and soil elements (brown circles). C. Soil water content distribution (white = dry, blue = wet).

As for the radial conductance, both permanent and transient features affect the axial conductance of individual root segments. Structural features include the number, size, degree of inter-connection and decorations of xylem vessels and tracheids (Domec et al. 2006; Vercambre 2002), Figure 1.1. The number and size of xylem vessels increase during the maturation of root segments, and decrease with branching order in

cereals (Watt et al. 2008). The xylem diameter also somehow reflects the root segment history. For example, it tends to be lower in shallow roots than in deep roots for woody plants growing in environments subject to drought or freezing conditions (Gebauer and Volařík 2013). The anatomy of xylem vessels also displays a large variability in grasses (Burton et al. 2013), rice (Uga et al. 2013), legumes (Purushothaman et al. 2013) or coniferous (McCulloh et al. 2010). Transient modifications of the axial conductance occur as a result of xylem vessel embolism following the nucleation and rapid expansion of gas bubbles under high tension (known as cavitation). As embolized vessels are not hydraulically conductive, the flow of water through the root segment is restricted to the remaining, non-cavitated vessels. Species are not equally susceptible to cavitation (Cochard et al. 2008) or even cultivars (Li et al. 2009) (but not always (Lamy et al. 2014)). Susceptibility to cavitation has been linked to the large xylem vessels, anatomy of walls and pits (Delzon et al. 2010). It has to be noted that xylem vessels cavitation is a reversible event although the exact mechanisms underlying the refilling processes are not yet fully known (Zwieniecki and Holbrook 2009) even though aquaporins were shown to play an important role in the recovery process (Zwieniecki and Secchi 2017). For more information about refilling mechanisms, see Brodersen and McElrone (2013). It is often considered that the axial conductance does not limit water flow in the root system by virtue of the large conductivity of xylem vessels (Steudle 2000a). However, recent experimental evidence has revealed the negative effect of cavitation on the plant water status (Johnson et al. 2012; Zufferey et al. 2011). At the opposite, breeding programs to reduce the diameter of the major xylem vessel in the seminal roots of wheat (and thus towards limiting xylem conductivities of these roots) demonstrated positive effects on grain yield in dry rain-fed environments (Richards and Passioura 1989).

The spatial geometry of the root system and its temporal evolution are other major determinants of water uptake capacity, as root location in the soil domain delineates the extent of soil exploration and sets up an upper limit to the volume of potentially accessible water at any time. Root insertion angles, interbranching distances or maximal root length are architectural characters that have been all suggested, among others, as potential breeding targets for root water uptake since they have a sig-

nificant impact on root location in four dimensions (three-dimensional space and time) and their possible coicindence and colocation with water sources. In addition, several traits that should contribute to a deep root phenotype have been proposed or identified. Increasing the diameter of the main roots is thought to be linked with a greater growth potential (Pagès et al. 2010) and a greater ability to explore hard soil (Bengough et al. 2011). In rice, the gene *DRO1* has been shown to steepen the root insertion angle and increase the rooting depth, conferring improved drought resistance (Uga et al. 2013). In groundnut, *DREB1A* has been shown to increase drought resistance by promoting root development in deep soil layers. Additionally, increasing the proportion of aerenchyma in main root axes reduces the metabolic cost of root exploration (Fan et al. 2007). The manipulation of root branching in different layers, which is part of the deep root ideotype (i.e. an ideal root system for a specific function, here for root water uptake), is expected to be more difficult to achieve for practical observation constraints. While considering those traits, it should be reminded that deep rooting could be obtained in different ways between tap-rooted or monocot species; the latter producing gravitropic adventitious root axes continuously for the whole crop cycle.

1.2.1 Root systems ideotypes and local phenes

Novel root hydraulic architectures are being proposed to improve drought tolerance. Wasson et al. (2012) advocate for greater axial and radial conductivities in deep roots to increase the uptake and transport capacity of water from deep soil layers. In conditions of scarce deep water, Comas et al. (2013) recommend to decrease the axial conductance in order to save water for the end of the crop cycle. More generally, the importance of the ratio between axial and radial conductivities has also been stressed from modeling studies (Doussan et al. 2006; Draye et al. 2010). Large values of this ratio should lead towards a uniform distribution of the uptake throughout the entire root system, while low values would favor preferential uptake in the topsoil, as shown numerically by Levin et al. (2007), among other illustrations. Lynch (2013) also designed a theoretical optimal maize root system for water and nitrogen uptake. His description of the perfect below-ground plant was

an exhaustive combination of architectural and hydraulic properties that together determine the root system hydraulic architecture. Unfortunately, in many occasions, the proposed traits are simply qualitative with general statements such as "long", "thin", "many" or "few" that remain unclear and do not fix a clear target for breeding. Furthermore hydraulic properties are not systematically accounted for whereas geometric properties alone are not sufficient to characterize uptake capacity. In addition, the temporal aspect of the ideotypes should also be taken into account, which is usually forgotten by now.

Understanding the contribution of specific root phenes (or equivalently traits, i.e. a characteristic property of the plant system) to root system function is critical for crop improvement because it allows identification of properties that contribute to desired functions (Lynch and Brown 2012). Phenes may be defined as the units of the plant phenotype. All together, phenes determine the plant phenotype and thus the root system hydraulic architecture at any time. Any particular phene may take different forms and functions, which is called the phene state. And any phene is expected to have a positive, negative or neutral impact on plant performance according to pedo-climatic conditions. However experimental evidence that the manipulation of root hydraulic architecture can improve the water status of plants under water deficit remains scanty (Passioura 2012). Designing a root hydraulic architecture to improve drought tolerance is thus likely to be specific to the species, climatic scenario, soil hydraulic properties and management practices (Draye et al. 2010). As reminded by Tardieu (2012), the perfect root system for water uptake does not exist, it always depends on the drought scenario, i.e. on the timing and magnitude of drought.

The identification of root ideotypes is further complicated by the fact that root growth and development are strongly influenced by the soil environment. Root architecture modeling in response to a wide range of nutrients deficiencies have been recently described and partly elucidated in Arabidopsis (Gruber et al. 2013). Changes in root architecture in response to phosphate starvation occur under the control of OsMYB2P-1 for example in rice (Dai et al. 2012). Interestingly, alternative adaptations to the same adverse conditions exists among different genotypes, as illustrated by altered primary or lateral root growth conferring resistance to K starvation (Kellermeier et al. 2013). Local environmental

conditions also contribute to root architecture remodeling. Individual roots are able to reorient towards water (hydrotropism) in Arabidopsis(Iwata et al. 2013). Similarly, PIN2 activity influences the capacity of individual roots to escape high salinity patches (halotropism) (Galvan-Ampudia et al. 2013). This plasticity of root development should not be overlooked in drought resistance studies given the role of water for nutrient mobility and uptake.

1.2.2 Macroscopic parameters

The root water uptake of a three-dimensional architecture whose individual segment is characterized by specific hydraulic properties according to its age, type and history is potentially extremely complex to predict. However, the concept of hydraulic architecture makes the understanding of its behavior potentially simpler as it may enable one to calculate so-called macroscopic parameters, or plant-scale parameters that determine plant behavior in terms of water uptake. Under uniform soil water distribution, it has been shown indeed that the hydraulic architecture allows one to predict the expected contribution of every root segment to the water uptake (Doussan et al. 2006), recently referred to as the standard uptake fraction distribution (Couvreur et al. 2012). In similar conditions, the ability of a root system to sustain a certain transpiration rate under a given potential difference between the roots and the collar is defined as its equivalent conductance (Couvreur et al. 2012), that can be calculated when the root system hydraulic architecture is perfectly known using a numerical solution of the water flow equations. Recently, Couvreur (2013) stated that these plant-scale properties could also be derived analytically by Thevenin theorem ((Thévenin 1883), this theorem states that the equivalent conductance of a linear network can be calculated analytically) but much is left to derive the macroscopic parameters from local root phenes.

When soil water potential distribution is no more uniform, water uptake compensation from one site to another occurs and the root distribution becomes then a very poor indicator of the distribution of the uptake sites, as root length density and uptake profiles become dissimilar (Javaux et al. 2013). Under heterogeneous conditions, at places where the soil water potential is low, soil capillary forces retain water more

strongly in the remaining fraction of the soil porosity, comprised of small micropores. As this reduces the soil hydraulic conductivity, the flow of water towards the root surface is locally restricted and water uptake by other root segments, located in portions of the soil where water is more readily available, should increase to maintain the global transpiration stream. This passive adjustment of the distribution of water uptake among root segments occurring as a consequence of the heterogeneity of soil water potential and conductivity was called compensatory root water uptake (Jarvis 1976). Interestingly, simulations studies indicate that compensatory root water uptake precedes the moment where transpiration is affected (Couvreur et al. 2012) since compensations occurs as soon as soil water potential distribution is no more uniform. These results converge to a contribution of compensatory root water uptake to the maintenance of transpiration and assimilation.

Couvreur et al. (2012) recently highlighted that the compensatory uptake could be also predicted using plant-scale parameters. The compensatory water uptake would then be formulated as the product of three terms: (i) the standard uptake fraction, (ii) the difference between the local and spatially averaged soil water potential, and (iii) the root system conductance; which suggests that, in addition of defining the standard sites of water uptake, the root hydraulic architecture simultaneously contributes to the adjustment of the uptake to the soil water potential distribution and influences soil water potential heterogeneity.

In their theory, Couvreur et al. (2012) demonstrated that root system water flow could be efficiently (in terms of computation cost) and accurately (in terms of water uptake flow) represented by these emerging properties of the hydraulic architecture, i.e. the standard uptake fraction, the root system conductance and the compensatory root water uptake conductance. Together they form the set of macroscopic parameters that can be easily calculated for a specific root system architecture and that allow predicting the water uptake sites and potentially the plant water stress. Unfortunately, as of today, there is no clear link between local root phenes and these macroscopic parameters for complex root system architectures.

1.3 The environment as an heterogeneous medium

The distribution and amount of water uptake in the root zone is also influenced by the distribution and amount of available soil water. The root hydraulic architecture essentially matters in water deficit conditions, when the soil hydraulic conductivity becomes limiting (Passioura 1984). Because the array of intermediate situations where the soil is neither completely dry nor wet is large, it has become obvious in the last decade that an appropriate framework to analyze water uptake should consider both root hydraulic architecture and soil hydraulic properties.

Figure 1.3 illustrates how flexible a mature root system can be and may adapt its water uptake to wet zones. Coincidence and colocation between root location and high water content soil sites impact the plant water status and *in fine* its performance.

1.3.1 Coincidence and colocation between root and soil

The importance of root placement for water extraction depends on the ability of the soil to redistribute its water in order to sustain the uptake of water that occurs in the rhizospheric compartment of the soil. In soils with high water conductivity throughout the season, fast soil water redistribution from the bulk soil to the rhizosphere limits the role of root growth as long as the root system conductance is large enough. In drying soils, however, the smaller hydraulic conductivity of the soil reduces soil water redistribution and the soil volume from which individual root segments are able to obtain their water narrows down accordingly. In such conditions, even transient, the placement of roots and its correlation to the distribution of soil water sets an upper limit to the amount of water that can be extracted.

In transient or cyclic drought environments, the reserve of soil water can be temporarily restricted to deeper layers because water uptake (and evaporation) occurs preferentially in the topsoil, where the root length density (cumulated root length per unit soil volume) is the highest and the path to extract water the shortest. This situation is most pronounced under terminal drought, as the soil water reserve is not refilled over the growing season and is gradually restricted to deeper

soil layers. Increasing the root system depth and tailoring deep water extraction was therefore proposed as a key element of a root system ideotype adapted to water-limited environments (Comas et al. 2013; Wasson et al. 2012). Considering the construction and maintenance costs of root systems, the ideotype should preferably have few and long laterals, evenly distributed along the depth axis (Lynch 2013). The rationale is that few long laterals have a small weight on the carbon budget and allow the exploration of a larger soil volume. Aerenchyma is also considered as a feature reducing the root construction cost, in favor of deep root extension. Wasson et al. (2012) also advocate for a greater root length density at depth and reduced density in the top-soil in order to favor deep soil water extraction.

The benefit of deep root system in drought prone environment has been experimentally demonstrated in rice (Steele et al. 2012), wheat (Manschadi et al. 2010), maize (Hammer et al. 2009), legumes (Vadez et al. 2012) or trees (Pinheiro et al. 2005). However, other results seem to indicate that deep root systems are not always linked to an increase in yield. Experiment with chickpea (Zaman-Allah et al. 2011) and wheat (Schoppach et al. 2014) indicate that drought tolerance, especially in terminal drought conditions, can be linked to a conservative use of water throughout the season rather than deep rooting. In such cases, plants tailored for improved root length density at depth are likely to use too much water early in the season and reduce the reserve of water in the profile during grain filling. A similar behavior has been reproduced using modeling tools (Vadez et al. 2012).

A particular scenario of soil water redistribution involving the root hydraulic architecture can occur under low or negligible transpiration flux. In such conditions, the xylem water potential at the root collar is a weighted value of the soil water potentials sensed by root segments, intermediate between the soil water potential of the driest and wettest soil parts in contact with roots. As long as root segments (and the rhizosphere) are radially conductive to water, the root system offers a long distance path of low hydraulic resistance that allows the hydraulic lift phenomenon, i.e. soil water redistribution through the root system from the wetter soil regions towards the drier ones. This phenomenon, which has long been a matter of debate, would contribute to the night restoration of the soil hydraulic conductivity that decreased around

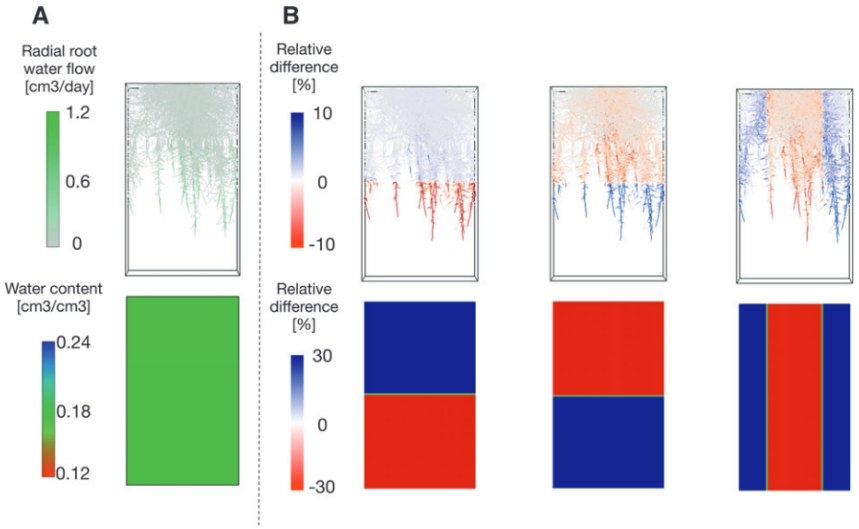


Figure 1.3: Influence of the soil water potential distribution on the water uptake process. The R-SWMS model (Javaux et al. 2008) was used to simulate the root radial water flow under different soil water potential distribution. A. Radial water flow (top) under hydrostatic equilibrium (bottom). B. Compensatory root water uptake (top) for different soil water potential distribution (bottom). Relative changes in water content and uptake rate given as a function of the standard scenario A.

part of the root system as a result of root water uptake during the day (McMichael and Lascano 2010).

Other factors reducing the soil hydraulic conductivity have recently been underlined. Following the mass conservation principle, the flux density of water (motion speed) increases as it gets closer to the root surface and, in parallel, its water potential decreases as well as the soil conductivity. The rhizosphere is thus susceptible to a local drop of hydraulic conductivity, that is favored by high rates of root water uptake and by soil properties, such as coarse textures, that steepen the relationship between soil conductivity and water potential (Schroeder et al. 2008). Soil hydraulic properties and water potential around each root segment therefore set a maximum uptake rate above which a soil restriction to water flow is likely to occur. This phenomenon would be

difficult to distinguish from the limitation imposed by root hydraulic properties that is observed under drought (Schoppach and Sadok 2012).

The specific hydraulic properties of the rhizosphere have been reviewed recently (Carminati and Vetterlein 2012). Strikingly, root exsudates seem to generate hydrophilic or hydrophobic behaviors depending on the environmental conditions and on its constitution (Carminati et al. 2011). The role of this ambiguous effect is not yet fully understood but is proposed to participate in the control of the soil conductivity by the roots themselves, which would add a level of complexity in the modelling of the regulation of water uptake.

1.3.2 The transpiration demand

Soil hydraulic conductivity and retention are not the only properties that determine the environmental conditions of growth and development of the plant. The atmospheric conditions (air temperature, humidity, wind velocity) establish the water demand to be sustained by the plant to avoid drought stress. This top boundary condition for the plant is the driver of the water flow in the soil-root system continuum and defines the water quantity to be taken up at any moment. To keep its stomata open and continue to assimilate air carbon dioxide, an equilibrium must be found between the atmospheric demand and the soil water supply by root systems. In case of limited soil water supply, plants may (partially or totally) close their evaporative sites in order to avoid too low water potential that would dramatically impact their hydraulic behavior (Draye et al. 2010).

Climate is usually defined as the statistics of meteorological variables over long time periods (typically 30 years) and therefore encompasses both mean dynamics of meteorological variables over the year (such as as temperature, humidity, wind and precipitation) and their variability. Extreme events are entirely comprised in the definition of climate. But climate conditions are not fixed once for all. As it is well known for more than 10 years now, human well beings are extremelily likely the main responsible of observed climate change all around the globe. According to IPCC (2007), climate changes and will keep doing so. Trajectories of these changes highly depend on emission scenarios and still now, in many regions of the world, climate could move in different conditions,

depending on global strategies of development, which underlines the usefulness of physically-based predictive models.

1.4 Modeling can help to understand the root water uptake

Despite the fact that water uptake follows simple rules of passive flow driven by water potential gradients and following paths of lowest resistance, and despite the current knowledge of the main paths and factors affecting their conductivities, the forecast capacity of water uptake at the plant and seasonal scale and of crop performance remains limited by the difficulties to integrate those interacting paths and factors, at the appropriate scales and in a spatial and temporal framework. Many of those factors have been evoked in the above sections, but many others have been deliberately set aside, such as the feedback effect of water uptake on root growth via its effects on, e.g. assimilation and soil mechanical impedance. Because direct experimental observations are necessarily capturing limited aspects of water uptake, systems approaches gained much interest in the last decade (Dunbabin et al. 2013).

Doussan et al. (2006) presented the first model that simulates water flows explicitly in the soil-root continuum. Using the concept of hydraulic architecture to solve plant water flow (Doussan et al. 1998a) and soil water flow through Richards equation in unsaturated soils, they developed a coupled model of the water flow in soils and plants, able to simulate compensatory uptake and hydraulic lift in heterogeneous soil conditions. A very similar approach was taken by Javaux et al. (2008) to create the R-SWMS model. Using the latter model, Schroeder et al. (2008) illustrated the negative impact of local conductivity drops around roots in drying soils on the water uptake process. The importance of the ratio between axial and radial root conductivities and of the soil type was also highlighted (Draye et al. 2010) by the same modelling tools. On the soil side, the model can be instrumental to investigate the influence of the root water uptake on water flow and nutrient transport in the surrounding soil (Schröder et al. 2012). Recently, it was used to assess the impact of salinity on the plant transpiration reduction (Schröder et al. 2012). In order to streamline the adoption of these

concepts (hydraulic architecture) and tools (coupled soil-plant models) by the plant science community, Couvreur et al. (2012) proposed a simplified version of R-SWMS that can be used at the crop level, but still relies on a precise parameterization of root hydraulic architecture. This simplified model, whose plant parameters were presented above, has also been shown to simulate behaviors such as compensatory uptake and hydraulic lift from hydraulic principles (Javaux et al. 2013).

In this uncertain context of climate change and increased food production demand, models have a critical role to play to clarify the picture. Modelling and particularly detailed process-based modelling can be used to unravel the underlying processes in an attempt to guide future management practices and best G x E x M interactions. There is not limit but imagination in designable simulations for models: any desired combination of plant-environment-management (even unrealistic) with any environmental conditions (even not currently existing) can be tested *in silico*. Process-based models are therefore a perfect tool to highlight best associations for specific pedo-climatic conditions for now and the next century. Models also allow one to bring out the mechanisms and feedbacks that dramatically contribute to plant performance and to determine the mechanisms promoting positive and/or negative interactions. Finally, it is also possible, with models, to cross scale and to predict the impact of deterministic relations, observed on a certain time and space scale, on the overall system behavior in a specific context. In this research, models will be used to assess the performance of particular G x E x M associations even though the management will be restricted to irrigation issues only. Other aspects of management such as sowing density or date will be ignored in this research (see assumption section in Chapter 2).

1.5 Methods to investigate root water uptake dynamics

The development of measurement techniques and observation methods has been instrumental in many recent advance of the understanding of root water uptake dynamics. While traditional methods to investigate either plant or soil properties are mainly used at the plant scale, new

techniques have empowered a more detailed approach of the system, down to the centimeter scale.

Several 2D and 3D observation methods have been developed that enable better or faster characterization of root system architecture. Pouches dipping in nutrient solution are becoming increasingly popular to screen early stages of root systems development in two dimensions (Hund et al. 2009). Recently, a scanning technique has been proposed for digitizing entire root systems of plants grown in rhizoboxes (Lobet and Draye 2013). The two-dimensional restriction of pouches and rhizotrons was recently released by stereo-imaging of root systems grown in tubes filled with gellan gum (Iyer-Pascuzzi et al. 2010). Lastly, X-ray computed tomography (Mooney et al. 2011) or magnetic resonance imaging (Jahnke et al. 2009; Stingaciu et al. 2013), widely used in medical sciences, are now entering the plant research domain. These allow the 3D non invasive monitoring of root growth in realistic soil cores and, in the future, should provide much details on the precise soil conditions around individual root segments, including soil water content.

Following the development of these observation techniques, specific free software solution were developed for the analysis of root system architecture and root anatomy. For example, RootNav (Pound et al. 2013), SmartRoot (Lobet et al. 2011) and EZ-Rhizo (Armengaud 2009) were developed for the analysis of 2D root images while RooTrak (Mairhofer et al. 2012) and RootReader3D (Clark et al. 2011) were designed for the analysis of stereo-images. These tools ease the digitizing and analysis of complex root system architecture. At the organ scale, RootScan (Burton et al. 2012) was developed for the high-throughput analysis of the anatomy of root sections. The software automatically computes the area of multiple root tissues including the aerenchyma or the xylem vessels. These tools have been recently included on the plant-image-analysis.org database (Lobet et al. 2013).

The quantification of root hydraulic properties remains certainly one of the biggest challenges. Techniques suitable for global measurements have been established for many years. The pressure chamber is widely used and estimates the conductance from the measurement of the water flow induced by a known pressure differential. Other techniques estimate the conductance of individual root segments, yet remain extremely time consuming (e.g. pressure clamp (Bramley et al. 2007a) and pressure

probe (Steudle and Peterson 1998)). Part of the challenge lies in the difficulty to measure the variability of root hydraulic properties as a function of segment type and age and environmental conditions, and in the variability between measurement methods (Bramley et al. 2007a).

On the opposite, techniques exist to monitor changes of environmental variables linked to root water uptake like soil water content or mobile tracer concentrations. This include time domain reflectometry (Robinson et al. 2003), electrical resistance tomography (Vanderborght et al. 2005) or, more recently, ground penetrating radar (Lambot et al. 2008) also for locating roots (Moore and Ryder 2015), or others (Nadezhdina and Čermák 2003). The spatial resolution of these techniques ranges in the decimeter scale and is appropriate to study the distribution of water in rows or inter-rows. Recently, two techniques have been successfully tested for the observation of water flow down to the centimeter level. Light transmission imaging can be used to finely map changes in soil water content in transparent rhizotrons (Garrigues et al. 2006). Unfortunately, the technique is restricted to a specific type of substrate (white sand) and does not estimate water uptake by individual roots due the unknown redistribution of the water in the substrate (Javaux et al. 2008). More recently, the use of neutron radiography (Esser et al. 2010), that is not bound to any specific type of substrate, has been used to investigate water movement and determine water uptake sites in lupin root systems. Using D_2O injection in combination with a convection-diffusion model, water uptake by individual segments could be quantified in a complete root system (Zarebanadkouki et al. 2013). On the other hand, Haber-Pohlmeier et al. ("Quantitative mapping of solute accumulation in a soil-root system by Magnetic Resonance imaging") used Gadelinium as tracer that accumulates at the root surface and NMR to quantitatively map concentrations of this tracer in a complex root-soil system to decipher to determine where and by which plant roots water is taken up. These technical evolutions are therefore promising new insights on the water dynamics at smaller scales, while systems analysis frameworks will help to integrate this information.

1.6 Conclusive remarks

The determinants of water flow through the soil-root system are well known and have been largely studied individually. However, their integration at the plant and canopy scales and over a whole crop cycle remains very limited. The spatial and temporal heterogeneity of the soil, the interactions between the soil and the root at multiple scales and the need to combine very different disciplines makes this integration particularly challenging. With the development of functional-structural soil-plant models, root system biological modelling is bringing novel analytical tools to turn a vast amount of data into biological questions crossing scales and disciplines. New root system ideotypes could emerge from a more comprehensive and quantitative consideration of the many determinants of water flow during a whole crop cycle and in the framework of a cost-benefit analysis at the system level. These next-generation root system ideotypes should be set in relation with the considered drought scenario, more quantitative than qualitative and they should include dynamics of change. They would be defined by a series of positive quantified phenes, or phenes state, specific to given pedo-climatic conditions or better by macroscopic parameters that lead to the desired plant behavior and that define root ideal strategies for root water uptake adapted to their local environment.

OBJECTIVES

2

THE main goal of this Ph.D. thesis is to advance the current understanding of optimal water uptake and growth strategies for crops - defined through macroscopic parameters and determined by ensemble of phene states - for maximising yield. Such plants would minimize the water stress over their crop cycle and particularly at critical development stages. These plants display what is defined as an ideal plant water uptake strategy (i.e. they do not experience water stress). To achieve this objective, methodological developments are needed. New tools and methods to define quantitative crop root system ideotypes for water uptake, defined as crop root systems perfectly adapted to their heterogeneous changing environment will thus be created, coupled or developed. At many occasions throughout this thesis, maize will be used for illustration purpose as model of crop species.

To address this main goal, three general objectives (GO) that pave the way were defined and listed below. Their interconnections to respond to the main goal are schematically represented in Figure 2.2.

2.1 General objectives

GO.1: Linking local architectural and hydraulic root phenes and plant-scale parameters

Root architectural and hydraulic phene states are appropriate to represent plant static properties but as such do not represent the plant behavior. On the other hand, macroscopic parameters adequatly represent uptake properties and depend on local hydraulic and architectural phene states. Yet, there is no direct link between macroscopic parameters and local phene states. The first general objective of this thesis is to develop analytical relationships between local and whole plant parameters. These relations would not only allow predicting plant scale behavior but also speeding up computational modelling of plant water uptake in variable environments. To do so, describing accurately the

water flow in root system hydraulic architecture is mandatory. This is why the third chapter of the Ph.D. thesis will be dedicated to the description of water movement in such architecture and improvement of current resolution methods of the water flow equations. In Chapter 4, analytical relationships between local root phenes (e.g. elongation rate, hydraulic properties) and macroscopic parameters will be developed at the branch scale. Finally, direct links between ensembles of root phenes and main macroscopic parameters are presented in Chapter 5 in order to progress towards fully implicit root systems and the plant-scale parameters analytically determined.

Figure 2.1 details the existing links and the current research gaps between local phenes and plant-scale parameters. The second part of this Ph.D. will focus on filling these gaps. In particular, analytical solutions of the water flow equations in root systems hydraulic architectures and fully implicit root system descriptions will be developed in Chapter 3 and Chapter 4-5, respectively.

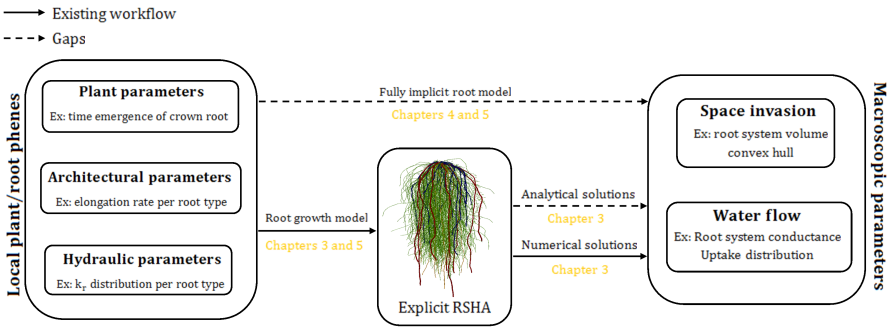


Figure 2.1: Workflow of the second part of the Ph.D.

Chapter 3 | Chapter 4 | Chapter 5

GO.2: Quantifying root hydraulic phenes

Root system hydraulic architectures are entirely described by two aspects: the root system topology and position in space on one hand and

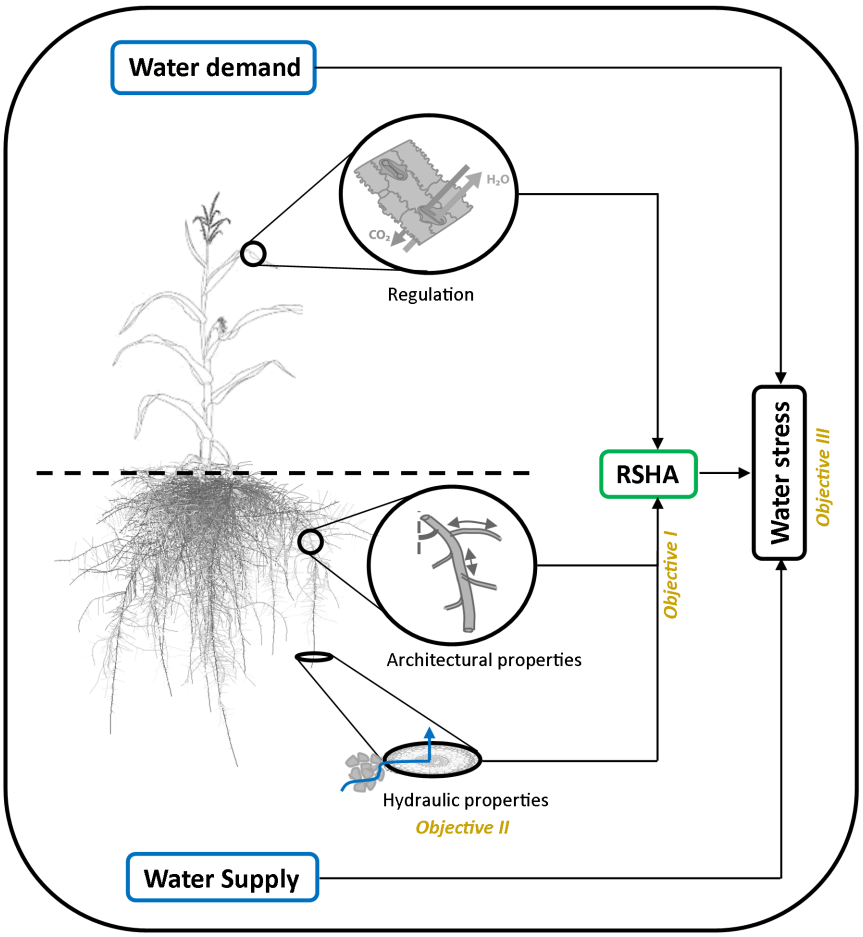


Figure 2.2: General objectives of the Ph.D. thesis represented in their general context. Water demand is determined by weather variable dynamics such as air temperature, humidity and wind velocity while water supply is supported by the root system and also depends on the soil hydraulic properties.

the age and order dependent hydraulic properties on the other hand. Even though new and ancient techniques to characterize the latter exist or arise in the last decades, the quantification of root hydraulic properties remains certainly one of the biggest challenges in the exploration of the root system hydraulic architecture properties.

Certain techniques already exist but they are only suitable for global measurements or they are too time-consuming to be applied at any time everywhere in the root system. In this thesis, the second methodological objective is therefore to develop novel procedures to accurately determine local hydraulic property distributions. The present methodology relies on a combination of global or local observations and inverse modelling in order to retrieve the most likely distributions of hydraulic properties of the observed roots, together with uncertainty of these distributions. The measurements used were the local water uptake flow (Chapter 6), the root conductance distributions (Chapter 7), the water content distribution (Chapter 8) or isotope profiles (Chapter 9). In the two first Chapters of this part, soils could be neglected while it was no more the case in Chapters 8 and 9.

Chapter 6 | Chapter 7 | Chapter 8 | Chapter 9

GO.3: Elaborating a novel definition of root water uptake optimal strategy: crop quantitative eco-ideotypes for root water uptake

The third and final objective is to revisit the concept of crop ideotypes for root water uptake. The new definition of ideotype has to be quantitative and must include the temporal evolution of the root system. The derived ideotypes will also be systematically associated to specific environments because no genotypes can perform ideally in all situations.

Since the advent of computers, many models have been developed to simulate the plant growth in its surrounding environment. Since then, functional-structural models have been developed and potentially provide better insights to investigate plant-environment interactions.

To reach the global objective, a functional-structural plant model able to simulate the water flow from the bulk soil to the atmosphere in three dimensions (Chapter 10), together with the plant growth and

development over a complete crop cycle (Chapter 11) has to be developed. This model has to be efficient enough to simulate many contrasted pedo-climatic conditions in short times and flexible enough to easily include new processes such as novel regulation mechanisms.

The model could then be confronted to field observations of water transpiration proxy such as yield and help to define best combination of genotype and management (irrigation only, Chapter 11) for a given environment using contrasted root phenotypes in contrasted pedo-climatic conditions.

Chapter 10 | Chapter 11

2.2 Methodological developments

To achieve the three main objectives of the present Ph.D. thesis, methodological developments are required. Eight current state of the art limitations were spotted and described here-below. Their interrelations are explicited in the flowchart of Figure 2.3.

MD1: The accuracy of current numerical solutions of the water flow equations in roots is too low to make numerical simulations useful tools to compare plant root water uptake

Methods for physically solving the water flow in hydraulic architecture exist nowadays. However the resolution is segment-size dependent: the root segment length directly influences the model prediction, which questions the maximal root segment dimension and the accuracy of the models itself. Such numerical limitations can be overcome by decreasing root segment size but then the computational time explodes.

MD2: Clear, direct relations between local root phenes and plant-scale parameters do not currently exist

The plant-scale parameters of the Couvreur et al. (2012) model can be numerically calculated for any root system hydraulic architecture. However part of the information is hidden in the resolution method. An analytical solution of the macroscopic parameters directly based on the ensemble of root system phene states would allow a direct calculation of the sensitivity of the plant-scale parameters and therefore, of the plant behavior in terms of water uptake.

MD3: The link between diversity of local phene observations and diversity of macroscopic parameters observations is currently missing

When the mathematical link is made between local root phenes and macroscopic parameters, the range of variation of the latter can be compared with direct observations using the observed root phene diversity as parametric space. Do the orders of magnitude of model and observations match or is there a mismatch between the predictions of the

plant-scale parameters generated from local observations and the direct measurements? Modelling can help bridging the gap between these two worlds.

MD4: Hydraulic property distributions within root systems is scarce

While they are key for understanding root water uptake distribution and intensity, the local distributions of root radial and axial conductivities can not be measured routinely in laboratory experiments today. New tools and methods must be investigated in order to assess their potential capabilities to do so. Results generated by such new tools should also be confronted to old measurements to see how consistent different techniques can be. Deterministic changes within root systems and stochastic variations between roots will be investigated.

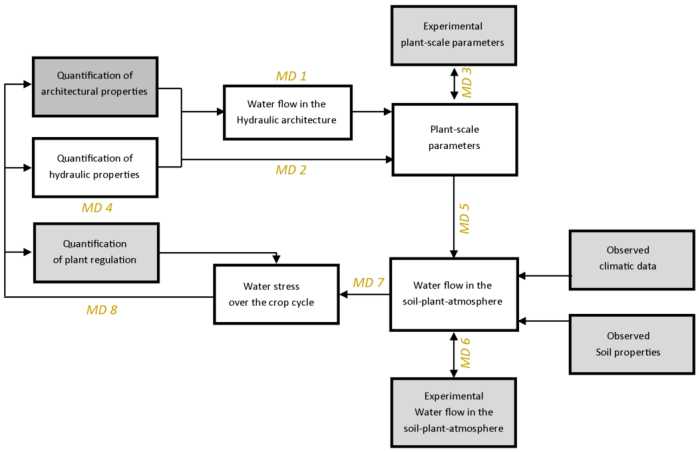


Figure 2.3: Flowchart of the methodological developments achieved in this Ph.D. Grey boxes represent inputs from literature, white boxes new developments contained in this thesis. MD = Methodological Development.

MD5: Current three-dimensional physically-based models of the water flow in the soil-plant-atmosphere continuum are too slow to be used at field scale over full crop cycles

Almost 20 years ago, Doussan et al. (1998a) suggested a method to solve the water flow in root systems. Eight years later, it was possible to solve the water flow in an unsaturated soil including a root system. But the implied numerical resolutions can be time-consuming. Then macroscopic models arose to speed-up the process and in parallel root growth model were developed to generate realistic root system architectures over the plant growth. While all the puzzle pieces exist, they still need to be glued together to model the water acquisition over the whole crop cycle in reasonable computational times.

MD6: The model of the water flow R-SWMS has not been validated yet with field observations

Methods to investigate water dynamics in soils and root system growth become more and more spread and accurate. This challenges the current ability to represent the dynamical behavior of the soil-plant system with the current state of the art of process understanding and models of the water flow in the soil-plant system such as R-SWMS.

MD7: Do different water uptake strategies emerge from combinations of individual root traits in contrasted drying scenarios?

When root or plant (such as stomatal properties) traits, mostly observed individually, are combined together to represent a plant phenotype, is it possible to catch crop diversity of behaviors when facing water stress? Does the plant efficiency depend on the drought conditions (i.e. the drying scenario) also in simulations as it was observed in field trials? In addition, it is worth investigating how these strategies arise from and how they can be defined.

MD8: Best quantitative root phenes specific to contrasted pedo-climatic conditions, defining ideal strategies and root systems ideotypes are currently not known

At any location in the world, specific pedo-climatic conditions apply, the question of plant sets of optimal phene states that would minimize water stress over the crop cycle is raised when considering the diversity

of plant performance in contrasted situations and the wide range of observed root system traits. In that sense, a plant is efficient when/if it can maintain its transpiration (i.e. supplying the requested water demanded) all over the crop cycle.

2.3 Research assumptions

To achieve the general objectives and respond to the research questions of this Ph.D. thesis, simplifying assumptions are needed. The most critical ones are enumerated in this section in a list that, of course, can not be considered as exhaustive.

On plant representation

First, it was assumed that a plant genotype could be perfectly represented by a regulated hydraulic architecture that changes and develops with time over the crop cycle. The functional and structural root system properties of a plant are then described by probability distributions. Parameters of the modeled processes (root growth and development) may be root type dependent, root age dependent or even genotype dependent but they do not change over time due to specific environmental conditions. The plants were not allowed to be plastic in their changing environment: they are genetically determined and their structural or functional properties do not change according to the surrounding medium.

In addition, since the focus is on the root system properties and its regulations, above-ground plant organ properties were generally simplified. As a consequence, when comparing plants in simulations, all plants are supposed to have similar canopies, at least in terms of total leaf surface, stomatal density and stomatal closure regulation. Stomatal aperture, carbon assimilation and transport in the plant architecture were oversimplified as compared to detailled approaches that currently exist. Again, these processes were assumed to be the same for all simulated plants. In the simulations, water stress impacts root growth and development in the sense that it decreases the total assimilated carbon and the consequent root system volume but observed behaviors such as an increase of carbon sent to roots in case of reduced transpiration was not modelled. Drought is also assumed not be fatal for the plant: the plants always survive water stress even for prolonged periods of time. Therefore, drought induces a signal, which slows down the carbon acquisition but never kills it nor impacts plant's strategy of carbon allocation.

On environmental description

The particular region of the soil known as rhizosphere was assumed to have hydraulic properties identical to the bulk soil while studies suggest that root mucilage exsudation affects the hydraulic behavior of the first millimiters of soil around the roots. While it has been shown that the specific properties of the soil surrounding the roots may have substantial effects on the plant water status and its transpiration, it was neglected everywhere in this manuscript. No preferential flow nor impact of the plant canopy on the rainfall dsitribution affected the water movement in all soil domains considered in this study.

The water stress was always considered alone in the present research. No other abiotic (i.e. nutrient stress for example) or biotic stresses (i.e. plant diseases) nor combination of stresses were considered in this study: it was here assumed either that they have no impacts on the plant performance and behavior or that they are simply absent. Furthermore, the environement was reduced to a combination of evaporative demand time series (that is in turn determined by atmospheric variables) and static soil hydraulic properties. Other aspects that are known as influencing plant growth and development, such as organic carbon distribution, soil density or structural properties were not directly taken into account in this study. They were only reflected somehow by the bulk soil hydraulic properties. These characteristics disserve deeper look in further studies.

On plant-environment interaction

While local root traits may reveal contrasting impacts on different plant functions (such as water and phosphorus uptake), this research focused on the role of the root system for water uptake, only. As a consequence, the plant that best perform in these simulations are not necessarly the ones that would optimize other root system functions. Looking at one particular aspect of the root system role could blind us from other fundatemental functions that could suffer from such changes.

Finally, as the water flow was modeled only and the interest *in fine* states in crop yield, ot was assumed that both aspects are strongly related. As suggested by many studies and authors for decades, it was considered here either that global cumulative transpiration or that cumulative transpiration at particularly critical stages are good predictive

proxies for crop yield. Therefore, simulating the plant water transpiration dynamics is enough to compare genotype performance in constrated pedo-climatic situations when focusing on the water stress. No much focus was put on the management side in this research except for the irrigation volume.

PART II

DECHIPHERING THE WATER FLOW IN ROOT SYSTEMS

In the second part of the manuscript, we develop the water flow equations that are necessary to decrypt the water dynamics in hydraulic architecture. In chapter 3, the basics of water flow in roots are recalled as well as the existing mathematical tools that currently exist. An improved version of the numerical resolution method of the water flow equations is then proposed using a hybrid numerical-analytical approach (Chapter 3). Finally purely analytical relationships between local root traits and macroscopic parameters are developed first at the branch scale (Chapter 4) and then at the root system scale (Chapter 4-5) to progress towards fully analytical root system macroscopic description.

In order to understand the universe, you must know the language in which it is written and that language is mathematics

Galileo Galilei

A HYBRID ANALYTICAL-NUMERICAL METHOD FOR SOLVING EQUATIONS OF WATER FLOW IN HYDRAULIC ARCHITECTURE

3

This chapter is a modified version of a manuscript accepted in Applied mathematical modelling

> Meunier F., Draye X., Vanderborght J., Javaux M. and Couvreur V. A hybrid analytical-numerical method for solving equations of water flow in hydraulic architectures. Applied Mathematical Modelling. In Press.

Abstract

We propose here a new method to calculate water flow and xylem water potential distribution in hydraulic architectures (such as root systems) of any complexity. It is based on the extension of the water flow equation analytical resolution of Landsberg and Fowkes for single roots. It consists in splitting the root systems in zones of homogeneous or homogeneously changing properties and deriving the xylem potential and water flow under any given boundary conditions (plant transpiration or collar potential, and potential at soil-root interfaces) without assuming a uniform xylem potential within each zone. The method combines analytical solutions of water flow within the segmented zones with the numerical solution of flow connectivity for the whole root system.

We demonstrate that the proposed solution is the asymptote of the exclusively numerical solution for infinitesimal root segment lengths

(and infinite segment number). As water uptake locations and magnitudes predicted by the latter solution for finite segmentation lengths deviate from the exact solution, and are computationally more intensive, we conclude that the new methodology should always be privileged for future applications. The new method resolution is as simple to implement as existing ones and was demonstrated more accurate and efficient. It should then systematically used when solving the water flow within root system hydraulic architectures.

The proposed solution can be easily coupled to soil modules (as already done with existing solutions) and further implemented in functional-structural plant models to predict water flow in the soil-plant atmosphere continuum with a better accuracy than current models. Finally the new solution may be used to calculate more accurately plant scale macroscopic parameters for crop models.

3.1 Introduction

Ensuring crop productivity under conditions of long term change of soil water availability and atmospheric demand for water requires a thorough understanding of crop bio-physical properties to acquire soil water (Javaux et al. 2013). Even though simple empirical models of crop transpiration benefit from consequent parameter libraries (Wesseling 1991), they may lose their predictive power under changing conditions, such as changing soil type or soil water content distribution (Hupet and Vanclooster 2005; Musters and Bouten 2000; Vandoorne et al. 2012). Bio-physical principles, such as water flow dynamics, integrated in crop water acquisition models might better address questions of water availability for future crop-climate combinations.

Root system water uptake and flow can be represented via a system of equations representing radial (between soil-root interfaces to xylem) and axial (within the xylem network) flow equations analogous to Ohm law (Passioura 1984). Axial law within xylem has been demonstrated to be similar to Poiseuille law (North and Nobel 1991). Radial water flow is known to be extremely complex due to the coexistence of several flow pathways but the ohm analogy has been shown to be relevant

(Fiscus 1977). Mass conservation allows one to link radial and axial flow equations, which can then be solved analytically for single roots with or without laterals (Landsberg and Fowkes 1978; Meunier et al. 2017). Analytical solutions for complete root system have also been developed (Biondini 2008; Roose and Fowler 2004) but they are based on several simplifying assumptions (as no pressure loss in the lateral roots, a simplified root architecture etc.).

In addition, numerical solutions have been developed to solve more complex root system hydraulic architecture (Alm et al. 1992). In 1998, Doussan et al. (1998a) proposed a model for solving water flow in a xylem network of a root system of any complexity as a function of the soil hydraulic status for any xylem collar boundary conditions (flux or potential). The root system architecture must first be split into small parts called segments of homogeneous hydraulic properties (i.e. radial and axial conductivity) and their connections (i.e., the root system architectural properties) are gathered in an incidence matrix. The model splits the water transfer from the soil-root interface in a radial pathway (driven by segment radial conductivity, mainly characterized by the Casparian strip) and an axial movement (driven by xylem vessels ability to transport the water, quantified by the segment axial conductivity). Assuming a constant potential in the xylem vessels of the segment, a set of linear equations can be solved to obtain the radial flow and the xylem potential in any position of the root system according to overall boundary conditions: plant collar water flux or potential, and water potential at soil-root interfaces (Doussan et al. 1998a). For further description of model assumptions and included processes, we refer to the original publication (Doussan et al. 1998a).

Methods for solving the water flow equations in hydraulic architectures have been used for many applications from inverse parametrization (Zarebanadkouki et al. 2016) to prediction (North and Nobel 1991) and process understanding (Schröder et al. 2009). The model was considered alone (Doussan et al. 1998a) or coupled to soil models (i.e., to simulate dynamic root water uptake and water transfer in three-dimensional soil-root continuum under changing atmospheric conditions, see for example (Javaux et al. 2008)).

However the assumption of a constant potential inside a root segment is not valid: the hydraulic potential cannot be uniform in a root

portion of finite length (the water movement would then be null within the segment). The resulting errors can be reduced by dividing the root system in smaller and smaller root segments but rapidly the computational time to solve the water flow inside the root system becomes limiting. As a consequence a compromise must be made between accuracy and efficiency.

All current models of root systems are flawed because of the segment constant potential assumption. One particular application of Doussan et al. model was to identify and calculate emergent plant scale hydraulic properties (or "macroscopic" hydraulic parameters) from root system architecture and local root hydraulic properties (Couvreur et al. 2012). Existing methods for calculating these macroscopic parameters have therefore the same limited accuracy as Doussan et al. model (Doussan et al. 1998a).

The objective of this study is to provide a new resolution of the water flow equations in a root system hydraulic architecture (RSHA) with better accuracy than existing methods. To do so, we implemented an analytical solution of the water flow at the root segment scale in a connection matrix representing the root system architecture. The central idea is thus to work at two different levels:

- at the plant root level, the root system (RS) architecture is divided into segments small enough to keep the features of the architecture, but potentially larger than in typical finite difference approaches;
- at the root segment level where an analytical solution is used to describe water flow. The new hybrid solution therefore does not require infinite refining of the root system to get closer to the exact water flow in the RSHA.

Both methodologies can be compared in terms of computer efficiency and accuracy. The hybrid (or combined) approach allows the calculation of the macroscopic parameters of RSHA more accurately and more quickly for using the Couvreur et al. model (Couvreur et al. 2012).

In this paper, we first detail the finite-difference method of Doussan et al. (Doussan et al. 1998a) hereafter referred alternatively to as the "Doussan model" or the "finite-difference approach", for solving the water flow in a RSHA (section 3.2.1) and the upscaled model of Couvreur

et al. (Couvreur et al. 2012), hereafter referred to as the "Couvreur model", for calculating the macroscopic parameters (section 3.2.1). We then develop the new resolution method of the water flow (section 3.2.2) using the analytical solution at the segment scale (Landsberg and Fowkes 1978) which has been extended by Meunier et al. (2017) (section 3.2.1) We refer to the new solution alternatively as the hybrid or the combined approach. Finally, we illustrate the benefits of using such a methodology as compared with existing methods in terms of accuracy and efficiency with five different tests mixing numerical simulations and experimental data (sections 3.3 to 3.4).

3.2 Theory

3.2.1 Existing approaches for modeling water flow

In this section, three existing models of water flow are presented, whose description is relevant before further developing the equations of the new model. The description is rather detailed in order to allow a final parallel comparison of the coefficients of each model and to clearly link their respective parameters. In this manuscript, we note the vectors and matrices as bold. We indicate the dimensions of the vectors and matrices between square brackets and units between regular parentheses.

Finite-difference solution of water flow in root systems

The finite-difference approach is part of van den Honert's lineage of physical models (van den Honert 1948) based on Ohm's analogy to describe water flow in plants of any complexity (Amenu and Kumar 2008; Javaux et al. 2008; Lhomme 1998; Nimah and Hanks 1973). However, for the first time, they proposed a matrix operation to solve water flow in three-dimensional HAs of any complexity.

Considering a root system made of root segments numbered from 1 to N, a vector $\mathbf{K_x}$ [N x 1] ($L^3P^{-1}T^{-1}$) contains root segments axial conductances, for axial water flow towards the upper root segment in xylem ($K_{x,1}$) being the axial conductance between the first root segment and plant collar, where a water flow, or water potential, boundary condition is imposed). A second vector $\mathbf{K_r}$ [N x 1] $\left(L^3P^{-1}T^{-1}\right)$ contains root segments radial conductances, for water flow between soil-root interface and root xylem. For each root segment, total water potential (P) (which is the sum of matric and gravitational potentials) is defined in root xylem and at soil-root interface and contained respectively in vectors $\mathbf{\Psi_x}$ [N x 1] and $\mathbf{\Psi_{sr}}$ [N x 1]. Note that both $\mathbf{K_x}$ and $\mathbf{K_r}$ depend on the segment size: they are not intrinsic properties of the root tissues (Javaux et al. 2008). Note also that conductance and water potential units differ from the standard usage in soil physics (where L^2T^{-1} and L are more commonly used): we use here water potential per volume rather than water head (water potential per weight) for consistency with plant physiology common units. Note also that our definition of the water potential includes the gravity, which allows the model to simulate

water flow in non-horizontal roots (and potentially in three-dimensional root systems).

An example of simple root system is represented in Fig. 3.1-A. It is made of a main root and three laterals and divided into 30 root segments numbered from 1 to N. The frame (Fig. 3.1-B) zooms in on a particular segment i characterized by radial $K_{r,i}$ and axial $K_{x,i}$ conductances, which we indicate by the subscript i.

By rearranging the system of mass conservation equations, Doussan et al. provided the following expression of xylem water potential under flux-type boundary condition (Doussan et al. 1998a):

$$\begin{bmatrix} \Psi_{collar} \\ \boldsymbol{\Psi_x} \end{bmatrix} = \boldsymbol{C^{-1}D} \tag{3.1}$$

where Ψ_{collar} (P) is the plant collar water potential, $\mathbf{D}$ [N + 1 x 1] contains T_{act} (L^3T^{-1}), the plant actual transpiration as imposed at plant collar, and $\mathbf{C^{-1}}$ [N + 1 x N + 1] is the inverse of $\mathbf{C}$ matrix of conductances. The detailed procedure to build $\mathbf{C}$ and $\mathbf{D}$ is described in Appendix A.

Under water potential-type boundary condition at plant collar, the expression for $\boldsymbol{\Psi_x}$ becomes:

$$\boldsymbol{\Psi_x = c^{-1}d} \tag{3.2}$$

Again the matrix $\mathbf{d}$ [N x 1] contains the top boundary conditions, the imposed collar potential Ψ_{collar} and $\mathbf{c^{-1}}$ is the inverse of $\mathbf{c}$, the reduced conductance matrix. Appendix A also details how to build $\mathbf{c}$ and $\mathbf{d}$.

Under both boundary condition types, equations of potential-driven water flow (Ohm's analogue) allow calculating RWU rates $\mathbf{J_r}$ (L^3T-1) [N x 1] at soil-root interfaces (positive from soil-root interfaces towards the xylem vessels):

$$\boldsymbol{J_r = \mathbf{diag}\,(K_r)\,(\Psi_{sr} - \Psi_x)} \tag{3.3}$$

In the next pages, Equations 3.1 to 3.3 will be referred to as "Doussan equations" and the method to solve the water flow problem as the "Doussan model" or the "finite-difference approach".

In Fig. 3.1-A-B, when the boundary conditions (in red) are known (i.e., soil-root interface potential and collar flow or potential), root system

variables (in blue) can be calculated using the Doussan model. The solution of the water flow equation in roots is instantaneous (as long as there is no hydraulic capacity considered, as it is here) but the solution can be applied for transient boundary conditions as long as small time steps that follow the boundary condition dynamics are used.

The Doussan model has the advantage to allow representing the complexity of RS architectures at a scale at which hydraulic parameters can be measured. Root system architecture information is contained in the **IM** matrix, which can either be built (i) using new or ancient techniques, destructive or not, to scan experimental RS (Flavel et al. 2012; Lobet and Draye 2013; Lobet et al. 2011; Stingaciu et al. 2013; Zarebanadkouki et al. 2016), or (ii) using softwares to generate virtual RS architectures (Pagès et al. 2004; Somma et al. 1998) based on information on root types, densities, branching and growth rates available in the literature, as carried out for maize, wheat and ryegrass and others (see for example (Couvreur et al. 2012, 2014b)). The emergence of a common format for storing root system architectures (i.e. RSML for root system markup language) opens new avenues for the plant and soil scientific community to share architectural information obtained from experiments to numerical models (Lobet et al. 2015a).

Information on root hydraulic properties is contained in vectors $\mathbf{K_x}$ and $\mathbf{K_r}$. They can either be (i) measured with direct techniques such as developed by Sanderson et al. (1988) and Frensch and Steudle (1989), (ii) estimated from flux measurements via inverse modeling (Zarebanadkouki et al. 2016) or (iii) taken from the literature, in which typical radial and axial root conductances are related to root age and type (Bramley et al. 2007a; Tazawa et al. 1997).

Macroscopic hydraulic architecture approach

Following Doussan model's basic assumptions, the Couvreur model provides a direct solution of water flow in root system HA of any complexity based on macroscopic parameters. This study uses the root system form of this model to stay consistent with the finite-difference approach.

The expression for RWU by individual root segments is the following:

$$\boldsymbol{J_r} = T_{act}\boldsymbol{SUF} + K_{comp}\left(\boldsymbol{\Psi_{sr}} - \Psi_{seq}\right) \odot \boldsymbol{SUF} \tag{3.4}$$

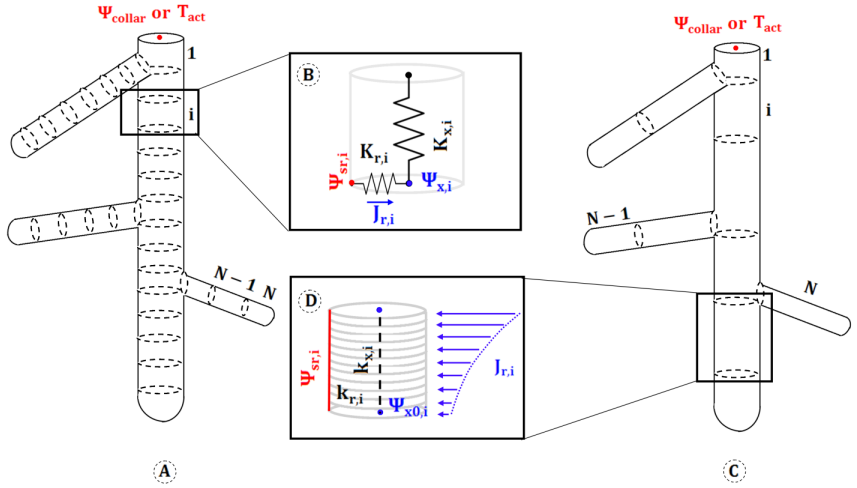


Figure 3.1: (A) Schematic of a simple root system made of 30 segments (N = 30) with (B) a zoom-in on a particular segment (numbered i). Each single segment is characterized by a radial conductance Kr and an axial conductance Kx. When the boundary conditions are provided (indicated here in red), water flow equations can be solved and lead to the xylem potential and radial flow distribution in the root system, solutions of the water flow equation. (C) Schematic of the same root system cut in 11 homogeneous (or homogeneously changing) zones (N=11) with (D) a zoom-in on a particular root zone numbered i and characterized by inherent radial conductivity and axial hydraulic conductance kr and kx. Again, the boundary conditions lead to the solution of the problem: the distal xylem potential and the proximal axial flow.

where **SUF** [N x 1] (-) is the vector of standard uptake fractions of root segments, K_{comp} ($L^3P^{-1}T^{-1}$) is the compensatory RWU conductance of the plant, $\odot$ indicates an Hadamard product and Ψ_{seq} (P) is the equivalent soil water potential sensed by the plant, which is a weighted-average of water potentials at soil-root interfaces:

$$\Psi_{seq} = \boldsymbol{SUF} \cdot \boldsymbol{\Psi_{sr}}$$

In Equation 3.4, the first term on the right-hand-side is interpreted as the "standard RWU", driven by plant actual transpiration, while the second term is interpreted as the "compensatory RWU", driven by

water potential heterogeneity at soil-root interfaces. As compared to the Doussan model, basic equations are the same (mass conservation and water potential-driven water flow equations), but an additional assumption is required for the compensatory RWU term: axial resistances need to be negligible as compared to radial resistances to water flow, which is not always fulfilled. The parameter K_{comp} only exists when the latter assumption is fulfilled, which makes it the only "non-exact" parameter of the simple macroscopic approach of root system HA. If this assumption is not valid, the Couvreur approach can also be used but with a more complex form for the second term of Eq. 3.4. Note that $\cdot$ designates a scalar product.

This approach also allowed to demonstrate the simple relationship linking Ψ_{seq}, Ψ_{collar} and T_{act}, which can be used to predict plant transpiration under water stress for isohydric plants:

$$T_{act} = K_{rs}\left(\Psi_{seq} - \Psi_{collar}\right) \tag{3.5}$$

where K_{rs} ($L^3P^{-1}T^{-1}$) is the equivalent conductance of the root system. In opposition to the compensatory RWU term of Eq. 3.4, this equation is an exact solution of Doussan set of equations.

The simplified macroscopic HA approach has the advantage to rely on few macroscopic parameters measurable and with physical meaning. Each of them contains information about both RS architecture and roots hydraulic conductances.

The numerical calculation of K_{rs} and **SUF** can be achieved by solving Equations 3.1 (or 3.2) and 3.3 under conditions of uniform water potential at soil-root interfaces:

$$\Psi_{sr} = \Psi_{seq}$$

which provides Ψ_{collar} and $\mathbf{J_r}$ for Equations 3.4 and 3.5:

$$K_{rs} = \frac{T_{act}}{\Psi_{seq} - \Psi_{collar}} \tag{3.6}$$

$$\boldsymbol{SUF} = \frac{\boldsymbol{J_r}}{T_{act}} \tag{3.7}$$

The calculation of K_{comp} requires solving Equations 3.1 (or 3.2) and 3.3 under conditions of heterogeneous water potential at soil-root interfaces. Then, K_{comp} can be estimated by linear regression using Eq. 3.4:

$$K_{comp} = \frac{(\boldsymbol{\Psi_{sr}} - \Psi_{seq}) \cdot (\boldsymbol{J_r} \oslash \boldsymbol{SUF} - T_{act})}{(\boldsymbol{\Psi_{sr}} - \Psi_{seq}) \cdot (\boldsymbol{\Psi_{sr}} - \Psi_{seq})} \tag{3.8}$$

Other parameterization methods exist. For instance K_{rs} can be calculated by using Thevenin theorem of equivalent conductances (Thévenin 1883). Experimental characterization of K_{comp} is also possible by using a water pressurisation technique and measuring outflow rate at plant collar (Hachez et al. 2012; Trillo and Fernández 2005). Eventually, given the low number of parameters (**SUF** then being approximated by a simple function of space), inverse modelling could be envisaged to estimate their values.

However, a parameterization is valid for a given root system architecture and distribution of root hydraulic properties. If any of these features evolve with time, a new parameterization would be required anytime they would change.

Analytical solution of water flow in a homogeneous root stretch

In the following, we define a root zone as a root segment or a combination of root segments without lateral branches in which root properties are uniform (but not the root xylem potential). The exact solution of the water flow equation in a root cylinder of length l_i (L) and radius r_i (L) (the subscript i indicates the root stretch) is given, according to Landsberg and Fowkes (1978) by:

$$\Psi_{x,i}(z) = \Psi_{sr,i} + c_{1,i} cosh\,(\tau_i z) + c_{2,i} sinh\,(\tau_i z) \tag{3.9}$$

where $\Psi_{x,i}$ (P) is the xylem potential along the root axis, z (L) is the position along this axis (comprised between 0 and l_i), $\Psi_{sr,i}$ (P) is the soil-root interface potential supposed to be uniform, $c_{1,i}$ (P) and $c_{2,i}$ (P) are coefficients that depend on the boundary conditions and τ_i (L^{-1}) is defined as:

$$\tau_i = \sqrt{\frac{2\pi r_i k_{r,i}}{k_{x,i}}}$$

with $k_{r,i}$ ($LP^{-1}T^{-1}$) and $k_{x,i}$ ($L^4P^{-1}T^{-1}$) the root radial conductivity and axial conductance, respectively. Both are inherent root tissue properties. The coefficients, $c_{1,i}$ and $c_{2,i}$, depend on boundary conditions applied on both sides of this root segment. Appendix B details their calculation under flux condition at the distal end, $J_{distal,i}$ (L^3T^{-1}) and collar condition at the proximal end of the root segment, $\Psi_{proximal,i}$ (P). They then can be used to obtain the distal potential $\Psi_{x0,i}$(P) and the proximal flow $J_{xl,i}$ (L^3T^{-1}) of the root cylinder of uniform hydraulic properties called stretch i (see Appendix B for details on their calculation). It yields:

$$\Psi_{x0,i} = \Psi_{sr,i} + \frac{\Psi_{proximal,i} - \Psi_{sr,i} + \frac{J_{distal,i}}{\kappa_i} sinh\left(\tau_i l_i\right)}{cosh\left(\tau_i l_i\right)} \tag{3.10}$$

$$J_{xl,i} = \left(-\Psi_{proximal,i} + \Psi_{sr,i} - \frac{J_{distal,i}}{\kappa_i} sinh\left(\tau_i l_i\right)\right) \kappa_i tanh\left(\tau_i l_i\right) + J_{distal,i} cosh\left(\tau_i l_i\right) \tag{3.11}$$

with $\kappa_i = \sqrt{2\pi r_i k_{r,i} k_{x,i}}$ ($L^3P^{-1}T^{-1}$)

Let us note that Eq. 3.9 can also be solved under a top flux $J_{proximal,i}$ boundary condition (imposed transpiration). Appendix C shows how it affects the coefficients $c_{1,i}$ and $c_{2,i}$. Other solutions when root hydraulic properties are not homogeneous also exist and can be used if desired (see next chapter).

3.2.2 Development of exact solutions

In this section, a new solution of water flow equations in RSHA is developed, where the simplifying assumption of constant water potential inside root segments (as in finite-difference approach) is released.

Hybrid water flow solution

As it can be directly seen from Equations 3.10 and 3.11, the solution of the water flow equation is linear in terms of distal flow and proximal

water potential so that for root system architecture, we can gather a set of N + 1 linear equations that can be numerically solved:

$$\begin{bmatrix} \Psi_{collar} \\ \boldsymbol{\Psi_{x0}} \end{bmatrix} = \boldsymbol{A^{-1}B} \tag{3.12}$$

where **A** [N+1 x N+1] and **B** [N+1 x 1] are constructed using Equations 3.10 and 3.11 and the incidence matrix **IM**, $\boldsymbol{\Psi_{x0}}$ [N x 1] is the vector of $\Psi_{x0,i}$. Appendix D explains in details how to build this matrix.

When imposing a potential boundary condition at the root system collar instead of a flux one, the water flow equation solution in the root system becomes:

$$\boldsymbol{\Psi_{x0}} = \boldsymbol{a^{-1}b} \tag{3.13}$$

where **a** [N x N] and **b** [N x 1] are fully described in Appendix D. **a** is **A** without its first line and row.

Figure 3.1-c illustrates the same root system as the one presented in Fig. 3.1-a. With the hybrid water flow solution formulation, the root system must be split either when root hydraulic property change (due for example to root tissue maturation) or at root branching sites. The total number of zones is here reduced to 11. Each single zone (as the one highlighted in the frame of Figure 3.1-d) is characterized by its intrinsic hydraulic properties: radial conductivity ($k_{r,i}$) and axial intrinsic conductance ($k_{x,i}$) and its geometrical characteristics: zone length and zone radius. We then need to determine 2 unknowns per root zone: the distal potential and the proximal flow (in blue in Fig. 3.1). A set of linear equations (Eq. 3.12 or 3.13) can be solved depending on the boundary conditions (in red in Fig. 3.1).

Hybrid macroscopic parameters calculation

As it was done in section 3.2.1., the exact water flow solution can be used to calculate the macroscopic parameters of the Couvreur model. Solving Eq. 3.12 or 3.13 under homogeneous soil conditions leads to K_{rs} and **SUF** while K_{comp} can be calculated when the water flows in the root system are known under heterogeneous soil conditions. We show in Appendix E that K_{rs} and **SUF** can be calculated analytically as well.

So K_{comp} remains the only non-exact macroscopic parameter of this approach.

3.2.3 Summary of all solutions and assumptions

Table 3.1 summarizes the four approaches detailed in sections 3.2.1 (Finite-difference approach), 3.2.1 (Macroscopic), 3.2.2 (Hybrid) and 3.2.2 (Hybrid macroscopic) and associated assumptions. It also describes the preparatory work required before generating a solution of the water flow equations in a RSHA. We call preparatory work all the tasks that need be done when either the root system architecture (e.g. growth, senescence) or the hydraulic properties (e.g. maturation, circadian cycle) change. The flow resolution includes the steps to calculate the water flow and xylem potential everywhere in the RS when the preparatory work has been already processed. The flow resolution steps need to be repeated whenever the boundary conditions change. Finally, in Table 3.1, the equations to solve the water flow equations in RSHA under either flux or potential top boundary conditions are provided as well.

Table 3.1 also includes the assumptions made by each resolution method. All models first assume that the potential at the soil-root interface is uniform for each single segment, i.e. the soil-root potential can differ between segments but must remain homogeneous for a particular root segment. The macroscopic approaches then include a non-exact parameter for describing the compensatory RWU. Finally the finite-difference (and therefore the macroscopic) method impose a constant potential within each single segment while this assumption is released in the hybrid model (and therefore the hybrid macroscopic).

Table 3.1: Summary of the assumptions made by each of the resolution method, the preparatory steps and the equations to be solved when applying a potential or a flux boundary condition at the root system collar

	Uniform $\Psi_{sr,i}$	Uniform $\Psi_{x,i}$	Simplified compensatory RWU	Preparatory calculation	Flow resolution (Potential collar BC)	Flow resolution (Flux collar BC)
Finite-difference	x	x		Build **C** and **D** or Build **c** and **d**	Eq. 3.1-3.3	Eq. 3.2-3.3
Macroscopic	x	x	x	Build **C** and **D** (or **c** and **d**) and Calc. K_{rs}, **SUF** and K_{comp}	Eq. 3.4-3.5	Eq. 3.4
Hybrid	x			Build **A** and **b** or Build **a** and **b**	Eq. 3.12	Eq. 3.13
Hybrid macroscopic	x		x	Build **A** and **B** (or **a** and **b**) and Calc. K_{rs}, **SUF** and K_{comp}	Eq. 3.4-3.5	Eq. 3.4

3.3 Material and Methods

In this section we describe the tests designed to assess the impact of using the finite-difference approach as compared to a hybrid method:

1. on the local water flow, the plant transpiration and the root macroscopic parameters in static conditions (section 3.3.1);

2. on dynamic variables of the root-soil continuum that are generated using a coupled model of the water flow in the root system and in the soil (section 3.3.2).

On total, five tests are presented illustrating the range of numerical errors that we deal with when using the Doussan model. All root systems used in this study are generated using RootTyp (Pagès et al. 2004) and maize root system parameters (Couvreur et al. 2012). For the dynamic

tests, we used R-SWMS as coupled soil-root system model (Javaux et al. 2008).

3.3.1 Discretization error in static conditions

Test 1: Impact of the radial to axial conductivity ratio

For the first test, we compute water flow in an 80-days old maize root system architecture for a prescribed water potential at plant collar ("potential boundary condition"). Segmentation lengths from 0.01 cm to 1 cm are tested. Results are compared in terms of (i) relative computational time and (ii) numerical accuracy of the calculated flow rate at plant collar resulting from the applied boundary condition. The former is the ratio of CPU times between the finite-difference and hybrid solutions (including the matrix building and parameter calculation steps). The numerical accuracy is the relative difference in percent between flow rates at plant collar calculated from both approaches, which is equivalent to the relative error on the total root system conductance. Note that here and in the following the hybrid method is always considered as the reference as infinite discretization imposed to the numerical method would lead to the same outputs.

In order to analyze the impact of the root radial to axial conductivity ratio $\frac{k_r}{k_x}$ (from 0.0001 cm^{-3} to 1 cm^{-3}), we used homogeneous hydraulic properties, i.e. constant with root age and order. More realistic hydraulic properties profiles are used in the next tests, whose root systems do not have unique $\frac{k_r}{k_x}$ ratios.

Test 2: CPU time and error variability in growing maize root systems

The second test assesses the variability of the model error resulting from the constant potential assumption in root systems with non-uniform hydraulic properties, and separates the components of the computational time of each approach. We used the software RootTyp (Pagès et al. 2004) to generate 100 maize phenotypes contrasted in terms of architectural and hydraulic properties. These properties were randomly selected from a parametric space delimiting the natural variability range of maize hydraulic and architectural properties reported in the literature (for more information, see (Meunier et al. 2016b)). We solved

water flow equations at daily stages of root system development over 60 days with average segment lengths of 0.5 cm. For each approach, we distinguished the mean time to prepare the calculations (building the conductance matrices, see Appendices A and D) and to solve the water flow problem (see section 3.2.3). The model error was quantified as the difference between root system conductances (K_{rs}) obtained from hybrid and finite-difference approaches. We were then able to compare the variability of the model error to the "natural variability" of K_{rs} within the species.

Test 3: Assessing errors applied to experimental data

In a third test, we assess how root system segmentation might affect interpretations of experimental observations of water uptake patterns. In practice, Zarebanadkouki et al. (2016) measured distributed root water uptake rates and total transpiration, then searched for root hydraulic properties profiles that best reproduce the experimental observations through root water uptake dynamics simulations (i.e. "inverse modelling"). Here we use a lupine root system architecture experimentally digitalized (Zarebanadkouki et al. 2016) and three different segmentation lengths for the Doussan model: 0.025, 0.25 and 2.5 cm. The homogeneous soil-root interface potential of -100 hPa measured experimentally (Zarebanadkouki et al. 2016) was applied as boundary condition for root segments. At the plant collar, a potential of -2500 hPa was measured by pressure probe (Zarebanadkouki et al. 2016) and set as top boundary condition. Eventually, we quantify, for the same optimal root hydraulic properties (Zarebanadkouki et al. 2016), how the simulated uptake pattern deviates from the original as a result of the finite difference model segmentation.

3.3.2 Propagation of errors in coupled models

Test 4: Root discretization impact on simulated water supply to the shoot

Using the same RS architecture as in the first test, we first ran simulations starring an 80 days-old maize root system whose total root length was 600m. We used two segment lengths to discretize the root

system: 0.1 cm and 1 cm. The root system was placed in a loamy soil at field capacity with no other water supply than soil water storage. The potential daily transpiration was fixed to 5.33 mm of water (with sinusoidal changes through day-night cycles, see (Couvreur et al. 2012)). We also defined a minimal collar potential (-15000 hPa) beyond which transpiration cannot meet the atmospheric demand. At the onset of water stress, the top boundary condition was switched from prescribed flux to constant water potential. Soil water flow was calculated with Richards equation (Richards 1931). Its coupling with root water dynamics is described in further details by Couvreur et al. (2012).

In a second series of simulations, we quantified the impact of maize root discretization on soil-root system water supply to the shoot over a two-month period. We used measured weather data from a French weather station located near Montpellier to calculate the daily potential transpiration. No feedback between plant water status and growth was accounted for (i.e. the actual growth rate is equivalent to the potential one).

Test 5: Impact of segmentation on variables of the soil-plant system

In the last test, we used the two root system phenotypes, generated in the second test, that were the most contrasted in terms of numerical error (minimal and maximal) to simulate the water flow in the soil-root-atmosphere continuum, hereafter referred to as phenotype min and max, respectively. We considered three root system ages: 20, 40 and 60 days and simulated water flow using the Couvreur et al. model with macroscopic parameters calculated either with the hybrid model or with the finite-differences approach in an initially homogeneous loamy soil. We used a sinusoidal transpiration function (maximal transpiration at midday, zero transpiration at midnight) with potential daily transpiration of 0.35 mm, 2.67 mm and 5.33 mm, respectively for the three ages. The minimal collar potential was anew fixed to -15000 hPa for all root systems and ages. Two initial soil conditions were considered: -300 hPa and -3000 hPa with an initial hydrodynamic equilibrium. We focused our analysis on key variables calculated by the root-soil model: the mean soil water content in the soil, the RS sink term, the cumulative transpiration and the collar potential.

3.4 Results

In this section, we highlight the benefits of using the hybrid solution presented above. With examples we show when and how significant errors may emerge from the finite-difference approach with low spatial resolution.

3.4.1 Discretization error in static conditions

Test 1: Impact of the radial to axial conductivity ratio

The flow rate at plant collar calculated with the finite-difference approach with the mature maize root system was off by up to 20% relative to the hybrid exact solution (see blue curves in Fig. 3.2). Yet, the relative error asymptotically tended to zero with finer root segmentations, the hybrid solution being equivalent to that of an infinitesimal root segmentation (and larger segment number). However, using fine root segmentations with the finite-difference method required higher computational times (24-fold for the 0.01 cm segmentation, see red curve in Fig. 3.2). The hybrid solution was faster than the finite-difference approach regardless of discretization, though computing times were fairly similar above 0.5 cm segmentation.

The position of lighter versus darker blue curves highlights that segmentation errors dramatically change with root hydraulic properties. For any given segmentation, the relative error varied by one order of magnitude from lowest to highest ratios of radial to axial conductivity (see blue curves in Fig. 3.2). Highest ratios yielded the largest errors. The assumption of constant water potential inside a root segment (inherent to the Doussan model) is indeed farther from being satisfied if axial pressure head losses are relatively important (low axial conductivity or high radial conductivity), particularly in longer root segments. As segmentation lengths of 1 cm are common in current models, typical simulations of root water uptake are likely subject to substantial errors.

Test 2: CPU time and error variability in growing maize root systems

Preparatory calculation times (i.e. building the conductance matrices) were two to four orders of magnitude larger than the time necessary

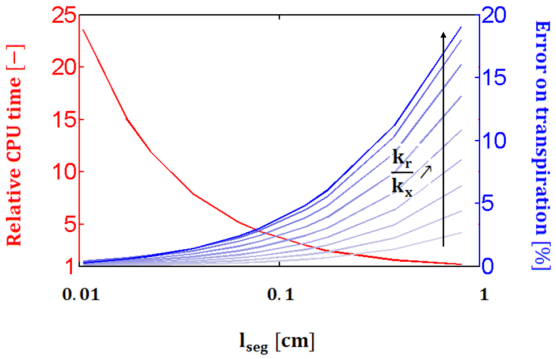


Figure 3.2: Finite-difference model relative error on plant transpiration calculation (blue curves) and relative CPU time (red curve) as a function of segmentation length. The figure presents results for different ratios of radial to axial conductivities (the darker, the higher the ratio).

to solve the flow solution (see Fig. 3.3, panel A versus B). This first step is required when the root system hydraulic architecture changes (e.g. root growth, development or senescence) but not when the boundary conditions alone evolve. Hence, there is a noteworthy tradeoff between the update of root system properties and the CPU time, particularly with the macroscopic models (see dotted and dashed-dotted curves in Fig. 3.3-B) whose second step is two orders of magnitude faster because they do not involve a matrix inversion (Couvreur et al. 2012). However, if preparatory calculations are needed, the fastest and most accurate method is always the hybrid approach (see solid lines in Fig. 3.3).

Figure 3.4 displays in blue the evolution of root system conductance (K_{rs}) over time in the 100 maize phenotypes covering the natural variability of hydraulic and architectural traits. The blue envelope encompasses more or less one standard deviation of the population K_{rs}. The mean finite difference model error (red solid line in Fig. 3.4, discretization of 0.5 cm) was 10% of K_{rs} on average, with 90% of errors comprised between 8 and 40% of K_{rs} (red envelope) after 60 days. This error is relatively high as compared to the estimated intraspecies variability (blue envelope). It must be noticed that the finite difference method always underestimates the root system outflow (such statement

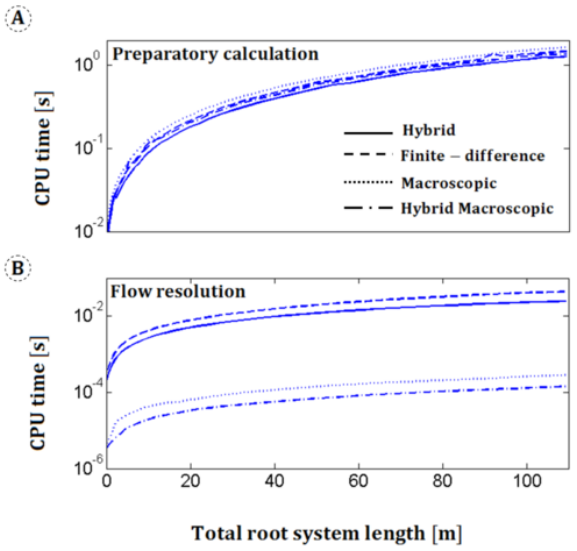


Figure 3.3: Comparison of the different methods in terms of computational time in growing root systems. The CPU time for preparatory calculations is shown in subplot A, while the flow solution CPU time is represented in subplot B.

can be demonstrated with simple considerations). Therefore as plotted here (hybrid approach minus finite-difference approach), the error is always positive.

As shown in Fig. 3.2, the relative model error depends on the local hydraulic properties of the root system which are phenotype key-traits. Consequently comparing contrasted phenotypes is automatically biased when using the finite difference method. This is also illustrated in Fig. 3.4 where the black curves represent the evolutions of K_{rs} of a representative phenotype using the hybrid (dashed) and finite difference (dotted) methods. Such differences do affect the results of virtual phenotype performance prospects under drought scenarios.

Test 3: Assessing errors applied to experimental data

In Fig. 3.5, we mapped deviations of root water uptake as com-

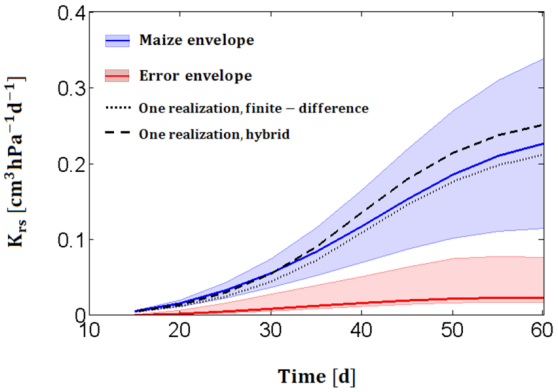


Figure 3.4: Simulated natural variability of maize root system conductance (blue solid line: average; blue envelope: standard deviation) in a population of 100 phenotypes growing for 60 days. The associated finite difference model (using 0.5 cm segments) mean error is shown in red (the envelope encompasses the 5% to 95% percentiles of errors). An example of phenotype root system conductances calculated with the hybrid (dashed black line) and finite-difference (dotted black line) approaches is included.

pared to the hybrid solution from coarse (2.5 cm) to fine (0.025 cm) segmentations. The root segment colors represent the relative error on the radial flux: blue means that the Doussan model underestimates the water uptake and red means that it overestimates it. When the Doussan and the hybrid models agree, segments appear gray. We also indicated the numerical error made on the plant total transpiration that reaches 33% of the global transpiration with coarse segments, 3.6% with intermediate segments and less than 0.1% with very fine segments. With segmentation lengths of the order of the centimeter, numerical errors would cause dramatic bias in the estimated root hydraulic properties, while the true hydraulic properties would be far from matching the observed uptake and transpiration rates as shown in the left panel.

While numerical errors tend to disappear in the right panel, the computation time explodes, which is a major issue in any inverse modelling scheme as tens of thousands simulations are typically necessary

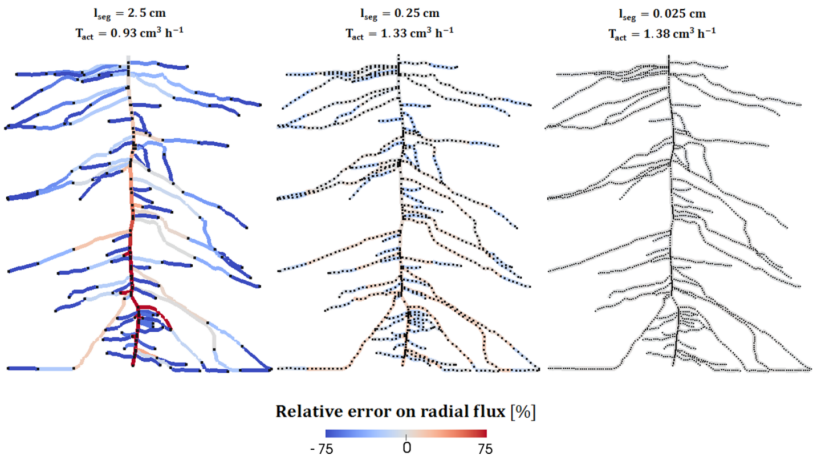


Figure 3.5: Segment size effect on local and total water uptake for three discretization levels (from coarse to fine, from left to right). The segment limits are indicated by black dots on the root laterals only.

before reaching the optimal parameter set. The hybrid method does not have such a limitation as it yields the exact solution with coarse segments.

3.4.2 Propagation of errors in coupled models

Test 4: Root discretization impact on simulated water supply to the shoot

In this test, the simulations of the water flow in the soil-root continuum are rigorously identical except for the root segment length. As shown in Fig. 3.6-A, the discretization size (red =1 cm, blue=0.1 cm) led to significant differences in the onset of water limitation. In case of finer segments, the stress appeared 3 days later (see red versus blue arrows). This is due to the discretization effect on root system conductance, which is underestimated by 20% with the coarse segmentation, thus limiting water supply to the shoot.

In the two-month scenario with growing root system, segmentation differences led to the actual (left axis, dashed blue lines) and cumulative

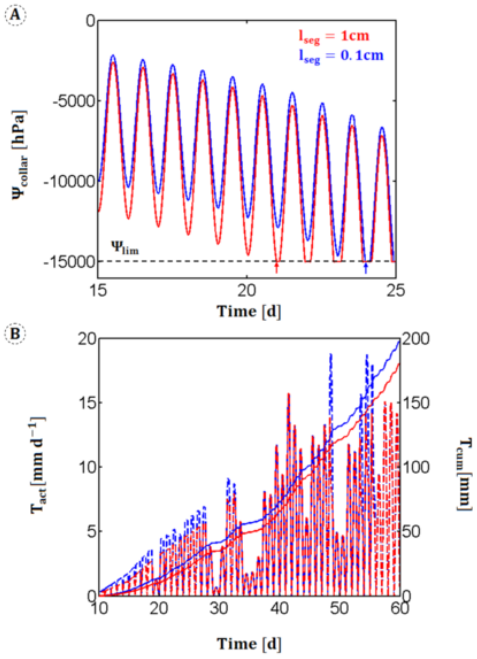


Figure 3.6: Simulated soil-plant water dynamics time series for 1 cm (red) and 0.1 cm (blue) segmentations. Panel A: Plant collar water potential. Red and blue arrows point at specific times of onset of water limitation. Panel B: Instantaneous (left axis) and cumulative (right axis) water supply from the soil-root system to the shoot.

(right axis, solid red lines) transpiration represented at Fig. 3.6-B. The difference of cumulative water supply after two months is about 15 mm of water. It was mainly constituted early stages of root system growth, when the xylem vessels are not developed yet (and the radial to axial conductivity ratio is high, hence generating large model errors, see Test 1).

Test 5: Impact of segmentation on variables of the soil-plant system

Finally, Table 3.2 summarizes minimal and maximal differences for several normalized state variables of a soil-plant hydraulic model (Javaux et al. 2008) run with macroscopic parameters calculated with

the hybrid and finite difference models. As it clearly appears, after normalization, errors are far from being negligible since they may represent up to 4% of the mean water content, 41% percent of the mean sink term, 2% of the total transpired water and 16% of the stress potential. As explained before, the hydraulic properties of the root systems dramatically affect the accuracy of the water flow resolution and hence the description of the water fluxes in the soil-plant-atmosphere continuum. There, even if not negligible most of the time, the errors on state variables of the phenotype min are always smaller (i.e. closer to zero) than those of the phenotype max. Note that the sink term is a local variable (soil voxel) while transpiration is a global one (root system) explaining possible mismatches between both.

In Fig. 3.7-A, the intrinsic property of the root segment τ_i multiplied by the segment length l_i is shown for the old root system of the phenotype max. Figure 3.7-B represents the relative errors of root water uptake in the same 60 days-old maize root system presented as a function of this product $\tau_i l_i$. The errors are calculated as the relative difference of root radial flow $J_r - J_{r,ex}$, (with the second term calculated with the hybrid solution and the first with the finite-difference approach, weighted by the mean exact radial flow $J_{r,ex}$). $\tau_i l_i$ is an indicator of the potential error of local water uptake, the error being located where the product $\tau_i l_i$ is high. When the root segment size is uniform within the root system (as it is here), the main errors are located at the lateral root tips, where the radial to axial conductivity ratio is the highest (and therefore τ_i is large). Let us note finally that the use of the finite-difference approach will always underestimate the root system total inflows under top potential boundary condition. Total root system conductances are thus always underestimated using the finite-difference approach.

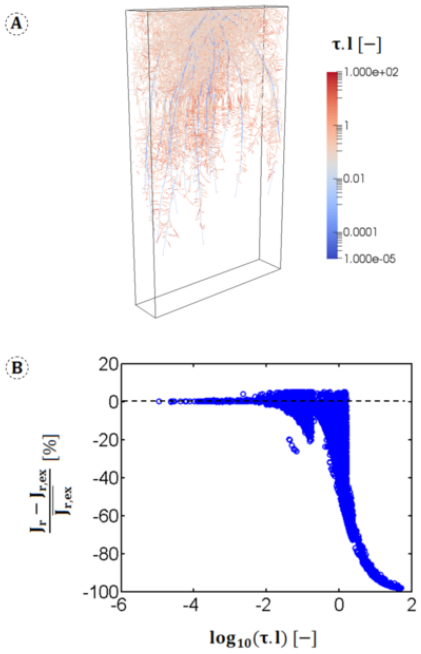


Figure 3.7: Distribution of the segment property τl as proxy of the water uptake error pattern in a virtual maize root hydraulic architecture (panel A). Relation between relative model error on the local water uptake rate and the segment property τl (panel B).

Table 3.2: Main relative differences between soil-plant model state variables. The simulations ran with macroscopic parameters calculated using the Doussan model or the hybrid model for two phenotypes generating maximum and minimum model errors at three different ages and under wet or dry condition. All numbers are in %.

			Young RS				Intermediate RS				Old RS			
			Phenotype max		Phenotype min		Phenotype max		Phenotype min		Phenotype max		Phenotype min	
			Dry	Wet	Dry	Wet	Dry	Wet	Dry	Wet	Dry	Wet	Dry	Wet
Relative Error on	Water content	Min	0.51	1.95	0.18	0.12	0.29	0.33	0.07	0.03	0.2	0.26	0.04	0.01
		Max	2.1	4.11	0.25	0.45	1.23	3.82	0.21	0.38	1.26	3.06	0.15	0.27
	Sink term	Min	13.46	24.94	1.87	1.57	22.44	25.52	2.48	2.36	21.15	25.97	1.86	1.86
		Max	25.03	40.95	3.43	2.41	53.76	27.34	9.37	5.37	36.29	29.07	9.67	2.23
	Total transpiration	Min	0	-0.02	0	0	-0.01	-0.01	-0.01	0	-0.01	0	0	0
		Max	1.64	0	0.38	0.01	2.26	0.01	0.75	0.01	2.05	0.02	0.35	0
	Collar potential	Min	-9.71	-16.59	-1.3	-1.61	-10.54	-13.36	-1.57	-1.61	-9.86	-10.33	-0.94	-0.6
		Max	1.46	4.81	0.31	0.33	1.36	0	0.1	-0.01	2	0.28	0.04	0

3.5 Conclusion

We developed and presented a hybrid solution of the water flow inside root system of any complexity under flux or potential boundary conditions. This method is based on the extension of Landsberg and Fowkes (1978) resolution of the water flow equation in a single root segment combined with a finite-difference approach of Doussan et al. (1998a). The hybrid approach improves the solution accuracy of transpiration fluxes as compared to traditional finite-difference model by up to 35%, with improved computational speed. In order to contain the finite-difference model error below 5%, the root system segmentation would have to be finer than 0.1 cm, which would imply 10 to 100-fold increases in CPU time as compared to the hybrid solution. The new methodology is the asymptotic solution of traditional resolution methods for infinitely small segments (and for infinite segment number), and can be implemented in any functional-structural root system model, as for instance SimRoot (Lynch et al. 1997).

The finite-difference method generates substantial errors on shoot water supply and water uptake location and intensity, which may result in erroneous estimations of root hydraulic properties from experimental observations of plant water uptake. The new hybrid approach prevents such numerical errors and is therefore safer to use. A new solution of plant scale parameters K_{rs} and **SUF** has also been provided, which opens the possibility to swiftly characterize virtual phenotypes hydraulic traits, and more accurately prospect on root ideotypes for water extraction in drought scenario analysis. As the new hybrid method is easy to implement in existing architectural models of the water flow, faster and more accurate than purely numerical approaches, it should be systematically promoted in the future when solving water flows in plant hydraulic architectures.

3.6 Appendices

Appendix A: Description of the IM, C, D, c and d matrices

We first introduce the incidence matrix as it was done in the work of Doussan et al. (1998a). This matrix **IM** [N + 1 x 2N], contains the information on connections between root segments and soil-root interfaces of the hydraulic architecture. In order to build the **C** matrix, only the upper half of the incidence matrix described by Doussan et al. (1998a) is necessary.

$$\boldsymbol{IM} = \begin{bmatrix} -1 & 1 & \cdots & \cdots & \cdots & 0 & 0 & 0 & \cdots & \cdots & \cdots & 0 \\ 1 & -1 & & & & \vdots & 1 & 0 & \cdots & \cdots & \cdots & 0 \\ 0 & 1 & & & & 0 & 0 & 1 & \ddots & & & \vdots \\ \vdots & \ddots & \ddots & & & -1 & \vdots & \ddots & \ddots & \ddots & & \vdots \\ \vdots & & \ddots & \ddots & & 0 & \vdots & & \ddots & \ddots & \ddots & \vdots \\ \vdots & & & \ddots & \ddots & \vdots & \vdots & & & \ddots & \ddots & 0 \\ 0 & \cdots & \cdots & \cdots & 0 & 1 & 0 & \cdots & \cdots & \cdots & 0 & 1 \end{bmatrix} \tag{A.1}$$

Each line of **IM** corresponds to a root segment. The first line is that of the collar, while the N next lines correspond to the ordered N segments. The N first columns of **IM** correspond to the ordered N segments, while the next N columns correspond to the ordered N soil-root interfaces. IM is almost full of zeros, with ones on the main diagonals of both square sub-matrices located below the first line (see Eq. A.1), which represent connections of segments with themselves and with soil-root interfaces. The first N columns contain each an additional "-1", which represent the connection of each segment with the previous segment in the architecture. IMi+1,j is "-1" if the i-th segment is the parent of the j-th segment in the architecture (each segment having only one parent). For instance, in the first column, the collar appears to be the parent of the first segment. In the second column, the first segment appears to be the parent of the second segment. Note that the third segment could have either the first or the second segment as parent. Since segments are ordered, the lower half of the first square sub-matrix can only contain

zeros (the third segment could, for instance, not be the parent of the first segment).

We then define the conductance matrix $\mathbf{C}$ [N+1 x N+1] ($L^3P^{-1}T^{-1}$) by:

$$\mathbf{C} = \mathbf{IM}.\mathbf{diag}\left(\begin{bmatrix} -\boldsymbol{K_r} \\ -\boldsymbol{K_x} \end{bmatrix}\right)\mathbf{IM}^t \tag{A.2}$$

where $\mathbf{diag}\left(\begin{bmatrix} -\mathbf{K_r} \\ -\mathbf{K_x} \end{bmatrix}\right)$ [2N x 2N] is a diagonal matrix containing the root segment axial and radial conductances $-\mathbf{K_r}$ on its diagonal and is 0 elsewhere. The vector $\mathbf{D}$ [N+1 x 1] (L^3T^{-1}) is defined as:

$$\mathbf{D} = \begin{bmatrix} T_{act} \\ \mathbf{diag}(-\boldsymbol{K_r}).\boldsymbol{\Psi_{sr}} \end{bmatrix} \tag{A.3}$$

where T_{act} (L^3T^{-1}) is the boundary condition for the root collar (flux condition), $\mathbf{diag}(-\mathbf{K_r})$ [N x N] ($L^3P^{-1}T^{-1}$) is a square matrix which contains on its diagonal and is zero elsewhere and $\mathbf{\Psi_{sr}}$ [N x 1] (P) contains the boundary conditions for the root segments.

In case of a top potential boundary condition, the root water flow equations are slightly modified. $\mathbf{c}$ [N x N] is $\mathbf{C}$ without its first line and column and $\mathbf{d}$ [N x 1] (L^3T^{-1}) is defined as:

$$\mathbf{d} = \left(\mathbf{diag}(-\boldsymbol{K_r}).\boldsymbol{\Psi_{sr}} - \begin{bmatrix} K_{x,1}.\Psi_{collar} \\ 0 \\ \vdots \\ 0 \end{bmatrix}\right) \tag{A.4}$$

with Ψ_{collar} (P) the potential boundary condition for the root collar.

Appendix B: Exact solution in a root zone

The solution of the water flow equation in a root branch as derived by Landsberg and Fowkes (1978) for generic boundary conditions is:

$$\Psi_{x,i}(z) = \Psi_{sr,i} + c_{1,i}.cosh\left(\tau_i z\right) + c_{2,i}.sinh\left(\tau_i z\right) \tag{B.1}$$

The axial water flow is powered by the potential gradient inside the xylem vessels and is consequently given by:

$$J_{x,i}(z) = -k_{x,i}\frac{d\Psi_{x,i}(z)}{dz} = -\kappa_i\left(c_{1,i}.sinh\left(\tau_i z\right) + c_{2,i}.cosh\left(\tau_i z\right)\right) \tag{B.2}$$

where $\kappa_{\mathrm{i}}\,[\mathrm{L}^3\mathrm{P}^{-1}\mathrm{T}^{-1}]$ is defined as:

$$\kappa_i = \sqrt{2\pi r_i k_{r,i} k_{x,i}} \tag{B.3}$$

We apply a potential $\Psi_{\mathrm{proximal,i}}\,[\mathrm{P}]$ and a flux $\mathrm{J_{distal,i}}\,[\mathrm{L}^3\mathrm{T}^{-1}]$ conditions respectively at the top (proximal end) and bottom (end) borders of this root cylinder, mathematically:

$$\begin{cases} \Psi_{x,i}(z = l_i) = \Psi_{proximal,i} \\ J_{x,i}(z = 0) = J_{distal,i} \end{cases} \tag{B.4}$$

Equations B.1 and B.2 yield:

$$\begin{cases} \Psi_{proximal,i} = \Psi_{sr,i} + c_{1,i}.cosh\left(\tau_i l_i\right) + c_{2,i}.sinh\left(\tau_i l_i\right) \\ J_{distal,i} = -\kappa_i c_{2,i} \end{cases} \tag{B.5}$$

Solving Eq. B.5 for both coefficients writes:

$$\begin{cases} c_{1,i} = \dfrac{\Psi_{proximal,i} - \Psi_{sr,i} + \frac{J_{distal,i}}{\kappa_i}.sinh(\tau_i l_i)}{cosh(\tau_i l_i)} \\ c_{2,i} = -\dfrac{J_{distal,i}}{\kappa_i} \end{cases} \tag{B.6}$$

The coefficients can be inserted in Equations B.1 and B.2 to obtain the distal potential and the proximal flow of the root branch:

$$\begin{array}{l} \Psi_{x0,i} = \Psi_{x,i}(z = 0) = \Psi_{sr,i} + \frac{\Psi_{proximal,i} - \Psi_{sr,i} + \frac{J_{distal,i}}{\kappa_i}.sinh(\tau_i l_i)}{cosh(\tau_i l_i)} \\ J_{xl,i} = J_{x,i}(z = l_i) = \left(\Psi_{proximal,i} - \Psi_{sr,i} + \frac{J_{distal,i}}{\kappa_i}.sinh\left(\tau_i l_i\right)\right)\kappa_i tanh(\tau_i l_i) + J_{distal,i} cosh(\tau_i l_i) \end{array} \tag{B.7}$$

Appendix C: Exact solution in a root zone for top-flux boundary condition

We apply a flux $J_{proximal,i}$ $[L^3T^{-1}]$ at the top (proximal end) of a root branch as well as a flux $J_{distal,i}$ $[L^3T^{-1}]$ at its bottom (distal end), mathematically:

$$\begin{cases} J_{x,i}(z = l_i) = J_{proximal,i} \\ J_{x,i}(z = 0) = J_{distal,i} \end{cases} \tag{C.1}$$

Combining the boundary conditions C.1 with Eq. B.2, it yields:

$$\begin{cases} J_{proximal,i} = -\kappa_i \left(c_{1,i}.sinh\left(\tau_i l_i\right) + c_{2,i}.cosh\left(\tau_i l_i\right)\right) \\ J_{distal,i} = -\kappa_i c_{2,i} \end{cases} \tag{C.2}$$

Solving C.2 writes:

$$\begin{cases} c_{1,i} = \frac{-J_{proximal,i} + J_{distal,icosh(\tau_i l_i)}}{\kappa_i sinh(\tau_i l_i)} \\ c_{2,i} = -\frac{J_{distal,i}}{\kappa_i} \end{cases} \tag{C.3}$$

Appendix D: Description of the A, B, a and b matrices

Top flux boundary condition

To construct matrix **A** [N + 1 x N + 1], we use the subscripts j that vary between 1 and N. **A** is a sparse matrix which is zero everywhere, except at the following locations (if j is connected to i):

$$
\begin{aligned}
A(i+1,i+1) &= A(i+1,i+1) - \frac{\kappa_j}{sinh(\tau_j l_j)} - \kappa_j tanh\left(\frac{\tau_j l_j}{2}\right) \\
A(j+1,i+1) &= A(j+1,i+1) + \frac{\kappa_j}{sinh(\tau_j l_j)} \\
A(i+1,j+1) &= A(i+1,j+1) - \kappa_j tanh\left(\frac{\tau_j l_j}{2}\right) + \frac{\kappa_j}{tanh(\tau_j l_j)} \\
A(j+1,j+1) &= A(j+1,j+1) - \frac{\kappa_j}{tanh(\tau_j l_j)}
\end{aligned}
$$

For **B** [N + 1 x 1], we must distinguish segments connected to the root system collar from those that are not (if j is connected to i, and for the last condition, if i is connected to the collar).

$$
\begin{aligned}
B(i+1,1) &= B(i+1,1) - \Psi_{sr,j}\kappa_j tanh\left(\frac{\tau_j l_j}{2}\right) \\
B(j+1,1) &= B(j+1,1) - \Psi_{sr,j}\kappa_j tanh\left(\frac{\tau_j l_j}{2}\right) \\
B(i,1) &= B(i,1) + J_{collar}
\end{aligned}
$$

Top potential boundary condition

a [N x N] is **A** without its first line and column. For **b** [N x 1], we must distinguish segments connected to the root system collar (i in the following lines) from those that are not. Again i and j indices can vary between 1 and N (if j is connected to i, and for the last condition, if i is connected to the collar).

$$
\begin{aligned}
b(i,1) &= b(i,1) - \Psi_{sr,j}\kappa_j tanh\left(\frac{\tau_j l_j}{2}\right) \\
b(j,1) &= b(j,1) - \Psi_{sr,j}\kappa_j tanh\left(\frac{\tau_j l_j}{2}\right) \\
b(i,1) &= b(i,1) - \Psi_{collar}\frac{\kappa_i}{sinh(\tau_i l_i)}
\end{aligned}
$$

Appendix E: Exact solution of macroscopic parameters

The exact solution of the water flow equation can also be used to calculate the macroscopic parameters of the Couvreur model instead of using the Doussan equations. We calculate the root system flow and xylem water potential under homogeneous soil-root interfaces conditions:

$$\mathbf{\Psi_{sr}} = \Psi_{\text{seq}}$$

with Ψ_{seq} (P) a constant. Under this condition, the distal flow can be related to the upstream conductance $K_{\text{rs,i+1}}$ ($L^3P^{-1}T^{-1}$) by:

$$J_{distal,i} = K_{rs,i+1}\left(\Psi_{sr,i} - \Psi_{x0,i}\right) \tag{E.1}$$

The axial flow at the top of this segment is given by equation B.2 evaluated in $z = l_i$. It yields

$$J_{xl,i} = -\kappa_i\left(c_{1,i}.sinh\left(\tau_i l_i\right) + c_{2,i}.cosh\left(\tau_i l_i\right)\right) \tag{E.2}$$

The difference of potential between the soil-root interface and the proximal end of this segment is calculated using Eq. B.1. It writes:

$$\Psi_{seq} - \Psi_{xl,i} = -\left(c_{1,i}.cosh\left(\tau_i l_i\right) + c_{2,i}.sinh\left(\tau_i l_i\right)\right) \tag{E.3}$$

The conductance of the root system including the upstream conductance and the present segment i, $K_{\text{rs,i}}$ ($L^3P^{-1}T^{-1}$) is given, in homogeneous conditions, by the total axial flow divided by the potential difference between the soil-root interface and the proximal end. Dividing Eq. E.2 by Eq. E.3, we obtain:

$$K_{rs,i} = \frac{J_{xl,i}}{\Psi_{xl,i} - \Psi_{xl,i}} = \kappa_i \frac{c_{1,i}.sinh\left(\tau_i l_i\right) + c_{2,i}.cosh(\tau_i l_i)}{c_{1,i}.cosh\left(\tau_i l_i\right) + c_{2,i}.sinh\left(\tau_i l_i\right)} \tag{E.4}$$

Combining Eq. B.1 evaluated in $z = 0$ and Eq. E.1, the distal flow yields:

$$J_{distal,i} = -K_{rs,i+1}.c_{1,i} \tag{E.5}$$

Equation B.5 allows one calculating the second coefficient:

$$c_{2,i} = \frac{K_{rs,i+1}}{\kappa_i} c_{1,i} \tag{E.6}$$

Combining Eq. E.4 and E.6, it yields:

$$K_{rs,i} = \kappa_i \left(\frac{\kappa_i.sinh\left(\tau_i l_i\right) + K_{rs,i+1}.cosh\left(\tau_i l_i\right)}{\kappa_i.cosh\left(\tau_i l_i\right) + K_{rs,i+1}.sinh\left(\tau_i l_i\right)} \right) \tag{E.7}$$

When no initial conductance is attached to the distal end of the system, Eq. E.7 simply becomes:

$$K_{rs,i} = \kappa_i.tanh(\tau_i l_i) \tag{E.8}$$

which is the formula derived by Landsberg and Fowkes (1978).

It appears that the root system conductance can be calculated recursively from the root tip towards the root collar. The first conductance is the total root system conductance. When calculated for all cumulative root zones from the root tips to the root collar, the root conductances can then be used to obtain the xylem potential, starting from the root collar to the root tips combining Eq. B.1, B.6 and E.5:

$$\Psi_{x,i}(z) = \Psi_{seq} + \left(\Psi_{proximal,i} - \Psi_{seq}\right) \frac{\kappa_i cosh(\tau_i z) + K_{rs,i+1}.sinh(\tau_i l_i)}{\kappa_i.cosh(\tau_i l_i) + K_{rs,i+1}.sinh(\tau_i l_i)} \tag{E.9}$$

$\Psi_{\text{proximal,i}}$ is derived from the previous calculations: it is calculated evaluating Eq. B.1 in z = 0. Equation E.9 is used to calculate the next proximal potential by taking anew z = 0:

$$\Psi_{x,i}(z) = \Psi_{seq} + \left(\Psi_{proximal,i} - \Psi_{seq}\right) \frac{\kappa_i}{\kappa_i.cosh(\tau_i l_i) + K_{rs,i+1} sinh(\tau_i l_i)} \tag{E.10}$$

Finally the radial flow is given by the integral of the radial flux per unit of length:

$$J_{r,i} = \int_0^{l_i} -2\pi r_i k_{r,i} \left(\Psi_{seq} - \Psi_{x,i}(z)\right) dz \tag{E.11}$$

Combining Eq. E.9 and E.11, we obtain:

$$J_{r,i} = 2.\kappa_i.tanh\left(\frac{\tau_i l_i}{2}\right)\left(\Psi_{sr,i} - \frac{\Psi_{x0,i} + \Psi_{xl,i}}{2}\right) \tag{E.12}$$

The radial flows as calculated by Equation E.12 can be used to calculate the Standard Uptake Fraction of each segment by dividing them all by the plant transpiration:

$$\boldsymbol{SUF} = \frac{\boldsymbol{J_r}}{J_{xl,1}} \tag{E.13}$$

TOWARDS QUANTITATIVE ROOT HYDRAULIC PHENOTYPING

4

This chapter is a combined version of two manuscripts published as:

> • Meunier F., Couvreur V., Draye X., Vanderborght J. and Javaux M. Towards quantitative root hydraulic phenotyping: Novel mathematical functions to calculate plant-scale hydraulic parameters from root system functional and structural traits. Journal of Mathematical Biology, 2017, 1-38
> • Meunier F., Couvreur V., Draye X., Vanderborght J. and Javaux M. Water movement through plant roots: Exact solutions of the water flow equation in roots with varying hydraulic properties. Hydrology and Earth Systems Sciences Discussions, 2017, 1-35 (Accepted subject to major revisions)

Abstract

Predicting root water uptake and plant transpiration is crucial for managing plant irrigation and developing drought-tolerant root system ideotypes (i.e. ideal root systems). Today, three-dimensional structural functional models exist, which allows solving the water flow equation in the soil and in the root systems under transient conditions and in heterogeneous soils. Yet, these models rely on the full representation of the three-dimensional distribution of the root hydraulic properties, which is not always easy to access. Recently, new models able to represent this complex system without the full knowledge of the plant 3D hydraulic architecture (HA) and with a limited number of parameters have been developed. However, the estimation of the macroscopic parameters a priori still requires a numerical model and the knowledge of the full three-dimensional hydraulic architecture.

The objective of this study is to provide analytical mathematical models to estimate the values of these parameters as a function of local plant general features, like the distance between laterals, the number of primaries (= main axes) or the ratio of radial to axial root conductances. Such functions would allow one to characterize the behaviour of a root system (as characterized by its macroscopic parameters) directly from averaged plant root traits, thereby opening new possibilities for developing quantitative ideotypes, by linking plant scale parameters to mean functional or structural properties. With its simple form, the proposed model offers the chance to perform sensitivity and optimization analyses as presented in this study. The originality of the new solutions is that they are purely analytical. In that sense, they are not tainted by numerical errors, they make the relationships between local root phene and macroscopic parameters straightforward and finally they dispense with the explicit root architecture.

4.1 Introduction

Global crop production is negatively affected by drought that is the most significant stress in agriculture (Cattivelli et al. 2008). Drought stress can be defined as the plant's inability to take up and transport the required amount of water to the shoot leading to stomatal closure and reduced yield (Campos et al. 2004). Transferring water from the soil to the shoot, thus preventing leaves from dehydration, is a major role of the vascular root systems (McElrone et al. 2013). Root water uptake (RWU) is driven by water potential gradients between soil and atmosphere and is mainly controlled by stomatal regulation, plant hydraulic resistance and soil water availability (Volpe et al. 2013). Both root system architecture and hydraulics are key for the location and intensity of water uptake (Leitner et al. 2014). These properties are encapsulated in the concept of root system hydraulic architecture (Lobet et al. 2014). Under high transpiration demand, from the root-soil interface to the evaporative sites, water crosses first radially the root tissues towards the root xylem vessels and flows then up to the leaves (Passioura 1980). The tissues' ability to transfer the water radially is called hydraulic radial conductivity while the capacity to conduct water

axially is the axial conductance or xylem conductance.

Measurements of root hydraulic properties demonstrated that radial conductivity and axial conductance both change with root tissue maturation for a given plant genotype (Doussan et al. 1998a; Frensch and Steudle 1989; Zwieniecki et al. 2002). The root anatomy and disposition of cell layers on water pathways impact root radial conductivity (Steudle 2000b). The development of endodermal and exodermal apoplastic barriers, first with a Casparian band, then with suberin lamellae and lignified tertiary walls constitutes major hydraulic impedances to water flow (Enstone et al. 2002). Aquaporins also play a central role in root radial conductivity by facilitating water flow across cell membranes (Chaumont and Tyerman 2014) and their location and expression change with the maturation of apoplastic barriers (Hachez et al. 2006). Besides, root axial conductance increases with abundance, shape and size of xylem vessels, increasing from apical regions with protoxylem to basal regions with late metaxylem vessels (McCully and Canny 1988). These maturation steps make younger (distal) root regions more functional for water uptake, while mature (proximal) regions are more adapted to water axial transfer, as confirmed by water flow measurements of Sanderson (1983) in barley or Zarebanadkouki et al. (2016) in lupine. Uniform root hydraulic properties would on the contrary concentrate water uptake on the proximal region (Landsberg and Fowkes 1978). Figure 4.1 (top) summarizes estimates and measurements of root radial conductivity and axial conductance of primary maize roots as a function of distance to root tip (Bramley et al. 2007b; Doussan et al. 1998a; Frensch and Steudle 1989; Frensch et al. 1996; Zwieniecki et al. 2002). Figure 4.1 (bottom panels) also illustrates the changes of primary root anatomy with distances to tip as observed by Steudle and Peterson (1998) with cross sections. With an inverse modelling approach coupled to tracer data from Varney and Canny (1993), Doussan et al. (1998a) produced an extensive estimation of root hydraulic property profiles with piecewise functions for both maize primary and lateral roots. The hydraulic conductivity profiles of Zwieniecki et al. (2002) comes as well from an inverse modelling exercise (Meunier et al. 2017).

Despite these evidences that uniform root properties are more the exception than the rule, today a majority of models assume explicitly (Biondini 2008; Roose and Schnepf 2008) or implicitly (Zhuang et al.

2001) that roots have homogenous properties. For instance, most crop and hydrological models assume that root water uptake is proportional to root length density, implicitly assuming uniform root radial properties and non-limiting xylem conductances while numerical models already showed that the arrangement of root hydraulic properties dramatically affects dynamics and efficiency of water uptake (Bechmann et al. 2014). It is important to realise that assuming uniform root properties will not only impact the root water uptake and water potential distributions, but also the total root conductance, when up-scaled to the full plant (Couvreur et al. 2012). Today, there is no easy way to predict how root property distribution impacts these plant scale properties.

An analytical solution for root water uptake and flow was developed by Landsberg and Fowkes (1978) but only for uniform roots. One noteworthy exception is the work of Ariyaratna (1990), which consider linear increase of the radial conductivity. Besides this study, no general analytical solution of the root water flow equation was found until now.

On the other hand, solving the water flow equation in the root system can also be achieved using finite difference for any root hydraulic property distribution (Alm et al. 1992) and for any root system architecture (Doussan et al. 1998a). Typically the water flow equation in the root system is solved by segmenting root system into small root parts called root segments. Water potentials within the structure are discrete so that each segment has (i) a unique xylem water potential connected to contiguous segment xylem potentials by axial conductances, and (ii) a soil-root interface water potential connected to the segment xylem potential by a radial conductance. Analogically to Ohm's law, radial and axial rates of water flow in each segment are proportional to the associated water potential differences. The water flow equations are solved for the generated root system hydraulic architecture by inverting a conductance matrix of the root system network (Doussan et al. 1998a; Javaux et al. 2008). If root segments were divided into smaller sub-segments though, water potentials and flows would slightly vary in each segment. The result is consequently an approximation of the exact solution that would be obtained for root segments of infinitesimal length. Developing analytical solutions would allow the community to verify numerical models' accuracy for heterogeneous roots.

In this paper we show that the assumption of uniform root property

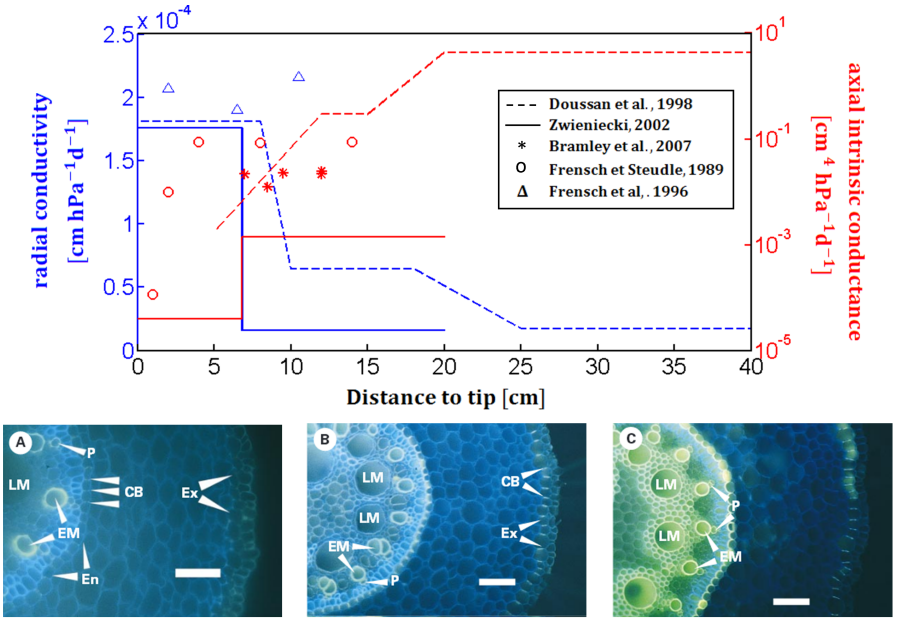


Figure 4.1: Top: Maize radial conductivity (left axis) and axial conductance (right axis) of primary roots as measured in several studies. Bottom: maize primary root cross-sections obtained at different development stages. The root cross-sections are the work of Steudle and Peterson (1998). The scale bars are 100 microns long. Ex = exodermis, En = endodermis, CB = casparian band, P = protoxylem, EM = early metaxylem, LM = late metaxylem. (a) Immature Ex, En with CB, mature P, mature EM and immature LM, (b) mature Ex, En with asymmetrically thickened walls, mature P and EM, immature LM (c) similar to (b) with mature LM. Reproduced by courtesy of Steudle and Peterson.

may be relaxed and yet analytical solutions of the water flow equation in roots are within our reach. Our objective is to present novel mathematical solutions of the water flow equation in roots with non-uniform radial and axial hydraulic properties closer to reality and more efficient than current existing models. We also developed solutions for growing roots at given elongation rates, which make the uptake distribution time-dependent. This widens the solution of Landsberg and Fowkes (1978) to roots growing at rates potentially decoupled from tissue maturation rate.

4.2 Theory

4.2.1 Water flow equation in a single root

In the following, we only consider single root, i.e. without laterals. Consequently we sometimes use simply the word roots for single roots. When used, the terms root stretch or root segment designate a portion of a single root characterized by specific root properties.

Assuming that root water content does not fluctuate, water mass balance in infinitesimal root segments of a cylindrical root of radius r [L] and total length l [L] under uniform soil-root interface water potential yields (Landsberg and Fowkes 1978):

$$\frac{dJ_x(z)}{dz} = -2\pi r k_r(z)\left(\Psi_x(z) - \Psi_{soil}\right) \tag{4.1}$$

where J_x [L^3T^{-1}] is the axial flow of water within the xylem in the root, k_r [$LT^{-1}P^{-1}$] is the root radial conductivity, Ψ_x [P] is the xylem water potential, Ψ_{soil} [P] is the uniform water potential at soil-root interface, and z [L] is the distance from the root tip along the root axis. We use the abbreviations P, T and P for length, time and pressure unit dimensions, respectively. The axis z is always chosen parallel to the root axis. Note that the right-hand side term corresponds to root radial flow rate per unit root length q_r [L^2T^{-1}]:

$$q_r = -2\pi r k_r(z)\left(\Psi_x(z) - \Psi_{soil}\right) \tag{4.2}$$

Axial flow is driven by the water potential gradient in the xylem vessels:

$$J_x(z) = -k_x(z)\frac{d\Psi_x(z)}{dz} \tag{4.3}$$

with k_x [$L^4T^{-1}P^{-1}$] the axial conductance of the root. Combining Eq. 4.1 and 4.3, we obtain:

$$\frac{d}{dz}\left(k_x(z)\frac{d\Psi_x(z)}{dz}\right) = 2\pi r k_r(z)\left(\Psi_x(z) - \Psi_{soil}\right) \tag{4.4}$$

which is the general equation of water flow equation in roots.

4.2.2 General solutions of root water flow

The differential Eq. 4.4 can be solved for various distributions of root properties and boundary conditions. Since Eq. 4.4 is a second-order differential equation, its general solution is of the form:

$$\Psi_x(z) = \Psi_{soil} + c_{1,i} f_{1,i}(z) + c_{2,i} f_{2,i}(z) \tag{4.5}$$

Where $c_{1,i}$ and $c_{2,i}$ are constants whose values depend on root hydraulic properties and boundary conditions at root's ends and $f_{1,i}$ and $f_{2,i}$ are differentiable functions of z whose type depends on the root hydraulic property profiles. The subscript i as it will be further explained is used to distinguish root stretches. It can vary between 1 and N, the total number of stretches in the single root. The length between the root apex and a root stretch proximal part is called l_i. When i = N, l_i = l.

For simple functions $k_x(z)$ and $k_r(z)$ (i.e. constant, linear and exponential), analytical expressions for $f_1(z)$ and $f_2(z)$, $c_{1,i}$ and $c_{2,i}$ are derived in Appendix A. However, $k_x(z)$ and $k_r(z)$ profiles along a root generally correspond to piecewise collections of these simple functions (see for example (Doussan et al. 1998a)). Hence, we establish a procedure to compute analytical expressions of water flow in a single root with segments connected in series with contrasted hydraulic property profiles. Figure 4.2 presents a sketch of a single root made of five stretches delimited by dashed vertical lines.

Deriving the coefficients $c_{1,i}$ and $c_{2,i}$ in any root stretch i requires boundary conditions at the limits of each stretch (i.e., at $z = l_{i-1}$, the root stretch i's distal end and at $z = l_i$, its proximal end). The bottom flux boundary condition at the distal end of stretch i is called J_{i-1} [L^3T^{-1}], and the xylem water potential at the proximal end of stretch i is $\Psi_{proximal,i}$ [P] as it appears in Fig. 4.2 and as stated in Eq. 4.6:

$$\begin{cases} J_x(l_{i-1}) = J_{i-1} \\ \Psi_x(l_i) = \Psi_{proximal,i} \end{cases} \tag{4.6}$$

Note that $J_0 = 0$ (no axial flow at the root tip), and $\Psi_{proximal,N} = \Psi_{collar}$ (the xylem water potential at the proximal end of the last root stretch N is the plant collar potential).

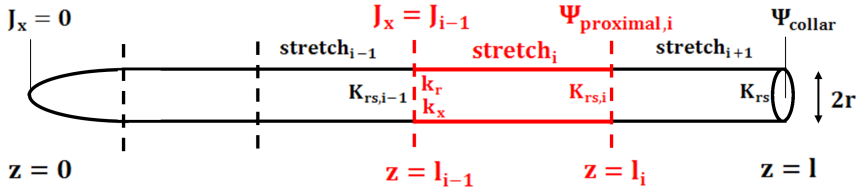


Figure 4.2: Single root made of five stretches (the dashed vertical lines are stretch boundaries). For root stretch *i*, boundary condition at $z = l_{i-1}$ (distal end) is the water flow J_{i-1} and at $z = l_i$ (proximal end) the xylem water potential $\Psi_{proximal,i}$. For details, see text.

4.2.3 Derivation of macroscopic root hydraulic properties

Only J_0 and $\Psi_{proximal,N}$ are predefined root boundary conditions and none of the root stretches has both boundary conditions known (J_{i-1} and $\Psi_{proximal,i}$) so the solution of the water flow equation is not straightforward unless the root is made of a single stretch. To solve this problem, the concept of root macroscopic parameters is used.

The root macroscopic parameters consist in the root system conductance K_{rs} [$L^3T^{-1}P^{-1}$] and the Standard Uptake Density SUD [L^{-1}] (Couvreur et al. 2012; Meunier et al. 2017). These parameters are used in soil-root water transfer models that stem from principles of water flow in root hydraulic architecture but do not rely on an explicit geometrical description of root system (Couvreur et al. 2012). In contrast to Couvreur, Meunier et al. (2017) revisited these definitions and applied them to any root or part of a root system. They are calculated in homogeneous soil conditions and are defined here as function of the root length l_i as:

$$\begin{cases} K_{rs,i} = \frac{J_x(l_i)}{\Psi_{soil} - \Psi_x(l_i)} \\ SUD_i(z) = \frac{q_r(z)}{J_x(l_i)} \end{cases} \tag{4.7}$$

These macroscopic parameters are always independent of the boundary conditions: they only depend on root geometric (radius and length) and hydraulic properties ($k_r(z)$ and $k_x(z)$). Let us note that the $K_{rs,i}$ and SUD_i as defined in Eq. 4.7 represent the root macroscopic parameters after addition of i stretches ignoring thus the root stretches after the

considered zone. The terms K_{rs} and SUD are used instead of $K_{rs,N}$ and SUD_N, respectively, and correspond to the macroscopic parameters of the entire root:

$$\begin{cases} K_{rs} = \frac{J_x(l)}{\Psi_{soil} - \Psi_x(l)} \\ SUD(z) = \frac{q_r(z)}{J_x(l)} \end{cases} \tag{4.8}$$

The macroscopic parameters may be calculated by a recursive equation (see Appendix B for demonstration):

$$\begin{cases} K_{rs,i} = k_x(l_i) \frac{\left(-K_{rs,i-1}f_{2,i}(l_{i-1}) + f'_{2,i}(l_{i-1})k_x(l_{i-1})\right)f'_{1,i}(l_i) + \left(K_{rs,i-1}f_{1,i}(l_{i-1}) - f'_{1,i}(l_{i-1})k_x(l_{i-1})\right)f'_{2,i}(l_i)}{K_{rs,i-1}f_{1,i}(l_{i-1})f_{2,i}(l_i) - K_{rs,i-1}f_{1,i}(l_i)f_{2,i}(l_{i-1}) - f'_{1,i}(l_{i-1})f_{2,i}(l_i)k_x(l_{i-1}) + f_{1,i}(l_i)f'_{2,i}(l_{i-1})k_x(l_{i-1})} \\ SUD_i(z) = \frac{2\pi r k_r(z)}{k_x(l_i)} \frac{\left(-K_{rs,i-1}f_{2,i}(l_{i-1}) + f'_{2,i}(l_{i-1})k_x(l_{i-1})\right)f_{1,i}(z) + \left(K_{rs,i-1}f_{1,i}(l_{i-1}) - f'_{1,i}(l_{i-1})k_x(l_{i-1})\right)f_{2,i}(z)}{\left(-K_{rs,i-1}f_{2,i}(l_{i-1}) + f'_{2,i}(l_{i-1})k_x(l_{i-1})\right)f'_{1,i}(l_i) + \left(K_{rs,i-1}f_{1,i}(l_{i-1}) - f'_{1,i}(l_{i-1})k_x(l_{i-1})\right)f'_{2,i}(l_i)} \end{cases} \tag{4.9}$$

where Lagrange notation is used for derivative. The recursive formulation is useful to solve the water flow equation when dealing with multiple-stretched roots. We start, in such a case, with the calculation of $K_{rs,1}$ (i.e., the conductance of the most distal stretch) using Eq. 4.9 (with $K_{rs,0} = 0$ because the axial flow is null at root apex). The obtained $K_{rs,1}$ is then used as $K_{rs,i-1}$ to calculate the effective conductance of the distal part from the second stretch $K_{rs,2}$ using Eq. 4.9. This procedure is then used again to derive the $K_{rs,i}$ of all stretches until the root collar is reached. The obtained set of $K_{rs,i}$'s or $K_{rs,i-1}$'s are then used to calculate the coefficients $c_{1,i}$ and $c_{2,i}$ for the different stretches using:

$$\begin{cases} c_{1,i} = \frac{\left(\Psi_{proximal,i} - \Psi_{soil}\right)\left(-K_{rs,i-1}f_{2,i}(l_{i-1}) + f'_{2,i}(l_{i-1})k_x(l_{i-1})\right)}{K_{rs,i-1}f_{1,i}(l_{i-1})f_{2,i}(l_i) - K_{rs,i-1}f_{1,i}(l_i)f_{2,i}(l_{i-1}) - f'_{1,i}(l_{i-1})f_{2,i}(l_i)k_x(l_{i-1}) + f_{1,i}(l_i)f'_{2,i}(l_{i-1})k_x(l_{i-1})} \\ c_{2,i} = \frac{\left(\Psi_{proximal,i-1} - \Psi_{soil}\right)\left(K_{rs,i-1}f_{1,i}(l_{i-1}) - f'_{1,i}(l_{i-1})k_x(l_{i-1})\right)}{K_{rs,i-1}f_{1,i}(l_{i-1})f_{2,i}(l_i) - K_{rs,i-1}f_{1,i}(l_i)f_{2,i}(l_{i-1}) - f'_{1,i}(l_{i-1})f_{2,i}(l_i)k_x(l_{i-1}) + f_{1,i}(l_i)f'_{2,i}(l_{i-1})k_x(l_{i-1})} \end{cases} \tag{4.10}$$

as demonstrated in Appendix B. Since in Eq. 4.10, only the potential at the proximal part of the stretch is needed as a boundary condition (in addition to the distal root conductance), the calculation starts at the proximal end of the root system where the root collar potential Ψ_{collar} is known. The obtained $c_{1,i}$ and $c_{2,i}$ for the proximal stretch are subsequently used in Eq. 4.5 to calculate the water potential at the distal part of the stretch. The water potential is then used to calculate the coefficients of the next stretch (towards the root tip). This procedure is used until the most distal stretch is reached. As SUD depends on

the collar water flow, it can not be calculated for each zone. However it can be derived at the end of the procedure when the xylem water potential is defined everywhere inside the root and when the total root conductance has been already calculated.

4.2.4 Resolution of the root water flow equation

We here analyse six cases of hydraulic conductance variations along a root axis: the uniform root (already developed by Landsberg and Fowkes (1978)), a single root with linear root hydraulic property profiles and a single root with exponential root hydraulic property profiles. For the two latter cases, the radial conductivity and the axial conductance may change alone or simultaneously. Table 4.1 summarizes the six cases with the corresponding local hydraulic properties. Note that the linear increase of axial conductance was already studied by Ariyaratna (1990). Table 4.2 summarizes the solutions of the root water flow equation obtained for the six considered cases. The resolution details are provided in Appendix A.

Table 4.1: Local hydraulic properties $k_r(z)$ and $k_x(z)$ for the different cases.

	$\mathbf{k_r(z)}$	$\mathbf{k_x(z)}$
Constant (uniform) root	$k_r(z) = k_{r0}$	$k_x(z) = k_{x0}$
Linear $\mathbf{k_r}$	$k_r(z) = a_0 z + b_0$	$k_x(z) = k_{x0}$
Linear $\mathbf{k_x}$	$k_r(z) = k_{r0}$	$k_x(z) = c_0 z + d_0$
Linear $\mathbf{k_r}$ and $\mathbf{k_x}$	$k_r(z) = a_0 z + b_0$	$k_x(z) = c_0 z + d_0$
Exponential $\mathbf{k_r}$	$k_r(z) = \gamma_2 exp(-\beta_2 z)$	$k_x(z) = k_{x0}$
Exponential $\mathbf{k_x}$	$k_r(z) = k_{r0}$	$k_x(z) = \gamma_1 exp(\beta_1 z)$
Exponential $\mathbf{k_r}$ and $\mathbf{k_x}$	$k_r(z) = \gamma_2 exp(-\beta_2 z)$	$k_x(z) = \gamma_1 exp(\beta_1 z)$

N.B.: Ai and Bi are the Airy functions of the first and second kind; M and U, the confluent hypergeometric function of the first and second kind; I_ν and K_ν, the modified Bessel function of the first and second kind of order ν and Γ is the gamma function.

The parameters used in Table 4.1 are gathered as well as their units in Table 4.3 (two first columns). To simplify the solutions of the root water flow equation, some parameters are combined. The definition of combined parameters is also given in Table 4.3 with their corresponding units (two last columns).

Table 4.2: Linearly independent functions f_1 and f_2 solutions of Eq. 4.4 according to the functions describing local root hydraulic properties.

	$\mathbf{f_1(z)}$	$\mathbf{f_2(z)}$
Constant (uniform) k_r and k_x	$cosh(\tau z)$	$sinh(\tau z)$
Linear k_r	$Ai\left(\frac{az+b}{a^{\frac{2}{3}}k_{x0}^{\frac{1}{3}}}\right)$	$Bi\left(\frac{az+b}{a^{\frac{2}{3}}k_{x0}^{\frac{1}{3}}}\right)$
Linear k_x	$\sqrt{\frac{2}{c}}I_0\left(2\sqrt{\frac{d+cz}{c^2}}\right)$	$\sqrt{\frac{2}{c}}K_0\left(2\sqrt{\frac{d+cz}{c^2}}\right)$
Linear k_r and k_x	$exp\left(-\frac{\sqrt{a}z}{\sqrt{c_0}}\right)M\left(\frac{\sqrt{a}c_0^{3/2}+bc_0-ad_0}{2\sqrt{a}c_0^{3/2}},1,\frac{2\sqrt{a}(c_0z+d_0)}{c^{3/2}}\right)$	$exp\left(-\frac{\sqrt{a}z}{\sqrt{c_0}}\right)U\left(\frac{-\sqrt{a}c_0^{3/2}-bc_0+ad_0}{2\sqrt{a}c_0^{3/2}},1,\frac{2\sqrt{a}(c_0z+d_0)}{c^{3/2}}\right)$
Exponential k_r	$I_0\left(\frac{2\sqrt{\gamma_r exp(-\beta_2 z)}}{\beta 2}\right)$	$K_0\left(\frac{2\sqrt{\gamma_r exp(-\beta_2 z)}}{\beta 2}\right)$
Exponential k_x	$\frac{\sqrt{\gamma_x exp(-\beta_1 z)}}{\beta_1}I_1\left(\frac{2\sqrt{\gamma_x exp(-\beta_1 z)}}{\beta_1}\right)$	$\frac{\sqrt{\gamma_x exp(-\beta_1 z)}}{\beta_1}K_1\left(\frac{2\sqrt{\gamma_x exp(-\beta_1 z)}}{\beta_1}\right)$
Exponential k_r and k_x	$\beta^{-\frac{\beta_1}{\beta}}\gamma^{\frac{\beta_1}{2\beta}}(exp(-\beta z))^{\frac{\beta_1}{2\beta}}\Gamma\left(1-\frac{\beta_1}{\beta}\right)I_{-\frac{\beta_1}{\beta}}\left(\frac{2\sqrt{exp(-\beta z)\gamma}}{\beta}\right)$	$\beta^{-\frac{\beta_1}{\beta}}\gamma^{\frac{\beta_1}{2\beta}}(exp(-\beta z))^{\frac{\beta_1}{2\beta}}\Gamma\left(1+\frac{\beta_1}{\beta}\right)I_{\frac{\beta_1}{\beta}}\left(\frac{2\sqrt{exp(-\beta z)\gamma}}{\beta}\right)$

Table 4.3: Local hydraulic property function parameters, their units, the expression of combined parameters and their corresponding units.

Parameter	**Unit**	**Combined parameter**	**Unit**
k_{r0}	$LT^{-1}P^{-1}$		
k_{x0}	$L^4T^{-1}P^{-1}$		
a_0	$T^{-1}P^{-1}$	$a = 2\pi r a_0$	$LT^{-1}P^{-1}$
b_0	$LT^{-1}P^{-1}$	$b = 2\pi r b_0$	$L^2T^{-1}P^{-1}$
c_0	$L^3T^{-1}P^{-1}$	$c = \frac{c_0}{2\pi r k_{r0}}$	L
d_0	$L^4T^{-1}P^{-1}$	$d = \frac{d_0}{2\pi r k_{r0}}$	L^2
γ_1	$L^4T^{-1}P^{-1}$	$\gamma_r = \frac{2\pi r\gamma_2}{k_{x0}}$	L^{-2}
γ_2	$LT^{-1}P^{-1}$	$\gamma_x = \frac{2\pi r k_{r0}}{\gamma_1}$	L^{-2}
β_1	L^{-1}	$\gamma = 2\pi r\frac{\gamma_2}{\gamma_1}$	L^{-2}
β_2	L^{-1}	$\beta = \beta_1 + \beta_2$	L^{-1}

These functions can be combined in complex root with several root stretches with Eq. 4.9, 4.10 and the entire root boundary conditions: Ψ_{collar} and $J_0 = 0$.

Figure 4.3 shows the procedure to solve the water flow problem in a root with variable hydraulic properties. First we need to know whether the root is made of one or several stretches. Then we have to determine the coefficients $c_{1,i}$ and $c_{2,i}$ for each single zone, $i \in [1\ N]$ by determining the type of root stretch we deal with and by using Eq. 4.10. Thanks to these coefficients, we obtain the root conductance after addition of each stretch by applying Eq. 4.9. Finally we calculate the xylem potential, the axial flow, the radial flow per root length and the macroscopic

parameters using the appropriate equations and analytical functions given in Table 4.2. The corresponding equations are mentioned in the figure.

If the root is made of only one stretch, there is no need to calculate intermediary root conductances. The solutions of Table 4.2 are then used with the no flux boundary condition coefficients to obtain the macroscopic parameters as well as the water xylem potential radial and axial water flow profiles along the root axis. This particular case is analysed in Appendix C.

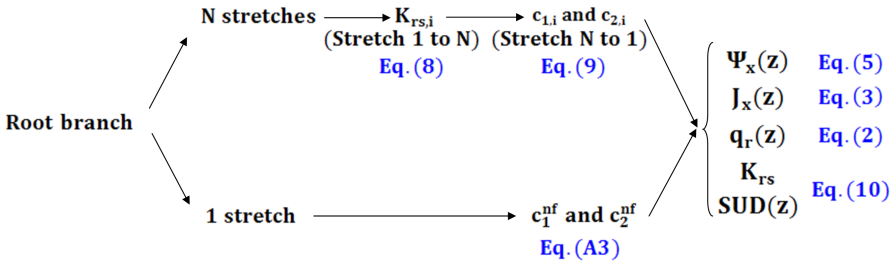


Figure 4.3: Flowchart of the water flow equation resolution in roots with heterogeneous hydraulic properties

4.2.5 Properties of an ageing root

The water flow equation resolution derived in the previous sections was obtained for a root of a specific length. In the next sections, we show how to modify the solution when the root is growing and developing.

Root growth

In this section we introduce the root elongation. As in many studies, the properties are measured as a function of emerging time instead of distance to tip, we provide here a tool to switch from one to another. Basically an equation of the root elongation rate is required. We consider here an instantaneous growth rate $v(t)\,LT^{-1}]$, function of the actual

time t [T], given by:

$$v(t) = v_0 exp\left(\frac{-v_0}{l_{max}}t\right) \tag{4.11}$$

where $v_0\,[LT^{-1}]$ is the initial elongation rate and $l_{max}\,[L]$ is the root maximal length (Pagès et al. 2004). Note that if $l_{max}\,[L]$ is large enough, then the elongation rate is almost constant and equals v_0. When the transition ages (i.e. root ages at which root hydraulic property change), $age_i\,[T]$, are known, the stretch lengths, $stretch_i(t)\,[L]$ are given by:

$$stretch_i(t) = \begin{cases} 0, t < age_i \\ l_{max}\left(1 - exp\left(\frac{-v_0}{l_{max}}(t - age_i)\right)\right), t \geqslant age_i \text{ and } t \leqslant age_{i+1} \\ l_{max}\left(exp\left(-\frac{v_0}{l_{max}}(t - age_{i+1})\right) - exp\left(-\frac{v_0}{l_{max}}(t - age_i)\right)\right), t > age_{i+1} \end{cases} \tag{4.12}$$

See Appendix D for details.

Root development

When roots get older, their macroscopic hydraulic parameters vary not only because they grow but also because of root tissue maturation. Maturation is defined here as an evolution of root hydraulic properties as a function of root age (and not of distance to root tip as done in the previous sections). This process is modelled by introducing root hydraulic properties depending on root age, such as:

$$\begin{cases} k_r = k_{r0} exp(-mt) \\ k_x = k_{x0} exp(mt) \end{cases} \tag{4.13}$$

where m $[\mathrm{T}^{-1}]$ is the maturation rate. These equations are similar to the ones used in the exponential root hydraulic properties subsection (see Sect. 4.6) except that they define the properties as a function of time instead of distance to tip. Other root development rate can be imagined, similar to the other functions developed in the previous sections.

4.2.6 Root System with laterals

Unlike the single root with analytical hydraulic property shape described in previous sections, no solution of the water flow equation could be

found for a root bearing regularly spaced laterals at first. Landsberg and Fowkes (1978) suggested an approximation when incorporating these laterals all over the principal root length by increasing the radial conductivity of the principal root. Yet it is possible to find the conductance of this idealized root system using a purely discrete approach or a hybrid numerical-analytical method.

The problem resolution for the discrete approach was described step by step by Meunier et al. (2017) and we redirect interested readers to the section 2.4 of the reference to explicit computations. We only explain here the main calculations. In a first step, it is possible to show that the analytical solutions presented above are the asymptotic solutions of the water flow equation resolution for discrete root elements. With infinitely small root segments (and infinite segment number), discrete and continuous solutions are rigorously identical. The finite element approach can thus be successfully applied for the simplest case: the uniform single root. We showed in Meunier et al. (2017) that the discrete root model indeed converges to the exact continuous model for sufficiently small root segments. But more interestingly, a similar mathematical solution could be applied to a more complex case of a single root bearing laterals and then an analytical solution of total root system conductance and root water standard uptake was within reach.

More simply, the hybrid method explained in details in Chapter 3 of the present document can also be successfully applied to a root bearing regularly-spaced laterals to obtain an analytical solution of the branch conductance and uptake distribution.

4.3 Model illustration

In this section, we highlight the potential of the newfunctions with a modelling exercises. We start with simple theoretical illustrations of the model. We then explain how pressure probe measurements can be used to derive local hydraulic properties. These results are then inserted first in a soil-root model to test the uptake efficiency of a heterogeneous root as compared to a uniform one, and then in an optimization algorithm to assess the breeding potential of the analysed roots (i.e. distance to an optimal root). Finally we show how root *vs* development rates can reveal very contrasted uptake strategies. Another added value of analytical solutions is their potential use to verify the current numerical solution. One example is given in Appendix E.

4.3.1 Comparison between uniform and heterogeneous roots

Roots with the same total conductance

First, three theoretical roots were simulated. Figure 4.4 represents how the radial conductivity (a) and the axial conductance (b) depend on distance to tip for these three roots. The blue solid lines represent a root with constant hydraulic properties while the dashed and dotted are roots with linear and exponential hydraulic property profiles (radially and axially), respectively. The numerical values are chosen so that the conductance K_{rs} of the three roots is rigorously the same.

The water flow equation is then solved for these three roots and the xylem potential as well as the radial and axial flow are computed to assess their divergences. Xylem water potential is obtained thanks to Eq. A.1 for the uniform root, A.4 for the linearly changing root and A.5 for the exponentially varying root. The calculations were performed for a constant Ψ_{collar} of -3000 hPa and a uniform soil water potential of 0 hPa. Radial flow per root length q_r and axial water flow J_x are obtained applying Eq. 4.2 and Eq. 4.3, respectively, to the three different cases.

We also define two root parameters combining root hydraulic and geometric properties:

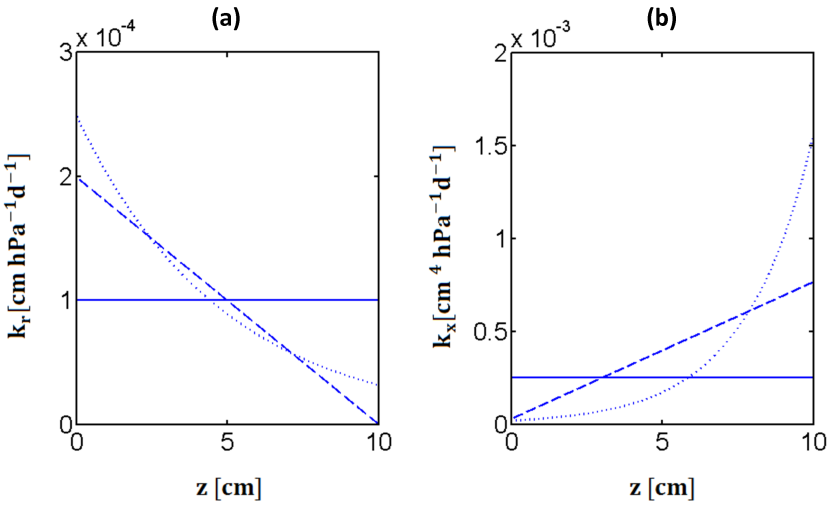


Figure 4.4: Variation with distance to root tip of radial conductivity (a) and axial conductance (b) along a single root with constant hydraulic properties (solid blue line), a single root with linear hydraulic profiles (dashed lines) and a single root with exponential hydraulic profiles (dotted lines). The origin of the z-axis is at the root tip.

$$\begin{cases} \tau(z) = \sqrt{\frac{2\pi r k_r(z)}{k_x(z)}} \\ \kappa(z) = \sqrt{2\pi r k_r(z) k_x(z)} \end{cases}$$

The units of these root parameters are $[\mathrm{L}^{-1}]$ and $[\mathrm{L}^{-3}\mathrm{P}^{-1}\mathrm{T}^{-1}]$, respectively. These parameters have the same definitions than in the case of the uniform root but they depend now on the position along the root axis (see Appendix A.1). τ indicates how fast the root system conductance changes and how homogeneous the water uptake along the root axis under homogeneous soil conditions is. κ is an indicator of the maximal possible root system conductance.

Water flow in a maize lateral root

Here, we compare single roots with complex hydraulic profiles (as they have been observed) and constant root hydraulic properties in terms

of distribution of water xylem potential, radial and axial flows and macroscopic parameters. Maize lateral root properties from Doussan et al. (1998a) are analysed here. This constitutes an illustration of the multiple-stretched single root. In their study, they described axial conductance and radial conductivity as stepwise functions of the root age or distance to tip. They justified it by the root tissue maturation and development. We converted the transition ages to distance to tip transition position as explained in the previous section. We considered a constant elongation rate of 1 cm per day (if not constant, the elongation rate change as described previously must be taken into account). Three other root hydraulic property uniform functions were also tested: minimal, maximal and mean values of observed profiles for both hydraulic properties. Whether constant root hydraulic properties could mimic more complex situations is consequently investigated comparing the different scenarios in terms of uptake, flow and macroscopic parameters.

4.3.2 Inverse modeling of root hydraulic properties

In this section, we illustrate how the novel solutions can help understanding an experiment conducted in 2016 by Mohsen Zarebanadkouki in Gottingen. For more details about the experimental conditions, see Material and Methods of Chapter 7. A root pressure probe was used to measure total root conductance as well as axial conductance of unbranched brace maize roots.

To do so, nine maize were grown in aluminium containers filled with silty soil. When plants were seven weeks old, the containers were opened, roots were carefully washed from the soil and selected maize brace roots were excised from the stem. They were then connected to a pressure probe in order to derive their hydraulic properties in an experiment really similar to the one first presented by Frensch and Steudle (1989). Only the general idea here is given here. For more details, we refer to the explanations of Frensch and Steudle (1989) or the fully detailed explanations of Chapter 7.

Unbranched intact roots were around 35 cm long when first connected to the root pressure probe. A series of pressure clamps were carried out (3-5 clamps) to induce a flow of water into the root after

a stable value of root pressure was reached, which took between 30 to 120 min. Increments of 20 to 50kPa were used for successive pressure clamps. Pressure was held constant at each increment for 10 to 120 s. The distance that metal rode (meniscus) inside the capillary had moved was used to calculate the water volume and as a consequence the flow rate by dividing by the duration of the step. The linear regression of flow rate plotted against the applied pressure difference led to the total root conductance for this specific length. The root was then cut towards its tip and reconnected to the root pressure probe to repeat the measurement until the root end was reached.

Axial hydraulic conductance was determined after cutting the root connected to the root pressure probe with a razor blade at a distance of 2 cm from its proximal end. Similar to the measurement of total conductance, a series of pressure clamps were carried out to induce water flow into the small root segment. The local axial conductance was calculated as the product of the segment length by the slope of the linear regression of flow rate plotted against the applied pressure difference.

The profile of axial conductance was first fitted using piecewise functions. Both axial conductances absolute values and positions of the transition were optimized. When axial conductances were obtained, further optimization was required to derive the profile of radial conductivity using measurements of total root conductances. Several scenarios, including uniform, single- and multi-stretches hydraulic properties, were tested. Since the number of fitting parameters was not constant between scenarios, adjusted coefficient of determination allowed us to discriminate the best scenario. A uniform root (both radially and axially) was also tested to compare the results with the solution of Landsberg and Fowkes (1978).

4.3.3 Root in a heterogeneous soil

The uniform and heterogeneous hydraulic profiles that best fitted the measurements of the previous experiments were then tested to compute the macroscopic parameters, $K_r s$ and SUD, for any root length. These calculations allowed us to simulate the water flow in the soil-root continuum. To do so, we used the model developed by Couvreur et al.

(2012) and Couvreur et al. (2014b) that only requires the macroscopic parameters (in terms of root parameters) to predict the water flow from the bulk soil to the root collar. The soil sink term is calculated as the sum of the local radial flow to the root which, in turn, are given by (Meunier et al. 2017)

$$q_r(z) = T_{act} SUD(z) + K_{rs} \left(\Psi_{sr}(z) - \Psi_{seq}\right) SUD(z)$$

with $\mathrm{T_{act}}\,[\mathrm{L^3T^{-1}}]$ the proximal end water flow, $\Psi_{\mathrm{sr}}(\mathrm{z})\,[\mathrm{P}]$ the soil-root interface potential and

$$\Psi_{seq} = \int_0^l SUD(z)\Psi_{sr}(z)dz\,[P]$$

the equivalent soil potential. In the simulations, the root were supposed to be vertical in a 3D loamy soil box of 10 cm x 10 cm x 30 cm with a constant total water uptake of 1 $\mathrm{cm^3 d^{-1}}$ and a constant elongation rate of 1 cm. When the root collar potential reached -1.5MPa, the root top boundary condition was switched from flux to pressure-head. A constant pressure was then maintained as top boundary condition and the total uptake was consequently reduced (Meunier et al. 2016b).

4.3.4 Optimal geometric properties

The new solutions of the water flow equation are key to estimate optimal geometric properties of roots. As an illustration we may want to maximize the root conductance $\mathrm{K_{rs}}$ of uniform roots and compare the results with those of roots with varying hydraulic property profiles. Using a carbon cost as a constraint, it writes:

$$\text{maximize } K_{rs}(r,l) \text{ subject to } V_0 = \pi r^2 l$$

where $\mathrm{V_0}\,[\mathrm{L^3}]$ is the volume constraint. To solve this optimization problem, Lagrange multipliers λ are useful. We define a new function Λ:

$$\Lambda(r,l,\lambda) = K_{rs}(r,l) + \lambda\left(\pi r^2 l - V_0\right)$$

whose maximum is found when:

$$\nabla_{r,l,\lambda}\Lambda = 0$$

The previous equation is equivalent to:

$$\begin{cases} \frac{\partial K_{rs}}{\partial r} + 2\lambda\pi r l = 0 \\ \frac{\partial K_{rs}}{\partial l} + \lambda\pi r^2 = 0 \\ V_0 = \pi r^2 l \end{cases} \tag{4.14}$$

Using appropriate equations to calculate the root conductance, we find an optimal radius and length that maximize root water uptake. As an illustration, we compare the optimal root radius of a root with constant hydraulic properties, a root whose constant root properties depend on the root radius (Biondini 2008) and a root with heterogeneous root properties as observed in the pressure probe experiment. Mathematically, it writes, respectively:

$$\begin{cases} \text{Constant } k_r \text{ and } k_x : k_r(z) = k_{r0} \text{ and } k_x(z) = k_{x0} \\ \text{Uniform } k_r(r) \text{ and } k_x(r) : k_r(r) = k_{r0}\frac{r_0}{r} \text{ and } k_x(r) = b^* r^5 \\ \text{Heterogeneous } k_r \text{ and } k_x : k_r(z) = f(z) \text{ and } k_x(z) = g(z) \end{cases} \tag{4.15}$$

The parametrization for the heterogeneous root and the uniform root are the best heterogeneous and uniform profiles derived from the pressure probe experiment for brace roots. For the root whose hydraulic properties depend on the root radius, we kept the parameters of Biondini (2008) for maize(r_0 [L], k_{r0} [$L^4P^{-1}T^{-1}$] and b^* [$L^{-1}P^{-1}T^{-1}$]). The constraint volume V_0 was the mean observed volume for the maize brace roots. $f(z)$ and g(z) are observed functions for the radial and axial hydraulic property, respectively.

4.3.5 Root water uptake strategy

In this last example, we again consider a single growing root whose development (ageing) and elongation rates can both vary. We varied the root parameters m (development) and $\frac{v_0}{l_{max}}$ (growth) between 0.05 and 0.5 [d^{-1}] and between 0.01 and 0.1 [d^{-1}], respectively to investigate the impact of relative growth and maturation processes on macroscopic parameters and uptake patterns.

4.3.6 Sensitivity of a mature root system to hydraulic phenes

The functions developed in the theory are of potential use for developing quantitative ideotypes, i.e., quantitative estimates of optimal root hydraulic or architectural traits for drought stress tolerance. We consider as an example a maize root system generated by RootTyp (Pagès et al. 2004). This root system is made of several primary roots attached to the basis of a stem. On these parallel primaries are attached regularly spaced laterals. We used the relationships of Doussan et al. (1998a) (see Figure 4) to represent the evolution of root segment radial and axial hydraulic properties with root segment age as a succession of plateau for both primaries and laterals. The conductance of single roots can be analytically derived using the solution of the water flow equation solved for single roots. To derive the total RS conductance we assume that the stem is not taking up water (its radial conductivity is zero) and that its xylem conductance is hydraulically non-limiting (its axial conductivity is very high). Consequently the RS conductance is simply the sum of the primary conductances. Actually, with the parametrization we used, the majority of the root primary surface for a mature maize RS are old so that we can consider with good approximation the primary root hydraulic properties as uniform when analysing a mature root system.

We can use the model including laterals to calculate the primary conductance and finally the RS conductance. The lateral interbanch distance parameter was given by the maize paramatrization of Couvreur et al. (2014a).

We considered a change of $\pm 50\%$ for the local conductivities of both primary (left) and lateral (right) roots, everything else kept constant.

The interest of such an example is to evaluate the potential benefit of increasing locally the root conductivity on RS conductance. Performing a sensitivity analysis on mature roots, we investigate which zone is the most resistive part of complex root systems. This sensitivity analysis is based on both hydraulic (obtained by Doussan et al. (1998a)) and architectural parameters (growth and shape parameters of the maize plant for RootTyp (Pagès et al. 2004)).

4.4 Results

4.4.1 Comparison between uniform and heterogeneous roots

Roots with the same total conductance

Solutions of the water flow equation are shown in Fig. 4.5 for three different root property distributions (the legend is the same as in figure 4.4): uniform, linear and exponential profiles. Are represented here xylem water potential (subplot a), the radial flow per root length (subplot b) and the axial water flow (subplot c).

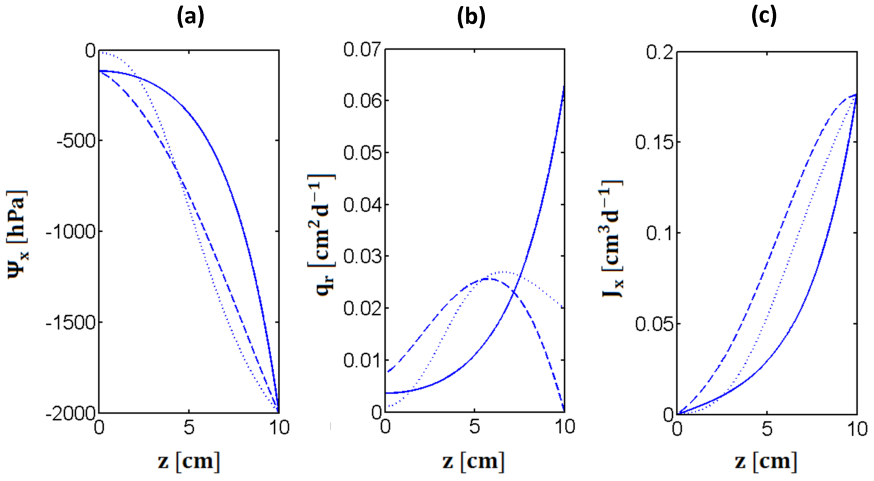


Figure 4.5: Solutions of the root water flow equation: xylem water potential (a), radial water flow per root length (b) and axial water flow (c) along a root with constant properties (solid blue line), a root with linear hydraulic profiles (dashed lines) and a root with exponential hydraulic profiles (dotted lines). The origin of the z-axis is at the root tip.

Even though the collar axial flow is identical for each root (because they have the same conductance), their xylem water potential and root water uptake profiles differ. The potential drop is more homogeneously distributed along the roots with heterogeneous properties. Furthermore, it is observed that q_r is a monotonic increasing function of distance in the case of the uniform root, but that the maximal uptake is not located

at the root collar anymore for the two other cases. Consequently the axial flow differ between these three cases.

Root parameters τ and κ are represented in Fig. 4.6, subplots (a) and (b), respectively. These parameters are constant for a uniform root. τ is monotonically decreasing for non-uniform roots because the radial conductivity is decreasing and the axial conductance is increasing along the root axis. The root with linear hydraulic property profiles has a non-monotonic κ while this parameter is always increasing for roots with exponentially changing hydraulic properties. These hydraulic parameters must be set in relation with the root macroscopic parameters represented in the bottom line of Fig. 4.6. In subplot (c) SUD is represented along the z-axis (note that this subplot is the same as the second subplot of Fig. 4.5 except that the curve is now normalized so that its integral on total root length is one). K_{rs} is plotted as a function of the root length in subplot (d). It is worth noting that the root system conductances differ very much between these cases. Depending on how k_r and k_x vary along the root, K_{rs} might even decrease with increasing root length (linear root case). This occurs when additional segments with a low k_r are added so that the extra inflow across these segments does not compensate for the extra pressure head loss due to axial flow through these segments. However, when k_r decreases with root length levels off and the k_x increases stronger with increasing root length, as it is the case in the exponential scenario, the root system conductance may increase steadily with root length.

Water flow in a maize lateral root

The local hydraulic property distribution for the lateral roots of maize, as derived by Doussan et al. (1998a), are shown in the two first subplots of Fig. 4.7 (blue solid lines). These subplots are equivalent to the Fig. 4B of the study of Doussan et al. (1998a) when a constant elongation rate of 1 cm per day is assumed. We removed the isolated distal region (whose axial conductance is null and that consequently does not affect root water fluxes). The red dashed, dotted and dashed-dotted lines correspond to hypothetical roots with uniform properties corresponding to minimal, maximal and mean values of observed hydraulic properties. When we compare the Doussan distribution of water radial flow per root

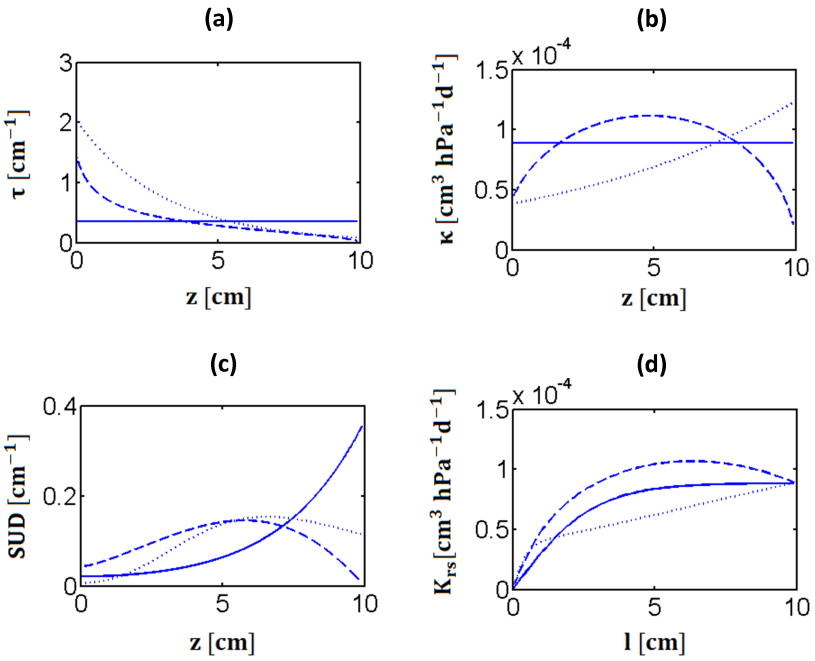


Figure 4.6: Variation along a single root of root (top line) and macroscopic (bottom line) hydraulic parameters: τ (a), κ (b), SUD (c) and K_{rs} (d) of a single root with constant properties (solid blue line), a single root with linear hydraulic profiles (dashed lines) and a single root with exponential hydraulic profiles (dotted lines).

length and potential with those of constant hydraulic property models (Fig. 4.7, c and d), we observe that it is not possible to represent its complex behaviour with an apparent/effective uniform model. The drop of water potential is much steeper with heterogeneous than with homogeneous properties (red lines). The decrease in water potential and the increase in axial flow are far more uniform along the composite root than along the homogeneous roots.

We used Eq. 4.9 to derive the macroscopic parameters of the four roots (the complex root and the three uniform roots). Again both the SUD and the K_{rs} could not be well represented by uniform root properties. It is indeed impossible with these solutions to represent non-monotonic functions as the standard uptake density (subplot (a), Fig. 4.8) and the root conductance (subplot (b), Fig. 4.8). This questions the

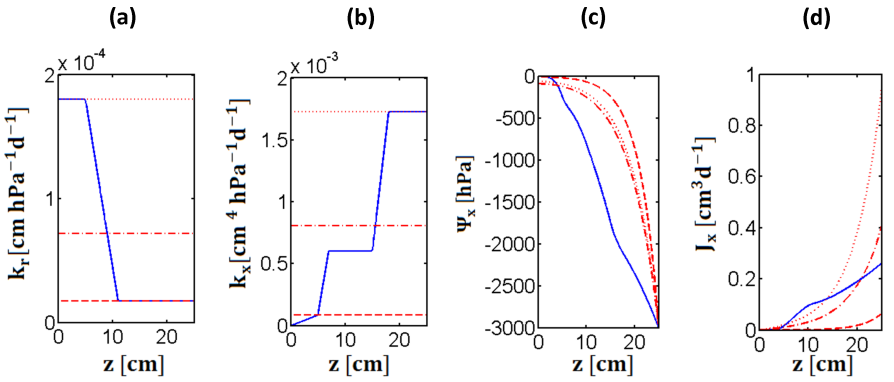


Figure 4.7: Distributions of radial conductivity (a), axial conductance (b), xylem water potential (c) and axial water flow (d) in a maize lateral root. We used hydraulic properties obtained by Doussan et al. (1998a) (blue solid line) for a maize lateral root or equivalent properties (red lines) with minimal (dashed), maximal (dotted) or mean (dashed-dotted) values. The origin of the z-axis is at the root tip.

typical assumptions made by hydrological and crop models, for which the root conductance is considered proportional to the root length density.

While K_{rs} increases monotonically towards the proximal end for uniform roots, this is no more the case for the heterogeneous root. When considering variations in hydraulic properties along the maize root axis, the analytical solutions that account for these changes revealed considerably different behaviours. The root conductance even decreases with root length. Similarly with the newly developed solutions, the maximal water uptake location was no more located at root proximal end. Non-monotonic functions of root water uptake emerged from the new solutions. Therefore, the search for optimal root systems (i.e. ideotypes) should also account for variations of root properties along roots.

4.4.2 Inverse modeling of root hydraulic properties

The analytical solutions developed here may serve as well to get local root hydraulic properties distributions along root axes. Here we used experimental measurements of the observed axial and total root conductances as measured by the root pressure probe (represented with black markers in the first and last subplots, respectively of Fig. 4.9). A perfect

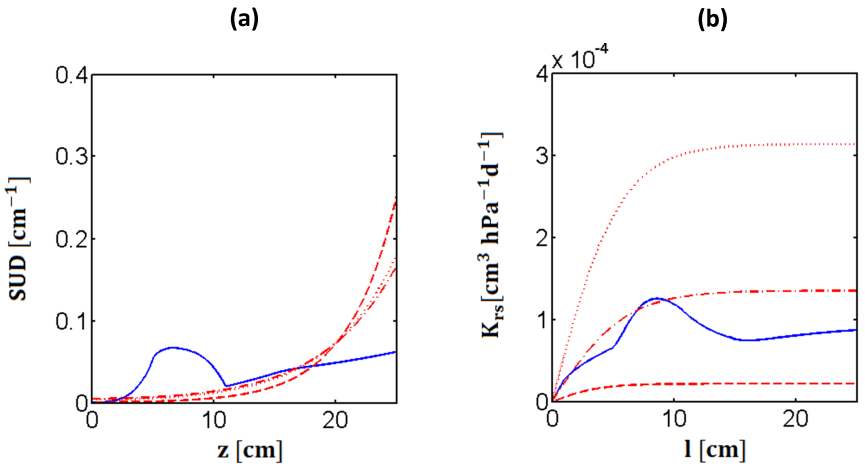


Figure 4.8: Macroscopic parameters: final SUD (a) and K_{rs} changes (b) for a growing maize lateral root with the local hydraulic properties estimated by Doussan et al. (1998a) (blue solid line) or the equivalent uniform roots (red lines) with minimal (dashed), maximal (dotted) or mean (dashed-dotted) hydraulic property values. The color legend is the same as in the previous figure.

fit of the xylem conductance profile could be obtained with a piecewise function (black dashed line, first subplot). The second subplot reveals the best radial conductivity profiles for some of the tested functions: linear (orange), exponential (yellow), stepwise (purple), 2 steps linear piecewise (light blue), 3 steps linear piecewise (green). The resulting total root conductance profiles are represented with the same legend in the last subplot with contrasting performances (the adjusted coefficients of determination are indicated as well). In the third subplot, radial to axial hydraulic properties ratios are plotted as a function of the distance from root tip. The best scenario is the stepwise function for the radial conductivity profile coupled to a piecewise function for the axial conductance profile (mauve scenario)

The last scenario that is represented in fig. 4.9 is an axially and radially uniform root (dark blue). If with such profiles, it is possible to reasonably fit the total root conductance profile (adjusted $r^2 = 0.81$), then, of course, the modelled xylem conductance profile does not fit at all, since high variations were observed between both root extremities.

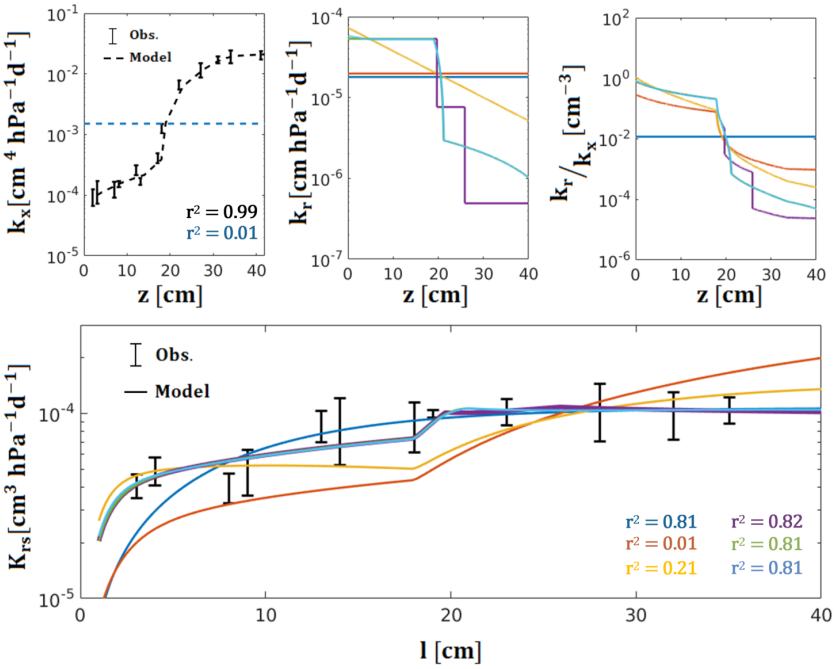


Figure 4.9: Hydraulic properties of the maize brace roots: axial and total hydraulic conductance of different root types as function of distance from root tip (dark symbols, first and last subplot, respectively). Data presented as dots are average of 5 measurements and the error bars represent the standard divisions. Profiles plotted as solid lines are the best profiles obtained from simulation of water flow into unbranched roots of varying length (last subplot). Second subplot: best fitted profiles of radial conductivity that reproduce measured profiles of total hydraulic conductance. Third subplot: ratio of radial conductivity to axial conductance derived from the analysis along the root axis. The best fitted axial conductance profile was used for each scenario except for the uniform root (dark blue).

The combination of pressure probe experiments with the newly developed solutions of the water flow equation in routine would allow us to derive the local hydraulic properties of roots that are critical for root system water uptake and plant performance (Vadez 2014). Different root types and plant genotypes will be compared in further experiments.

4.4.3 Root in a heterogeneous soil

When inserted in a soil-root model, the maize brace uniform root and the one with best scenario of hydraulic properties present contrasted uptake patterns and performances as revealed in fig. 4.10. In all subplots of this figure, the uniform and heterogeneous roots are represented with solid and dashed lines, respectively. The uniform root decreases its uptake after 6 days because its collar potential reaches the threshold at that time. At the very end of the simulation (20 days), this root had transpired 15% less water than the heterogeneous root, in total. This can be explained by the location of the root water uptake: while the uniform root always takes up water at the top, the heterogeneous root keeps looking for water at its tip. While, as a consequence, the heterogeneous root never feels a too low potential, the top water potential rapidly decreases for the uniform root and critical potential are reached within the xylem vessels that force the root reducing its water uptake. The uptake location can be seen from the clipped domain where water velocities at the end of the simulations are shown. A movie of the change in the main water uptake depth is also provided in the supplementary material. While after five days, the z-averaged soil potentials look similar for both roots, they diverge at the end of the simulation (bottom subplot).

This simulation underlines how critical the root water uptake location is for the root performance. The environment (that was not changed in the presented simulation) is, of course, important for the overall plant transpiration. The soil hydraulic properties (that redistribute more or less the water) and the climatic demand (that is more or less severe) strongly influence the results. What is needed to keep in mind at this stage, however, is that the water flow equation solutions, through the macroscopic parameters, can be inserted in water flow models, i.e. in heterogeneous environments to predict how efficient a particular root is. In further studies, the roots will be combined in an architecture and root systems performances will be assessed.

Here for the first time, the root was coupled to its surrounding medium, the soil. Note however that, as we simulate a single root, it was easy to finely discretize soil domain to accurately represent the water potential gradients around the growing root. Soil discretization and its

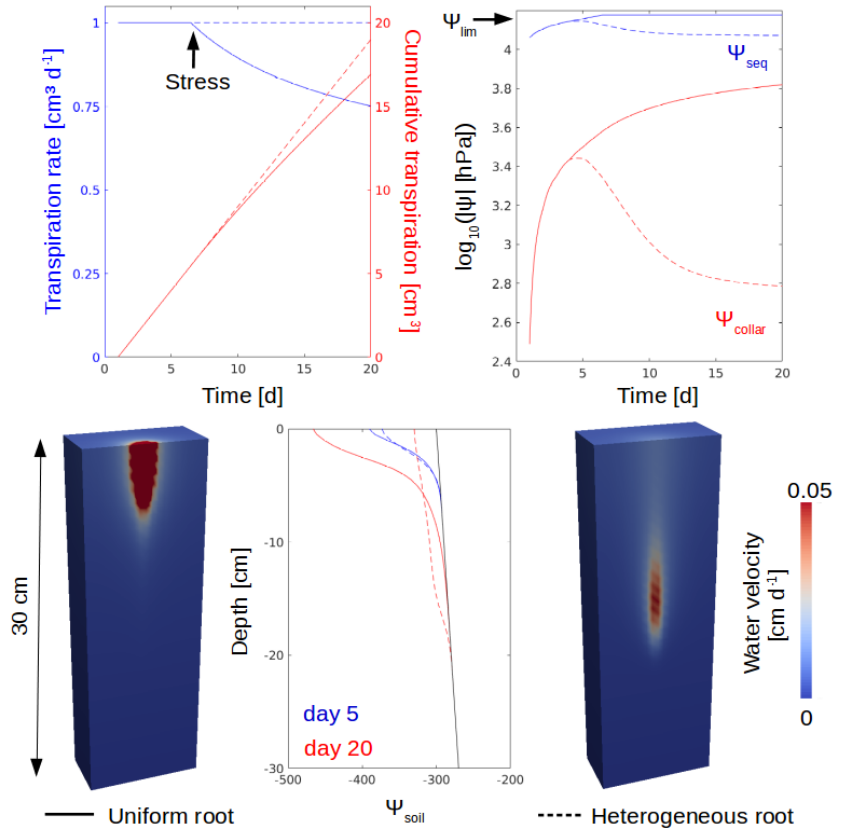


Figure 4.10: Root perfomances in a coupled soil-root model: changes of instantaneous and cumulative water uptake (top, left) and of collar and equivalent potential (top, right) for a uniform (solid) and heterogeneous (dashed) roots. In the bottom, the z-averaged profiles of soil potentials are plotted early and late in the simulation. The resulting water velocities at the end of the simulation are also shown in the clipped domain for both scenarios.

impact will be better discussed in Chapters where the simulations take place at the plant-scale.

4.4.4 Optimal geometric properties

In this section, we look for optimal root traits that would maximize the root water uptake. As an illustration, we compare the root conductances

of a uniform single root, a uniform single root with hydraulic properties varying with its radius, and a single root with exponential hydraulic property profiles. The root conductances of the three cases are shown in Fig. 4.11: the dashed line is the uniform root, the solid line is the uniform root whose hydraulic properties depend on the root radius and the dotted one is the heterogeneous root observed with the pressure probe experiment. The red stars point the optimal radii at which the conductances are maximal for the three scenarios. The black star is the observed pair radius-conductance of maize brace root.

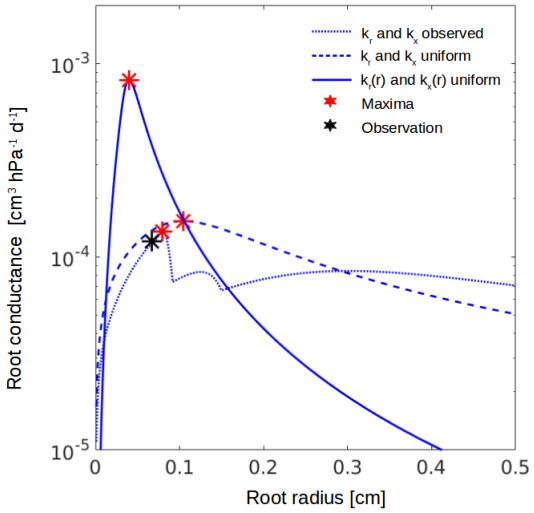


Figure 4.11: Root conductance as a function of root radius under a volume constraint for a uniform root whose hydraulic properties depend on the root radius (solid line), a uniform root (dashed line) and a root with observed heterogeneous conductivity profiles (dotted line). The red stars point the optimal radii (i.e., that maximize the root conductance), the black star the observed one.

Unlike previous approaches (Biondini 2008; Roose and Schnepf 2008) we consider here that the hydraulic properties may be functions of the root tissues and do not necessarily depend on the root radius. As highlighted by the red stars, the optimal root radii vary considerably when integrating this concept. We find that optimal root radius is closer to the observed one than with old approaches.

4.4.5 Root water uptake strategy

Figure 4.12-A shows the integral of K_{rs} over time when simulating 40 days of growth and maturation of a root whose l_{max} is 10 cm. Four extreme situations are represented: fast growth and slow maturation (case 1), slow growth and maturation (case 2), fast growth and maturation (case 3) and slow growth and fast maturation (case 4), respectively. The conductances of these particular roots are plotted as a function of time in Fig. 4.12-B. They exhibit very contrasted strategies in terms of total root conductance and uptake distributions. When the root growth is fast, the K_{rs} quickly reaches a high value. If the root maturation process is rapid, the final conductance is low. It can also be observed that the root properties change slowly when the root growth is low and rapidly when the root elongation rate is high. Figure 4.12-C represents the relative SUD(z) (i.e., multiplied by root length) as a function of the relative root position z (i.e., divided by root length) after 20 days of growth. Again contrasted strategies appear with a maximal water uptake location at the root tip for cases 3 and 4 or at the root collar for cases 1 and 2. It is worth noting that a constant elongation rate means a very small elongation rate to maximal root length ratio. So depending on the maturation rate, the constant elongation case rate is similar to case 2 or 4. This illustrates that plants might control their uptake patterns not only by changing their local conductances (Tardieu et al. 2015) but also by adapting their growth rate.

4.4.6 Sensitivity of a mature root system to hydraulic phenes

Results of one-by-one sensitivity analysis of local hydraulic phenes are plotted in Figure 4.13. In this panel the dashed lines stand for the radial conductivity while the solid lines represent the axial intrinsic conductances. The colour blue indicate the primary roots and the red colour, the laterals. The darker the lines, the younger the zones. We can first notice that hydraulic property relative changes of primaries would not have a big impact on the total RS conductance. Indeed the axial conductivity of mature primaries are high enough to conduct the total amount of water until the collar while their radial conductivity is so low that even if the pressure head drops until the collar would be

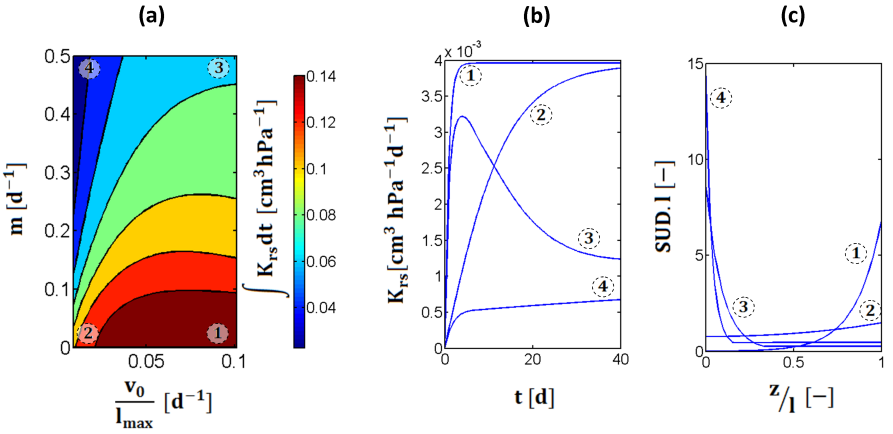


Figure 4.12: Integral of the root conductance over time when changing the elongation rate $\frac{v_0}{l_{max}}$ (x-axis) and the maturation rate m (y-axis) (a). Root hydraulic conductances of the four extreme cases numbered and indicated in (a) as a function of time (b). Relative uptake of the four single roots after 20 days as a function of the relative position to the root tip (l is the root length and z = 0 at the tip) (c).

negligible increasing them the consequent change in conductance would be tiny.

The radial conductivity of young segments of lateral roots will have an important (the biggest) impact on global conductance even though they are not the majority of lateral segments as it can be seen from the left top panel (they constitue only 14% of the lateral root surfaces).

Javot et al. (2003) reviewed the aquaporin expression in roots and its effect on the root hydraulic conductivity. They listed a set of examples demonstrating the possible regulation of the root conductance according to outer stimuli. Using the present model and this sensitivity analysis we can predict the magnitude of a change in local radial conductivity needed to induce a desired modification of the water uptake in a given soil (so far only in homogeneous soil conditions but the present model could and will be coupled in the future with a soil model to simulate transient flow). Another application would be the effect of drought period and its consequent root cells shrinkage leading to a decrease of the soil-root contact and thus of the root radial conductance on macroscopic behaviour (North and Nobel 1991). Finally, the benefits

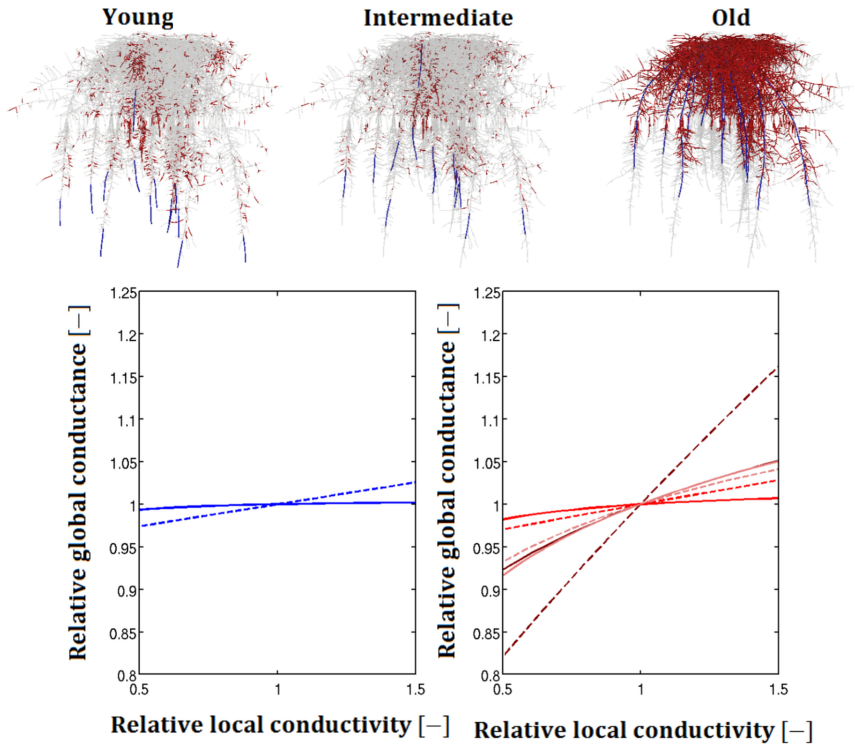


Figure 4.13: Sensitivity analysis of a maize root system the top panels represent a maize root system architecture highlighting the different root zones: young (left), intermediate (center) and old (right) root zones for both primaries (blue) and lateral (red) roots. Bottom subplots show the effect of modifying local radial (dashed) or axial (solid) conductivities of the primary (left) or lateral (right) roots on the RS conductance in a one-by-one sensitivity analysis. The curves are coloured as a function of the segment ages and consequently their hydraulic conductivities: the darker, the younger.

of increasing local xylem vessels (Vercambre 2002) or rise the radial conductivity of certain zones can be predicted using both this approach and/or complete simulations (Leitner et al. 2014). For example from the picture (Figure 4.13) it can readily be seen that increasing axial conductances of both young and intermediate lateral segments would allow raising the RS conductance significantly.

4.5 Conclusion

Six new solutions of the water flow equation in single roots with different hydraulic property distributions are presented in addition to the uniform hydraulic property solution of Landsberg and Fowkes (1978). These novel solutions account for root hydraulic properties that vary as a function of the distance to root tip. When the radial conductivity and the axial conductance change linearly or exponentially alone or in combination along the root axis, analytical solutions of the xylem potential and water flow inside the root were developed. Explicit equations for macroscopic parameters of the corresponding single roots were derived from these analytical solutions. Moreover, they were associated to make complex single roots of changing root hydraulic property profiles as observed in nature or combined with elongation to obtain the root macroscopic parameters and uptake profile as a function of root age, even in heterogeneous soils. These complex functions were not well represented by root of equivalent but constant root hydraulic properties.

This enabled us investigating the effects of root maturation or root tissue development and differentiation on root water uptake. This gave interesting perspectives to evaluate both growth and maturation and their combined effects on root water uptake. We demonstrated how combinations of different maturation and growth functions lead to different strategies of water uptake.

These solutions were also used to revisit optimal root geometrical parameters for water uptake. Indeed, Landsberg and Fowkes (1978) model had been used to define optimal root systems in terms of water uptake subject to minimal carbon cost (Biondini 2008). In contrast to their monotonic behaviour of root water uptake capacity with root length, we demonstrated that local root hydraulic conductivity varying with root length lead to very different behaviours. The root effective conductance may increase with root length more steadily than in case of a uniform root or even decrease with root length. Similarly, the maximal water uptake location was no more located at root proximal end. Non-monotonic root water uptake distributions emerged from the new solutions. Therefore, the search for optimal root systems (ideotypes) should not only focus on root architecture or general averaged root hydraulic properties but also account for variations of root properties

along roots.

The new models can be used to derive local hydraulic properties of roots or be combined as building blocks to generate complete root system hydraulic architectures defining plant genotypes in order to compare plant performances in contrasted environments using soil-root-atmosphere continuum model such as R-SWMS (Javaux et al. 2008). For the latter, first single roots will be associated in root system hydraulic architectures thanks to root growth architectural models. Plant macroscopic parameters will then be derived by combination of root growth and maturation analytical function at the single root scale. The generated root systems will be then tested in contrasted environments through calculated macroscopic parameters and the model of Couvreur et al. (2012) to look for best genotype by environment by management association.

These solutions of the water flow highlight the links between functional or structural traits and the plant behaviours in terms of macroscopic parameters. As analytical solutions, they are exact solutions of the water flow in roots in the sense that they do not contain numerical inaccuracies and they can reliably be used to compare plant behaviours.

4.6 Appendices

Appendix A: New solutions of the root water flow equation

In this appendix, we provide detailed solutions of the water flow equation when the root hydraulic properties are constant (Landsberg and Fowkes 1978) or when they vary linearly or exponentially, alone or together along the root axis. These solutions of the water flow equation 4.4 have been obtained using the symbolic calculation toolbox of Matlab. All solutions are summarized in Table 4.2.

Constant root hydraulic properties

The solution of the water flow equation in a uniform root has been proposed by Landsberg and Fowkes (1978). We present their methodology and principal results in this section to illustrate with the simplest case how to derive the water flow equation solution and the macroscopic parameters.

The simplest root is made of constant root properties: axial conductance k_{x0} [$L^4T^{-1}P^{-1}$] and radial conductivity k_{r0} [$LT^{-1}P^{-1}$]:

$$\begin{cases} k_r(z) = k_{r0} \\ k_x(z) = k_{x0} \end{cases}$$

Equation 4.4 becomes:

$$k_{x0}\frac{d^2\Psi_x(z)}{dz^2} = 2\pi r k_{r0}\left(\Psi_x(z) - \Psi_{soil}\right)$$

The general solution of this differential equation is given in terms of hyperbolic sinus and cosinus:

$$\Psi_x(z) = \Psi_{soil} + c_1 cosh(\tau z) + c_2 sinh(\tau z) \tag{A.1}$$

where we define τ [L^{-1}]:

$$\tau = \sqrt{\frac{2\pi r k_{r0}}{k_{x0}}}$$

Here, the independent functions $f_1(z)$ and $f_2(z)$ are thus $\cosh(\tau z)$ and $\sinh(\tau z)$.

The coefficients are obtained for the bottom no-flux boundary conditions in case of single stretch root (see Appendix C and particularly Eq. C.1):

$$\begin{cases} c_1^{nf} = \frac{\Psi_{collar} - \Psi_{soil}}{cosh(\tau l)} \\ c_2^{nf} = 0 \end{cases}$$

Here and in the following, the superscript nf stands for non-flux. Using these coefficients, we find the general solution of the xylem water potential profile:

$$\Psi_x^{nf}(z) = \Psi_{soil} + (\Psi_{collar} - \Psi_{soil}) \frac{cosh(\tau z)}{cosh(\tau l)}$$

The axial flow is then obtained using Eq. 4.3

$$J_x^{nf}(z) = -\kappa (\Psi_{collar} - \Psi_{soil}) \frac{sinh(\tau z)}{cosh(\tau l)}$$

And the macroscopic parameters are derived thanks to Eq. C.4

$$K_{rs}^{nf}(l) = \kappa tanh(\tau l)$$
$$SUD^{nf}(z) = \tau \frac{cosh(\tau z)}{sinh(\tau l)}$$

where tanh is the hyperbolic tangent and $\kappa\,[L^3T^{-1}P^{-1}]$ is the asymptotic root conductance defined by:

$$\kappa = k_{x0}\tau$$

For the bottom flux boundary condition (see Eq. 4.6), the coefficients are:

$$\begin{cases} c_1 = (\Psi_{proximal,i} - \Psi_{soil}) \left(\frac{\kappa}{\kappa cosh(\tau l_i) + K_{rs,i-1} sinh(\tau l_i)} \right) \\ c_2 = (\Psi_{proximal,i} - \Psi_{soil}) \left(\frac{K_{rs,i-1}}{\kappa cosh(\tau l_i) + K_{rs,i-1} sinh(\tau l_i)} \right) \end{cases}$$

And the solution of the water flow equation in the root becomes:

$$\Psi_x(z) = \Psi_{soil} + (\Psi_{proximal,i} - \Psi_{soil}) \frac{\kappa cosh(\tau z) + K_{rs,i-1} sinh(\tau z)}{\kappa cosh(\tau l_i) + K_{rs,i-1} sinh(\tau l_i)}$$

which leads to the following axial flow:

$$J_x(z) = -\kappa (\Psi_{proximal,i} - \Psi_{soil}) \frac{\kappa sinh(\tau z) + K_{rs,i-1} cosh(\tau z)}{\kappa cosh(\tau l_i) + K_{rs,i-1} sinh(\tau l_i)}$$

The macroscopic parameters become:

$$K_{rs,i}(l_i) = \kappa \left(\frac{\kappa sinh(\tau l_i) + K_{rs,i-1} cosh(\tau l_i)}{\kappa cosh(\tau l_i) + K_{rs,i-1} sinh(\tau l_i)} \right)$$

$$SUD_i(z) = \tau \left(\frac{\kappa cosh(\tau z) + K_{rs,i-1} sinh(\tau z)}{\kappa sinh(\tau l_i) + K_{rs,i-1} cosh(\tau l_i)} \right)$$

The flux boundary solutions are a generalization of the non-flux solutions as they converge towards the same results as $K_{rs,i-1} \to 0$.

Linear root hydraulic property profiles

In case of roots with linear hydraulic property profiles, different cases are distinguished and are investigated successively.

Linear k_r

Equation 4.4 can be solved with different root linear hydraulic property profiles. Let us consider a constant axial conductance and a radial conductivity varying linearly along the root:

$$\begin{cases} k_r(z) = a_0 z + b_0 \\ k_x(z) = k_{x0} \end{cases}$$

where $a_0\,[T^{-1}P^{-1}]$ and $b_0\,[LT^{-1}P^{-1}]$ are shape parameters. Equation 4.4 yields:

$$k_{x0} \frac{d^2 \Psi_x(z)}{dz^2} = 2\pi r (a_0 z + b_0) (\Psi_x(z) - \Psi_{soil})$$

and can be rewritten as:

$$\frac{d^2\Psi_x(z)}{dz^2} = \frac{(az+b)}{k_{x0}}\left(\Psi_x(z) - \Psi_{soil}\right)$$

where we have defined:

$$\begin{cases} a = 2\pi r a_0 \\ b = 2\pi r b_0 \end{cases}$$

with a $[\mathrm{LT^{-1}P^{-1}}]$ and b $[\mathrm{L^2T^{-1}P^{-1}}]$ the revised shape parameters. The general solution of this differential equation is now:

$$\Psi_x(z) = \Psi_{soil} + c_1 Ai\left(\frac{az+b}{a^{\frac{2}{3}}k_{x0}^{\frac{1}{3}}}\right) + c_2 Bi\left(\frac{az+b}{a^{\frac{2}{3}}k_{x0}^{\frac{1}{3}}}\right) \tag{A.2}$$

where c_1 and c_2 can anew be obtained using boundary conditions. Ai and Bi are the Airy functions of the first and second kind, respectively. It is worth noting that we obtain a similar solution if the root radius changes linearly along the root while k_x remains constant.

Linear k_x

If the root axial conductance varies while the radial conductivity is constant, i.e.:

$$\begin{cases} k_r(z) = k_{r0} \\ k_x(z) = c_0 z + d_0 \end{cases}$$

with c_0 $[\mathrm{L^3T^{-1}P^{-1}}]$ and d_0 $[\mathrm{L^4T^{-1}P^{-1}}]$ the shape parameters, the general water flow Eq. 4.4 yields:

$$(c_0 z + d_0)\frac{d^2\Psi_x(z)}{dz^2} + c_0\frac{d\Psi_x(z)}{dz} = 2\pi r k_{r0}\left(\Psi_x(z) - \Psi_{soil}\right)$$

Again we rewrite the equation as:

$$(cz+d)\frac{d^2\Psi_x(z)}{dz^2} + c\frac{d\Psi_x(z)}{dz} = \left(\Psi_x(z) - \Psi_{soil}\right)$$

with the following definitions of the revised shape parameters:

$$\begin{cases} c = \frac{c_0}{2\pi r k_{r0}} \\ d = \frac{d_0}{2\pi r k_{r0}} \end{cases}$$

The units of c and d are [L] and [L^2], respectively. The general solution becomes:

$$\Psi_x(z) = \Psi_{soil} + \sqrt{\frac{2}{c}} \left(c_1 I_0 \left(2\sqrt{\frac{d+cz}{c^2}} \right) + c_2 K_0 \left(2\sqrt{\frac{d+cz}{c^2}} \right) \right) \tag{A.3}$$

I_ν and K_ν are the modified Bessel function of the first and second kind of order ν ($\nu = 0$, here), respectively.

Linear k_r and k_x

We assume now a linear relation between the hydraulic properties and the distance to the tip:

$$\begin{cases} k_r(z) = a_0 z + b_0 \\ k_x(z) = c_0 z + d_0 \end{cases}$$

The water flow equation becomes:

$$(c_0 z + d_0) \frac{d^2 \Psi_x(z)}{dz^2} + c_0 \frac{d\Psi_x(z)}{dz} = 2\pi r (a_0 z + b_0) \left(\Psi_x(z) - \Psi_{soil} \right)$$

After rewriting the parameters it yields:

$$(c_0 z + d_0) \frac{d^2 \Psi_x(z)}{dz^2} + c_0 \frac{d\Psi_x(z)}{dz} = (az + b) \left(\Psi_x(z) - \Psi_{soil} \right)$$

with:

$$\begin{cases} a = 2\pi r a_0 \\ b = 2\pi r b_0 \end{cases}$$

This equation has now the general solution:

$$\Psi_x(z) = \Psi_{soil} + exp\left(-\frac{\sqrt{a}z}{\sqrt{c_0}}\right) \left(c_1 M\left(\frac{\sqrt{a}c_0^{3/2} + bc_0 - ad_0}{2\sqrt{a}c_0^{3/2}}, 1, \frac{2\sqrt{a}(c_0 z + d_0)}{c_0^{3/2}}\right) + c_2 U\left(\frac{-\sqrt{a}c_0^{3/2} - bc_0 + ad_0}{2\sqrt{a}c_0^{3/2}}, 1, \frac{2\sqrt{a}(c_0 z + d_0)}{c_0^{3/2}}\right)\right) \quad (A.4)$$

with M and U the confluent hypergeometric function of the first and second kind, respectively.

Exponential root hydraulic property profiles

Let us finally consider a root whose root hydraulic properties vary exponentially along the root axis:

$$\begin{cases} k_x(z) = \gamma_1 exp(\beta_1 z) \\ k_r(z) = \gamma_2 exp(-\beta_2 z) \end{cases}$$

with $\gamma_1\,[L^4T^{-1}P^{-1}]$, $\beta_1\,[L^{-1}]$, $\gamma_2\,[LT^{-1}P^{-1}]$ and $\beta_2\,[L^{-1}]$ are shape parameters.

The water flow equation becomes:

$$\frac{\partial^2 \Psi_x(z)}{\partial z^2} + \beta_1 \frac{\partial \Psi_x(z)}{\partial z} = \gamma exp\left(-\beta z\right)\left(\Psi_x(z) - \Psi_{soil}\right)$$

with $\gamma = 2\pi r \frac{\gamma_2}{\gamma_1}\,[L^{-2}]$ and $\beta = \beta_1 + \beta_2\,[L^{-1}]$. Solutions of this differential equation are of type:

$$\Psi_x(z) = \Psi_{soil} + \beta^{-\frac{\beta_1}{\beta}} \gamma^{\frac{\beta_1}{2\beta}} \left(exp\left(-\beta z\right)\right)^{\frac{\beta_1}{2\beta}} \left[c_1 \Gamma\left(1 - \frac{\beta_1}{\beta}\right) I_{-\frac{\beta_1}{\beta}}\left(\frac{2\sqrt{exp(-\beta z)\gamma}}{\beta}\right) + c_2 \Gamma\left(1 + \frac{\beta_1}{\beta}\right) I_{\frac{\beta_1}{\beta}}\left(\frac{2\sqrt{exp(-\beta z)\gamma}}{\beta}\right)\right] \quad (A.5)$$

with Γ the gamma function and I_ν, again, the Bessel function of the first kind.

The cases of mixed constant/exponential hydraulic property may be easily solved using the same methodology.

Appendix B: Macroscopic parameters

To calculate the general form of the macroscopic parameters defined as:

$$\begin{cases} K_{rs,i} = \frac{J_x(l_i)}{\Psi_{soil} - \Psi_x(l_i)} \\ SUD_i(z) = \frac{q_r(z)}{J_x(l_i)} \end{cases} \tag{B.1}$$

we need to combine combining Eq. 4.3 and 4.5 with the root stretch boundary conditions 4.6. The two unknowns, $c_{1,i}$ and $c_{2,i}$, are given, in matrix notation, by:

$$\begin{bmatrix} -k_x(l_{i-1})f'_{1,i}(l_{i-1}) & -k_x(l_{i-1})f'_{2,i}(l_{i-1}) \\ f_{1,i}(l_i) & f_{2,i}(l_i) \end{bmatrix} \begin{bmatrix} c_{1,i} \\ c_{2,i} \end{bmatrix} = \begin{bmatrix} J_{i-1} \\ \Psi_{proximal,i} - \Psi_{soil} \end{bmatrix} \tag{B.2}$$

Inverting the system, Eq. B.2 yields:

$$\begin{cases} c_{1,i} = \frac{k_x(l_{i-1})f'_{2,i}(l_{i-1})\left(\Psi_{proximal,i} - \Psi_{soil}\right) + f_{2,i}(l_i)J_{i-1}}{k_x(l_{i-1})\left(f'_{2,i}(l_{i-1})f_{1,i}(l_i) - f'_{1,i}(l_{i-1})f_{2,i}(l_i)\right)} \\ c_{2,i} = \frac{-k_x(l_{i-1})f'_{1,i}(l_{i-1})\left(\Psi_{proximal,i} - \Psi_{soil}\right) - f_{1,i}(l_i)J_{i-1}}{k_x(l_{i-1})\left(f'_{2,i}(l_{i-1})f_1(l_i) - f'_{1,i}(l_{i-1})f_{2,i}(l_i)\right)} \end{cases} \tag{B.3}$$

In homogeneous soil conditions, the proximal flow J_{i-1} may be expressed as the product of the upstream conductance ($K_{rs,i-1}$ root property) by the potential difference between the soil and the proximal xylem water potential of the root stretch:

$$J_{i-1} = K_{rs,i-1}\left(\Psi_{soil} - \Psi_x(l_{i-1})\right) = -K_{rs,i-1}\left(c_{1,i}f_{1,i}(l_{i-1}) + c_{2,i}f_{2,i}(l_{i-1})\right) \tag{B.4}$$

Substituting Eq. B.4 in Eq. B.3 for the i^{th} stretch, we obtain a set of two equations with two unknowns which after solving for $c_{1,i}$ and $c_{2,i}$ gives:

$$\begin{cases} c_{1,i} = \frac{\left(\Psi_{proximal,i} - \Psi_{soil}\right)\left(-K_{rs,i-1}f_{2,i}(l_{i-1}) + f'_{2,i}(l_{i-1})k_x(l_{i-1})\right)}{K_{rs,i-1}f_{1,i}(l_{i-1})f_{2,i}(l_i) - K_{rs,i-1}f_{1,i}(l_i)f_{2,i}(l_{i-1}) - f'_{1,i}(l_{i-1})f_{2,i}(l_i)k_x(l_{i-1}) + f_{1,i}(l_i)f'_{2,i}(l_{i-1})k_x(l_{i-1})} \\ c_{2,i} = \frac{\left(\Psi_{proximal,i-1} - \Psi_{soil}\right)\left(K_{rs,i-1}f_{1,i}(l_{i-1}) - f'_{1,i}(l_{i-1})k_x(l_{i-1})\right)}{K_{rs,i-1}f_{1,i}(l_{i-1})f_{2,i}(l_i) - K_{rs,i-1}f_{1,i}(l_i)f_{2,i}(l_{i-1}) - f'_{1,i}(l_{i-1})f_{2,i}(l_i)k_x(l_{i-1}) + f_{1,i}(l_i)f'_{2,i}(l_{i-1})k_x(l_{i-1})} \end{cases} \tag{B.5}$$

It is important to mention that these coefficients only depend on the properties of the distal stretches to the stretch of interest and on the effective conductivity that lumps the properties and their spatial variation in all distal stretches. Combining the coefficients B.5, the definitions of the macroscopic parameters B.1 and the general solutions 4.5, 4.2 and 4.3, the root system conductance and the standard uptake density after addition of i stretches become:

$$\begin{cases} K_{rs,i} = k_x(l_i)\frac{\left(-K_{rs,i-1}f_{2,i}(l_{i-1})+f'_{2,i}(l_{i-1})k_x(l_{i-1})\right)f'_{1,i}(l_i)+\left(K_{rs,i-1}f_{1,i}(l_{i-1})-f'_{1,i}(l_{i-1})k_x(l_{i-1})\right)f'_{2,i}(l_i)}{K_{rs,i-1}f_{1,i}(l_{i-1})f_{2,i}(l_i)-K_{rs,i-1}f_{1,i}(l_i)f_{2,i}(l_{i-1})-f'_{1,i}(l_{i-1})f_{2,i}(l_i)k_x(l_{i-1})+f_{1,i}(l_i)f'_{2,i}(l_{i-1})k_x(l_{i-1})} \\ SUD_i(z) = \frac{2\pi r k_r(z)}{k_x(l_i)}\frac{\left(-K_{rs,i-1}f_{2,i}(l_{i-1})+f'_{2,i}(l_{i-1})k_x(l_{i-1})\right)f_{1,i}(z)+\left(K_{rs,i-1}f_{1,i}(l_{i-1})-f'_{1,i}(l_{i-1})k_x(l_{i-1})\right)f_{2,i}(z)}{\left(-K_{rs,i-1}f_{2,i}(l_{i-1})+f'_{2,i}(l_{i-1})k_x(l_{i-1})\right)f'_{1,i}(l_i)+\left(K_{rs,i-1}f_{1,i}(l_{i-1})-f'_{1,i}(l_{i-1})k_x(l_{i-1})\right)f'_{2,i}(l_i)} \end{cases} \tag{B.6}$$

Appendix C: Special case of a single-stretched root

If the root system consist in a single stretch, the distal boundary condition is no-flux and the proximal boundary conditions corresponds to the root collar water potential Ψ_{collar} [P]. l_1 is equivalent to l. Mathematically, the boundary conditions become:

$$\begin{cases} J_x(0) = 0 \\ \Psi_x(l) = \Psi_{collar} \end{cases} \tag{C.1}$$

The boundary conditions C.1 used in case of a root made of a single stretch can be rewritten as:

$$\begin{bmatrix} -k_x(0)f_1'(0) & -k_x(0)f_2'(0) \\ f_1(l) & f_2(l) \end{bmatrix} \begin{bmatrix} c_1^{nf} \\ c_2^{nf} \end{bmatrix} = \begin{bmatrix} 0 \\ \Psi_{collar} - \Psi_{soil} \end{bmatrix} \tag{C.2}$$

As in Appendix A, the superscript nf means no-flux bottom boundary condition. It is used when the root is made of only one stretch. Inverting the matrix we obtain the constants:

$$\begin{cases} c_1^{nf} = \frac{f_2'(0)(\Psi_{collar} - \Psi_{soil})}{f_2'(0)f_1(l) - f_1'(0)f_2(l)} \\ c_2^{nf} = \frac{-f_1'(0)(\Psi_{collar} - \Psi_{soil})}{f_2'(0)f_1(l) - f_1'(0)f_2(l)} \end{cases} \tag{C.3}$$

The 'non-flux' coefficients C.3 are actually a particular case of the 'flux' coefficients B.5 since the latter tend to the former as $K_{rs,i-1} \to 0$ (or $J_{i-1} \to 0$).

The macroscopic parameters of the single-stretch root are finally given by (using the no-flux coefficients C.3 or equivalently evaluating Eq. B.6 with $K_{rs,i-1} = 0$):

$$\begin{cases} K_{rs}^{nf} = k_x(l) \left(\frac{f_2'(0)f_1'(l) - f_1'(0)f_2'(l)}{f_2'(0)f_1(l) - f_1'(0)f_2(l)} \right) \\ SUD^{nf}(z) = \frac{2\pi r k_r(z)}{k_x(l)} \left(\frac{f_2'(0)f_1(z) - f_1'(0)f_2(0)}{f_2'(0)f_1'(l) - f_1'(0)f_2'(l)} \right) \end{cases} \tag{C.4}$$

Appendix D: Stretch lengths in heterogeneous roots

Let us consider a growing single root with an initial elongation rate v_0 [LT^{-1}] and a maximal length l_{max} [L]. Its actual elongation rate v(t) [LT^{-1}] is given, as in Pagès et al. (2004), at any time t [T] by:

$$v(t) = v_0 exp\left(\frac{-v_0}{l_{max}}t\right) \tag{D.1}$$

Integrating Eq. D.1 between 0 and time t, we obtain the actual root length l [L]:

$$l(t) = \int_0^t v(t')dt' = l_{max}\left[1 - exp\left(\frac{-v_0}{l_{max}}t\right)\right] \tag{D.2}$$

In the case of the root made of one stretch, the root length can be easily substituted by Eq. D.2 to obtain the macroscopic parameters as a function of time instead of root length. If the root is split in distinct stretches, as we substitute l by t, we need to replace the transition positions by transition ages. An equation of the different root stretch lengths $stretch_i$(t) [L] is required (we use the indices i to indicate the zones from the tip to the collar).

Inverting Eq. D.2, the root age age(z, t) [T] at any distance z to the root tip z and at any time t yields:

$$age(z,t) = t + \frac{l_{max}}{v_0} ln\left(\frac{z}{l_{max}} + exp\left(\frac{-v_0}{l_{max}}t\right)\right), \forall z \in [0\ l(t)] \tag{D.3}$$

Equation D.3 is then used to derive the macroscopic parameters and the water flow equation solution of a single root as a function of age or when the root hydraulic properties are defined as a function of time instead of as a function of the distance to the tip. We can also calculate the stretch lengths, $stretch_i$. When the root is older than any transition age (called hereafter age_i[t]), it is simply the length differences between two successive transition ages. When the root is younger, then either

the root zone length is zero (if the young transition age is not reached yet) or growing limited by the total root length:

$$stretch_i(t) = \begin{cases} 0, t < age_i \\ l_{max}\left(1 - exp\left(\frac{-v_0}{l_{max}}(t - age_i)\right)\right), t \geqslant age_i \text{ and } t \leqslant age_{i+1} \\ l_{max}\left(exp\left(-\frac{v_0}{l_{max}}(t - age_{i+1})\right) - exp\left(-\frac{v_0}{l_{max}}(t - age_i)\right)\right), t > age_{i+1} \end{cases} \tag{D.4}$$

Appendix E: Use of the analytical solutions to verify numerical models

One of the main advantages of analytical solutions is their possible use to verify the accuracy of numerical algorithms. All the developed solutions should be asymptotic solutions provided by numerical algorithms for infinitely small root segments. In fig. 4.14, we show how we tested the numerical accuracy of Doussan et al. (1998a)'s algorithm for single root with varying hydraulic properties. In the illustrated case, exponential radial and axial hydraulic functions are chosen for a single root that is 10 cm long. The analytical solution is the solid black line, while blue lines are numerical solution for smaller and smaller root segments (darker and darker blue).

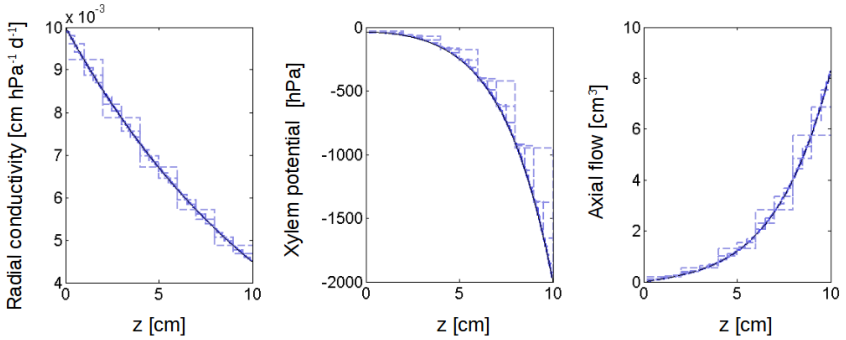


Figure 4.14: Numerical approximation (blue dashed line) *vs* analytical solution (dark solid line). The smaller the segment size, the better the numerical accuracy.

As the root segment size decreases, the numerical solution tends towards the analytical solution in terms of both xylem potential and axial flow.

TOWARDS FULLY IMPLICIT MAIZE ROOT SYSTEM HYDRAULIC ARCHITECTURE

5

This chapter is the current version of a manuscript in preparation entitled:

> Meunier F., Lobet G., Draye X. and Javaux M. MARSHAL: towards fully implicit maize root system hydraulic architecture

---

Abstract

Existing literature about maize root system hydraulic and architectural properties is abundant and could serve as input for contrasted root system hydraulic architecture generation such as CRootBox. To so so, root hydraulic and architectural observations in field and/or laboratory experiments should be converted into parameters for feeding root growth model and water flow algorithms. We describe here MARSHAL, a new tool that couples a fast and efficient root growth model, CRootBox, improved (see Chapter 3) water flow algorithms of Doussan et al. (1998a) and plant-scale parameter calculation method of Couvreur et al. (2012). Existing maize root system architecture parametrizations as well as measured hydraulic functions were gathered as well in a common database.

MARSHAL is an online and flexible tool that generates contrasted root system hydraulic architectures, calculates the water flow within the root system under user-provided boundary conditions (transpiration and soil water potential distribution) and saves the plant-scale macroscopic parameters. The generated root systems hydraulic architectures can be saved in common formats such as RSML (Lobet et al. 2015b) to

be easily used in other models. Finally, MARSHAL is also coupled with sensitivity and optimization algorithms in order to investigate the sensitive input parameters for a used-defined objective function or to provide an optimal set of parameters that minimize an error function, alongside with parameter uncertainty.

As illustration of the model's potentiality, we used MARSHAL to generate maize contrasted hydraulic architectures and we compared them with plant-scale observations of both architecture (root length density profile field measurements) and hydraulics (root system conductance direct measurements). The macroscopic parameters could be fitted with the model and the observed local variability of root phenes. We also calculated the sensitivity of mature root system conductance, depth of standard uptake, volume and convex hull volume to the input parameters. Finally, MARSHAL served to validate a purely analytical model of the root system hydraulic architecture that is described here-below.

Regarding the root system morphology and the nomenclature of the different root types, we used the same definitions as Hauck et al. (2015). Similarly to the observations of Hochholdinger et al. (2004), the maize root system development is divided into two stages (embryonic and post-embryonic growth). The former is constituted by the root primary and seminal roots emerging from the seed alongside with their laterals. The post-embryonic root system starts developing around 1 week after the emergence of the primary and seminal roots and becomes prominent approximatively 2 weeks after seed germination. It is made of crown roots, shoot-borne roots that develop from nodes below the soil surface and brace roots, shoot-borne roots developing from nodes above the soil surface several weeks later as the plant matures. These two types of roots also exhibit lateral branching, although the brace roots will not branch until they penetrate the soil. This nomenclature was consistently kept throughout the whole manuscript.

5.1 Introduction

Drought in agriculture represents the most significant abiotic stress worldwide and maintaining yield under dry conditions is one of the major challenges of plant breeding (Cattivelli et al. 2008). To do so, breeders have been looking for decades for ideal structural and functional plant phene states which would allow cultivars to avoid or resist drought stress episodes (Mir et al. 2012). Because of their key-role in water uptake and transfer to aerial parts but also thanks to their wide variability and high regulation level, root systems are excellent candidates for contributing in such a task (Wasson et al. 2012). Several authors, such as Lynch (2013) for maize, or Comas et al. (2013) for wheat, suggested that a specific combination of optimal phene states would lead to plant species ideotype for water uptake, i.e. a plant model which is expected to yield a greater quantity or quality of products when developed as a cultivar (Donald 1968).

However, many traits conferring drought tolerance present dual effects: positive in a range of scenarios and negative under different circumstances (Tardieu 2012). According to the pedo-climatic conditions, the effects associated with positive traits may be consolidated or disappear (Leitner et al. 2014). Deciphering genotype by environment by management interaction is therefore critical to breed new drought-tolerant cultivars (Chaves and Davies 2010). In addition, many traits are studied alone and it is not always clear where combinations of potentially positive traits would lead to or whether such a combination is even genetically feasible.

To clarify the picture, functional-structural models of the water flow in soil-plant-atmosphere continuum have a crucial role to play. Because they can investiate the behavior of any desired combination of plant traits (even unrealistic) within any environmental condition (even not currently existing), they are a perfect tool for virtual breeding (Chapman 2008). They also allow one to highlight mechanisms, regulation rules and feedbacks that dramatically contribute to plant transpiration and ultimately performance (Huber et al. 2015). Finally models enable one to cross scales and to predict the impact of deterministic relations, observed and valid on short timescales, on the overall relations within a system in given pedo-climatic conditions (Hammer et al. 2009).

Existing root growth models are numerous in the current literature (see (Dunbabin et al. 2013) for a review or (Pagès et al. 2004; Schnepf et al. 2017) for examples). They have been already parametrized for several species thanks to various architectural observations of root systems in laboratory or field experiments. Nowadays models are also able to accurately simulate water flow in any root system hydraulic architectures (RSHA) with existing water flow algorithms provided that root hydraulic property distribution is accurately characterized (see Chapter 3). Water uptake distribution of the generated root system hydraulic architectures can be simulated in three dimensional heterogeneous soils using coupled model of the water flow in the soil-plant-atmosphere continuum. R-SWMS (Javaux et al. 2008), for example, uses as input root system architecture generated by root growth model coupled with hydraulic property functions experimentally measured or found in the literature.

Unfortunately, the heavy computational load and the high time requirement for running a single simulation in 3D explicit numerical models does not allow currently such models to be used in routines to predict genotype performance in contrasted pedo-climatic conditions. However, recently, fast and simple approaches for solving root water uptake equations arose (Couvreur et al. 2012). They describe the root system no more as a complex ensemble of local root traits but rather by a reduced number of plant-scale parameters that determine their behavior in terms of water uptake with satisfactory accuracy (Couvreur et al. 2012).

Glued together, root growth models, water flow equation resolution algorithm and macroscopic representation of root systems would allow generating contrasted root system hydraulic architecture, parametrized for different crop species, that could be used, in turn, in coupled soil-plant models for water uptake performance forecasting. In Chapter 4, we have developed analytical solutions to solve the water flow equations in root branches. How to extend this on a full, evolving root architecture is however still missing.

The first objective of this study is thus to develop and validate a fully analytical methodology tool able to generate contrasted maize root system hydraulic architecture estimates and their corresponding macroscopic parameters. To do so, we first develop analytical solutions

to estimate root architectural evolutions based on simple input root architectural models. Then we coupled our analytical solutions for water flow with the analytical estimate of the root architecture to predict plant scale parameters related with hydraulics (root system conductance, standard uptake fraction) and root system geometry (total root system volume, convex hull). A second objective is then to use this methodology to investigate how local root hydraulic and architectural parameters control macroscopic plant parameters.

Maize was chosen as illustrative crop species because of the abundant literature about its architectural and hydraulic properties. In addition, it is a widely spread crop species that does not have to prove its agronomic relevance. However, the flexibility of the model makes it suitable for any crop species as soon as information is available about its hydraulic architecture.

This new methodology is implemented together with a traditional numerical model within a new sofware called MARSHAL, which combines a root growth model, namely CRootBox (Schnepf et al. 2017), the water flow equation resolution algorithm of Doussan et al. (1998a), including the analytical solution of Landsberg and Fowkes (1978) extended for a whole root system (see Chapter 3) and the macroscopic approach of Couvreur et al. (2012). It generates maize realistic root system hydraulic architectures that can be compared with functional or structural observations of maize root systems. Outputs (generated hydraulic architectures) are exportable in common formats in order to serve as inputs in other modeling tools. MARSHAL was also coupled to global sensitivity and optimization algorithms. Use of MARSHAL in combination with such powerful inverse methods leads to the identification of sensitive parameters for specific output variables or optimal set of parameters for a given objective function, as illustrated in this study.

5.2 Theory: towards a complete RSHA analytical model

In this section, we explain the steps to build a purely analytical root system hydraulic architectural model. We first detail how to derive an

estimated root system architecture (section 5.2.1), then we describe how we derive macroscopic parameters for the whole root system (sections 5.2.2 and 5.2.3). The principal root parameters are described in Fig. 5.1 and will be explained throughout the theory and material and methods sections.

We consider that the maize root system is made of first order axes (primary + seminal taken together, crown and brace roots) that have specific root architectural and hydraulic properties (defined by root type) and that bear regularly spaced laterals. We only consider two root orders in this study: main axes and lateral roots. However in total, we have more root types since primaries can be seminal, crown or brace root and lateral can be short or long (see below).

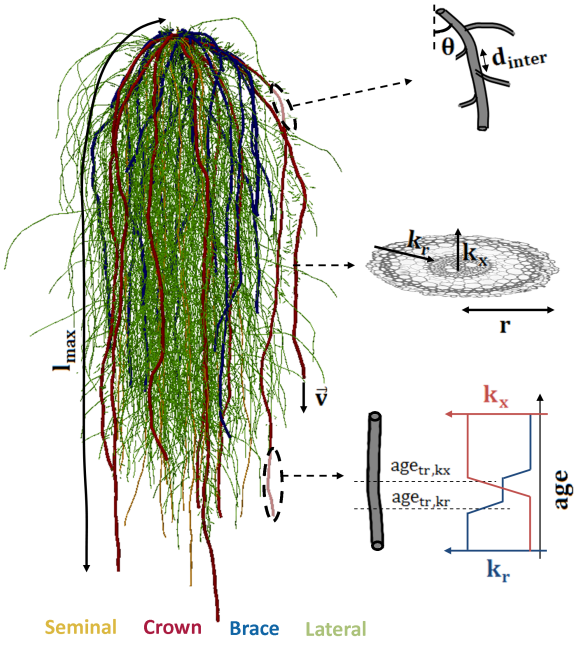


Figure 5.1: Maize mature root systems and the architectural and hydraulic parameters

5.2.1 Analytical estimate of root system architecture

Growing root

Root elongation rate v(t) [LT^{-1}] according to Pagès et al. (2004) is given by:

$$v(t) = v_0 exp\left(\frac{-v_0}{l_{max}}t\right) \tag{5.1}$$

with v_0 [LT^{-1}] and l_{max} [L] the initial elongation rate and the maximal root length, respectively. Let us note that if the maximal root length is very large, then the elongation rate is almost constant ($v(t) \simeq v_0$).

Integrating equation (5.1) between 0 and t we obtain the actual root length l [L]:

$$l(t) = \int_0^t v(t')dt' = l_{max}\left[1 - exp\left(\frac{-v_0}{l_{max}}t\right)\right] \tag{5.2}$$

If the root is split in age classes, their lengths is given (we use the subscripts i to indicate the zone from the tip to the collar, see Chapter 4 for details):

$$\begin{aligned}
Zone_0(t) &= l(t) - l_{max}\left[1 - exp\left(\tfrac{v_0}{l_{max}}(age_0 - t)\right)\right] \\
Zone_1(t) &= l_{max}\left[exp\left(\tfrac{v_0}{l_{max}}(age_1 - t)\right) - exp\left(\tfrac{v_0}{l_{max}}(age_0 - t)\right)\right] \\
Zone_2(t) &= ...
\end{aligned}$$

with age_i [T] the transition ages (root properties are assumed to be homogeneous within a certain age class).

Primary root with laterals

We consider now a growing primary root on which laterals can appear and grow. The total primary length l is given by equation (5.2). If the interbranching distance d_{inter} [L] is constant, the number of laterals N_{lat} [-] is given by:

$$N_{lat}(t) = \frac{l}{d_{inter}} - 1 = \frac{l_{max}}{d_{inter}}\left[1 - exp\left(\frac{-v_0}{l_{max}}t\right)\right] - 1$$

Their ages $\mathrm{Age_{lat}}$ [T] are also easily obtained:

$$Age_{lat}(t) = t + \frac{L_{max}}{v_0} ln\left(1 - \frac{d_{inter}}{l_{max}}\left[1 : N_{lat}\right]\right)$$

And finally their length $\mathrm{l_{lat}}$ [L] can be calculated at any time:

$$l_{lat}(t) = L_{max,lat}\left[1 - exp\left(\frac{-v_{0,lat}}{l_{max,lat}} Age_{lat}(t)\right)\right] \tag{5.3}$$

with $\mathrm{v_{0,lat}}$ [$\mathrm{LT^{-1}}$] and $\mathrm{l_{max,lat}}$ [L] the initial elongation rate and maximal length of the laterals, respectively. As we restrict at two root orders in this study, equations 5.2 and 5.3 allow one to get the length of any root at any time.

Growth direction

The root tip position depends on root tropisms and elongation rates. In CRootBox, the expected angular change in root tip heading because of root gravitropism per unit length is δ [$\mathrm{L^{-1}}$] (see next section). The insertion angle θ(t) [-], changes with time and is then given by, if the elongation rate is constant:

$$\theta(t) = \theta_0 - v_0 \delta t$$

with θ_0 [-] the initial insertion angle. For a root whose initial position is [0,0,0], in the XZ plane (z is positive upwards), the root tip position X(t) is given at any time by:

$$X(t) = \frac{1}{\delta}\left[cos\left(\theta_0 - v_0\delta t\right) - cos\left(\theta_0\right), 0, -sin\left(\theta_0\right) + sin\left(\theta_0 - v_0\delta t\right)\right] \tag{5.4}$$

Now if the insertion angle is constant with time:

$$\theta(t) = \theta_0$$

The root tip position is simply given by:

$$X(t) = \left[l(t) sin\left(\theta_0\right), 0, -l(t) cos\left(\theta_0\right)\right] \tag{5.5}$$

with equations 5.4 and 5.5, we have two asymptotic solutions with constant elongation rate (and gravitropism) and constant insertion angle (and changing elongation rates). The former is used for primary axes whose elongation rates are usually larger and maximal length important and the latter is applied for lateral whose small length does not impact too much their vertical position in space.

5.2.2 Analytical estimate of macrosocpic parameters

As it was done in Chapter 4, the root system total conductance is given by the sum over all primary axes, N_I [-] of their respective conductance K_{rsI} [$L^3T^{-1}P^{-1}$].

$$K_{rs}(t) = \sum_{i=1}^{N_I} K_{rsI,i}(t)$$

The root primary conductances are calculated by summing up all lateral conductances if there is no xylem limitation or by the methodology developed by Meunier et al. (2017) in case of xylem limitation.

Similarly in case of high xylem conductances (see Chapter 3 for discussion about optimal radial to axial conductivity ratio), the root standard uptake fraction SUF_{root} [-] (the standard fraction of water taken up by a specific root) is simply obtained by dividing root conductances K_{root} $L^3T^{-1}P^{-1}$] by the root system conductance K_{rs} $L^3T^{-1}P^{-1}$]:

$$SUF_{root} = \frac{K_{root}}{K_{rs}}$$

if the xylem limits the water flow, we must anew use the equations of Meunier et al. (2017) for calculating root standard uptake fractions.

5.2.3 Analytical estimate of macroscopic geometric factors

The total root system V_{RS} [L^3], proxy of the carbon spent in the root system, is given by the sum over all roots, mathematically:

$$V_{rs}(t) = \sum_{i=1}^{N_{order}} \sum_{j=1}^{N_i} \pi r_i^2 l_{ij}(t)$$

where N_{order} [−] is the number of root orders, N_i [−] is the number of roots of order i, r_i [L] is the root order i radius and l_{ij} [L] is the length of root j of order i. We can also calculate the root exploration volume based on the convex hull $V_{convexhull}$ [L^3] determined by the estimated position of all root tips.

5.3 Material and methods

5.3.1 MARSHAL: a online tool to generate RSHA

Numerical model for root architecture

The root growth model we use is CRootBox. Its main parameters and processes are explained hereafter. For a more detailed description, see Schnepf et al. (2017). CRootBox considers several root types. For each root, we consider three zones: the basal zone lb at the base of the root, the branching zone, and the apical zone l_a at the end of the root (Fig. 5.2, left). After the basal and apical zones have developed their lengths stay constant during root growth, while the branching zone develops. New lateral roots are only created within the branching zone with the inter-spaces d_{inter}.

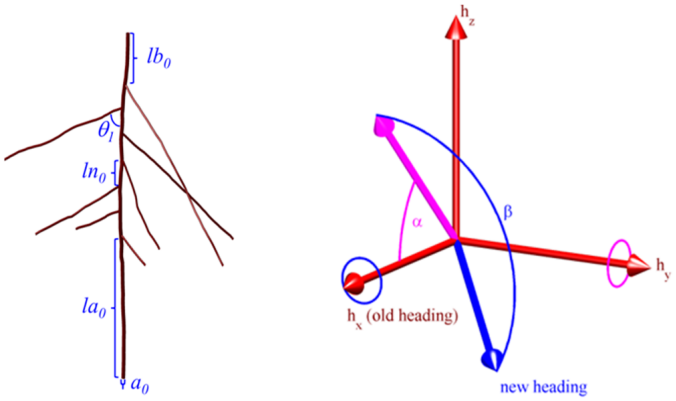


Figure 5.2: Root growth parameters of the RootBox model (left) and change of root tip heading due to two random angles α and β (right)

The maximal root length is calculated for each individual root by

$$L_{max} = l_b + l_a + d_{inter}(n_{ob} - 1) \tag{5.6}$$

where n_{ob} is the maximal number of lateral branches. New lateral roots are initiated with an insertion angle θ which describes the angle between the parent root and the initial direction of the new lateral root. Each root has a constant radius r.

Therefore, we describe each root type in a specific soil by seven parameters: l_a [L], l_b [L], d_{inter} [L], n_{ob} [-], v_0 [LT^{-1}], θ [L^3L^{-3}] and r [L]. To add randomness to this deterministic approach each parameter is given by its mean value and its standard deviation.

Additionally, we describe random changes in direction during root tip elongation by randomly choosing two angles (Fig. 5.2, right). First, we choose the angle α, which describes the angle between current and new root tip heading by a rotation around the local axis (h_y). The angle α is a random number and normally distributed with a mean of 0 and a standard deviation of δ per root length. Thus, the expected angular change in root tip heading per unit length is δ . Second, we choose the radial angle β uniformly distributed between 0 and 2π , which rotates the root tip heading around the local axis (h_x).

To describe root growth towards a preferential direction, we randomly calculate N pairs of angles (α, β) and then choose the most suitable pair regarding to an objective function. N is the number of trials to find optimal values for α and β, the larger N, the more likely the root will grow in the preferred direction. The objective function is dependent on the type of tropism: for gravitropism headings into the z-direction are favoured, for exotropism headings into the initial direction, and for hydrotropism headings towards higher water content. Therefore, tropism is modelled by three parameters for each root type: δ [L^{-1}], N [-], and type [-].

The main root axes of the maize plant can be implemented as crown or brace roots that start to grow after predefined times and predefined depths (z-position on the stem). The parameters for the initiation times are called $t_{0,1}$ to $t_{0,M}$, and the predefined depths are given by the z-coordinates z_1 to z_M, where M is the maximal number of main root axes. The root axes are initiated at a predefined angle θ_0 .

Five root types are considered for maize root systems: primary and seminal (order = 1), short and long laterals (order = 2 and 3, respectively), crown (order = 4) and brace (order = 5) roots. To differenciate architectural parameters that are order dependent, we used subscript i that consequently varies between 1 and 5. Maize parametrizations already exist for maize in CRootBox and are therefore available for root system architecture generation. Moreover, Lynch (2013) reviewed ranges of variations of most of the architectural parameters and are included as input variability ranges in the model.

Maize hydraulic model and parameters

The water flow model included in MARSHAL is the water flow algorithm developed by Doussan et al. (1998a) and improved by ourselves including an analytical solution of the water flow at the segment scale (see Chapter 3). In summary, it solves the water flow equations in a given hydraulic architecture when boundary conditions (i.e. plant transpiration and water potential at any soil-root interface position).

As stated in Chapter 3, the solution of the water flow equation is numerically solved by:

$$\boldsymbol{\Psi_{x0}} = \boldsymbol{a^{-1}.b} \tag{5.7}$$

where **a** [N x N] and **b** [N x 1] are constructed based on the root system architecture generated by CRootBox and the hydraulic properties that are genotype dependent. **b** contains the top-boundary condition, i.e. the plant collar potential Ψ_{collar} (or plant transpiration), and the soil-root interface water potentials while **a** contains the segment connections and their hydraulic properties.

$\boldsymbol{\Psi_{x0}}$ is a vector containing water potential everywhere within the root system hydraulic architecture and is the solution of the water flow equations. This allows MARSHAL to calculate the root water uptake distribution and the axial flow everywhere within the root system as explained in previous Chapters.

Several studies measured hydraulic axial and radial conductivites for different maize root types at different ages and for different genotypes. We gathered all this information in a common database and we define the genetic range of variation of axial and radial hydraulic per root

type as extreme values. Root properties used as reference were the ones obtained by Doussan et al. (1998b).

Macroscopic parameters

Solving the water flow in homogeneous soil conditions lead to the macroscopic parameters of Couvreur et al. (2012) model, i.e. the root system total conductance K_{rs} and the Standard Uptake Fraction **SUF**. The numerical calculation of these plant-scale parameters are achieved by solving Equations 5.7 under conditions of uniform water potential at soil-root interfaces, i.e. Ψ_{seq} (fixed), which provides local inflow $\mathbf{J_r}$ and total plant transpiration T_{act} under constant collar potential. They are then calculated as:

$$K_{rs} = \frac{T_{act}}{\Psi_{seq} - \Psi_{collar}} \tag{5.8}$$

$$\boldsymbol{SUF} = \frac{\boldsymbol{J_r}}{T_{act}} \tag{5.9}$$

Summary and online application

A summary of MARSHAL's capacity is shown in Fig. 5.3. Reference maize root system hydraulic architectures are generated using literature hydraulic and architectural parameters. The latter can be modified and resulting hydraulic architectures are visible simultaneously. Hydraulic and architectural parameter modifications affect the water uptake spatial distribution and water flow within the root system, which may also be seen from 3D plot of the root system hydraulic architecture or z-averaged profiles of water flow. Finally the soil-root interface water potential profile may also be changed to assess the impact of local soil water content heterogeneity on root water uptake distribution. Equation (5.7) is then solved under heterogeneous soil conditions.

Other statistics such as root length density, macroscopic parameters or total root length and surface are also plotted and can be exported. MARSHAL also saves previous simulations and historical changes can be recorded. When a root system hydraulic architecture is suitable for the user, he can easily export it in a common format, e.g. RSML or

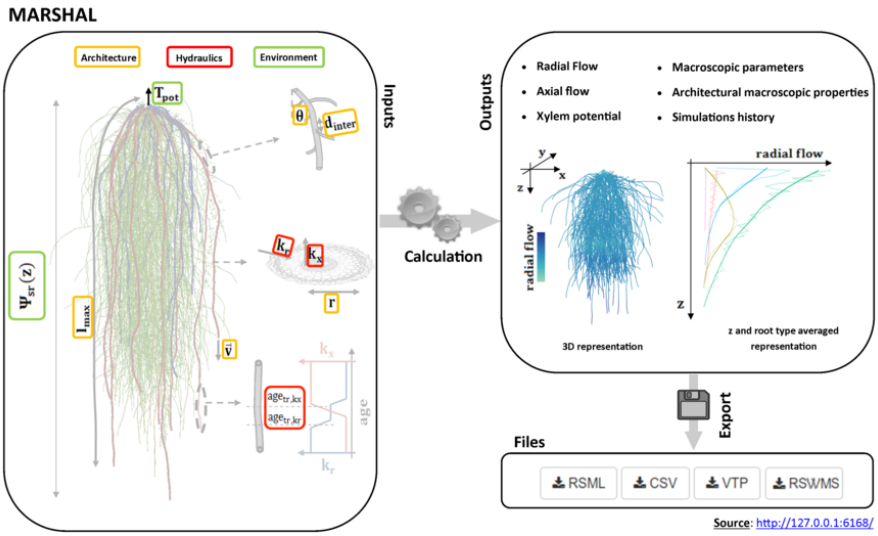


Figure 5.3: MARSHAL online application: input parameters to be changed (left), available outputs (top right) and export formatss (bottom right). Coloured boxes indicate the parameters that can be changed according to their type (environmental, hydraulic or architectural)

R-SWMS input files, for example to simulate simultaneous water flow and root system growth and development in a specific pedo-climatic situation.

MARSHAL will be available online soon (currently in alpha-version) and is written in R. It runs CRootBox (written in C), calculates local hydraulic properties of the root segments, solves (5.7)-(5.9) to calculate macroscopic parameters and local flow under homogeneous or heterogeneous soil potential distribution.

5.3.2 Model cross-validation

In the two previous Chapter, analytical solutions of macroscopic properties were derived for ideal cases: single root with or without changes of radial and axial conductivity and root with regurlaly spaced laterals. These relations are deterministic while parameters for root system hydraulic architecture generation are probabilistic. The purely analytical solution developed in section 5.2 are based on a estimated root system

architecture while numerical approaches generate explicit root system architectures. The analytical model estimates root system architectures at any time, the total root number by order and their ages and uses analytical solution to calculate single root conductances K_{root} $[L^3T^{-1}P^{-1}]$. The numerical model explicitely generates root system hydraulic architecture, builds connection matrixes and solves the linear system of equations. In a second step, both models calculate macroscopic parameters based on analytical or numerical solutions, respectively. MARSHAL can make the link between both approaches, which are schematically represented in Figure 5.4.

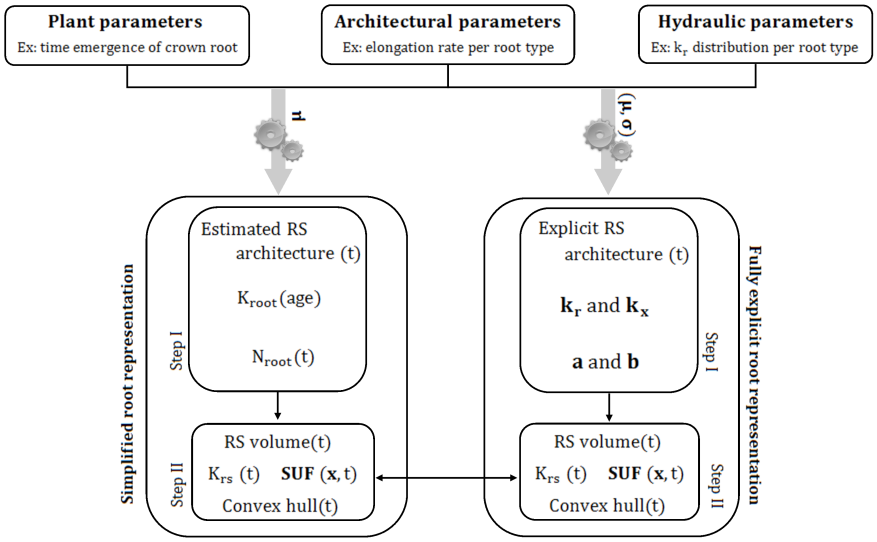


Figure 5.4: Analytical *vs* numerical approaches. μ and σ stand for the mean and standard deviations of the parameters, respectively.

We illustrate this statement by calculating analytically the root system conductance of maize root system over a full crop cycle generated by MARSHAL. Hydraulic and architectural parameter standard deviations were progressively increased until they reached 100% of the mean parameter values. Predictions of the analytical model were then confronted to numerical solutions of the resulting root systems.

5.3.3 Model applications

Meta-analysis

The analytical and numerical approaches can be used for comparison with field or laboratory observations to confront local root phene state variability and macroscopic parameters - hydraulic, architectural or combination of both using meta-analysis. First we show how local architectural property parameters can be used for root system architecture generation and comparison with root length density profile observations.

10 000 root system architectures were generated using MARSHAL in the architectural parametric space reviewed by Lynch (2013) with a relative standard deviation of 10%. For each model realization, an objective function was calculated to compare with field observations of root length density profiles at different times t and different distances to the stem x, achieved by Gao et al. (2010) for sole maize plots. Mathematically, the objective function OF was the RMSE of observed $\mathrm{RLD_{obs}}$ and simulated RLD root length density profiles:

$$OF = \sqrt{\frac{\left(RLD(x,t) - RLD_{obs}(x,t)\right)^2}{N}} \tag{5.10}$$

with N the number of observations. The generated root systems were then sorted according to their performance (root length densities) and the eight best simulations were set aside. For all realizations, we also calculated the macroscopic parameters of Couvreur et al. (2012)'s model using the analytical approach described above and root hydraulic properties provided by Doussan et al. (1998b), considered here as fixed (they did not vary between model realizations).

In a second example, we reviewed the literature to collect all maize complete root system conductance measurements and corresponding approximative ages of the root systems. The analytical approach was run to generate 10 000 root system estimates using the complete hydraulic and architectural parametric space to compare observed variability of observations *vs* variability of generated root system conductances based on ensemble of observed local root phenes.

Quantifying group of phene states

To illustrate the potential interest of coupling MARSHAL (or the analytical solutions) with sensitivity analysis algorithms, we also generated 100 000 root systems thanks to MARSHAL and we used the global sensitivity algorithm of Cannavo (Cannavó 2012) to compute model macroscopic parameters sensitivity to local root phenes. The plant-scale parameters are the root system conductance, the depth of standard uptake defined as $z_{SUF} = \sum_{i=1}^{N_{seg}} SUF_i.z_i$, the root system volume and the convex hull, all calculated 60 days after sowing. In these sensitivity analyses, parameters were allowed to vary $\pm 50\%$ of their reference values.

The explanatory local root phenes were then gathered by parameter family (either hydraulic or architectural) at the exception of the convex hull and the root system volumes that are function of architectural parameters, only. They were then assembled according to their corresponding root type or parameter type.

In order to know the direction of change and the significance of phene states, multilinear regression algorithms were applied to the macroscopic parameters. Resulting slope coefficients indicate whether the macroscopic parameters is expected to increase when increasing the local root phene value. Confidence intervals are also provided by the algorithm, which allows one to assess the parameter significance.

5.4 Results

5.4.1 Model cross-validation

First, we compare how the derived analytical model compares with the numerical growth and hydraulic, purely numerical, model. As mentionned before, the full analytical model neglects the randomness of a typical growth model (see Figure 5.4, which allows estimating tip, primary and lateral locations in a fully analytical and deterministic way. The objective of this section is to assess the error due to that simplification and how it affects macroscopic parameter estimates.

As it can be seen from Fig. 5.5 where we plotted the quality of regression between both approaches for the root system conductance, the analytical performance decreases as the hydraulic and architectural parameters become uncertain. From a perfect relationship when there is no parameter variance, we progressively reach a null quality performance of the analytical due to the larger parameter uncertainty.

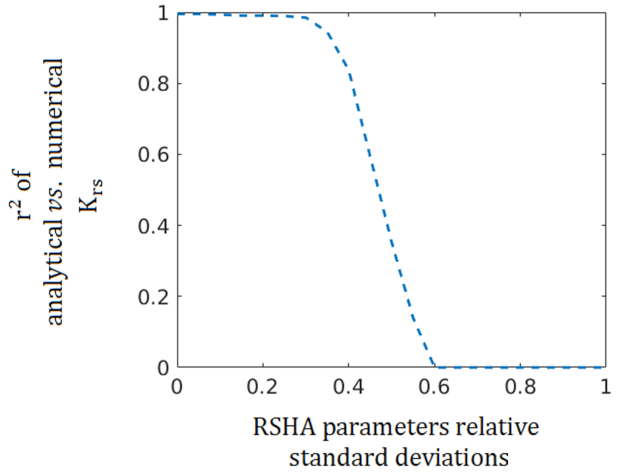


Figure 5.5: Impact of standard deviation of root system properties on analytical *vs* numerical solutions for the root system conductance of maize.

However, if the local parameters remain well characterized (typically between 0 and 0.4 mean parameter value), the analytical predictions perform very well (r-square of analytical *vs* numerical comprised between 1

and 0.8). Similar performance curve can be analyzed for other mascroscopic parameters and lead to very similar results (data not shown). From such figure, it can be concluded that a fully analytical approach, wich is faster and more informative about the parameter sensitivity, is valid until a certain parameter uncertainty, which should always be kept in mind when following this approach.

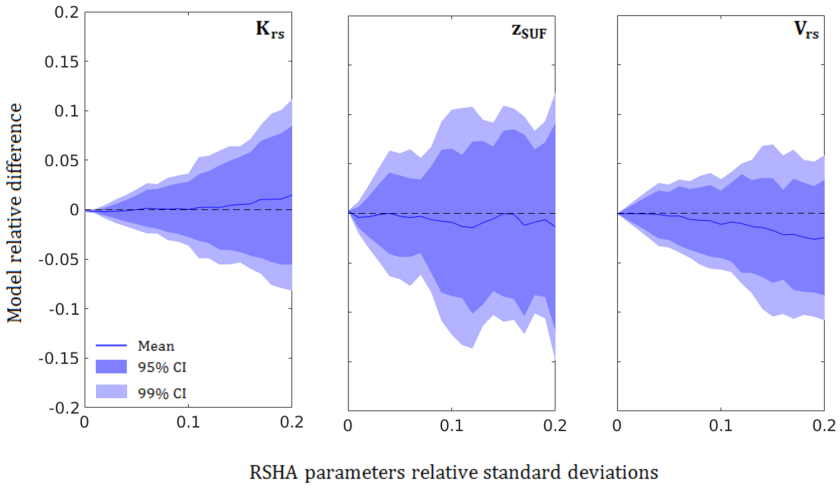


Figure 5.6: Model cross validation

5.4.2 Model applications

In the following, we use our new anaytlical tools and MARSHAL to investigate how ensembles of maize phene states impact macroscopic maize hydraulic and architectural parameters. First, we performed a meta-analysis of the literature on maize root system scale properties and compare these properties with MARSHAL estimates of parameters evolution with time. Second, we demonstrate how sensitivity analyzes can help to understand the most important local root phenes for specific macroscopic parameters.

Meta-analysis

First, MARSHAL-generated root system architectures were confronted to measured root length density profiles measured in maize plot by Gao et al. (2010). From the 10 000 estimates (generated and analyzed in less than 1h by MARSHAL), we kept the 8 best (in terms of fit of the observed RLD) root systems whose realizations are plotted in Figure 5.7 (top). r-square of measured *vs* modelled RLD profiles were all larger than 0.9 for the best simulations. Interestingly, the range of variations of the latter was dramatically reduced as compared to the entire variability of the dataset (see Fig. 5.7 bottom, blue enveloppe *vs* grey enveloppe). This suggested that if no unique solution is findable in the parametric space, functional parameters could be conserved between best solutions. Somehow, Figure 5.7 indicates that under constraints (parametric space of the maize root system and measurements of root length density profiles), the range of variability of plant-scale parameters is considerably reduced, leading to a good knowledge of the root system behaviour. The initial variability (light blue enveloppe) was due to the total length uncertainty og the root system and this information provided as the evolution of the root length densities constrained the inverse problem.

The problem to find a root system architecture fitting a (or several) root length density profile(s) is not unique: different ensemble of phene states could lead to similar goodness of fit. However Figure 5.7 suggests that these solutions could be not too much distant in terms of macroscopic parameters such as their root conductances since somehow their architecture is constrained to certain limits.

In the second example of comparison of model predicition with macroscopic observations, we related predicted root system conductance variability over time due to phene states observed variability and observed maize root system conductances. These results are plotted in Figure 5.8 where the blue enveloppe encompasses the whole simulated variability of maize root system conductance changes with time. Measurements are reported in Fig. 5.7 with grey boxes and are numbered according to the reference we return to.

Interestingly, orders of magnitude are similar and grey observations are entirely contained in the blue enveloppe, suggesting that MARSHAL

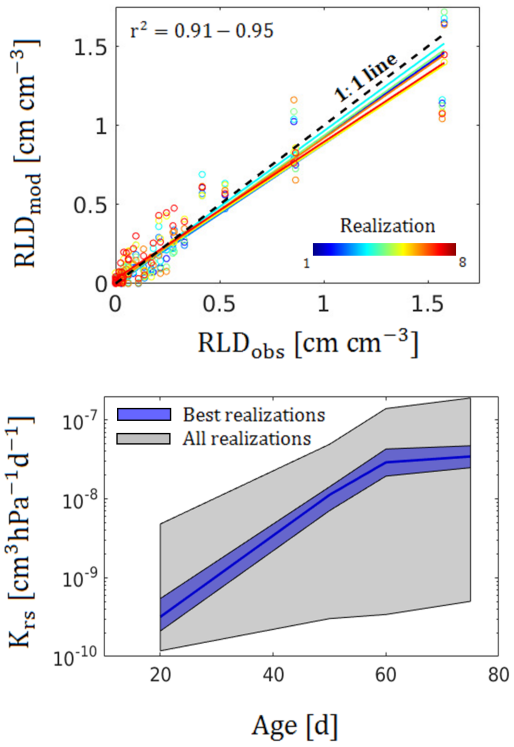


Figure 5.7: Maize root length density profile goodness of fit using MARSHAL (top) and corresponding macroscopic parameter (conductance) of whole set and best simulations (bottom)

can bridge the gap between local root phene observations and plant-scale parameter measurements. The local root phene state variability is able to explain the observed variability of root system conductance.

Quantifying group of phene states

In this last section, we take advantage of the coupling between MARSHAL and global statistical algorithms to perform sensitivity analyses of the macroscopic parameters: the root system conductance (Fig. 5.9), the depth of standard water uptake (Fig. 5.10), the root system volume (Fig. 5.11 left) and the convex hull (Fig. 5.11 right) after 60 days of

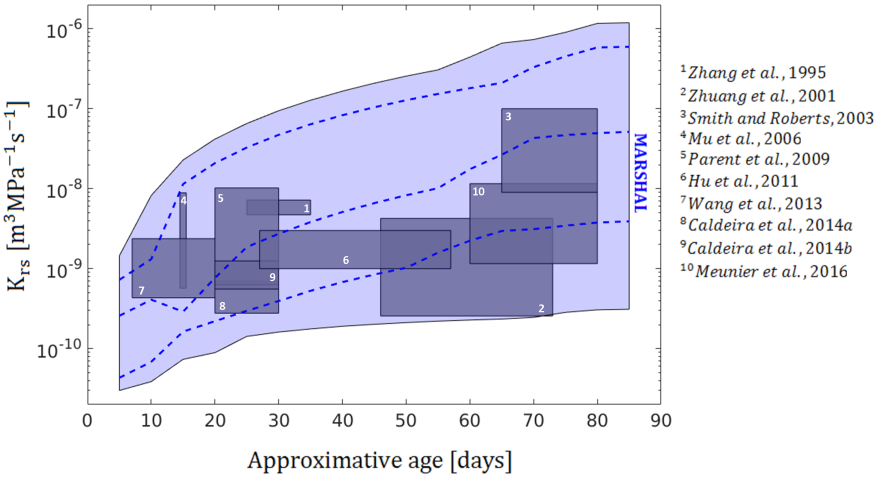


Figure 5.8: Comparison between maize root system conductances observed in the literature and the range of conductance simulated using MARSHAL over the full crop cycle. Dashed lines are particular realizations of root system conductance evolutions.

growth and development.

Let us note that together all parameters do not explain the entire macroscopic variance because only primary effects (and combined effects) were taken into account in the algorithm. Impact of combined local root phenes are not accounted for in the variance decomposition.

These sensitivity analyses highlight the most sensitive parameters for each considered macroscopic parameter. For example, insertion angles do not affect the maize root system conductance as the topology and the hydraulics only drive the absolute value of the equivalent conductance (Figure 5.9). The insertion angles only position the root tip in space which does not affect the root system conductance. However insertion angles of adventive roots (brace and crown) are critical for depth of standard uptake (Figure 5.10).

Similarly, brace roots are the main explicative variable for the root system volume because of the size of their radius which is much larger than for other root types. However, root radius do not play an important role for other macroscopic parameters (root conductance for example), which makes them good candidates for more efficient root

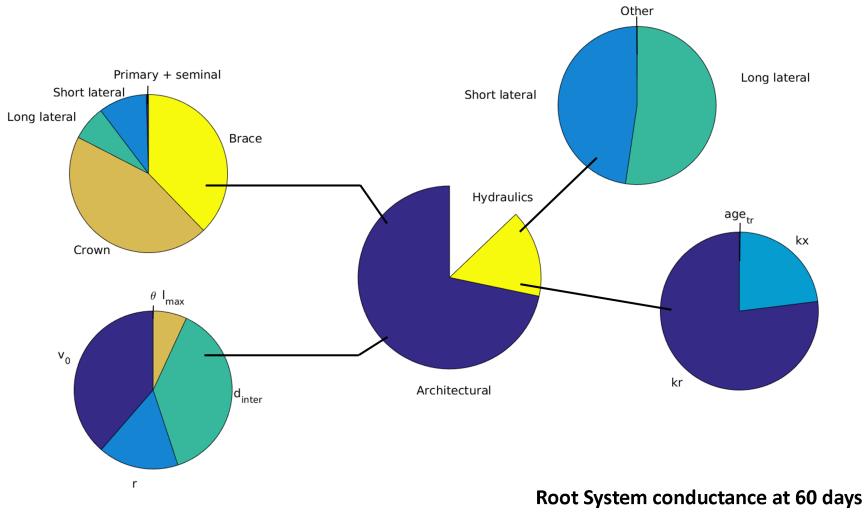


Figure 5.9: Sensitivity analysis of maize root system conductance at 60 days. The parameters are sorted in hydraulic and architectural parameters, root types and parameter types.

system hydraulic architectures.

Finally, if these pie-charts help to picture the most sensitive variables for macroscopic parameters, they do not allow the reader to know the direction of change. To do so, one may applied multilinear regression algorithm of the plant-scale parameters. For example, we performed such an analysis on z_{SUF} and K_{rs} as affected by the local root phene states. Resulting significant linear coefficients are plotted in Figure 5.12 together with their 95% confidence intervals. A positive effect on K_{rs} means that increasing the corresponding local parameter make the root system conductance grow, a positive effect on z_{SUF} deepens the standard root water uptake fraction. Note that the linear coefficient has the same unit as the corresponding macroscopic parameter because the linear regressions were achieved between the relative changes of the local root phenes and the macroscopic parameters. So the estimated change on the macroscopic parameter is obtained by multiplying the root local phene change by the linear coefficient plotted in Figure 5.12.

Breeding for more water-spending and deeper root system could

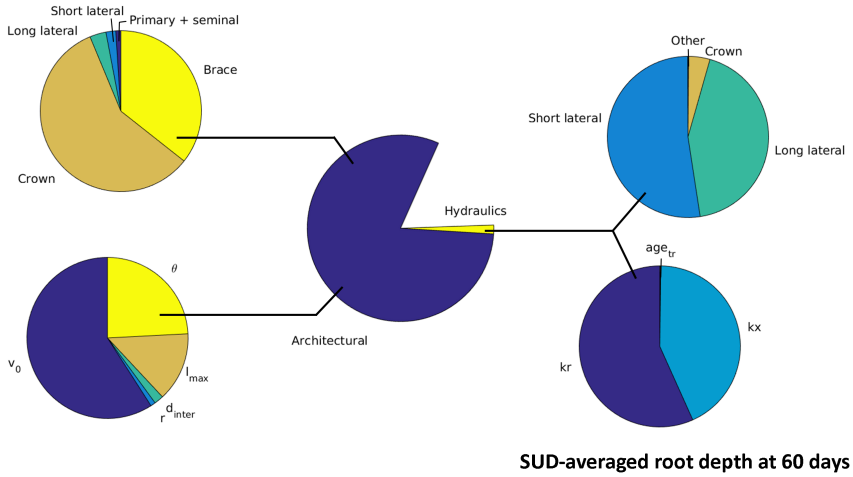


Figure 5.10: Sensitivity analysis of maize root water uptake depth at 60 days. The parameters are sorted in hydraulic and architectural parameters, root types and parameter types.

therefore focus for example on elongation rate of crown ($v_{0,4}$) and brace ($v_{0,5}$) roots as well as their maximal lengths ($L_{max,4}$ and $L_{max,5}$).

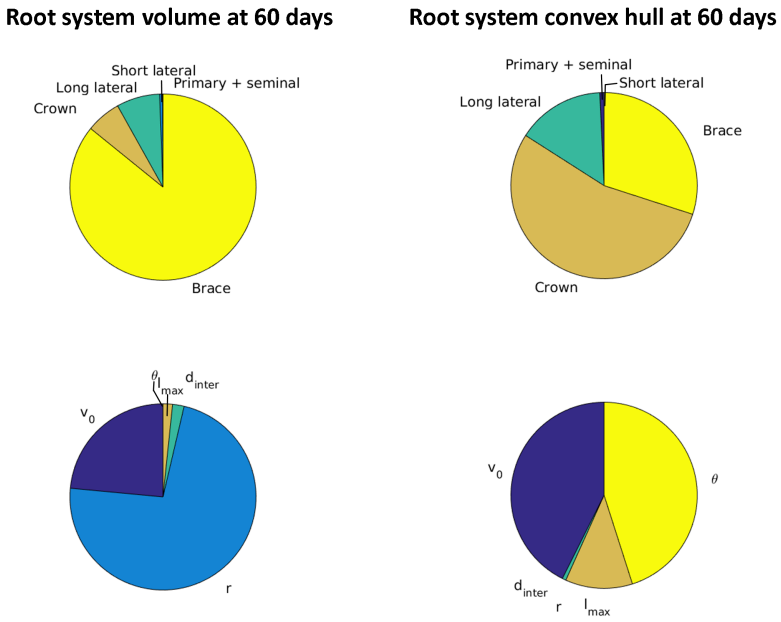


Figure 5.11: Sensitivity analysis of maize root system (left) and convex hull (right) volumes at 60 days. The parameters are sorted in root types and parameter types.

5.5 Conclusive remarks

We first developed a purely analytical model of the root system hydraulic architecture that generates estimates of the root system architecture, uses analytical relations to calculate root conductances and assembles them to derive the plant-scale parameters. The model is fed with mean growth and hydraulic parameters to predict the macroscopic architectural and hydraulic parameters.

In parallel, MARSHAL, a novel purely numerical tool, glued together different models and algorithms: a root growth model, CRootBox, a water flow algorithm in root system hydraulic architecture, macroscopic parameter calculation, sensitivity and optimization algorithms. It is available online and also gathers observation of local root hydraulic and architectural parameters of maize.

We used MARSHAL to validate the purely analytical approach.

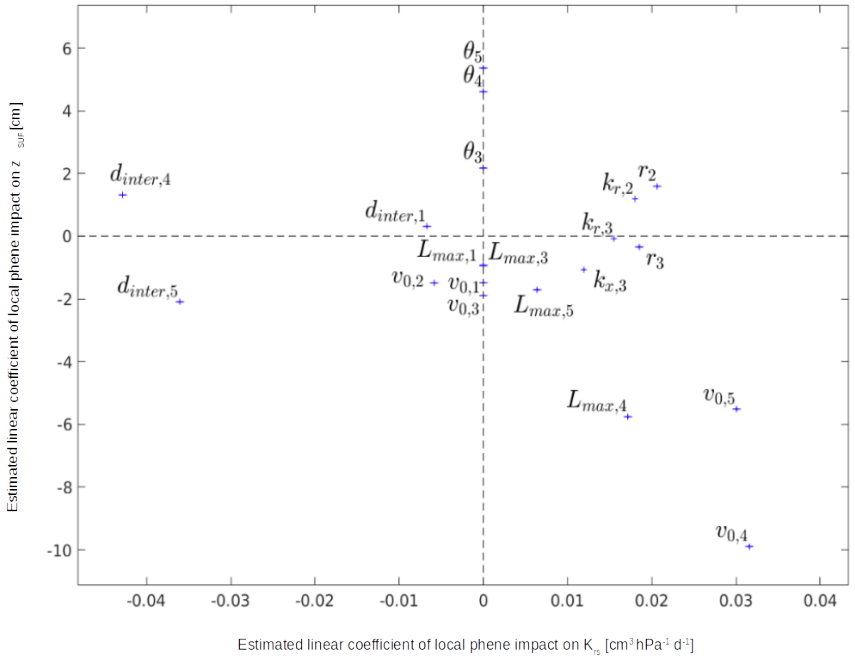


Figure 5.12: Linear coefficient estimated by multilinear regression of macroscopic parameters on local root phenes: z_{SUF} *vs* K_{rs}.

As the latter is deterministic while the former is probabilistic, we progressively increase the standard deviation of the growth and hydraulic parameters and observed the decreasing performance of the analytical estimations. Until a relative standard deviation of 40% however, the goodness of fit was pretty good.

Explicit or estimated root system hydraulic architectures are compatible with macroscopic observations such as root length density profiles and root system conductance changes with time as demonstrated in a meta-analysis of the literature. Finally, sensitivity analysis and multilinear regression algorithm highlighted sensitive local phenes to macroscopic parameters such as root system conductance, depth of standard uptake, root system volume and root system convex hull.

Root system architectures can be exported in common format such as RSML by the model users. They can then be used as inputs in other

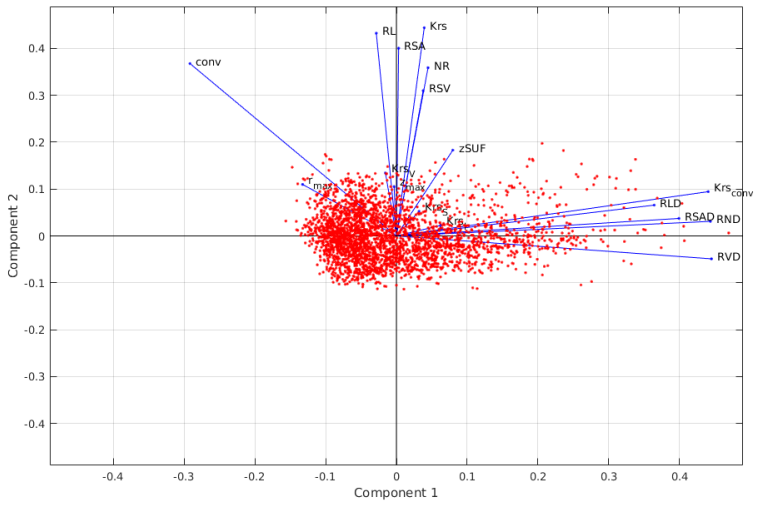


Figure 5.13: PCA of the macroscopic parameters.

functional-structural model such as R-SWMS. In the future, MARSHAL will be coupled to contrasted pedo-climatic condition generator to look for best G x E interaction (see Chapters 10 and 11).

Note that, at this stage, the analysis focuses on root and root systems properties only, which is a component of the soil-plant-atmosphere continuum, as explained in Chapters 1 and 2. The attention was put on the properties of the root systems emerging from local root phenes. How these emergent, macroscopic parameters interact with a heterogeneous changing medium will be introduced and discussed in Chapters 8 to 11.

PART III

RETRIEVING HYDRAULIC ROOT PROPERTIES USING INVERSE MODELLING

In the third part of this PhD thesis, we develop new experiments that can be used to retrieve, by inverse modelling, the local hydraulic properties of roots along their axis. In the two first chapters, soil impact can be neglected as we work in homogeneous conditions while in next two chapters, it is no longer the case. The soil resistance must be then taken into account in order to properly derive the root conductivity we are interested in.

The roots below the earth claim no rewards for making the branches fruitful

Rabindranath Tagore

ESTIMATION OF THE HYDRAULIC CONDUCTIVITIES OF LUPINE ROOTS BY INVERSE MODELLING OF HIGH-RESOLUTION MEASUREMENTS OF ROOT WATER UPTAKE

6

This chapter is a modified version of a research article published as:

> Zarebanadkouki M., Meunier F., Couvreur V. Cesar J., Javaux M. and Carminati A. Estimation of the hydraulic conductivities of lupine roots by inverse modelling of high-resolution measurements of root water uptake. Annals of botany, 2016, 118(4), 853-864.

Abstract

Radial and axial hydraulic conductivities are key parameters for proper understanding and modelling of root water uptake. Despite their importance, there is limited experimental information of how the radial and axial hydraulic conductivities vary along roots growing in soil. Here, we introduced a new approach to inversely estimate the profile of hydraulic conductivities along the roots of transpiring plants growing in soil.

We used a three-dimensional model of root water uptake to reproduce the measured profile of root water uptake along roots of lupine

plants grown in soil. The profile of fluxes was measured using neutron radiography technique combined with injection of deuterated water as tracer. The aim was to inversely estimate the profiles of the radial and axial hydraulic conductivities along the roots.

We calculated the profile of hydraulic conductivities along the taproot and the lateral roots of lupine using three flexible scenarios. For all scenarios, we found that the radial hydraulic conductivity increases towards the root tips, while the axial conductivity decreases. Additionally, we found that in soil with uniform water content: (1) lateral roots were the main location of root water uptake; (2) water uptake by laterals decreased towards the root tips due to the dissipation of the gradient of water potential along the root; (3) water uptake by the taproot was higher in the distal segments and was negligible in the proximal parts, which had a low radial conductivity. Here proximal and distal regions consistently refer to the zones close the root collar and root tips, respectively.

The proposed approach allows the estimation of the root hydraulic properties of plants growing in soil. This information can be used in advanced model of water uptake to predict the water uptake of different root types or different root architectures under varying soil conditions.

6.1 Introduction

Transpiration is driven by the difference in vapour pressure between the atmosphere and the leaves and depends on the stomatal conductance (Tardieu et al. 2015). The water loss from leaves generates a suction that is transmitted along the xylem down to the roots (Wheeler and Stroock 2008). The resulting gradient in water potential between leaves and soil drives root water uptake (Passioura 1988). The radial flow of water from the root surface into the xylem vessels is controlled by the radial conductivity, which depends on several anatomical features of the root tissue (Steudle and Peterson 1998). The axial flow of water in the xylem vessels up to the shoot is controlled by the axial conductivity, which depends on the maturation, size and abundance of the xylem vessels (Martre et al. 2001). The distribution of radial and axial conductivities

and along the root system influences rate and location of root water uptake (Javaux et al. 2008)

Although the distribution of hydraulic conductivities along the root system is a key parameter to understand how plant roots function in acquiring water from the soil (Leitner et al. 2014), quantitative measurement of these parameters for plants growing in soil remains challenging (Vadez 2014). Currently, most of the experimental data reporting the spatial distributions of hydraulic conductivities along roots are based on measurements of water flow into excised roots grown in soilless cultures. Frensch and Steudle (1989) employed the root pressure probe technique to measure the hydraulic properties of excised primary roots of maize. They determined the hydraulic conductivity of root segments by applying gradients of hydrostatic and osmotic pressure across (to induce water flow across root). Their results indicated that: (a) except for the apical zone (first 2 cm of root tip), the radial hydraulic conductivity was much more important in limiting water uptake than the axial hydraulic conductivity; (b) the radial conductivity was rather constant along the rest of the root segment in hydrostatic, but not in osmotic experiments where it decreased with distance from root tip; and (c) the change in axial conductivity along the root was much bigger than in the radial conductivity. Zwieniecki et al. (2002) employed a pressure chamber technique to measure water flow into excised nodal roots of maize that were successively cut into smaller segments. These results were numerically simulated to reconstruct the profile of radial and axial resistance along the root. Tyree et al. (1994) and Tsuda and Tyree (2000) used the high pressure flow meter technique to measure root hydraulic conductivity.

To separate the contribution of axial and radial conductivity, all these techniques rely on measuring water flow into excised roots that are successively cut into smaller segments. Alternatively, the axial conductivity can be estimated based on anatomical features such as abundance and size of xylem vessels (Biondini 2008; Frensch and Steudle 1989). Frensch and Steudle (1989) showed that the measured values of axial conductivities were smaller by a factor of 2 and 5 than those calculated according to the Poiseuille's equation.

The hydraulic properties of roots grown in soil may differ from those of roots grown in soil less culture; for instance root hydraulic proper-

ties change in response to soil drying (North and Nobel 1991). Under drought stress early development and modifications of endodermis and exodermis, main resistances to water flow, have been reported (Enstone et al. 2002). Additionally under drought stress, the expression and activity of aquaporins, which are proteins in the cell membrane that regulate the flow of water, may also vary affecting the root radial conductivity (Caldeira et al. 2014; Knipfer et al. 2011; McLean et al. 2011).

Root water uptake models can be divided in empirical, macroscopic models, such as those of Feddes and Zaradny (1978) and more detailed models that explicitly couple the water flow into and along the root architecture with the water flow in soils (Doussan et al. 2006; Javaux et al. 2008; Roose and Fowler 2004). The latter type of models can be used to simulate the response of different root systems to varying external conditions, such as drought (Doussan et al. 2006; Lobet et al. 2014). However, these models require detailed information about the spatial distribution of the root hydraulic conductivity, whose measurement is still challenging. A method that allows estimating the spatial distribution of hydraulic conductivity along roots growing in soil is thus needed to properly model and predict root water uptake.

Doussan et al. (1998a) modelled the hydraulic architecture of a maize root system to inversely estimate the spatial distribution of hydraulic conductivities along the roots based on the fluxes of water measured by Varney and Canny (1993). Doussan et al. (1998a) were aware that without a priori knowledge of the distribution of hydraulic conductivities along the roots the same set of experimental data could be fitted by different profiles of hydraulic conductivities – in other words, the solution of the inverse problem was not unique. To solve this problem, the authors imposed simple constraints to the root conductivity distribution as a function the distance to tip.

We combined the root architecture model of Doussan et al. (1998a) with recent high resolution images of root water uptake by Zarebanadkouki et al. (2012) and Zarebanadkouki et al. (2013), who measured the profile of water uptake of three-week old lupines at a spatial resolution of ca. 5 cm. The objective of this study is to inversely estimate the profile of conductivities fitting the water fluxes measured by Zarebanadkouki et al. (2013).

6.2 Material and methods

We used the Hydraulic Tree Model of Doussan et al. (1998a) to fit the local flow of water reported by Zarebanadkouki et al. (2013). Zarebanadkouki et al. (2013) measured the local fluxes of water into different root segments of three week-old lupines grown in soil. The root system was made of one taproot and 66 individual lateral roots. The root system was split into an upper and a lower zone. In each of these two zones, the roots were sub-grouped according to their length in three types: long roots (> 12 cm), middle roots (8-10 cm), and short roots (< 4 cm). The radial fluxes of water were estimated for ten different segments along the root system as illustrated in Figure 6.1.

In addition to these data sets, we used the two-dimensional root system architecture, the measured xylem potential at the collar of plant, the soil water potential distribution and the actual transpiration. Note that the actual transpiration was measured just before measuring the xylem potential at the root collar. As the latter is a destructive measurement, they can not indeed be measured at the same time. Root architecture and soil water potential were extracted from the neutron radiographs according to the protocol described in Zarebanadkouki et al. (2012). Transpiration rates were taken from Zarebanadkouki et al. (2013). For the soil water potential we assumed a uniform water potential in the soil based on the measured soil water contents and the retention curve reported in Zarebanadkouki et al. (2013). In their samples, soil water content varied from 0.1 to 0.2 $cm^3.cm^{-3}$ which corresponded to a soil water potential range of -150 to -50 hPa. Since these variations are small compared to their difference with the xylem water potential (-2500 hPa), we assumed that the soil water potential was constant. As these measurements all correspond to wet soil, it was assumed that the soil resistance could be neglected and that the root resistance was then the only driver of water uptake. The xylem water potential at the collar of the plant was measured by pressuring the aboveground part of the plant with a Scholander bomb (Scholander et al. 1965). The pressure at which the first drop of water came out from the cut end of the xylem tissue gave the absolute value of the water potential in the xylem. This measured xylem water potential of -2500 hPa was used as the top boundary condition for the root collar of the modelled plant.

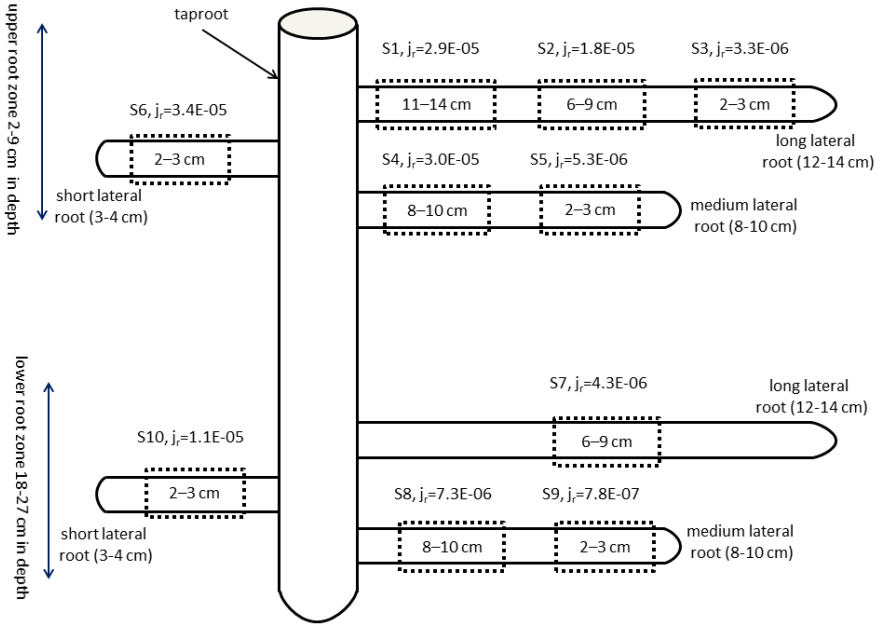


Figure 6.1: Schematic diagram of a lupine root system and the locations along the root system where radial fluxes of water were measured in Zarebanadkouki et al. (2013). The radial fluxes (j_r) are given in $m.s^{-1}$. The value given in rectangular shows the distance from root tip where the radial fluxes are averaged. The root system was divided into upper and lower root zone. In each zone three roots with different lengths were selected and the water fluxes were measured at different locations along each root (ten root segments).

6.3 Hydraulic tree model

Doussan et al. (1998a) developed an algorithm to solve the steady-state water flow within the root system by taking into account the spatial distribution of soil water potential. They simplified the root architecture as a system of interconnected nodes in which water flows radially from the soil into the roots and longitudinally inside the xylem vessels. The root system is split in small segments with typical length of 0.25cm and the root hydraulic properties is assumed homogeneous within each single segment (as well as the xylem potential). The radial water flow $\boldsymbol{J_r}$ [$\mathrm{L^3T^{-1}}$] between the soil-root interface and the root xylem nodes is written as:

$$\boldsymbol{J_r} = \boldsymbol{k_r S_r} \left(\boldsymbol{\Psi_{sr}} - \boldsymbol{\Psi_x} \right) = \boldsymbol{K_r} \left(\boldsymbol{\Psi_{sr}} - \boldsymbol{\Psi_x} \right) \tag{6.1}$$

where $\mathbf{\Psi_{sr}}$ and $\mathbf{\Psi_x}$ are the total water potential at the root surface in the soil and in the xylem (P), $\mathbf{k_r}$ is the intrinsic radial conductivity of the root [$\mathrm{LP^{-1}T^{-1}}$], $\mathbf{S_r}$ is the surface area of the root segment [$\mathrm{L^2}$], and $\mathbf{K_r} = \mathbf{k_r S_r}$ [$\mathrm{L^3P^{-1}T^{-1}}$] is defined as the radial conductance of the segment with surface $\mathbf{S_r}$. In the present notation, matrices and vectors are bold. The total water potential is the sum of the hydrostatic potential (in plant) or matric potential (in soil) and the gravitational potential, while the osmotic potential is neglected. The axial water flow in the root $\mathbf{J_x}$ [$\mathrm{L^3T^{-1}}$] is given by the the method presented in chapter 3.

$$\boldsymbol{J_x} = -\frac{-\boldsymbol{k_x}}{\boldsymbol{l}} d\boldsymbol{\Psi_x} = -\boldsymbol{K_x} \left(d\boldsymbol{h_x} + d\boldsymbol{z} \right) \tag{6.2}$$

where $\mathbf{\Psi_x}$ is the total water potential in the xylem, $\mathbf{h_x}$ is the hydrostatic potential in the xylem, l is the length of the root segment [L], $\mathbf{K_x} = \frac{\mathbf{k_x}}{\mathbf{l}}$ is the axial conductance of the root segment of length $\mathbf{l}$ [$\mathrm{L^3P^{-1}T^{-1}}$] and $\mathbf{k_x}$ is here called axial conductivity [$\mathrm{L^4P^{-1}T^{-1}}$] – note that in other studies (e.g. (Doussan et al. 1998a)) $\mathbf{k_x}$ is called conductance, as it includes the information of the cross-section of the xylem vessel; we call $\mathbf{k_x}$ axial conductivity to distinguish it from the axial conductance $\mathbf{K_x}$ and also because $\mathbf{k_x}$ is an intrinsic propertiy that does not depend on the length of the root segment $\mathbf{l}$, while $\mathbf{K_x}$ decreases with increasing $\mathbf{l}$.

When generalized to all the nodes of the root system, the water potential distribution in the xylem is obtained by solving a system of linear equations. Under water potential boundary condition, Ψ_{collar} [P], the equations can be written in matrix notation as:

$$\boldsymbol{\Psi_x} = \boldsymbol{c}^{-1} \left(\boldsymbol{diag}(-\boldsymbol{K_r})\boldsymbol{\Psi_{sr}} - \begin{bmatrix} K_{x,1}\Psi_{collar} \\ 0 \\ \\ \vdots \\ \\ 0 \end{bmatrix} \right) \tag{6.3}$$

where $\mathbf{c}$ (dimensions N × N with N being the number of root nodes) is derived from the so-called "conductance matrix" $\mathbf{C}$ described in Couvreur (2013) ($\mathbf{c}$ is obtained retrieving the first column and the first line of $\mathbf{c}$), Ψ_{collar} is the collar water potential [P], $\mathbf{diag}(-\mathbf{K_r})$ (dimensions N × N) is a diagonal matrix containing the radial conductances on its diagonal, $\mathbf{\Psi_{sr}}$ (dimensions N × 1) contains the total soil water potentials and $\mathbf{\Psi_x}$ (dimensions N × 1) is the unknown xylem water potential vector. $K_{x,1}$ is the axial conductance of the first segment. The conductance matrix $\mathbf{C}$ is a combination of both hydraulic conductances and architecture:

$$\boldsymbol{C} = \boldsymbol{IM}.\boldsymbol{diag}\left(\begin{bmatrix} -\boldsymbol{K_x} \\ -\boldsymbol{K_r} \end{bmatrix} \right).\boldsymbol{IM}^t \tag{6.4}$$

$\mathbf{IM}$ (dimensions (N +1) × 2N) is the connectivity matrix whose "(i, j)" entry is 1 if root node "i" is connected to root or soil node "j", and 0 elsewhere, see (Doussan et al. 1998a), $\mathbf{diag}\left(\begin{bmatrix} -\boldsymbol{K_x} \\ -\boldsymbol{K_r} \end{bmatrix} \right)$ (dimensions 2N × 2N) stands for the diagonal matrix whose diagonal elements are the axial and radial conductances and $\mathbf{IM}^t$ is the transpose of the matrix $\mathbf{IM}$.

Combination of equation 6.1 and 6.4 gives the fluxes from the root-soil interface to the xylem vessels as well as the collar water potential:

$$\begin{cases} \boldsymbol{J_r} = \boldsymbol{diag}(\boldsymbol{K_r})\left(\boldsymbol{\Psi_{sr}} + \boldsymbol{c}^{-1}\boldsymbol{diag}(\boldsymbol{K_r})\boldsymbol{\Psi_{sr}} + \Psi_{collar}\boldsymbol{c}_1^{-1}K_{x,1}\right) \\ T_{act} = \sum \boldsymbol{J_r} \end{cases} \tag{6.5}$$

where $\mathbf{c}_1^{-1}$ is the first column of the $\mathbf{c}^{-1}$ matrix and T_{act} is transpiration rate at the collar of plant [L^3T^{-1}]. Equation 6.5 was built and solved in Matlab under known water potential boundary condition at the root collar and constant and homogeneous water potential boundary condition at the soil-root interfaces. The latter assumption could be made because (i) the soil water content was measured homogeneous in different compartments of the rhizotron and (ii) the soil was rather wet and therefore the main resistance to the water movement was the root resistance (Draye et al. 2010).

6.3.1 Modelling approach

We applied the Hydraulic Tree Model of Doussan et al. (1998a) to the lupine root system studied in Zarebanadkouki et al. (2013). The root architecture was implemented in Matlab. The entire root architecture of the lupine was split into 1977 nodes by dividing the root system into small segments with typical length of 0.25 cm and using their centres as simulation nodes. Each node was connected to the neighbouring nodes from the same root or from the taproot by an oriented link accounting for the axial conductance between two successive compartments. Each node was connected to the soil-root interface node by an oriented link having a given radial conductance. Nodes were numbered serially from root collar, starting from taproot first, and then branched roots Doussan et al. (1998a)). The soil nodes were numbered in the same way as the root nodes. Finally, we built matrixes **C**, **c**, and **IM** for the whole set of nodes based on the protocol given above and in Doussan et al. (1998a).

We inversely estimated the radial and axial hydraulic conductivities (k_r and k_x) of the root system to reproduce the profile of root water uptake measured at ten different locations along the root system in Zarebanadkouki et al. (2013) (Fig. 6.1). The inverse problem was solved by minimizing a predefined objective function using the global optimization toolbox in Matlab (pattern search algorithm). Pattern search algorithm finds the global minimum of a predefined objective function. This solver has the advantage of accepting lower and upper predefined boundaries for the solution. It also allows imposing linear and nonlinear constrains to the solution. The objective function to be minimized was defined as the root mean square of relative differences

between measured and simulated radial fluxes of water at ten different locations presented as s1 to s10 in figure 6.1 and the measured and simulated actual transpiration (Eq. 6.5). Note that consequently during optimization we had 11 known parameters.

$$OF = \Sigma \left(\frac{\left(\begin{bmatrix} T_{act} \\ \boldsymbol{J_r} \end{bmatrix} - \begin{bmatrix} T_{act,obs} \\ \boldsymbol{J_{r,obs}} \end{bmatrix} \right)^2}{\begin{bmatrix} T_{act} \\ \boldsymbol{J_r} \end{bmatrix}^2} \right) \tag{6.6}$$

with $\mathrm{T_{act,obs}}$ $[\mathrm{L^3T^{-1}}]$ and $\mathbf{J_{r,obs}}$ $[\mathrm{L^3T^{-1}}]$ the observed actual transpiration and the radial fluxes $[\mathrm{LT^{-1}}]$, respectively. Note that the radial fluxes inserted in this equation for each location were first averaged along the root segments with given length as were reported in Zarebanadkouki et al. (2013). Equation (6.6) indicates that the radial fluxes and the actual transpiration (measured and modelled) are concatenated in a single column vector gathering all the observations and all the outputs of interest. The error is then calculated by summing up all the relative squared differences between measurements and simulations.

Finding a unique solution for the profile of hydraulic conductivities at the resolution of 0.25 cm was challenging - i.e. in the inverse problem there will be far more unknowns than the 11 measurements (10 radial fluxes plus the total transpiration). To reduce the number of unknowns in the inverse problem we made the following assumptions: 1) the root system was made of one tap root and several lateral roots, and we neglected secondary laterals and cluster roots; 2) the radial and axial conductivities of the tap root and the laterals were functions of the distance from the root tip.

Then we investigated different shapes of the profiles of hydraulic conductivities along the root. In scenario 1 and 2 we assumed that the conductivities were linear and exponential functions of the distance to the root tip. Scenario 1 and 2 allowed either, increasing or decreasing conductivities towards the root tips; however, the functions had to be monotonic. In scenario 3 we described the conductivities as step-wise functions. To reduce the number of parameters, we assumed that the roots had a maximum of three zones with different radial and axial conductivities. The location and extent of the zones were let vary. The

advantage of scenario 3 is that it allows a flexible and non-monotonic shape of the conductivities. The three scenarios are described in details in the following sections.

6.3.2 Scenarios

Scenario 1

The profiles of the lateral radial and axial conductivity were described with linear functions:

$$\begin{aligned} \boldsymbol{k_r} &= a.\boldsymbol{z} + b \\ \boldsymbol{k_x} &= c.\boldsymbol{z} + d \end{aligned} \tag{6.7}$$

where a, c can be positive or negative numbers and b and d are positive numbers. If a is negative the radial conductivity (k_r) linearly decreases with distance from the root tip (z [L]) and if it is positive it increases. The same applies to the profile of axial conductivity (k_x): if c is negative, the axial conductivity decreases with distance from the root tip and if it is positive, it increases. Note that for each individual root type (lateral and taproot) these four parameters are optimized. This scenario contains 8 parameters to optimize.

Scenario 2

The profiles of the lateral radial and axial conductivity were described with exponential functions:

$$\begin{aligned} \boldsymbol{k_r} &= aexp(b.\boldsymbol{z}) \\ \boldsymbol{k_x} &= cexp(d.\boldsymbol{z}) \end{aligned} \tag{6.8}$$

where b, d can be positive or negative numbers, while a and c are positive numbers. If b is negative the radial conductivity (k_r) decreases with increasing distance from the root tip (z [L]), while if b is positive k_r increases. The same applies to the axial conductivity (k_x); if d is negative k_x decreases with distance from the root tip, while if d is positive k_x increases. Note that for each individual root type (lateral and taproot) these four parameters are optimized. This scenario contains 8 parameters to optimize.

Scenario 3

The profiles of hydraulic conductivity along the lateral roots were described using a stepwise function with two transition points separating three zones. We chose three zones because also the radial fluxes were measured at three locations along an individual lateral root (Zarebanadkouki et al. 2013) and a similar scenario was also tested in Doussan et al. (1998a). The position of the three zones was let vary during the optimization. The parameters to be optimized in this scenario are three radial conductivities of laterals ($k_{r,1}$, $k_{r,2}$, $k_{r,3}$), three axial conductivity of laterals ($k_{x,1}$, $k_{x,2}$, $k_{x,3}$), two locations separating the three zones, n_1 and n_2. The radial and axial conductivities were defined as:

$$\begin{aligned} &\boldsymbol{k_r}(z) = k_{r,1} \text{ and } \boldsymbol{k_x}(z) = k_{x,1} \text{ for } z > n_2 \\ &\boldsymbol{k_r}(z) = k_{r,2} \text{ and } \boldsymbol{k_x}(z) = k_{x,2} \text{ for } n_2 \geqslant z \geqslant n_1 \\ &\boldsymbol{k_r}(z) = k_{r,3} \text{ and } \boldsymbol{k_x}(z) = k_{x,3} \text{ for } z < n_1 \end{aligned} \tag{6.9}$$

where z is the distance from the root tip. Estimation of the hydraulic conductivities along the taproot is problematic since there was no information about water fluxes into the taproot. To reduce the number of unknowns, we impose constant radial and axial conductivity along the taproot. Our sensitivity analysis also showed that our model is not sensitive to the radial conductivity of the taproot (discussed in details in the result section). This scenario requires 10 parameters.

6.3.3 Sensitivity analysis and parameter uncertainty

A sensitivity analysis was performed for scenario 2 around the optimal solution. We considered each single couple of variables of scenario 2. The range of variation for each parameter was ± 20% for two reasons. First, we considered only small variations of the parameters to evaluate the local sensitivity. Second, the exponential shape of the functions in scenario 2 led to significant changes of the simulated conductivities even with small parameter changes. The uncertainty of the resulting parameters was quantified by estimation of confidence intervals of parameters. We estimated 95% confidence intervals for the estimated profiles of radial and axial conductivity using linear regression analysis for our nonlinear problem following the approach of Lambot et al. (2002).

6.4 Results

Figure 6.2 shows the profiles of radial conductivity (k_r) and axial conductivity (k_x) along the roots that best fitted the measured water fluxes. The results of all scenarios showed that the radial hydraulic conductivity was higher at the distal parts of the root and decreased towards the proximal parts. The axial conductivity showed the opposite trend. In scenario 2 and 3, k_r of lateral roots decreased by 3 and 7 times from the distal to the proximal segments, respectively. k_x of lateral roots increased by ca, 300 times in both scenario 2 and 3. k_r predicted by scenarios 1 and 2 was rather similar. Scenario 2 predicted a larger variation in k_x of lateral roots from the distal to proximal parts. The differences between k_r and k_x predicted by the different scenarios were always smaller than 1 order of magnitude. We also estimated the 95% confidence intervals for both estimated k_r and k_x of the lateral root. In general, the ranges of estimated confidence intervals were small in all scenarios, particularly in scenario 3. The range of estimated confidence intervals were bigger for distal root segment than the proximal segment. The small confidence interval indicates that the best solutions were reached and had a sharp global minimum.

Estimated k_r and k_x of the tap root showed a bigger variation among different scenarios. These larger variations are in fact due to the lack of having measured fluxes along the taproot. The 95% confidence intervals showed big uncertainties in the estimation of k_r and k_x of the taproot. It is worth noting here that the optimized radial conductivities in the three scenarios were always smaller than the ones of the laterals. Combined with a much lower total surface area of this root type we observe that this root does not affect significantly the plant actual transpiration. This explains the uncertainty on the radial conductivity of the laterals. For this plant, the taproot is mainly a conducting rather than extracting organ. Therefore, its k_x needs to be large enough to conduct water and k_r small enough not to extract water. Higher k_x and lower k_r will not affect much the root water uptake distribution, which leads to a wide 95% confidence interval.

Figure 6.3 shows the measured and the simulated radial fluxes of water into different locations along the root segment. The radial fluxes were modelled using the scenarios 1, 2 and 3. The model was able to

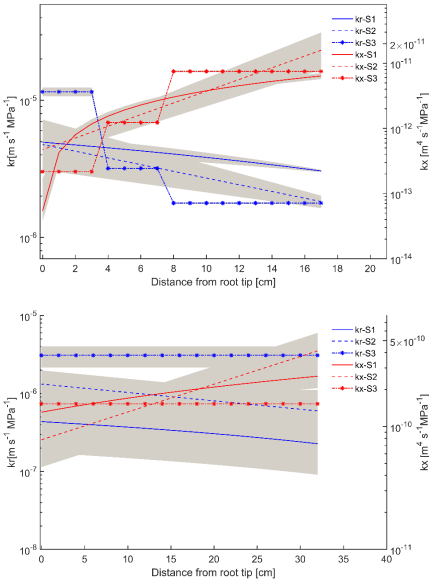


Figure 6.2: Profile of hydraulic conductivities as a function of distance from root tip. a) Profile of radial conductivity (k_r) and axial conductivity (k_x) along lateral roots. b) Profile of radial and axial conductivity along the taproot. We used three different scenarios to estimate the profile of the conductivities. In scenario 1 and 2, we imposed a linear and exponential function to estimate the profile of conductivities, respectively. In scenario 3, k_r and k_x of lateral root were estimated using a stepwise function with three transition zones and the ones of taproot was fitted to be homogenous along the taproot. The grey strips around the lines show 95% confidence interval of estimated conductivities. The data of k_r and k_x obtained from scenario 2 are given in the supplementary information.

fit the profiles of root water uptake in all scenarios, in particular with scenario 2 and 3.

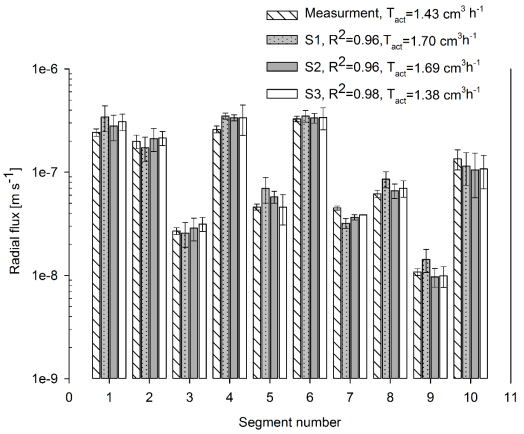


Figure 6.3: Measured and simulated radial fluxes into different locations along the root system illustrated in Fig. 6.1. Error bars show the standard deviations of average fluxes into different segment types (S1-S10) s. r^2 refers to correlation coefficient between measured and simulated fluxes and Tact is the transpiration rate.

Taking advantage of the 3D architectural model of Doussan et al. (1998a), we visualized the spatial distribution of water flux and the xylem water potential along the entire root system of lupine (Fig. 6.4). The results are based on scenario 2 but do not change dramatically if the other scenarios are used. The simulations show that: (1) root water uptake was not uniform along the root system; (2) lateral roots were the main location of root water uptake in homogeneous soil conditions; (3) the lateral roots in the upper soil were more involved in water uptake than the laterals located in the lower zone; (4) root water uptake in the proximal parts of the lateral roots was higher than in the distal parts; (5) water uptake by the taproot was high in the distal part, but it was negligible in the proximal part; (6) root water uptake was not only function of the distance from root tip and it depended mainly on the architecture of root system (this means that the axial conductivity of the taproot is limiting). A similar pattern of root water uptake was reported by Dara et al. (2015) who estimated root water uptake of

lupines based on soil water depletion.

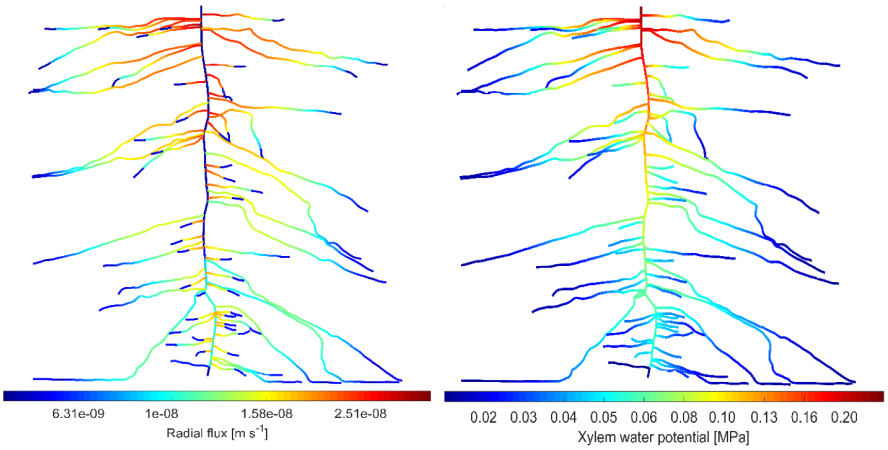


Figure 6.4: Radial fluxes [cm s-1] (left) and (minus) absolute xylem water potential [MPa] (right) along a three weeks old root system of lupine simulated in in scenario 2 The root system is extracted from the neutron radiographs of Zarebanadkouki et al. (2013).

The profiles of root water uptake and xylem water potential along an individual lateral root are shown in figure 6.5. The selected root was 14.5 cm long and located at a depth of 5 cm from the soil surface. We found that the highest radial flux occurred at a distance of 11 cm from the root tip. Excluding the first 1.5 cm of the root tip, where the xylem conductivity was low (probably because the xylem vessels were not yet developed (Frensch and Steudle 1989), root water uptake increased by 20 times from a distance of 1.5 to 11 cm from the root tip. Water uptake decreased by 1.5 times from a distance of 11 to 14.5 cm from the root tip. As expected, the lowest xylem water potential was found in the proximal parts of the root and increased towards the distal parts where it approached the soil water potential (Fig. 6.5-B). Figure 6.5 also shows the profile of root water uptake along a root as a function of the radial conductivity and xylem water potential. We did not find a simple correlation between root water uptake and radial conductivity (Fig. 6.5-C), and the same conclusion holds for the xylem water potential (Fig. 6.5-D).

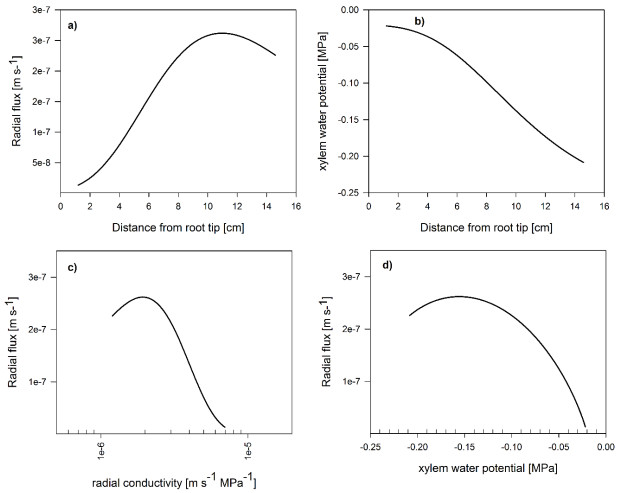


Figure 6.5: (a) Profile of root water uptake and (b) xylem water potential as a function of distance from the root tip. (c) Relation between root water uptake and radial hydraulic conductivity. (d) Relation between root water uptake and xylem water potential. The simulated root had a length of 14.5 cm and it was located at a depth of 5 cm from the soil surface. The results are based on scenario 2.

Finally, we tested the sensitivity of the model to the parameters of the radial and axial conductivities. The question was to find out with our set of available data whether the model of Doussan et al. (1998) is sensitive to the profile of conductivities. Since the profile of simulated root water uptake and hydraulic conductivities in scenario 3 and 2 were rather close, we decided to test the sensitivity of the model only for the parameters used in scenario 2. In scenario 2, we needed only 8 parameters to describe the profile of hydraulic conductivities/conductances along roots, which makes the sensitivity analysis easier and more straightforward.

Figure 6.6 shows the results of the sensitivity analysis. Indeed, in scenario 2 radial conductivity of the taproot can be considered as constant without affecting dramatically the results. The model was insensitive to the radial conductivity of the principal in the here-considered range of variation. Indeed, the radial conductivity of the taproot was very low as compared to the one of laterals and increasing its value by 20% did

not affect the water uptake. From the other subplots, we can draw the following conclusions: the parameters a and b as well as c and d were correlated (the parameters are defined in Eq. 6.8). This is due to the shapes of the functions: i.e. increasing the argument of the exponential can be compensated by decreasing the multiplying factor of this function. The parameters (except k_{rI}) were well defined: a clear valley in the objective function was found corresponding to the global minimum. The solution was unique with the considered scenario and d is the most critical parameter: small variations of its value lead to large changes in the objective function and in the water uptake. This parameter is critical: it explains how fast the xylem vessels matur and allows the transport of the water absorbed at the root tip.

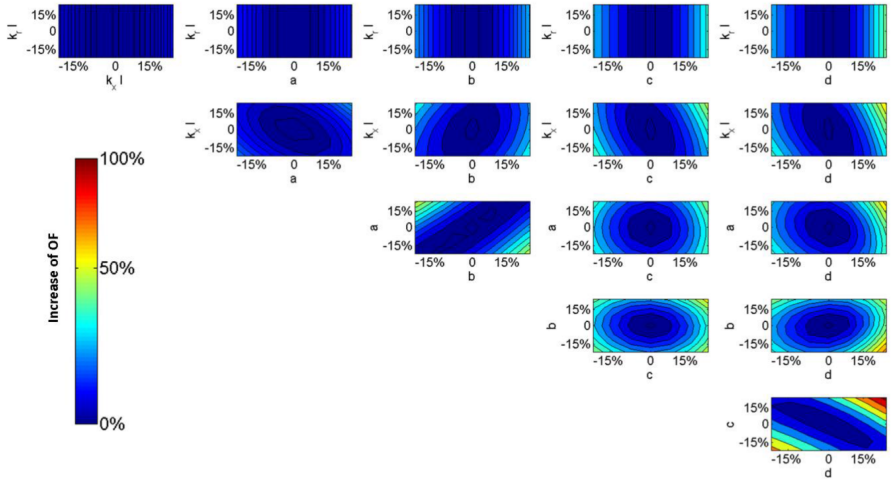


Figure 6.6: Sensitivity analysis of the model parameters. The colour intensity shows increase of the objective function defined in Eq. 6.6. The results are based on the radial and axial conductivities calculated in scenario 2 (see equation 6.8 and main text for the explanation of the parameters names).

6.5 Conclusive remarks

We estimated the profile of radial and axial conductivities along the roots of a transpiring plant grown in soil. To this end, we used Hydraulic Tree Model of (Doussan et al. 1998a) to reproduce the profile of root water uptake along the root system of lupines reported in Zarebanadkouki et al. (2013). To reduce the number of unknown of the inverse problem and ensure uniqueness of the inverse solution, we used three flexible and different functions of the profiles of conductivities along the roots. The results of all scenarios showed that the radial conductivity increases towards the root tips, while the intrinsic axial conductivity decreases. This result confirms the current opinion of how root anatomy and root maturation affect the root conductivities: over time, the radial conductivity decreases due to the formation and maturation of casparian strips and suberin lamellae. In contrast, the axial conductivity increases due to the development and maturation of conductive xylem vessels (Enstone et al. 2002; Steudle and Peterson 1998).

Besides revealing the spatial distribution of hydraulic conductivities along roots, another important significance of this work is to predict the distribution of root water uptake along root system with a high spatial resolution. The results showed that root water uptake was not uniformly distributed along the root system even in homogeneous soil conditions. Similar findings were also reported by Dara et al. (2015) for lupines growing is soil. We found that the profile of root water uptake along the roots cannot be simply described by the developmental stage of the root (distance from the root tip), but it depends on the architecture of the root system. The distal parts of the roots (young segments) showed different contributions in root water uptake depending on the distance from the taproot. By increasing distance from the taproot, the contribution of young root segment in root water uptake decreased due to the increasing axial resistance that water has to overcome.

In Zarebanadkouki et al. (2013), the profile of root water uptake was estimated with a spatial resolution of 4 cm and it was concluded that root water uptake increased towards the most proximal parts. Simulations of root water uptake at a finer resolution showed that along an individual lateral root, the maximum water uptake occurs at a distance of 11 cm from root tip and it decreases towards both proximal and

distal parts. This results differ from the simulations of Landsberg and Fowkes (1978), who found an increasing uptake towards the proximal part in soil with homogenous soil water potential. The reason is that they assumed uniform root conductivities. In our case, the increase of axial conductance and the decrease of radial conductivity in the proximal parts favour the uptake in the more distal parts, resulting in a maximum at 11 cm. The results also show that water uptake by the taproot was negligible due to its low radial conductivity. The combination of low radial conductivity and high axial conductance confers to the taproot an excellent ability to collect water from lateral roots and transport it to the shoots.

It is interesting to estimate how the ability of root to extract water from soil changes as root elongates. Does water uptake increase linearly with root length or is there a trade-off between root length and water uptake capacity? The answer to this question is not straightforward and can not be simply estimated from the profile of conductivities. We used our model to simulate the total water uptake by a single growing root (from 1 to 17 cm), using the profile of conductivities obtained from scenario 2. The results showed that root water uptake increases with root length (Fig. 6.7). For roots shorter than ca. 7 cm, the increase in water uptake is rather linear. As roots grow further, root water uptake starts to increase less rapidly. With further root growth the uptake reaches a constant value. These results show that there is a trade-off between root growth and maximum root water uptake. The explanation is that as the root grows the total root surface increases but the radial conductivity of the proximal segments decreases as the root ages. Additionally, as the roots elongate the axial path becomes longer and the dissipation of pressure along the root becomes more significant. However, the maturation of the xylem vessels and their increasing axial conductivity facilitates the longitudinal transport of water along the old, proximal segments. This combination of increasing axial conductivity and decreasing radial conductivity with age explains the profile of water uptake shown in Fig. 6.5 and the total uptake for varying root lengths shown in Fig. 6.7.

Interestingly, these results are consistent with those found in next Chapter (see Chapter 7) and other studies (Hamza and Aylmore 1992; Zarebanadkouki et al. 2013). They indicate that the root conductance

of lateral roots rapidly reach a plateau. It corresponds to the function of these roots: as short roots, they look for local water but are not dedicated to the deep exploring of the soil water resources. This task is devoted to the main axes that position all the lateral roots in space at appropriate locations.

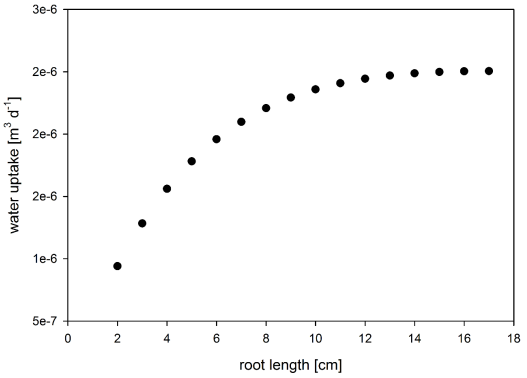


Figure 6.7: Root water uptake as a function of root length. Root water uptake (total water taken up by root at the basal end of root) was simulated using the radial and axial conductivities obtained in scenario 2.

The fluxes reported here refer to plants growing in uniformly wet soils, when the soil conductivity is not a limit for root water uptake. However, as the soil dries, its hydraulic conductivity decreases and becomes relevant for water uptake (Draye et al. 2010; Passioura 1988). Measurements and models of root water uptake showed that in wet soils root water uptake mainly occurs in the upper part of the root system; but as the top soil layers dry, root water uptake moves downwards to the lower part of the root system (Couvreur et al. 2012; Dara et al. 2015; Doussan et al. 2006; Garrigues et al. 2006; Roose and Fowler 2004). Roose and Fowler (2004) simulated root water uptake in soil with heterogeneous water content and showed that the regions near the base of the root system (i.e. close to the ground surface) and near the root tips will take up more water than the middle region of the root system, due to the highly nonlinear nature of water flow in the soil. Yet, Schwartz et al. (2016) showed that the specific non-equilibrium rhizosphere properties

may generate more uniform uptake profiles. Furthermore, in dry conditions the interface between roots and soil undergoes complex dynamics. It has been shown that under dry conditions roots shrink and lose their contact with the soil (Carminati 2013). It has also been shown that in dry conditions the rhizosphere turns hydrophobic (Ahmed et al. 2014; Carminati 2012; Carminati et al. 2010; Moradi et al. 2014). The rhizosphere hydrophobicity is more pronounced in the proximal, older root segments, while the rhizosphere of the distal root segments is rapidly rewetted (Carminati 2013). Therefore, after repeated drying/wetting cycles we can expect a shift of water uptake towards the distal, younger root segments.

Here, for simplicity, we assumed that root segments with equal distance from the root tip had identical hydraulic properties. This assumption implies that the rates of root growth and root maturation were constant. However root growth rate depends on the supply of water, oxygen and nutrients, as well as on the developmental stage of the plants (Bengough et al. 2006). Detailed measurements of root growth would help to remove this assumption and to obtain detailed information on the profiles of root conductivities.

The significance of this study is to propose a method to estimate the hydraulic properties of a root system. Using the model of Doussan et al. (1998a) and measurements of local fluxes into the roots (Zarebanadkouki et al. 2012), we reconstructed the potential profiles of radial and axial conductivities along the roots. The estimated root properties can be used to simulate root water uptake under different scenarios, for example as the soil dries, assuming no time variation of root hydraulic properties. These data can be also used to understand "which type of roots and root architecture better extract water from drying soil" (Lynch 2013). The answer to this question relies on modelling approaches which require a good knowledge of root hydraulic properties (Leitner et al. 2014). Finally, this experiment could be repeated to several genotypes to compare their hydraulic properties and try to understand their different water uptake behaviours.

Finally, it must be said that the actual transpiration observed during the experiment was pretty low. In our model, the boundary flux imposed at the root collar has no impact on the water uptake distribution in homogeneous soil conditions and hence the root conductivities

obtained by inverse modelling. However, several authors suggest that the transpiration rate impacts the plant conductances (see for example Tardieu et al. (2015)). As local properties could play a role in this process, the network of resistances might be locally impacted and therefore uptake distribution could change even in soils homogeneously wet. This is why the experiment should be repeated in different conditions, especially under different collar fluxes. It would be then worth looking at the relative changes of hydraulic conductivity distribution within the root system.

It also must be added that, if the plant conductance varies with the transpiration rate, then a low demand implies low root conductances and hence conductivities. The parameters obtained in our analysis would then correspond to a certain, low transpiration rate and would be larger in a context of increased atmospheric demand.

In next Chapter, absolute values of these modelled radial and axial conductivities will be compared with other studies reported in the literature as well as with outputs of another experiment applied to lateral roots of lupine. It will be shown that our observations globally correspond to findings of other studies even though the lupine radial and axial conductivities stand in the upper and lower range of observations, respectively.

ESTIMATION OF THE HYDRAULIC CONDUCTIVITIES OF MAIZE ROOTS BY INVERSE MODELLING OF PRESSURE PROBE CONDUCTANCE MEASUREMENTS

7

This chapter is a modified version of a research article in preparation:

> Meunier F., Zarebanadkouki M., Ahmed M., Carminati A., Couvreur V. and Javaux M. Hydraulic conductivity of soil-grown lupine and maize unbranched roots and their junction to the stem, In preperation, To be submitted to the special issue "Plant water relations" of Journal of Plant Physiology

---

Abstract

A root pressure probe technique was used to measure hydraulic conductance of maize and lupine roots. Lupine and maize plants were grown for in rhizoboxes filled with sandy soil for seven weeks in 14 h days with 500 µmol.m^{-2}.s^{-1} PAR and day/night temperatures of 24°C and 19°C, respectively. Thereafter, unbranched segments of different root types of maize (lateral, seminal, crown and brace) and lateral roots of lupine were excised from plant root systems and the total root conductance was then measured under steady-state conditions for the segments of varying length. To do so, proximal root regions were progressively shortened and the resulting root segment axial conductance

was measured as well. The corresponding profiles of total root conductance and axial conductance were used in an optimization exercise to fit the intrinsic root hydraulic property function that drives the water flow transfer in roots. Interestingly, the total root conductance were measured similar between root types and even species but since the axial conductance profile were shown to be significantly different, the fitted root radial conductivity display significant differences between the different root orders. In a final experiment, a similar measurement methodology was applied to the connection of the different maize root types to the stem. The connection conductances highly depended on the root types: maize crown root connections were an order of magnitude more conductive than the other brace and seminal roots, suggesting potential regulation mechanism for root water uptake location. The obtained axial and radial conductivities were compared to literature measurements and were found in the lower range of observed hydraulic properties of herbaceous species.

7.1 Introduction

Both architectural and hydraulic properties of the root systems are determinant for the location and the rate of water uptake (Leitner et al. 2014). These characters are encapsulated in the concept of hydraulic architecture (Lobet et al. 2014): any root system can be split into individual segments (defined as a root portion with homogeneous hydraulic properties) connected together to form the complete root system (Doussan et al. 1998a). Under sustained transpiration demand, from the root-soil interface to the above-ground plant part, water first radially crosses root tissues towards the root xylem vessels and then flows up to the shoot (Passioura 1980). Radial flow of water is controlled by root radial conductivity whose numerical value depends on anatomical properties of the root cross-section (Steudle 2000a). On the other hand, axial conductivity is controlled by the size, the abundance and the maturation level of the xylem vessels (Martre et al. 2001).

Recently, plant root system and its architecture has received increasing attention as a promising target for breeding crops more tolerant

to drought stress (Comas et al. 2013). Root systems of plants consist of many different root types. For instance, in plants with adventitious root systems, such as maize, wheat and barley, the root system consists of four different root types classified as seminal (+ primary), crown, brace root (Lynch and Brown 2012), see schematic (left) of Fig. 7.1. These roots are main axes which may host several lateral roots with different degrees of branching orders. Such a complexity of root system is believed to secure efficient acquisition of resources from soil at different developmental stages of plant growth and particularly varying environmental conditions (Lynch 2013). For a more accurate definition of the different root types, the readers are referred to Chapter 3 or other readings (see for example Hochholdinger et al. (2004)). Lupine root system is simpler and made of a vertical taproot hosting lateral roots more or less horizontally (see schematics (right), Fig. 17.1).

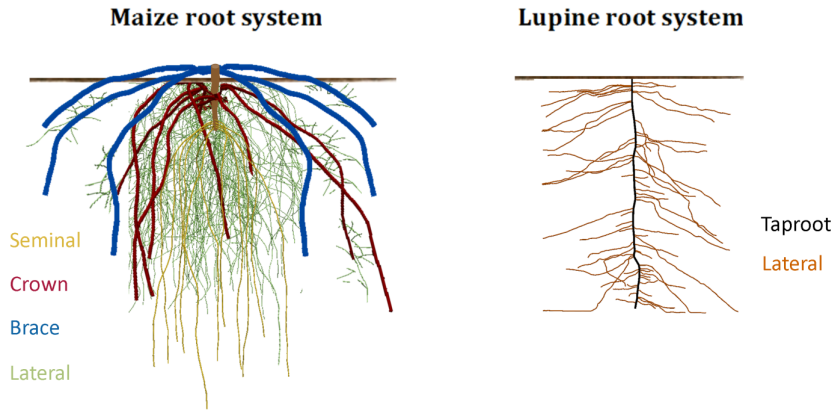


Figure 7.1: Schematics of the root system of maize (left) and lupine (right) and the root nomenclature

The maize root system illustration was generated using CRootBox (Schnepf et al. 2017) and the one of the lupine comes from a rhizotron experiment (Zarebanadkouki et al. 2016). The roots are coloured according to their type with a consistent colour code throughout the manuscript.

Although root hydraulic properties are critical for decrypting the water uptake pattern in heterogeneous environments (Javaux et al. 2008) and have an important breeding potential (Schoppach et al. 2014; Vadez 2014), their measurement for plants growing in soil remains challenging. Yet, their accurate determination in laboratory experiment routines would allow their use in three-dimensional physically-based models of the water flows in the soil-plant-atmosphere continuum to compare species and/or genotypes performances in contrasted environmental conditions (Meunier et al. 2017; Tardieu et al. 2015). Additionally, in spite of the importance of understanding the function of different root types in extraction of water from soil particularly in the context of breeding for better root traits, little experimental information is available to show the relative importance of different root types in extraction of water from soil. The relative importance of different root types depends on their hydraulic properties and architecture of root system.

In this study, we aimed to measure hydraulic properties of different root types and compare the ability of different root types to extract water from soil. A root pressure probe technique was used to measure profile of hydraulic conductances along roots of maize and lupine plants growing in soil. These measurements were combined by an inverse modeling approach to retrieve the profile of radial and axial hydraulic conductivities which are intrinsic properties of each root. These values are compared with direct or inverse measurements obtained from other studies in the literature. The paper first explains the material and methods we used in the laboratory and the necessary theory to describe water flow in unbranched roots and the parametrization scheme used in our experiments (section 2). The results are provided and discussed in the next two sections.

7.2 Material and Methods

7.2.1 Soil and plant material

Nine maize and nine lupine plants were grown in aluminum containers (size of 40 cm × 40 cm × 1cm) filled with sandy soil (92% sand - 5% silt - 3% clay). The aluminum containers consisted in two aluminum

plates of 40×40 cm, which were held together at the edges by aluminum bars of 1 cm × 1 cm × 1 cm. This construction enabled us to open the container from one side and carefully dig out roots from soil. Maize seeds were soaked in 10% H_2O_2 solution for 10 minutes and then germinated on moist filter paper for 48 hours. One seedling was then planted at a depth of 1 cm into each container and the upper soil layers were covered with a 1 cm layer of quartz gravel to reduce evaporation from soil surface. The plants were grown with a daily light cycle of 14 h and 10 h of darkness, a light intensity of 500 µmol.m^{-2}.s^{-1}, day and night temperature of 24 and 19 °C, respectively and relative humidity of 60%. During the growth period, plants were irrigated every four days to keep the soil at an average water content of 0.20-0.25 cm^3.cm^{-3}. When plants were seven weeks old, the containers were opened from one side and roots were carefully washed from the soil. Unbranched segments of different root types of maize (lateral, seminal, crown, and brace roots) and lateral roots of lupine were excised and connected to a pressure probe to measure their hydraulic properties (Frensch and Steudle 1989). The methodology was applied to the different species and root types. For lupine, we only considered the lateral roots since the taproot is rapidly branched. For maize, we analysed seminal, crown, brace and lateral unbranched roots as well as the conductance of the root-shoot junction.

7.2.2 Root pressure probe

Root pressure probe consists in a pressure transducer to measure the pressure and a capillary that connects an excised root system to the probe. A root was connected to the probe with seals prepared from silicone material (Xantopren L blue, Heraeus Kulzer GmbH, Germany) to ensure root pressure was maintained without blocking xylem vessels. The root pressure probe was laid horizontally and the root was supported inside a glass container (10 cm × 30 cm) in which root was kept immersed in water. Half of the capillary (diameter of 600 µm) was filled with silicon oil and the other half of the capillary facing the root was filled with water. The meniscus between water and oil was used to measure water volume injected into and sucked from the root. The probe was equipped with a metal rod that could push or suck water into

or out of the root. Both total and axial conductances obtained from root pressure probe measurements depend on the length and radius of root segment connected to the pressure probe. In contrast, axial and radial conductivities are intrinsic properties of each root independent of root length. To extract the profile of axial and radial conductivities, measurements of root pressure probe was combined by an inverse modelling approaches described in the following sections.

7.2.3 Total root conductance

Unbranched roots that were 5–40 cm long were connected to the root pressure probe. When the root pressure reached a stable value (it took around 30 to 120 min), a series of pressure clamps was carried out (3-5 clamps) to induce a flow of water into the root. Root pressure was increased in 20 to 50 kPa increments and held constant at each increment for 10–120 s by continually adjusting the metal rod inside the pressure chamber of the probe. The distance that the metal rod had moved was used to calculate the cumulative water volume, and retrieve the average flow rate [L^3T^{-1}] across the root. The slope of the linear regression of flow rates plotted against the applied pressure differences yielded the total root conductance for this root length. The root was then cut towards its tip and reconnected to the root pressure probe to repeat the cycle until the root end was reached.

It can be shown that the root collar flow under uniform soil-root interface potential is given by (see Appendix A):

$$J_x(l) = K_{root}\,(\Psi_0 - \Psi_i) \tag{7.1}$$

with K_{root} the unbranched root conductance (Meunier et al. 2016a). For a given length l, the axial flow should be consequently a linear function of the applied pressure. Isolating the root conductance from Eq. 7.1 yields:

$$K_{root} = \frac{J_x(l)}{\Delta\Psi_i} \tag{7.2}$$

with $\Delta\Psi_i = (\Psi_0 - \Psi_i)$. As a consequence, the root conductance can be obtained by measuring simultaneously the root axial flow and the

collar potential, as done by a root pressure probe. As the profile of xylem water potential and the axial flow depend on the local hydraulic property distributions, so does the root conductance. Figure 7.2-A illustrates the procedure to estimate K_{root}. Initially the entire root length is l_1 and its total conductance, $K_{root,1}$, is deduced from the slope of a linear regression between root fluxes and applied pressures. The root conductance is measured for several root lengths by cutting a small portion of the root at its proximal end and repeating the pressure probe measurement.

7.2.4 Axial conductance

Axial hydraulic conductance was determined after cutting the root connected to the root pressure probe with a razor blade at a distance of from its proximal end. Similar to the measurement of total conductance, a series of pressure clamps was carried out to induce water flow into the root segment. The slope of the linear regression of flow rate plotted against the applied pressure difference gave axial conductance of the root segment. The axial intrinsic conductance was calculated as the product of the measurement by the segment length (see Appendix A for details).

When solving this differential equation, we obtain for the axial flow:

$$J_x(l_{seg}) = \frac{k_x}{l_{seg}} \Delta\Psi_i = K_x \Delta\Psi_i \tag{7.3}$$

where l_{seg} is the root segment length. The axial conductance K_x, equal to the ratio $\frac{k_x}{l_{seg}}$, can be obtained by measuring the flow and the potential together. The axial conductance measurement was assigned to the middle position of the root segment:

$$k_x \left(z_n = l_n - \frac{l_{seg}}{2} \right) = K_{x,n}.l_{seg} \tag{7.4}$$

where n designates the measurement index (comprised between 1 and the total number of measurements). Four to five replicates per root type were considered.

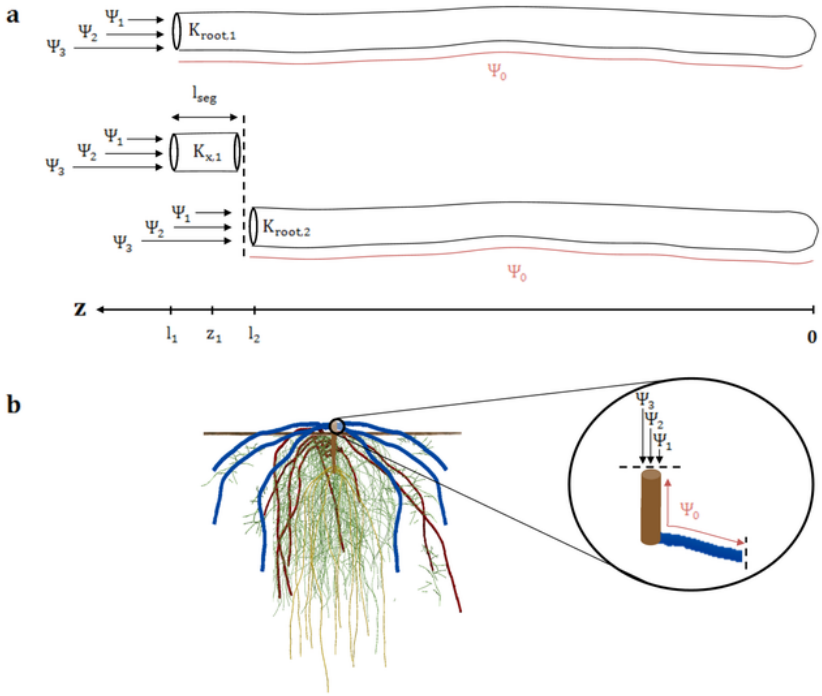


Figure 7.2: Principle of the conductance measurements. Total root conductance is estimated by increasing the pressure applied to the root extremity and measuring the corresponding flow. The root is then cut, the proximal (short) part is used to assess the axial conductance of the root tissues at this position and the distal (long) part is the raw material for repeating the experiment from step one (a). The root-shoot connection conductance is measured on a small portion of the root and the stem as highlighted in the second subplot, the bottom stem outflow was avoided by sealing this part of the system (b).

7.2.5 Junction root-shoot conductance

A simple version of the high pressure flowmeter method was used to determine the axial hydraulic conductance of root-shoot junction. Both roots and stem were cut at distance of 2 cm from the junction points. Then the stem was connected to a tube designed to perfuse water into the base of the stem with stepwise increasing pressures. Twenty minutes after applying a given pressure, the volume of water that passed through each root type (length of ca. 2 cm) was determined by weighing a soft tissue before and ten minutes after absorbing water from cut end of roots. The slope of the linear regression of flow rate plotted against the applied pressure yielded the axial conductance of the root segment. Four to five replicates were taken for these experiments. Note that the axial conductances measured here refer to axial conductance of root-shoot junction of seminal, crown and brace roots at a distance of 58-65cm, 45-52, and 3-40 cm from root tip, respectively. Here we were constrained to the maximum length of each root type.

Figure 7.2-B shows how we adapted the procedure to the root-shoot junction of maize roots.

7.2.6 Optimization scheme

The objective of the optimization procedure was to obtain the distribution of k_r along root axes of different root types. First (scenario 1, table 1), we optimized k_x and k_r based on $k_r$oot measurements only, assuming that they were unique (uniform values). In the first scenario, the measurements of k_x were not used. In the next scenarios, (2 to 5) we assume that k_r and k_x were a function of distance to root tips and k_x measurements were used as extra information to total root conductance measurements. The axial conductance function was optimized independently by linear piecewise function of root age and several scenarios of root radial conductivity (scenarios 2-5, table 1) were tested to match the total root conductance. Comparison of scenarios was based on the adjusted r-square as the total number of model parameters is scenario-dependent. The four considered k_r functions were: constant, exponential, stepwise (max. 3 steps) and piecewise (max. 5 points). The scenarios were selected for their simplicity and flexibility (Zarebanadkouki et al.

Table 7.1: Summary of the considered scenarios for fitting the measurements

Scenario	$k_x(z)$ function	$k_x(z)$ parameters	$k_r(z)$ function	$k_r(z)$ parameters	Unknowns
1	constant	1	constant	1	2
2	Linear piecewise	4-8 (separate fit)	constant	1	5-9
3	Linear piecewise	4-8 (separate fit)	exponential	2	6-10
4	Linear piecewise	4-8 (separate fit)	stepwise	5	9-13
5	Linear piecewise	4-8 (separate fit)	Linear piecewise	6	10-14

2016) and their relatively low number of parameters as compared to the number of observations (Meunier et al. 2016a).

The optimizations were achieved in MATLAB with the Multistart heuristic algorithm (Optimal Methods Inc., USA) as global solver. The analytical solutions of Landsberg and Fowkes (1978) and Meunier et al. (2016a) were used to compute analytical solutions of water flow equation for scenario 1 and 2-5, respectively.

7.3 Results

7.3.1 Example of pressure probe experiment

An illustration of the pressure clamps transduced to the measured root is shown in Figure 7.3 (left). Three successive clamps are applied to a maize crown root of 13 cm long including its tip (Ψ_1, Ψ_2 and Ψ_3) after an initial equilibrium was reached (Ψ_0). The observed water flows are reported as a function of the pressure difference in the right subplot of Figure 7.3. A linear regression is finally applied to the observations. The slope of the linear relationship is the root conductance.

Good fits (r2 between 0.95 and 1) were obtained from the regression between the water flow and the pressure transduced by the pressure probe.

7.3.2 Conductance results and fits

Figure 7.4 shows the profile of hydraulic properties along different root type of maize plant. Subplots 7.4-A and 7.4-B show total hydraulic conductance and axial hydraulic conductance obtained from root pressure probe measurements, respectively (data presented as dots). Both total and axial hydraulic conductances increased with increasing length or

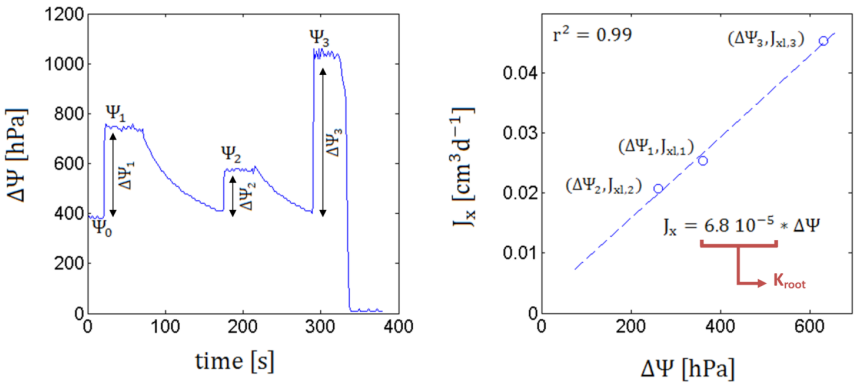


Figure 7.3: Example of root conductance measurement. A series of three successive clamps are applied to a specific root (left) and the corresponding water flows are recorded as well. When plotted ones against the others, a linear regression can be applied between axial flow and the difference of pressure imposed. The conductance is the slope of this linear regression.

distance from root tip and reached a plateau at a varying length or distance from root tip in each root type. After simulation of water flow into unbranched roots of varying length, the profiles of axial conductance and radial conductivity were obtained for each root type (Figure 7.4-B and 7.4-C, respectively). Here, for given boundary condition, profiles were optimized to best reproduce the measured profile of total and axial conductance (solid line). The resulting total conductance with the local hydraulic properties are plotted as solid lines in subplot a. The root mean radii were 0.067, 0.052, 0.037, 0.03 and 0.025 cm for brace, crown, seminal, maize lateral and lupine lateral roots, respectively.

Then the ratio of root axial conductance and radial conductivity along the root axis is plotted in subplot 4d. Throughout the whole manuscript, we keep the same colours that represent the different root types.

Similarly, hydraulic properties of lateral roots of lupine are represented in Figure 7.5. The y-axis limits have been kept the same as the ones presented in Figure 7.4 to easily compare the absolute values of measurements between the two species.

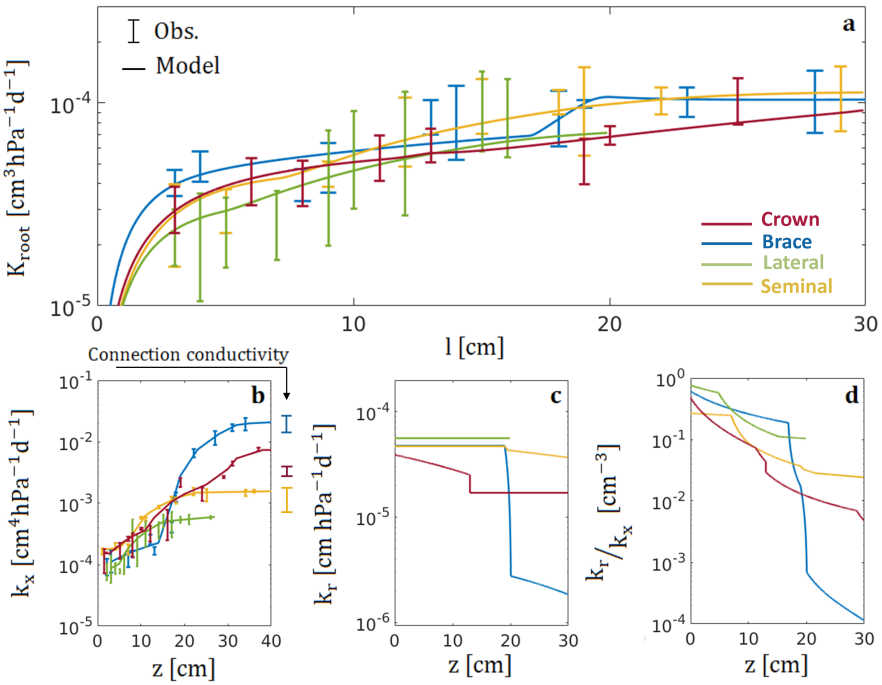


Figure 7.4: Hydraulic properties of the different root types of maize. Subplots a and b: total and axial hydraulic conductance of different root types as function of distance from root tip, respectively. Data presented as dots are average of 3 to 7 measurements and the error bars the standard divisions. Profiles plotted as solid lines are the best profiles obtained from simulation of water flow into unbranched roots of varying length. Subplots c: best fitted profiles of radial conductivity that reproduces measured profiles of total hydraulic conductance. Subplot e: ratio of radial conductivity to axial conductance derived from the analysis along the root axis.

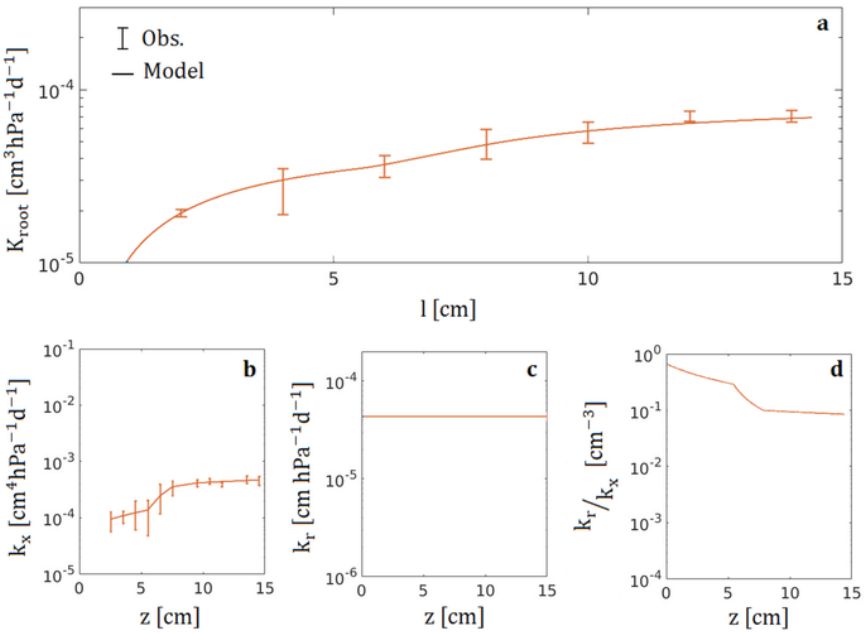


Figure 7.5: Hydraulic properties of the lateral roots of lupine. Subplots a and b: total and axial hydraulic conductance of different root types as function of distance from root tip, respectively. Data presented as dots are average of 3 to 7 measurements and the error bars the standard divisions. Profiles plotted as solid lines are the best profiles obtained from simulation of water flow into unbranched roots of varying length. Subplots c: best fitted profiles of radial conductivity that reproduces measured profiles of total hydraulic conductance. Subplot e: ratio of radial conductivity to axial conductance derived from the analysis along the root axis.

Finally, the axial conductances of root-shoot junction of three main maize root types are illustrated in Figure 7.6 with their mean values and the standard deviation of the observations. These axial conductances refer to axial conductance of root-shoot junction of seminal, crown and brace roots at a distance of 58-65cm, 45-52, and 3-40 cm from root tip, respectively.

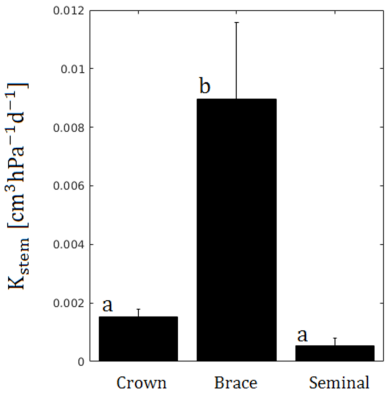


Figure 7.6: Junction conductance between the main maize roots (seminal, crown and brace) and the stem. Different letters indicate significant differences between measured means.

It appears that brace roots have the greatest axial hydraulic conductance and the seminal roots have the smallest. The difference between axial conductance of brace and seminal roots was 11.46 times and the difference between crown and seminal roots was 2.79 times. These results suggests that brace roots and then crown roots has a significantly better connection to the stem. In this figure, the letters designate the corresponding statistical groups.

7.3.3 Goodness of fit

The corresponding hydraulic functions are given in tables 2 and 3, respectively, in the form of conductivity/position couples for both species and all root types. The adjusted correlation coefficients for best sce-

Table 7.2: Best fit for the axial conductance profile of maize and lupine roots given as distance from root tip, axial conductance couples. The hydraulic functions were optimized as piecewise functions. The coefficients of determination are given as well for each root type.

Species	Root type	Best scenario	z [cm]	k_x [$10^{-4} \times cm^4 hPa^{-1} d^{-1}$]	r^2
Maize	Seminal	4-linear piecewise	0 - 7 - 10 - 21 - 40	1.76 - 1.91 - 5.45 - 14.85 - 15.85	0.98
	Crown	4-linear piecewise	0 - 11.2 - 28.7 - 34.3 - 40	0.82 - 3.71 - 24.44 -73.63 - 73.63	0.97
	Brace	4-linear piecewise	0 - 16.9 - 27 - 32.6 - 40	0.78 - 2.56 - 122 - 196 - 225	0.99
	Lateral	3-linear piecewise	0 - 4.8 - 15.2 - 30	0.74 - 0.98 - 5.04 - 5.99	0.93
Lupine	Lateral	3-linear piecewise	0 - 5.5 - 7.92 -15	0.62 - 1.44 - 4.22 - 4.95	0.99

Table 7.3: Best fit for the radial conductivity profile of maize and lupine roots given as pairs of distance from root tip and radial conductivity values. The adjusted r-square are provided as well for each root type.

Species	Root type	Best scenario	z [cm]	k_r [$10^{-4} \times cm.hPa^{-1} d^{-1}$]	r^2
Maize	Seminal	5	0 - 19 - 19.5 - 30	0.47 - 0.47 - 0.43 - 0.28	0.88
	Crown	5	0 - 13 - 13.1 - 30	0.39 - 0.25 - 0.17 - 0.17	0.72
	Brace	5	0 - 19 - 20 - 30	0.48 - 0.48 - 0.028 - 0.02	0.83
	Lateral	1	0 - 15	0.56 - 0.56	0.65
Lupine	Lateral	1	0 - 15	0.432 - 0.432	0.97

narios are indicated as well. They are always higher for the best fit of axial conductance profiles (0.93-0.99) and lower for the best fit of radial conductivity profile (0.65-0.97). For the latter, the scenario 4 is always privileged except for the maize and lupine lateral roots where the constant radial conductivity profile reached the highest adjusted r^2 for both species.

The measurements and fittings are represented all together in Figure 7.7 for both the axial conductances (bottom) and the total conductances (top). The two general cases may be compared in terms of goodness of fit: the scatter plot represent the fitted scenario 0 and the crosses, the best fitted function between the four other scenarios (1-4). The two simulation sets reach similar fitting quality for the total root conductance (r-square a little bit larger than 0.8) but have abilities of fitting the axial conductances pretty contrasted. Constant scenarios could not catch such a variation with satisfactory fitting.

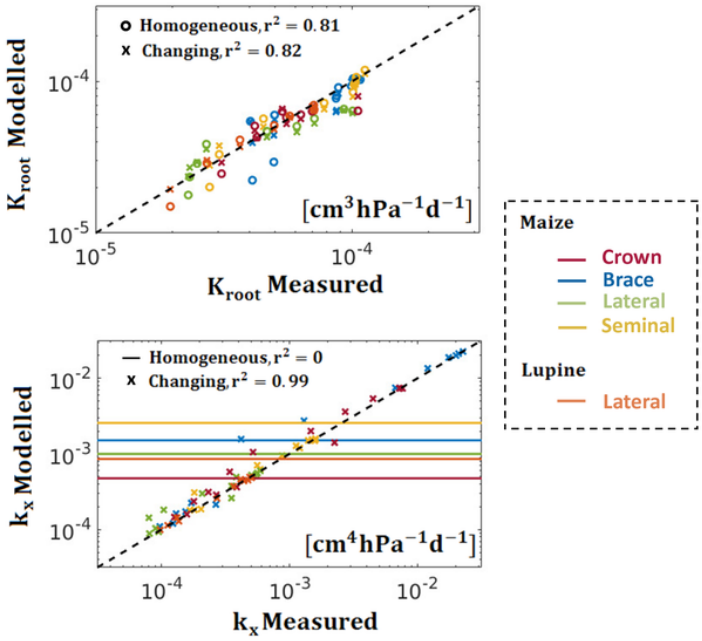


Figure 7.7: Overall goodness of fit for the total root conductances (top) and the axial conductance (bottom). Scenario 1 (circles and lines) and best scenario (crosses) are compared in terms of correlation coefficient.

7.4 Discussion

Interestingly, the measured total conductances (K_{root}) of different root types and plant species root were in the same order of magnitude (see Figures 7.4 and 7.5, top), while the observed axial conductances were quite different (Figure 7.6, bottom: more than two orders of magnitudes between the smallest and largest measurements). The latter result is expected when comparing roots of different orders and ages, the former is surprising. The lupine root conductances are in average smaller but the measurements correspond to smaller lateral roots. When compared, the lateral roots of the two species are rather similar (r^2 of 0.85) and the best fits were both obtained with homogeneous radial conductivity functions. This is opposite to what was obtained in the previous Chapter.

As a consequence the radial profiles of hydraulic conductivity are similar between the species. In Fig. 7.8, we plotted the relative water uptakes in homogeneous soil-root interface potential for the different root types along its longitudinal axis. They were calculated using a single root scenario just as in Zarebanadkouki et al. (2016).

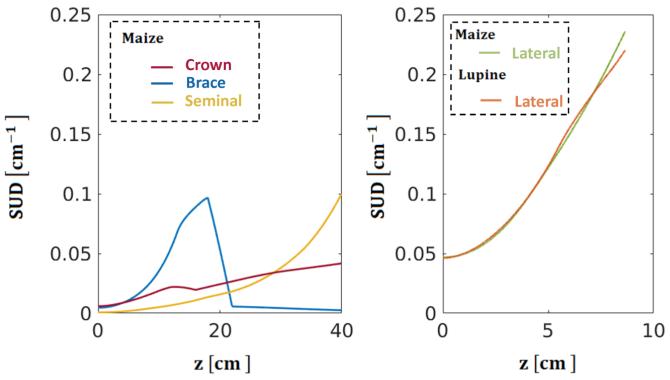


Figure 7.8: Root water uptake location in the different root types.

From empirical observations reported in the literature, the opening of early metaxylem vessels progressively occurs in the region from 4 to beyond 14 cm from the root tip in maize (Wenzel et al. 1989). Our measurements suggest that the timing of early metaxylem vessels opening varies among root types. In brace roots, the dramatic increase of root axial conductance related to early metaxylem opening took place in the narrow range between 15 and 25 cm from the apex. In contrast, our observations suggest that in crown roots early metaxylem vessels start opening closer to the root tip and new vessels of that type keep on reaching maturity beyond 30 cm from the apex. Late metaxylem vessels reportedly reach maturity 40 to 50 cm from the root tip in maize, increasing the axial conductance by an extra order of magnitude (Doussan et al. 1998a; St. Aubin et al. 1986), and thus were likely not open in our root samples.

The cellulosic diaphragms, or "pit membranes", that separate a branch from its mother root xylem vessels were reported to filter out

particles as small as 5 nm (Shane et al. 2000), like common primary cellulosic walls (hydraulic conductivity: 7×10^{-3} $m^2s^{-1}MPa^{-1}$(Steudle and Boyer 1985)). Assuming 50 x 50 micron connective xylem junction surface, and 1 micron thick diaphragms (Shane et al. 2000), yields a junction hydraulic conductance of 1.7×10^{-3} $cm^3d^{-1}hPa^{-1}$, which corresponds to the range measured in our seminal and crown roots (Fig. 7.6). Corresponding anatomical analyses for brace roots were not documented in the literature. The higher junction conductance of brace roots might for instance be due to larger pore size in junction diaphragms as reported in the literature for various plants (Sperry and Tyree 1988; Van Alfen et al. 1983).

The optimized root radial conductivities (k_r) tended to decrease with distance from the tip in principal roots, and remained stable in laterals. Longitudinal variations of k_r were not always observed in maize principal roots (e.g. (Frensch et al. 1996)). In cases they were, anatomical features such as the systematic development of hydrophobic barriers (Tylová et al. 2017) and aerenchyma were considered responsible for the k_r spatial gradient (Fan et al. 2007). Note that our experiments were achieved in saturated conditions and therefore the aerenchyma was probably saturated (this was not checked) and should therefore rather increase the radial conductivity of these regions. Cell plasma membrane permeability was reported not to vary longitudinally (Zimmermann et al. 2000) and would thus not contribute to k_r variations.

Maize laterals systematically form an endodermal Casparian strip, but the development of other apoplastic barriers remains quite limited when grown in well-watered soil (Tylová et al. 2017), which may explain why we do not observe variations of k_r along laterals (Figure 7.5). The longitudinal k_r gradients previously observed in lupine laterals (Zarebanadkouki et al. 2016) may be the result of the sandy growth medium that is prone to generate water stress and foster the development of suberin lamellae in both endodermis and exodermis, as demonstrated experimentally in maize laterals by Tylová et al. (2017).

In order to compare the radial and axial root hydraulic properties derived from the pressure probe experiments, we compared them to root radial and axial conductivities from the literature (Figs 7.9 and 7.10). In these graphs, all the studies are sourced in the bottom panels and the colours correspond to the plant species: blue for maize plant (any

genotype), red for lupine (any genotype) and black for other herbaceous species. Most of the presented values come from the reviews of Draye et al. (2010) and Rieger and Litvin (1999).

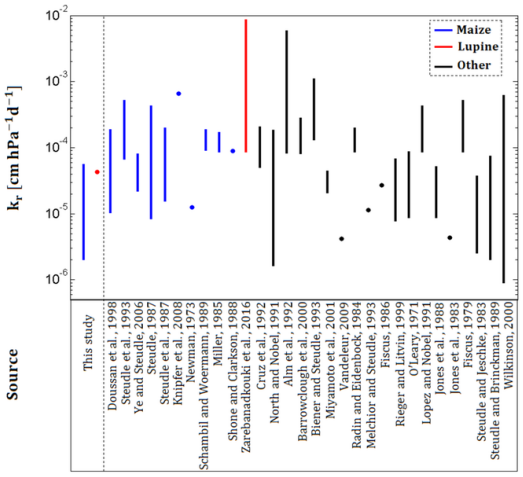


Figure 7.9: Comparison of the root radial conductivity obtained in this study and the ones measured in the literature for maize (blue), lupine (red) and other herbaceous species (black)

Bars indicate ranges of variation observed in the corresponding studies. The range of radial conductivity observations covers four orders of magnitude (see Figure 7.9). The k_r values in our study are rather low as compared to other values for the same species, but correspond on average to observed radial conductivity values of herbaceous plants.

Root conductance (K_{root}) is frequently assumed to be a linear function of root length for simplicity (Ehlert et al. 2009; Hachez et al. 2012). Here we show empirically that the K_{root}(length) function saturates for all of the considered root types, which was demonstrated theoretically to be a consequence of axial hydraulic limitation (Meunier et al. 2017). Hence the typical empirical assumption that k_r is the measured K_{root} per unit root surface could generate substantial bias (underestimation of k_r), particularly for long roots.

More than five orders of magnitudes difference exist between the lowest and highest observed root axial conductances, even in herbaceous

species only (see Figure 7.10). Including woody plants would have further enlarged this range. Again, the axial conductances obtained from our experiments are in the overall range of non-woody species even though they are rather equivalent to the lowest values of the corresponding species.

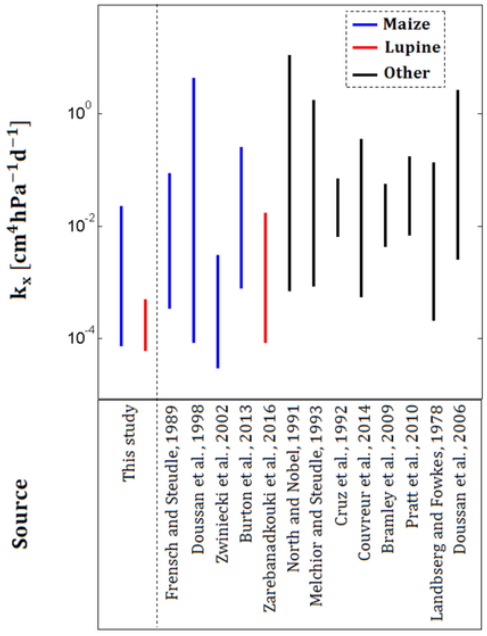


Figure 7.10: Comparison of the root axial conductance obtained in this study and the ones measured in the literature for maize (blue), lupine (red) and other herbaceous species (black)

In our study, it was systematically impossible to fit simultaneously the root axial and total conductances with constant hydraulic functions. While pretty good results can be obtained for total root conductances alone (see Figure 7.5, top), axial measurements highlighted the xylem conductivity changes while the root grows and develops. It indicates that measuring root conductances with different root lengths is not sufficient to successfully reproduce the conductivity profiles along the roots: it would have been impossible to discriminate a constant hydraulic model

from complex ones from these measurements only. The combination of axial and total root conductances only allows one to do so.

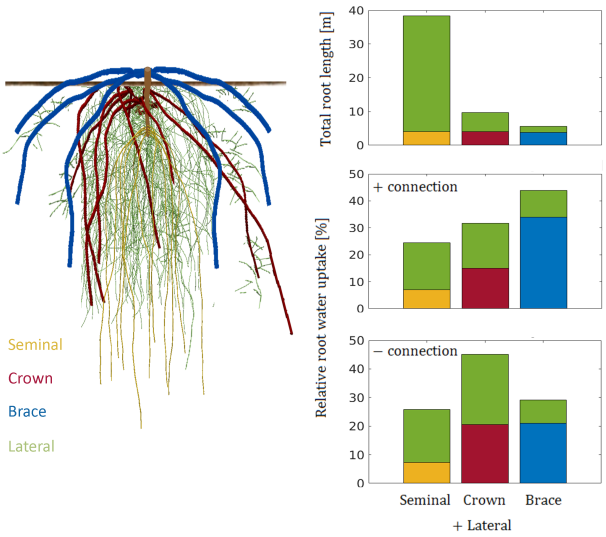


Figure 7.11: Comparison of the relative water uptake with or without the measured connection conductances at root-shoot junction and the total root length of the different root types.

When comparing the root-stem connection conductances with the axial conductances measured from the root tips (the former must be multiplied by the sample length, i.e. around 2 cm), we see that similar values appear only for the crown roots. For both the brace and the seminal roots, the junction hydraulic conductivity is much smaller than the axial conductivity of the corresponding roots close to this point, with a probably large water flow reduction due to this bad connection issue. It suggests a potential plant regulation mechanism for root water uptake location. Instead of finely tuning radial properties locally to adapt the water uptake to the local environment, plant could roughly decide to stop taking up water from one entire root by shutting its connection with the stem and switch water uptake from one root (or one root type) to another.

Lateral-to-primary connections could also be investigated between

main axes (seminal, crown and brace) in the future as the lateral roots seem to have different properties in function of the mother root type. However it is likely that the potential observed differences are not as large as the ones measured on the root-shoot connections as in the latter case, different root systems truly develop and grow at different plant stages with potentially different purposes and/or preferential pathways to leaves.

All together the measurements derived from this study give a complete description of the hydraulic properties of the maize plant. Combined with architectural properties, it allows building root system hydraulic architecture models fully parametrized that would tackle open questions such as root water uptake distribution in growing root systems and relative roles of the different root types in contrasted environments. As illustration example, we generated a mature root system using MARSHAL (see Chapter 5) and root segment hydraulic properties were allocated according to root distance to tip and age. Root-shoot connection conductances were either assignated to their measured values or to extrapolated ones according to their root types. Both root system representation and water uptake with or without taking the connection conductances are represented in Figure 7.11 under homogeneous soil conditions.

Connection conductance significantly impact the water uptake distribution within the root system as it dramatically reduces the relative uptake of the crown root system and increases the relative uptake of brace root system. In all cases, the root length distribution is not a good proxy for root water uptake when xylem may limit the flow and hydraulic properties are not uniform within the root system. It is also worth saying that the uptake of the lateral roots is despite their length not so important compared to the uptake by the all main roots. The relative small lengths of these axes are partially compensated by their large radii that increase their total surface and their preferential connection with the shoot. Both together these properties explain why more water than expected from the distribution of lengths is taken by primary roots.

7.5 Conclusion

Total and axial root conductances of maize and lupine unbranched roots were measured using a pressure probe technique. The methodology allowed us to compute root water flows in single roots under different scenarios of radial and axial hydraulic conductivity profiles. The best scenarios fitted the measurements pretty well for both axial (r-square between 0.93 and 0.99) and total (r-square between 0.65 and 0.99) conductances. While the axial properties revealed significant differences between root types and species, the total root conductances were rather similar which implies changes of root radial conductivity between root order and ages. The analysis showed that the root-stem connection conductances deeply depended on the maize root type with the highest values for the crown roots. Regulation mechanism for location of root water uptake could be the cause of such contrasts between root types. Comparison with the literature unveiled discrepancies between studies for both radial and axial root properties within and between species. Our results were in the low middle.

7.6 Appendix

Appendix A: Exact solution of macroscopic parameters

The local root water uptake in a cylindrical root of radius r [L] and length l [L] is usually represented by a membrane-like equation (Landsberg and Fowkes 1978). The radial flow of water per root length along the root axis z [L] is driven by the water potential difference between the xylem vessels and the soil-root interface, hereafter referred to as and, respectively. It depends also on the inherent radial conductivity of the root tissues:

$$q_r(z) = -2\pi r k_r(z) \left(\Psi_x(z) - \Psi_0\right) \tag{A.1}$$

All the state variables here may vary along the root axis except for the soil-root interface potential that is considered as uniform because in our experiments the roots were entirely contained in the same water solution. The root axial flow that takes place within the xylem vessels is powered by the water potential gradient in these conduits and is regulated by their axial conductance:

$$J_x(z) = -k_x(z)\frac{d\Psi_x(z)}{dz} \tag{A.2}$$

Mass conservation implies that the radial flux as described by Eq. A.1 leads to incremental changes of the axial flow given by Eq. A.2:

$$\frac{d}{dz}J_x(z) = q_r(z) \tag{A.3}$$

Combining Eq. A.1-A.3 yields the most general form of the water flow equation in an unbranched root in homogeneous soil potential (Frensch and Steudle 1989):

$$\frac{d}{dz}\left(k_x(z)\frac{d\Psi_x(z)}{dz}\right) = 2\pi r k_r(z)\left(\Psi_x(z) - \Psi_0\right) \tag{A.4}$$

Equation A.4 is a potentially non-linear differential equation of the second order that can be solved either analytically for several root hydraulic conductivity distribution (constant, linear, exponential or any

complex combination of these three functions (Meunier et al. 2016a) or numerically for any complex shape of root hydraulic properties (Alm et al. 1992; Doussan et al. 1998a). Solving Eq. A.4 requires two boundary conditions. Here we consider the case of a constant water potential applied at the proximal end (z = l), and a no-flux at the distal root end (z = 0):

$$\begin{cases} J_x(z=0) = 0 \\ \Psi_x(z=l) = \Psi_i \end{cases} \tag{A.5}$$

The solution of Eq. A.4 with particular boundary conditions A.5 to the xylem potential distribution that, in turn, provides the radial flux and axial flow along the root axis through Eqs. A.1 and A.2, respectively. The water flow can be written as:

$$J_x(l) = K_{root}\left(\Psi_0 - \Psi_i\right) = K_{root}\Delta\Psi_i \tag{A.6}$$

with K_{root} the total root conductance and $\Delta\Psi_i = (\Psi_0 - \Psi_i)$.

When the root is cut, the methodology (pressure clamps and flow measurements) is also applied to the short root segment to compute the axial conductance. For short segments of length l_{seg} [L], we can neglect the radial flow and consider that the root hydraulic properties are homogeneous, Eq. A.4 becomes:

$$\frac{d^2\Psi_x(z)}{dz^2} = 0 \tag{A.7}$$

That, solved with the following boundary conditions,

$$\begin{cases} \Psi_x(z=0) = \Psi_0 \\ \Psi_x(z=l_{seg}) = \Psi_i \end{cases} \tag{A.8}$$

leads to the solution:

$$J_x(l_{seg}) = \frac{k_x}{l_{seg}}\Delta\Psi_i = K_x\Delta\Psi_i \tag{A.9}$$

where we noted $K_x = \frac{k_x}{l_{seg}}$.

INVESTIGATING SOIL-ROOT INTERACTIONS WITH THE NUMERICAL MODEL R-SWMS

8

This chapter is a modified version of a book chapter submitted for Methods in Molecular Biology as:

> Meunier F., Couvreur V., Draye X., Lobet G., Huber K., Schroeder N, Schnepf A., Vanderborght J., Vereecken H. and Javaux M. Investigating soil-root interactions with the numerical model R-SWMS. Submitted to Methods in Molecular Biology

Abstract

In this chapter, we present the Root and Soil Water Movement and Solute transport model R-SWMS, which can be used to simulate flow and transport in the soil-plant system. The equations describing water flow in soil-root systems are presented and numerical solutions are provided. An application of R-SWMS is then briefly discussed, in which we combine in vivo and in silico experiments in order to decrypt water flow in the soil-root domain. More precisely, Light Transmission Imaging experiments were conducted to generate data that can serve as input for the R-SWMS model. These data include the root system architecture, the soil hydraulic properties and the environmental conditions (initial soil water content and boundary conditions, BC). Root hydraulic properties were not acquired experimentally, but set to theoretical values found in the literature. In order to validate the results obtained by the model, the simulated and experimental water content distributions were compared. The model was then used to estimate variables that were not experimentally accessible, such as the actual root water uptake distribution and xylem water potential.

8.1 Introduction

Root water uptake (RWU) is a passive process essentially driven by water potential gradients between the soil around roots and the xylem (water conducting tissue within the root), and controlled by hydraulic properties at the soil-root interface and of the roots themselves (Steudle and Peterson 1998). At the plant scale, evaporation from leaf mesophyll surface decreases the water potential in the leaf, which propagates via cohesion-tension through plant xylem and decreases the root water potential as compared to the surrounding soil, thereby extracting soil water. Understanding transpiration and RWU processes is important not only at the small scale but also at the global scale. According to a recent analysis of isotopic data (Brooks 2015), at the global scale, transpiration represents 47.8% $\pm$ 10.4% of the continental precipitations. Yet, the investigation and the modeling of root water uptake processes has remained a scientific challenge for decades (Green et al. 2006). Estimates of transpiration via land surface models were shown to be affected with a high uncertainty (Wang and Dickinson 2012), mainly due to the poor representation of root water uptake in particular under dry conditions (Canal et al. 2014) and compensation mechanisms (Tang et al. 2015). Today however new technological advances on monitoring soil-water fluxes (e.g. (Zarebanadkouki et al. 2013)) and improved understanding of the biological processes controlling RWU (Lobet et al. 2014) open new opportunities for detailed biophysical models.

Numerous models for RWU simulation already exist. They principally differ in two aspects: their dimensionality, i.e. the way they account for root architecture and soil complexity, and the degree of empiricism in functions describing water uptake reduction and redistribution when water is depleted in parts of the root zone. Typically, these models use Richards equation (Richards 1931) to describe water flow in soils under usual assumptions of incompressibility of the porous matrix and isothermal single phase flow. Soil water extraction is implemented in this equation by subtracting from the water flow divergence a sink term S, which aggregates the local uptake by roots up to the macroscopic

scale of representative elementary soil volumes (REV):

$$\frac{\partial \theta}{\partial t} = \nabla . \left[K \nabla \left(h + z \right) \right] - S \tag{8.1}$$

where θ [-] is the volumetric water content, K $[\mathrm{LT}^{-1}]$ the hydraulic conductivity tensor, h [L] the matric head, z [L] the elevation, which is defined positive upward, and S $[\mathrm{T}^{-1}]$ a sink/source term, positive for RWU and negative for water release. Functional relationships between water content, matric head and hydraulic conductivity (called retention, $\mathrm{h}(\theta)$, and conductivity, $\mathrm{K}(\theta)$, functions) are needed to solve Eq. 8.1. The sink term represents the water flow from soil to root by volume of soil and can be related to the actual plant transpiration $\mathrm{T_{act}}$ $[\mathrm{L}^3\mathrm{T}^{-1}]$ as

$$T_{act} = \int_{\Omega_r} S dx \tag{8.2}$$

where Ω_r $[\mathrm{L}^3]$ is the total soil volume occupied by roots, dx $[\mathrm{L}^3]$ an infinitesimal soil volume around location x. Many different forms of the sink-term function have been experimentally developed in the literature (e.g., (Feddes and Zaradny 1978; Gardner 1960; Herkelrath et al. 1977; Jarvis 1976; Molz and Remson 1970)). They are typically composed of four factors: (i) a root distribution function, (ii) a soil resistance function, (iii) a stress function, and (iv) a compensation function (Javaux et al. 2013). Due to the difficulty to characterize root architecture and hydraulic properties (Feddes and Raats 2004), most of these models use a probability density function for potential RWU. Vrugt et al. (2001) for instance showed the potential of using this probability representation for describing RWU of an almond tree in 3-D. However, the in situ-characterization of the 3-D root length distribution remains tedious (Kuchenbuch et al. 2009). In addition, thanks to recent advances in 3-D root growth models (Pagès et al. 2004) and in novel methods to image and map root architecture (Mooney et al. 2011; Stingaciu et al. 2011), the requirements of models using root architectures have become more reachable. Clausnitzer and Hopmans (1994) proposed one of the first 3-D RWU models based on an explicit detailed description of the root architecture. A root growth model was coupled to the Richards equation, and RWU was simulated based on root length density distributions derived from root architectures (Somma et al. 1998). Yet,

water flow within the root was not modeled. An additional step was performed by (Doussan et al. 2006) who developed that 3D approach by implementing water flow through the root system. Javaux et al. (2008) built the R-SWMS model based on the same principles: solving and coupling both root and soil water flow equations. They explicitly modeled isohydric water stress, i.e. the water stress of a plant that can regulate the water potential in the leaves and keep it at a constant level by closing stomata. Several additional features were then added in R-SWMS, like microscopic water flow towards roots (Schröder et al. 2012), cavitation (Lobet and Draye 2013), gap formation at soil-root interfaces (Couvreur et al. 2014b), solute transport in soil and solute/nutrient uptake (Schröder et al. 2012), uptake in saline soils including osmotic potential gradients beween the bulk soil, the soil-root interface and the plant xylem (Schröder et al. 2014), solute transport in the root and chemical signaling production and transport to the shoot (Huber et al. 2014), anisohydric stomatal regulation as a function of chemical signal concentrations in the roots (Huber et al. 2015), coupled root growth and water/nutrient uptake (Koebernick et al. 2015). Today other three-dimensional models explicitly modeling root water flow exist (Schneider et al. 2010; Tournier et al. 2015) but none of them has all the features of R-SWMS (Dunbabin et al. 2013).

This model also has limitations due to its hypotheses. Although each root segment is characterized by a diameter and a length, it does not account for the physical presence of root as an impeding feature for soil water flow. The anatomy of root cross section is not explicitly described and implicitly considered as uniform on the segment length, i.e. the finest scale is the root segment. Plant canopy and beyond-ground architecture are not explicitly represented. Stomatal conductance is thus modeled through an effective function. As mentioned before, the existence of a REV for the soil is assumed, allowing the description of the water flow and solute transport as a continuum.

Such a model, by explicitly representing the root architecture and the bio-physical laws controlling the water flow, allows one investigating how processes at the root segment scales may alter plant scale water relations. This model can be used as a mean to investigate scientific assumptions or hypotheses. Schröder et al. (2014) used R-SWMS numerical simulations compared with historical data of Hamza and Aylmore

(1992) to demonstrate that there was no osmotic adjustments and a constant reflection coefficient for solute uptake. R-SWMS can also be used to explore new hypotheses and study the impact they might have in a quantitative way. For instance, it has been used to assess the role of specific root traits on the plant resistance to drought (Leitner et al. 2014). Couvreur (2013) used it to investigate how potential aquaporin regulation by the soil hydraulic status would affect plant water uptake. Recently Schwartz et al. (2016) studied how the mucilage could affect the distribution and magnitude of water uptake and the stress onset. Combined with data R-SWMS can also be used to characterize local parameters or variables at which we do not have a direct access. Koebernick et al. (2015) for instance used R-SWMS to elucidate the role of impeding layers on the plant transpiration monitored in a split root experiment and to estimate water fluxes between soil layers. Finally this model can also be used to design soil plant experimental set-up.

The objectives of this chapter are threefold: (1) to introduce the basic physical equations governing the water flow in the soil-root system; (2) to present the finite element numerical solution for these equations, and (3) to provide an example of the use of R-SWMS to analyze experimental data and test local scale hypotheses.

8.2 Model description

8.2.1 Water flow

Soil water flow can be described using the 3-D Richards equation 8.1. Flow in the root system can be modeled based on radial and axial flow equations. When osmotic potential is not considered, the radial flux density entering a root segment, q_r $[L^3L^{-2}T^{-1}]$ at a position x and a time t is given by:

$$q_r(x,t) = L_r\left(h_{sr}(x,t) - h_x(x,t)\right) \tag{8.3}$$

where L_r $[T^{-1}]$ is the root radial conductivity and h_{sr} [L] and h_x [L] are the pressure heads at the soil-root interface and in the xylem respectively.

The axial volumetric flow along root, J_x [L^3T^{-1}] is described by:

$$J_x(x,t) = -K_x(x,t)\left(\frac{dh_x(x,t)}{dl_{seg}(x)} + \frac{dz}{dl_{seg}(x)}\right) \tag{8.4}$$

where dl_{seg} [L] is the arc length of a root segment and defined positive in the direction of root growth, and K_x is the xylem axial conductance [L^3T^{-1}]. A negative J_x then implies a flux towards the root collar. The volume balance on an unbranched root segment dl_{seg} with a diameter r [L] is:

$$2\pi r q_r = \frac{dJ_x}{dl_{seg}} \tag{8.5}$$

In the following, we define the radial volumetric flow of a root segment J_r [L^3T^{-1}] as:

$$J_r = 2\pi r q_r l_{seg} \tag{8.6}$$

8.2.2 Boundary conditions

Equation 8.6 can be written and solved for each segment of a complex root system provided that we know the root system architecture, the soil water potential, and the BC at the root tips and the root collar. The BC for the axial flow at the root tips is considered to be a no flux boundary. At the root collar, the following BC can be defined:

(a) Imposed flux: a potential transpiration is imposed at the collar: $J_x = -T_{pot}$ [L^3T^{-1}] where T_{pot} is the prescribed transpiration rate estimated based on climatic conditions and plant properties (e.g., crop coefficient). When the prescribed transpiration cannot be met due to low soil water potential, water stress occurs, which decreases the transpiration. We describe it as an isohydric stress process, in which a plant maintains its water potential at the collar (or, by extension in the leaf) above a critical value hx,lim. This can be written mathematically as:

$$\begin{cases} J_{x,1} = T_{act} & \Psi_{collar} \geqslant \Psi_{lim} \\ \Psi_{collar} = \Psi_{lim} & \Psi_{collar} < \Psi_{lim} \end{cases} \tag{8.7}$$

where Ψ_{collar} is the water potential at the plant collar.

(b) Imposed pressure head: The pressure head at the collar Ψ_{collar} is defined as a constant or function of time.

Solving Equation 8.5 for each time step and location yields the distribution of radial flux densities to root nodes (q_r). To estimate the water sink term S of Eq. 8.1, an integration of q_r located in a given soil element V can be performed (Leitner et al. 2014):

$$S = \frac{1}{V} \int_V 2\pi r \delta_2 \left(\chi(x)\right) q_r dx \tag{8.8}$$

where V [L^3] is the voxel volume, χ(x) is a function that is 0 when x is on the centerline of a root segment located in V and δ_2 [L^{-2}] is a 2-dimensional Dirac delta function.

8.3 Application : Use of R-SWMS for hypothesis testing

In this section, we present an application where R-SWMS is used in combination with an in vivo experiment on maize to investigate water uptake process by plant roots. As possibilities to measure root water fluxes and xylem water potential distribution still remain quite limited (Zarebanadkouki et al. 2013) the combination of biophysical modeling and experimentation offers the opportunity to gain novel insights into the spatio-temporal distribution of these variables (Doussan et al. 2006). In this experiment, the soil water content in the root zone of a maize plant under water limitation was monitored with a light transmission imaging (LTI) setup (Garrigues et al. 2006). In addition, R-SWMS was parametrized with both experimental observations and parameter values from the literature. The water content distribution observed during the experiment was used to validate the model and reveal the root water potential and flow information hidden in the raw data.

8.3.1 Material and methods

Figure 8.1 summarizes our methodology. Some of the experimental outputs are used as inputs for the simulation, such as the soil characteristics,

the root system architecture and the environmental conditions (see arrows marked with an A, more details further in this section). The root hydraulic information (xylem and root radial conductivities) was derived from the literature (arrow marked with a B in Fig. 8.1). Simulated outputs were compared to the independent empirical data to evaluate model performance (arrow marked with a C in Fig. 8.1), in our case the water content distribution. The model generates output variables that were inaccessible during the experiment such as water uptake location and xylem water potential distribution in the root system (see arrows marked with a D in Fig. 8.1).

The LTI experiment was run during the first month of 2012 in a greenhouse (Lobet 2012). The mean temperature, relative humidity and vapor pressure deficit (VPD) in the greenhouse during the three days of WSE were 19.6°C $\pm$ 2.1°C, 53.4% $\pm$5.4% and 1.1kPa $\pm$ 0.2kPa, respectively. Experiments were conducted with eight maize plants but only the results obtained for one plant will be presented here. Details are given in Lobet (2012).

Three days after germination, the seeds were transplanted in a rhizotron filled with a previously saturated mixture of Fontainebleau sand and Hectorite clay (98.5% - 1.5% in volume) freely drained out from the bottom. After 21 days, another cycle of saturation – free drainage was applied to set the soil water at field capacity. The plant was then submitted to a Water Stress Episode (WSE) of three days. Four times a day, pictures of the rhizotron were taken to evaluate the water content distribution, and the rhizotron was weighed. The actual transpiration of the plant was evaluated from weight differences (soil evaporation was not a significant part of the water balance due to the plastic sheets at the top, and the small drainage holes at the bottom of the rhizotron).

After the WSE, the root system was collected to digitize its architecture and to generate a root system input file for R-SWMS (note that the simulation presented here includes a single plant). The morphological and topological data (see figure 8.2-A) were taken directly from the Smartroot database (Lobet et al. 2011). Root segment ages were inferred from the root growth rates observed during the growth period preceding the water shortage episode assuming linear growth between daily observations of root architecture. Hydraulic properties of the roots were assumed to be function of the root segment type and

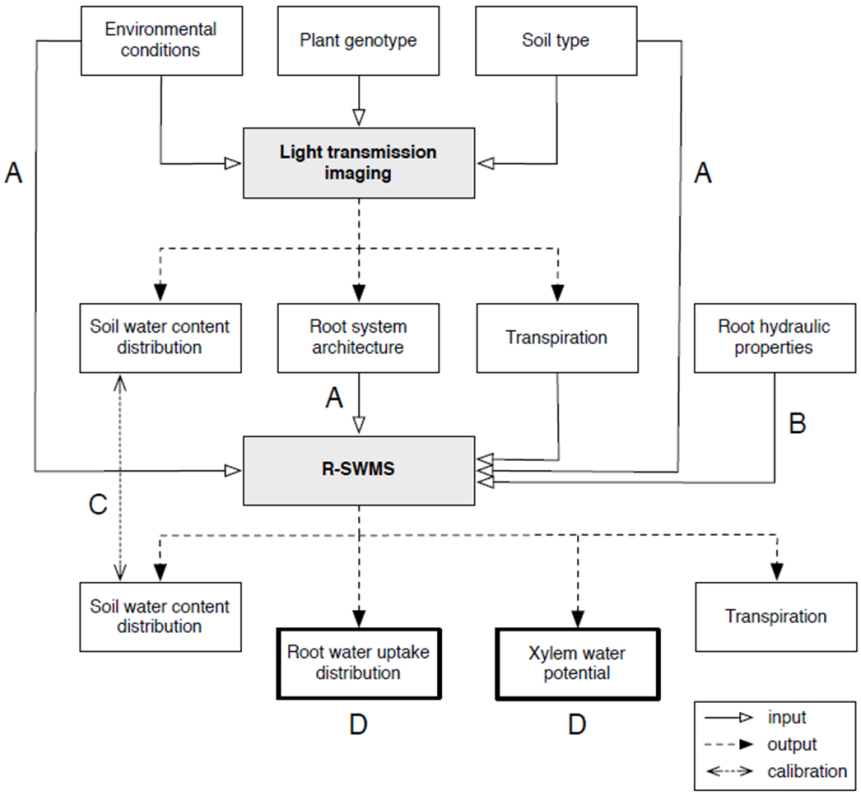


Figure 8.1: Methodology used to decrypt water flow in the soil-root domain using both experimental and modeling data. A. Experimental outputs used as simulation inputs. B. Some simulation inputs are not acquired experimentally, but obtained from literature. C. Simulated and experimental outputs are compared to validate the simulations. D. Simulation outputs gives access to data that were not accessible experimentally.

age (see figure 8.2-C with primary root properties on top and laterals at the bottom), as in Doussan et al. (1998a).

Additional experimental data were used as input parameters for the R-SWMS simulations. This included the soil water retention and hydraulic conductivity curves of the substrate as a function of soil water status (see figure 8.2-B, respectively top and bottom) that were determined in sandbox, pressure plate, and multi-step outflow experiments (Van Dam et al. 1994). Note that the substrate had a very steep hydraulic conductivity curve, with high conductivity values at saturation and very low values below pF 2. Hence the soil hydraulic conductivity was very low during most of the WSE.

The cumulative transpiration is shown in Figure 8.3. The red dots represent the weight losses measured during the experiment. In order to provide to R-SWMS a higher temporal resolution for the boundary conditions, the following equation was fitted to the cumulative transpiration data (see Figure 8.3):

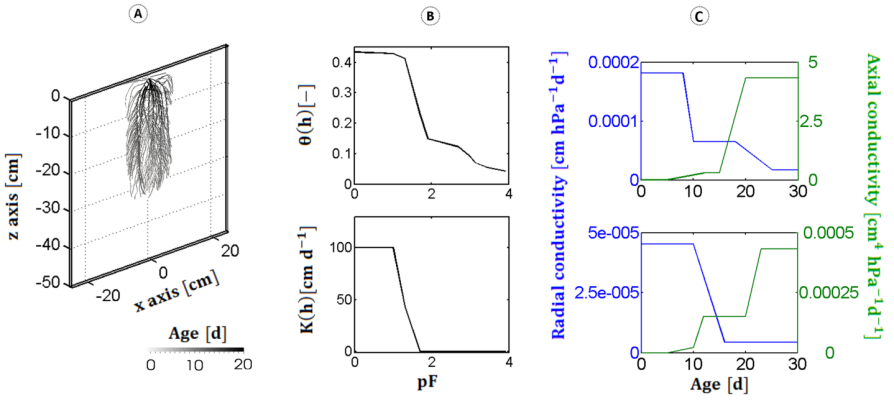


Figure 8.2: Inputs for R-SWMS simulations. (A) Root system architecture and segment ages. (B) Soil water retention (top) and hydraulic conductivity curves (bottom). (C) Root hydraulic properties of both primary (top) and lateral segments (bottom) as a function of their age.

$$T_{cum} = \frac{-T_d}{2\pi} cos\left(2\pi t - \frac{\pi}{2}\right) + T_d.t \tag{8.9}$$

with T_d [L^3T^{-1}] the daily transpiration rate, and T_{cum} [L^3] the cumulative transpiration of the corresponding day. Instantaneous transpiration was provided to R-SWMS with the following equation, with optimized T_d values for each individual days of the experiment:

$$T_{act} = T_d sin\left(2\pi t - \frac{\pi}{2}\right) + T_d \tag{8.10}$$

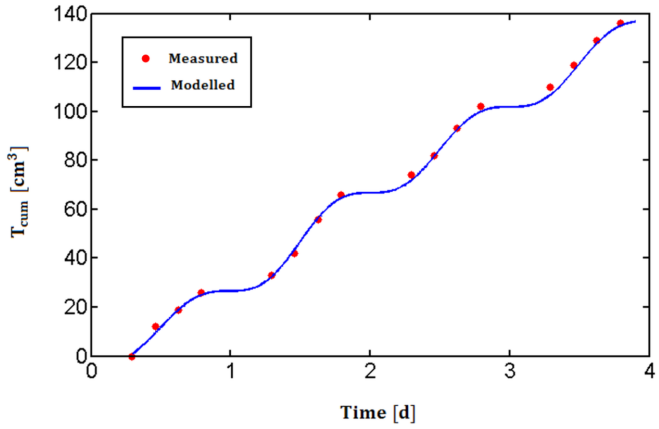


Figure 8.3: Cumulative transpiration measured by rhizotron weight loss (red dots) and interpolated with equation 8.9 (solid blue line) to generate the flux boundary condition at plant collar.

8.3.2 Representing experimental results

A comparison between the water content distributions measured by LTI (top line) and simulated with R-SWMS (bottom line) at three specific times (after 28, 56 and 84 hours after the start of the WSE) is presented in Figure 8.4. Globally there is a good correspondence between the model and the experiment, even though R-SWMS is unable to reproduce all the heterogeneity and complex patterns observed during the WSE. In particular, local variations of water content due to soil compaction heterogeneity visible at the end of the experiment could not be reproduced as the soil hydraulic properties were considered as

uniform in the simulation. Yet, the main feature of the WSE, i.e., the downward moving water front, was well represented by the model.

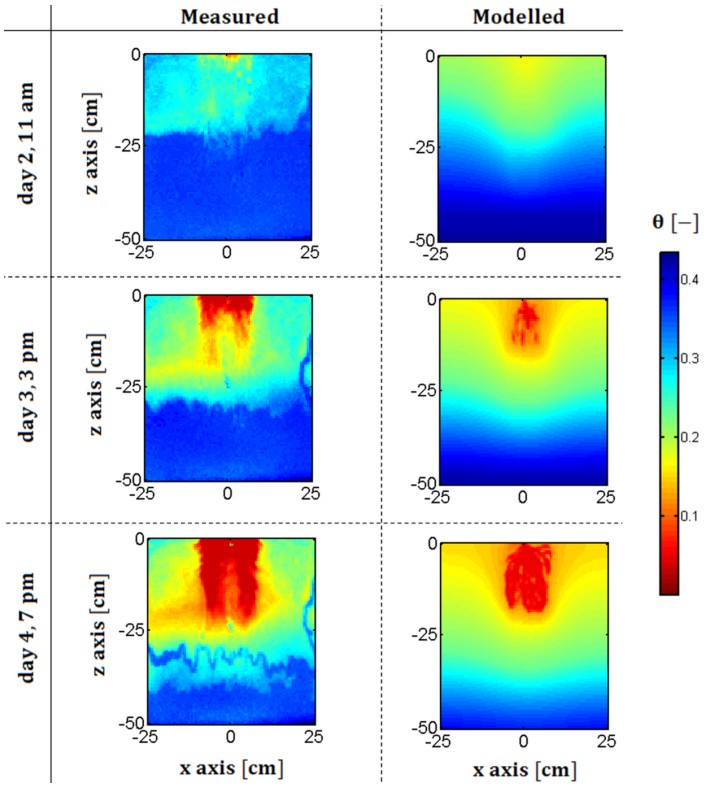


Figure 8.4: Comparison between experimental and simulated water content distributions after 28, 56 and 84 hours of experiment/simulation. The first row shows the experimental results at these times while the second one represents the results as simulated by R-SWMS.

Figure 8.5 compares the simulated versus measured water content in each soil voxel (blue crosses). The black solid line is the 1:1 line representing a perfect agreement. A coefficient of correlation of 81% and a root mean square error $cm^3.cm^{-3}$ of 0.05 were obtained without any optimization procedure. These values indicate that the root hydraulic parameters obtained from the literature (arrow C in Figure 8.1) are in the good range of magnitude. Optimizing them would likely

improve the correlation coefficient and the rmse further. Yet, given the uncertainty in the observed water content calibration curve and the fact that the variation in soil properties was not accounted for (see Fig. 8.4), this result can be considered as satisfactory. Two satisfactory results patterns could be well reproduced by model simulations. First the overall water content distribution with a very dry zone close to the root collar and a small lateral and vertical extension was captured by the parameterized simulations. Second the z-moving resulting from deeper and deeper uptake in a drying soil (data not shown) was also captured by the reference simulation. However it is worth saying that the model does not reproduce perfectly the experimental observations as the r-square reaches 0.67. While it is impossible to reproduce small heterogeneities due to cracks or increased medium densities with the current model, the poor knowledge of the soil conductivity curve and the coarse soil model resolution (0.5cm) could both explain a part of the discrepancy between the outputs of simulation and the observations. Both disserve a deeper look especially with the sandy medium we used for the experiment.

Modeling the change in water content with R-SWMS allowed us to get access to variables which are currently impossible to measure. Figure 8.6 shows at the three corresponding times the water potential distribution inside the root system (top row) and the sink term S of the Richards equation (bottom row) as simulated by R-SWMS. It mainly shows that the water uptake distribution is shifted towards wetter areas of the root system periphery as the experiment runs, and that RWU already takes place below 25 cm depth at the start of the experiment even though soil water content changes are not visible at that location yet.

In Figure 8.7, we represent the modeled water content changes between two successive measurements and the integrated sink term over time during this period for all pixels. Sometimes the change of water content is used as a proxy of the root water uptake described here by the Sink term S. As shown in Fig. 8.7, no unique relations between these variables exist, which highlights the importance of the model to decipher the RWU distribution.

To make that point clearer, the model clearly states that changes of water content between two observation times does not necessarily

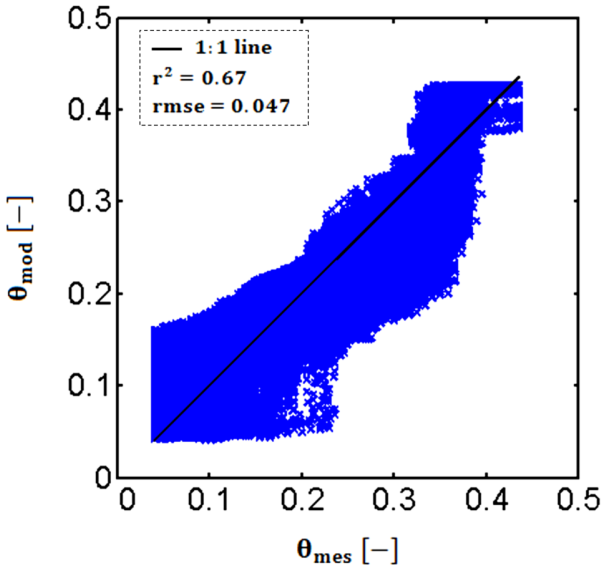


Figure 8.5: Modeled *vs* measured soil water content (blue crosses). The black line is the 1:1 line.

imply a root water uptake/release as the soil may redistribute the water as well. If it were the case, all the dots in Figure 8.7 would fall on a straight line. It indicates that the soil cannot be neglected in our study at least and probably in most cases. Therefore, measuring evolution of water content is not a good proxy of water uptake and is not sufficient information to derive root water uptake. Models have a role to play to depict soil and root effects.

8.3.3 Hypothesis testing

The R-SWMS model can be used to test hypotheses of plant functioning or assess the impact of scientific assumptions at the segment scale processes on plant scale behavior. For instance, R-SWMS could be used to challenge the assumption of constant root hydraulic properties presented above in the simulation of the LTI experiment. Indeed, different processes may alter root radial and axial hydraulic properties. First,

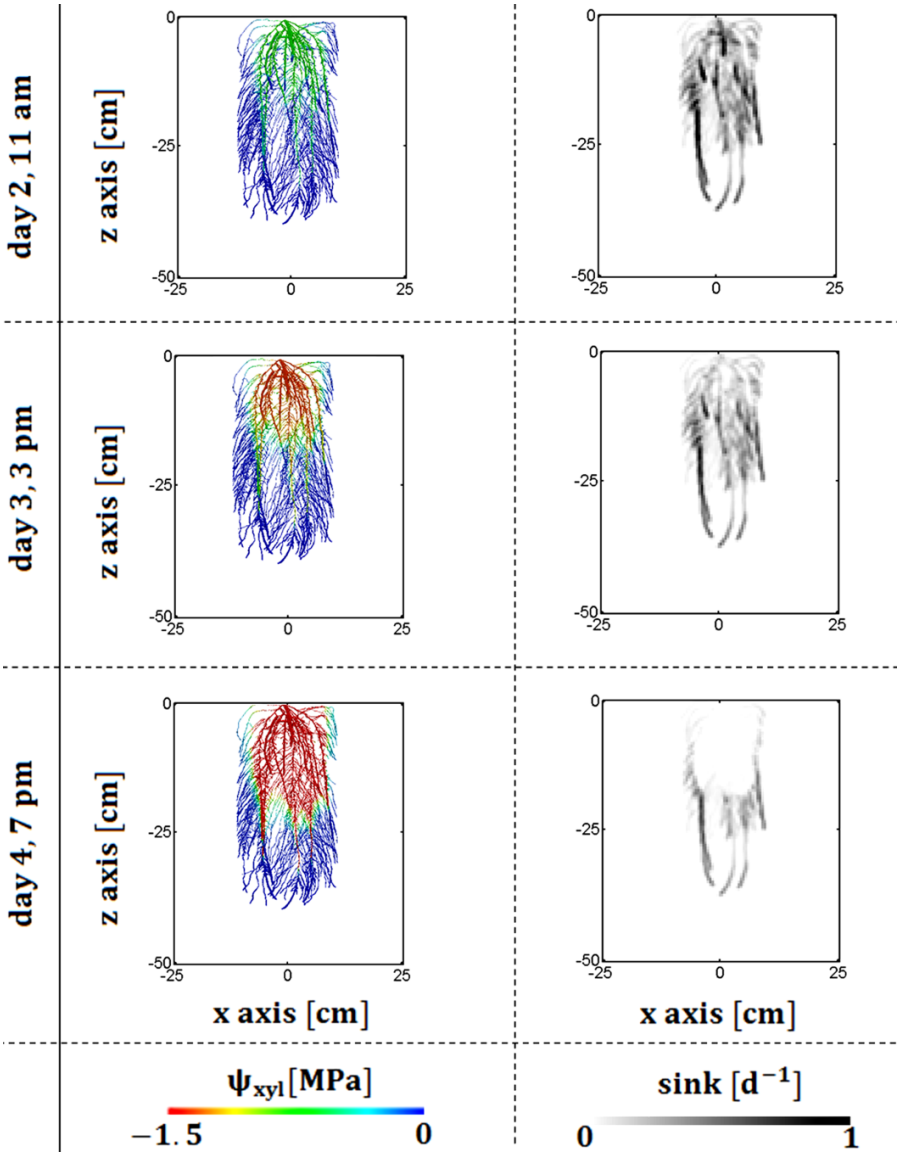


Figure 8.6: Outputs available in RSWMS: water potential inside the root system (top) and sink term distribution (bottom) after 28, 56 and 84 hours of experiment/simulation. These results are not available in the raw data; the model only can give an insight into these state variables.

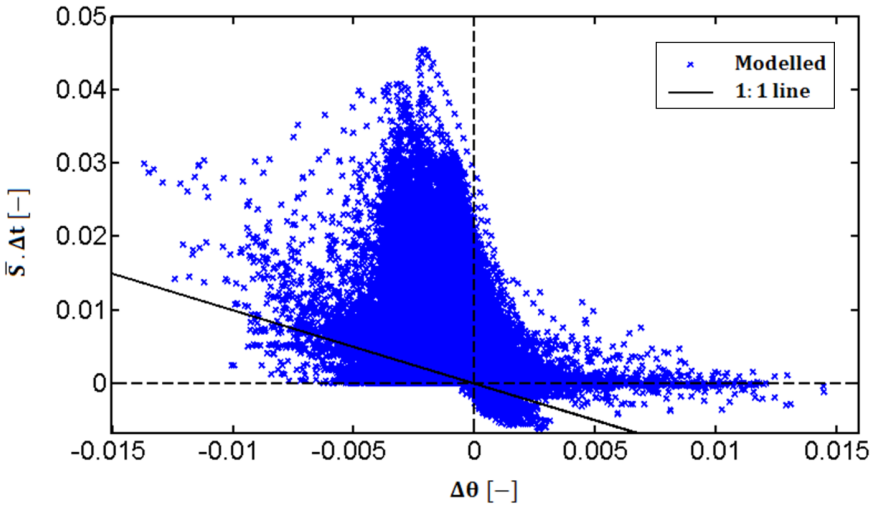


Figure 8.7: Comparison between the simulated water content change and simulated integrated sink term over time for all the pixels along the simulation. No clear relation exists between these variables as shown by the difference between the blue crosses (simulated) and the dark solid line (1:1 line).

transient modifications of the axial conductance may occur as a result of xylem vessel embolism, or cavitation, following the nucleation and rapid expansion of gas bubbles under high tension. Cavitation has been shown to be a reversible event. However, recent experimental evidence has revealed the negative effect of cavitation on the plant water status (Zufferey et al. 2011). Second, radial root conductivity can also be affected by the soil hydraulic status. Root shrinking under low water potentials can cause loose of contact between soil and roots leading to a decline of the effective root radial conductivity in dry regions, for instance. In addition, the presence of aquaporins that facilitate water diffusion across membranes of cell located in specific water-limiting tissues may also affect root segment radial conductivity. Indeed aquaporins are highly regulated at different levels, providing plants with the means to rapidly and reversibly modify the cell water permeability (and potentially root segment radial conductivity) at different developmental stages and under varying environmental conditions (Chaumont and Ty-

erman 2014). Third, one may also want to check whether variations in the root hydraulic conductivity affect root water uptake, and whether simpler models without any variations in hydraulic properties would be able to reproduce plant water relations. We illustrate these hypotheses in Figure 8.8 in which we compare the initial experiment (scenario S0, solid lines in the three subplots) with three plants with modified hydraulic properties (scenarios S1, S2 and S3, dashed lines of the left, middle and right subplots respectively). In the first scenario S1 (left), the root radial and axial conductivities of both primaries and laterals are considered homogeneous while in S0 they were a function of both segment age and order. In a second test S2 (middle), we include xylem cavitation by decreasing the axial conductivities when the xylem potential becomes too high using a Weibull distribution. In the last scenario S3 (right), we assume (1) an increase of the radial conductivity of the laterals for moderate soil dryness as a result of aquaporin regulation but (2) a dramatic decrease of the radial conductivity for very dry soils due to root skrinking.

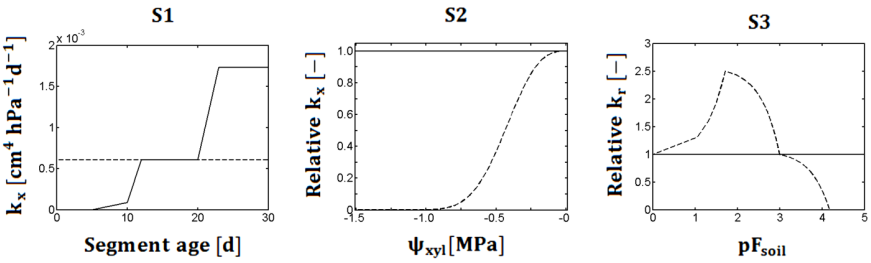


Figure 8.8: Scenarios tested with R-SWMS (dashed lines) as compared to the original (S0, solid line). In scenario S1 we consider homogeneous root conductivities for both primaries and laterals and for both radial and axial (shown in the left subplot) transfer. In scenario S2 the cavitation process is included by reducing the axial conductivities as a function of the xylem potential (middle subplot). And finally in scenario S3 the radial conductivity of the laterals is changed as soil becomes dry (right subplot).

Comparing the 3 scenarios under the same conditions allows evaluating the effect of these processes on both soil and plant variables and to determine the experiment information content (Figure 8.9). In subplot

8.4-A, the evolution of collar water potential is shown. In subplot 8.9-B, the vertical sink term profiles after 1.5 days are compared, and the corresponding root xylem potential distributions for the 4 cases are shown in subplot 8.9-D. In subplot C, the differences of water content between each considered scenario and the reference one are also represented. From this subplot it appear the z-averaged water content is significantly affected by the considered scenario with a mean change that can reach up to 1% for certain layers in volumetric water content. This is a consequence of the difference of water uptake location according to the scenario and could be reflected by the LTI experiment. It is observed that changes in the hydraulic properties deeply impact the pressure in the root system (Figures 8.9-A and C), although the distribution of the RWU remains similar, except for S1 (Figure 8.9-B). This suggests that the dependency of the hydraulic properties to the root segment age (included in all scenarios but S1) is of major importance to reproduce LTI data. Yet, hypotheses S2 and S3 cannot be discriminated from S0 with the help of LTI only. It suggests that additional measurements of the root water potential would be needed, or other experimental conditions generating further differences between the scenarios (e.g. lower xylem water potentials would generate more significant amount of cavitation). Xylem potential in primary roots in particular seems to be very sensitive to the different hypotheses.

Finally it must be added that water potential measurements in the root collar or in some other parts of the plant (see figure 8.9) contain much information about the root hydraulic conductance. When assumptions are made about the relation between water potential in the collar and the stomatal conductance, then this information also becomes available indirectly from measuring the fluxes or transpiration rates when the water potentials in the shoot reach levels that influence the stomatal conductance.

8.4 Conclusion

In this chapter, we have presented the theoretical and numerical development of the water flow equations in soil and root. These equations are implemented in the software R-SWMS, which allows one to simulate

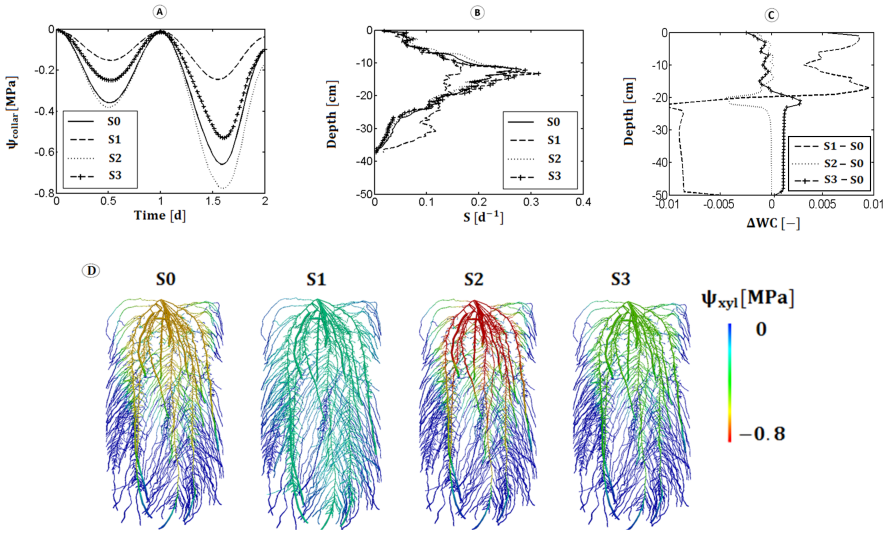


Figure 8.9: Comparisons of results as simulated by R-SWMS for the 4 considered scenarios. In subplot A, the collar potential change during the simulation of the four plants is plotted. The subplot B and C represent respectively the sink term profiles S of the different scenarios after 1.5 days of water stress and the differences of water content between all scenarios as compared to the reference one after 1.5 day of the water stress episode. Finally subplot D shows the xylem water potential distribution in the root system after1.5 days of simulation.

water uptake by plant roots under variable environmental conditions. An application of the model to simulate the evolution of the water potential in the root system and the RWU is presented. It demonstrates that RWU cannot be inferred from soil water content changes only, and that such detailed models in combination with experimental data allow one to have access to unmeasurable variables. In addition, R-SWMS can be used as a prospective tool to evaluate how to set-up an experiment, check the impact of scientific hypotheses or make scenario analyses.

MEASURING AND MODELLING HYDRAULIC LIFT OF LOLIUM MULTIFLORUM USING STABLE WATER ISOTOPES

9

This chapter is a modified version of a research article published as:

> Meunier F., Rothfuss Y., Bariac T., Biron P., Richard P., Durand J.,Couvreur V., Vanderborght J. and Javaux M. Measuring and modelling hydraulic lift of Lolium Multiflorum using stable water isotopes. Vadose Zone Journal. 2017.

Abstract

The present study proposes a method to quantify and locate hydraulic lift (HL, defined as the passive upward water flow from wetter to dryer soil zones through the plant root system) by combining an experiment using the stable water isotope $^{1}H_2{}^{18}O$ as a tracer with a soil-plant water flow model. Our methodology consisted in (i) establishing the initial conditions for HL in a large rhizobox planted with Ryegrass (*Lolium multiflorum* Lam.); (ii) labeling water in the deepest soil layer with a ^{18}O-enriched solution; (iii) monitoring the water oxygen isotopic composition in soil layers in order to find out changes in the upper layers that would reflect redistribution of ^{18}O-enriched water from the bottom layers by the roots; (iv) confronting the observed soil water oxygen isotopic composition to simulation results of a three-dimensional model of the water flow and the isotope transport in the soil-root system.

Main findings were that (i) the depth and strength of the observed changes in soil water oxygen isotopic composition could be well reproduced with a modelling approach (RMSE = 0.2‰, i.e., equivalent to the

precision of the isotopic measurements); (ii) the corresponding water volume involved in HL was estimated to account for 19% of the plant transpiration of the following day, i.e. 0.45 mm of water and was in agreement with the observed soil water content changes; (iii) the magnitude of the simulated HL was sensitive to both plant and soil hydraulic properties.

9.1 Introduction

Hydraulic Lift (HL) is defined as the upward water flow from wetter to dryer soil layers through passive root transport (Richards and Caldwell 1987) and has been reported for numerous plant species (Neumann and Cardon 2012). In principle, HL takes place when in upper soil layers the root water potential is higher than the soil water potential containing these roots, while in deeper layers the soil water potential is higher than the root water potential contained in this layer. HL is a particular case of hydraulic redistribution, which may happen in any soil direction, e.g., from shallower to deeper layers or in the horizontal direction (Burgess et al. 1998).

The quantitative and qualitative implications of HL on plant water balance, nutrient mobilization, and competition for space and nutrients between plants are still unclear among the scientific community (Burgess 2011). From a hydrological perspective the absolute volume of hydraulically lifted water is debated: it has been reported to vary by nearly two orders of magnitude depending on the species and environmental conditions (representing between 2 and 143% of the plant transpiration with a mean of 30%) (Neumann and Cardon 2012). Discriminating between soil and root hydraulic redistribution is also very challenging (Katul and Siqueira 2010). This leads to divergences between authors on the importance of HL: in some studies it was estimated to be a negligible term of the water budget (e.g., (Meinzer et al. 2004; Scholz et al. 2010)), while according to other studies it might impact evapotranspiration and net ecosystem carbon exchange significantly at the stand and catchment scales (Domec et al. 2010; Jackson et al. 2000). The ecological interest of HL might be not only to improve water uptake from soils, but also

to mobilize nutrients and enhance rhizosphere microbial communities (e.g., see reviews of Prieto et al. (2012)).

The stable water isotope $^{1}H_2{}^{18}O$ is a tracer of ecosystem processes (Javaux et al. 2016; Rothfuss and Javaux 2017; Werner et al. 2012). As plant Root Water Uptake (RWU) does not lead to fractionation of stable water oxygen isotopes for a wide variety of plants, when the soil water natural abundance ratio (-, expressed in permil on the international accepted scale and referred in the following to as $\delta^{18}O$; (Gonfiantini 1978)) varies within the root zone, the stem xylem $\delta^{18}O$ is a valuable tool for determining origin of water extracted by the root system (e.g., (Asbjornsen et al. 2007; Dawson and Ehleringer 1991; McCole and Stern 2007). When RWU and release do not lead to fractionation, stem xylem water $\delta^{18}O$ of plants with different rooting depths can also be used to identify the injection of the isotopic signal from deeper soil layers into shallower ones. Caldwell and Richards (1989), for example, inferred from measurements of stem xylem water $\delta^{18}O$ that isotopically labeled water injected in deep roots of Artemisia tridentata and released through HL was extracted by shallow roots of Agropyron desertorum. HL is often inferred from diurnal variations of soil surface water potential (Dawson 1993; Ludwig et al. 2003) and water content (Brooks et al. 2002; Warren et al. 2005). Only a very few direct observations of changes in soil water isotopic composition were made (e.g.,(Zegada-Lizarazu and Iijima 2004)). Since no accurate isotopic "anomaly" in the soil water isotopic profile was reported, the depths where HL occurs and the water volumes that are involved could not be determined accurately.

HL can be explicitly simulated with existing models of the soil-plant-atmosphere continuum that describe the water flows in one (Couvreur et al. 2012; Guswa 2012; Volpe et al. 2013) or three dimensions (e.g., (Javaux et al. 2008)) as a passive process based on soil water potential gradients. Recently, Couvreur et al. (2012) developed a 1-D solution of the RWU based on water flow equations in roots. He demonstrated that the RWU was a sum of two terms: one proportional to the root distribution and another one function of the soil water potential distribution. At locations where this second term exceeds the first one, RWU term is negative and HL occurs. It implies that existence and intensity of such a phenomenon depend on both environmental conditions and plant properties: low transpiration, high soil water potential variability and

high root conductance are the three conditions for HL (see Appendix A for more details). Interestingly, several authors have found similar root water uptake models (Javaux et al. 2013), confirming that this was an appropriate way to model HL (Volpe et al. 2013). Such models and their predictions can help to build an experiment in which the environmental prerequisites are met and quantifying the water and isotope flow in the soil-root system continuum.

The general objective of this study is to develop a methodology to quantify hydraulic lift in the soil plant system and investigate and understand the factors controlling the magnitude and location of the water efflux. This objective will be addressed by combining experiment and modeling tools. First, we set up a unique controlled experiment in which stable water isotope $^{1}H_2{}^{18}O$ was supplied to the deepest soil layers of a rhizobox and monitored in soil and plants. In addition an existing soil-root model (R-SWMS, (Javaux et al. 2008)), which included all relevant processes to simulate root water uptake and HL according to basic physical principles, was extended to the transport of the $^{1}H_2{}^{18}O$ isotope. This model was used to test whether the observed distributions of $^{1}H_2{}^{18}O$ could be reproduced using meaningful parameters and to assess the water volumes that were involved in HL.

9.2 Material and Methods

9.2.1 Experimental setup

A macro-rhizobox with transparent polycarbonate sides (dimensions L x l x H = 100 cm x 20 cm x 160 cm, Figure 9.1-A) was filled up with soil (District Cambisol, particle size distribution: sand 15% – silt 65% – clay 20%, sieved at 2 mm) layer by layer of 10 cm in order to reach a bulk density similar to the field, i.e., 1.42 g cm^{-3} (Rothfuss et al. 2010). It was placed in a greenhouse (Lusignan, France 46.44°N, 0.13°E) and continuously weighed (KE1500, Mettler-Toledo, range 1500 kg, resolution: 20 g) to monitor the soil water balance and calculate water effluxes (i.e., evapotranspiration). Underneath the rhizobox and in contact with the soil bottom surface, a water reservoir (height: 10 cm) filled with gravel acted as water table and allowed the discontinuous supply of water from the bottom, see figure 9.1 for illustration. Soil water content $\theta\,[L^3L^{-3}]$ and pressure heads h_{soil} [P] were monitored within the soil at five depths (z = -5, -10, -25, -60, -90, and -130 cm) with water content reflectometers (CS 616, Campbell Scientific, precision: around 2.5%), micro-psychrometers (Soils – PST55, WESCOR) and tensiometers (SMS 2000 with pressure transducers SKT850, SDEC, France).

In the greenhouse, atmospheric temperature and relative humidity were measured but not regulated. The amount and isotopic composition of water applied to the soil from the reservoir were controlled during the experiments. The rhizobox soil was initially saturated with input water ($\delta_{IW} = -8.1‰$) from the bottom reservoir. Italian ryegrass (*Lolium multiflorum* Lam.) was seeded (seeding density = 0.03kgm^{-2}) when the soil surface reached field capacity, and emerged 12 days later.

The water isotopic tracer experiment was carried out 116 days after seeding (DaS 116). At that time, there was a strong soil water potential gradient between deep (100 – 140 cm) and superficial (0 – 30 cm) soil layers as measured by the tensiometers and micro-psychrometers and roots were observed to reach the water reservoir (see the experimental results section). At 2:00 pm, the water reservoir was labeled with a 18O-enriched water solution ($\delta_{LW} = +400‰$) and put in contact with the soil outlet. To assess the impact of this tracer, soil water isotopic composition profiles were determined at two moments: on DaS 116 at

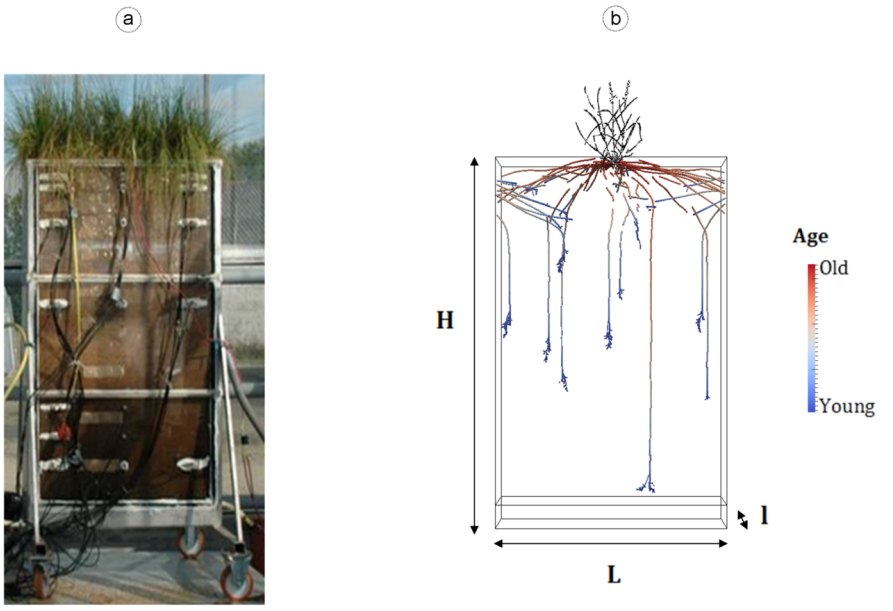


Figure 9.1: Soil macro-rhizobox experimental setup with Lolium multiflorum cover and different profiles of soil probes (a) and sketch of the macro-rhizotron with a representation of a single plant root system (b).

3:15 pm and on DaS 117 at 5:20 am. To do so, horizontal soil samples were extracted with a 1.2 cm diameter auger (corresponding to a soil sampling volume ranging from 0.6 to 1.7 cm^3) from the surface down to 130 cm-depth with 5 to 15 cm increments and then subject to isotopic composition analyses (see next section).

At 14 times between from 2:00 am to 5:20 am on DaS 117, three tillers were sampled homogeneously from the vegetation's cover and pulled together in a single vial. All dead material and the sheath of the oldest living leaf around each tiller were discarded in order to remove any organ which could have been transpiring (Durand et al. 2007).

After the second soil sampling for isotopic analyses, additional soil samples were taken between the polycarbonate sides using the same 1.2 cm diameter auger to determine the root length density (RLD) profile. Each depth was sampled twice or thrice and compounded in a single

vial per sampling depth. From each sample, soil particles were washed off and roots were manually collected over a 0.2 mm mesh filter, and dried at 60°C for 48h. RLD was determined from the obtained root dry masses using the specific root length for Italian ryegrass (181 $m.g^{-1}$) as determined by Gonzalez-Dugo et al. (2005).

9.2.2 Isotopic analysis

Water was removed from soil and tiller samples by cryogenic vacuum distillation (−196°C), and sealed in closed glass containers. Recovery was higher than 98.5% and a correction, ranging from 0 to 0.4, was applied according to the distillation yield by a Rayleigh-type law (Araguás-Araguás et al. 1995). Stable water oxygen isotope composition was measured by isotope ratio mass spectrometry (Aquaprep Micromass Isoprime) after $CO_2 - H_2O$ equilibration (Gilson X222 system) using the Epstein and Mayeda (1953) technique.

9.2.3 Modelling

A fully mechanistic 3-D model of the soil-plant system is used to analyze the isotopic dataset and quantify the HL: R-SWMS. This model is based on a physical representation of the water flow in the soil and in the root system (Javaux et al. 2008). Yet, in order to ease the optimization procedure, we first made use of the root-rhizosphere module of this model, thereby neglecting bulk soil water flow (section 9.2.3). Based on the assumption that bulk water flow was minimal during a short period, we used this fast module with a global optimization algorithm to adjust root and rhizosphere hydraulic parameters. Then the full R-SWMS (section 9.2.3) accounting for water flow and solute transport in the bulk soil was used to verify these assumptions and to fine-tune our model parameters. Note that to generate a realistic 3-D root system architecture for R-SWMS and the root-rhizosphere module, the root growth model RootTyp was used (section 9.2.4).

Root-rhizosphere model

The root-rhizosphere model solves water flow from the bulk soil to the root collar. In this module, bulk water flow and $^1H_2{}^{18}O$ transport are ne-

glected in soil and bulk water potential and water isotopic compositions are model boundary conditions.

The water flow equation in the root system is solved with the finite difference approach of Doussan et al. (1998a). The root system is divided in N segments leading to N linear equations that are solved for root water potential given known boundary conditions at the root collar and soil-root interfaces. Once solved, these equations allow calculating the radial water flows in a root segment i, $J_{r,i}$ [L^3T^{-1}]:

$$J_{r,i} = k_{r,i}.S_{r,i}\left(\Psi_{sr,i} - \Psi_{x,i}\right) \tag{9.1}$$

where $k_{r,i}$ [$LP^{-1}T^{-1}$] is the radial conductivity of the root (i.e., between the root surface and xylem of root segment i), $S_{r,i} = 2\pi r_i l_i$ [L^2] the surface of the root segment of radius ri [L] and length ri [L] and $\Psi_{sr,i}$ [P] and $\Psi_{x,i}$ [P] the soil-root interface and the root xylem water potential of the segment, respectively. The radial flow is defined positive towards the root. Here and in the following we distinguish the total water potential Ψ and the matric potential h [P]. The latter is simply the former without the gravitational component. The subscripts associated to the water potentials locate them. It is worth noting that we used in this study the nomenclature and the units of soil/root conductivity/conductance of Javaux et al. (2013). To account for the soil hydraulic resistance in the rhizosphere, the (Doussan et al. 1998a) hydraulic architecture was extended by an extra soil shell around the roots with an hydraulic conductivity k_{soil} [$L^2P^{-1}T^{-1}$] through which radial flow from the bulk soil to the soil-root interface takes place. The equivalent conductance between the bulk soil around and the xylem of root element i, $K_{i,eq}$ [$L^3P^{-1}T^{-1}$], can be defined as a function of the flow rate to the segment $J_{r,i}$ and the water potential difference between the xylem and the bulk soil, Ψ_{soil}, as:

$$J_{r,i} = K_{i,eq}\left(\Psi_{soil} - \Psi_{x,i}\right) \tag{9.2}$$

with $K_{i,eq} = \frac{k_{r,i}k_{soil}2\pi l_i r_i B}{Bk_{soil}+r_i k_{r,i}}$ expressed in [$L^3P^{-1}T^{-1}$], the equivalent conductance between the soil node and the xylem of root element i and B [-] a geometric parameter. Appendix B describes the calculation for $K_{i,eq}$ and analyzes the limiting cases of the equivalent soil-root conductances. In this approach, soil water flow is not explicitly modelled

but soil hydraulic conductivity was accounted for through k_{soil} and its dependency to soil water potential. k_{soil} is indeed a function of the soil water matric potential h [P] through the hydraulic conductivity curve :

$$k_{soil} = \frac{\int_{h_{soil}}^{h_{sr,i}} k(h)dh}{|h_{soil} - h_{sr,i}|} = \frac{\Phi_{sr,i} - \Phi_{soil}}{|h_{soil} - h_{sr,i}|} \tag{9.3}$$

where $\Phi_{sr,i}$ and Φ_{soil} are the matric flux potential of the soil-root interface and of the soil, respectively (de Jong van Lier et al. 2008). The matric flux potential is defined as the integral of the soil conductivity curve. Figure 9.2-A illustrates one of the numerous segments of the whole root system and its surrounding soil. The total xylem potential of this segment $\Psi_{x,i}$ (black node), the soil-root total potential $\Psi_{sr,i}$ (brown node), and the bulk soil potential total Ψ_{soil} (blue node) are represented as well as the soil and root radial conductances K_{soil} and $K_{r,i}$ (see Appendix B). It is worth mentioning that several studies reported different root conductivities for in- and outflows but this aspect was not implemented in our modelling exercise. Other authors showed that shallow and deep roots may have different root hydraulic conductivities (Wan et al., 1994) but this is explicitly accounted for in our model through root ages and types (see section 9.2.4).

R-SWMS: Transient soil-root water flow model

In a second step, we used the full transient soil-root water flow model, R-SWMS to account for the soil flow in addition to water flow in the root and in the rhizosphere. The R-SWMS model (Javaux et al. 2008) solves the coupled problem of water flow in the soil-root continuum by iteratively solving soil and root water flux equations until convergence at each time step. A convection-dispersion equation is solved for describing the solute movement in soil and the soil water movement is modeled by Richardson (2007) equation with sink term to account for RWU. The sink term S_j [T^{-1}] for each soil element j (having a volume V_j [L^3]) in this equation is calculated summing up the radial water fluxes for each root segment i contained in this particular soil element:

$$S_j = \frac{1}{V_j} \sum_{i \in j} J_{r,i} \tag{9.4}$$

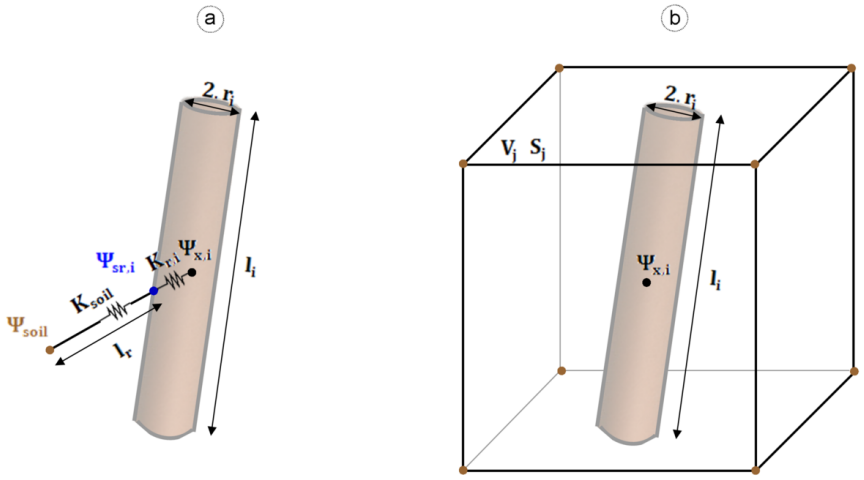


Figure 9.2: Root segment layout in the Root-rhizosphere model (a) and the same root segment situated in a soil element in R-SWMS (b).

Calculation of $J_{r,i}$ is obtained via the root-rhizosphere module explained before (see section 9.2.3). Transport of isotopes in the soil was modeled via a classical convection-diffusion equation with passive uptake only (Schröder et al. 2012). This model thus explicitly accounted for soil water flow, isotopic dispersion in soil, and root water uptake and release. Figure 9.2-B shows one of the root segments compounding the whole hydraulic architecture, numbered i, in the surrounding soil element j, the element sink term and its volume V_j.

Isotope uptake modeling

The prognostic variable for the computation of isotopic flow is the oxygen isotopic liquid concentration C [ML^{-3}], which can be obtained from the oxygen isotopic liquid composition δ [-, expressed in ‰] (Braud et al. 2005) at any time t [T]:

$$C(t) = \rho R_{ref} \frac{M_i}{M_w} \left(\frac{\delta(t)}{1000} + 1 \right) \tag{9.5}$$

with ρ [ML^{-3}] the volumetric mass density of water, R_{ref} [-] the Vienna-Standard Mean Ocean Water (V-SMOW) oxygen isotopic ratio (R_{ref} = (2005.2 $\pm$ 0.45) 10^{-6}), M_w and M_i [$Mmol^{-1}$] the molar masses of $^1H_2{}^{16}O$ and $^1H_2{}^{18}O$ water, respectively. Considering a perfect mixing inside the root xylem and no root capacitance (no water stored in root compartments), we define an equivalent oxygen stable isotopic concentration inside the root system, $C_{Ti}(t)$ [ML^{-3}] as a sink-weighted average oxygen isotopic concentration of absorbed water:

$$C_{Ti}(t) = \frac{\sum_{S_j>0} S_j(t)C(t)dz}{\sum_{S_j>0} S_j(t)dz} \tag{9.6}$$

where the local sink term is defined positive if water is taken up. When HL occurs, the outgoing flow is supposed to have the equivalent stable oxygen isotopic concentration assuming an instantaneous mixing of all the water sources within the plant. We model in this study the stable water isotope as a "standard" non-excluded solute: we assume that root uptake does not lead to fractionation and we do not consider evaporation.

9.2.4 Model-data comparison

Root system architecture

The root system architecture needed by the models was inferred by inverse modeling of measured RLD with a root growth model, RootTyp (Pagès et al. 2004). Lolium multiflorum root growth parameters (maximal length and initial velocity) of both primary and lateral roots as well as the intermodal distance between two successive lateral roots were optimized to fit the measured RLD data. RootTyp was thus used to generate a realistic root system architecture that is needed as input for the Root-rhizosphere module and R-SWMS.

Boundary conditions for soil and root

The weight loss was considered due to transpiration solely (this assumption is justified thanks to observations; see section 9.3.1 on experimental

Table 9.1: Soil (optimized) and reservoir (fixed) van Genuchten (1980) and Brooks and Corey (1964) retention and conductivity curves' parameters

	θ_s [$cm^3.cm^{-3}$]	θ_r [$cm^3.cm^{-3}$]	α [cm^{-1}]	n [-]	k_S [$cm.d^{-1}$]	λ [-]
Soil	0.4	0.044	0.0285	2.29	0.26	6.67
Reservoir	0.45	0.4	0.000344	1.42	1500	0.5

results). The actual transpiration rate per plant, T_{act} [L^3T^{-1}], was obtained by dividing the weight loss by the number of plants, which was derived from the plant density, observed 12 days after sowing. The transpiration rate was used as boundary condition for the root system (flux boundary condition) at the root collar in both modeling steps. The soil water content profile measured at the beginning of the HL experiment (DaS 116 15:15) was used as initial condition. The bulk potential used as boundary conditions for the Root-rhizosphere model came from the measured tensiometers/psychrometers profiles. No flow and a pressure condition were used as boundary conditions for R-SWMS at the top- and bottom soil, respectively. The pressure values used were obtained with the tensiometers at the very bottom of the soil profile.

The time step in the root-rhizosphere model is fixed to 10^{-2} day. During a time step, the boundary conditions, i.e. the transpiration rate at the collar and the bulk water potentials in the soil were assumed to be constant. The time step is adaptive in R-SWMS but always comprised between 10^{-5} and 10^{-2} day.

Soil parameterization

The rhizobox was simulated as a bi-layered medium formed by the soil and the reservoir underneath. Experimental retention curve data were derived from simultaneous measurements of soil water content and potential provided by collocated water reflectometers, micro-psychrometers, and tensiometers. Van-Genuchten parameters were obtained by fitting the water retention function to the observed soil water content and soil water matric potential pairs. A Burdine-type condition was used to link shape parameters m and n (m=1-2/n; (Burdine et al. 1953)) of the water retention curve.

The retention and conductivity function parameters of the reservoir were imposed so that it stayed always saturated and much more

(i.e., three orders of magnitude) conductive than the soil during the experiment.

As the RWU model simulates one single plant scale while many distinct plants were present in the rhizobox, a continuous soil domain was used. It mimics the presence of plant neighbors by considering the vertical boundaries to be periodic for soil and root water fluxes and root system architecture. In particular outgoing roots reappear at the opposite face of the domain in x and y directions (Couvreur et al. 2012).

Optimization scheme

Missing information on root and soil hydraulic conductivities were obtained by inverse modelling from the experimental dataset using in a first step a global single-objective optimization of the root-rhizosphere model that neglects soil water flow (see section 9.2.3). The parameters provided by the global optimization algorithm were then further locally optimized taking into account the soil water movement using R-SWMS. The optimizations were achieved in MATLAB with the Multistart heuristic algorithm OQNLP (Optimal Methods Inc., USA) for the global optimization and with a local algorithm (Nelder-Mead simplex direct search) for the local one. Both root and soil hydraulic parameters were optimized. The optimized soil properties were the soil saturated conductivity (k_S [L T^{-1}]) and the shape parameter of the Brooks and Corey (1966) conductivity function (λ [-]) whereas the other soil hydraulic parameters were derived directly from the retention curve. Root hydraulic conductivity functions consisted of monotonic (increasing for axial conductivities/decreasing for radial conductivities) piecewise linear curve function of the root age. To reduce the number of parameters to be optimized, the following simplifying assumptions were made: (i) root conductivity depended on the age and order of the root segment only (see, e.g., (Bramley et al. 2009; Zwieniecki et al. 2002)); (ii) the transition ages between successive conductivity plateaus were considered as fixed and (iii) the primary roots were not responsible for root water uptake. The latter assumption is pretty strong: main axes are probably responsible for at least a part of the water uptake (see previous Chapter) but doing so the number of fitting parameters was considerably decreased. Neglecting the uptake by primary roots will probably

lead to an overestimation of the radial conductivities of the lateral roots that needs to be kept in mind when using the resulting optimal parameter set.

The root and soil hydraulic properties functions are presented in Figure 9.3-A. The following terminology for the root hydraulic properties was used: x and r subscripts stand for axial and radial conductivities, respectively, Roman numerals I and II describe the root order, i.e., primary and secondary (i.e., lateral) roots and finally, a and b refer to the age of the root section (respectively "young" and "old").

Two objective functions were used. The first objective function, OF_1 [-, expressed in ‰], was defined as the RMSE of measured ([-, expressed in ‰]) vs simulated ([-, expressed in ‰]) isotopic composition profiles:

$$OF_1(P) = \sqrt{\frac{\sum \left[\delta_{meas} - \delta_{sim}(P)\right]^2}{N - N_p}} \tag{9.7}$$

where P is the soil and root parameter set, N and N_p and are the number of observations and parameters, respectively.

The second objective function, OF_2 [-, expressed in ‰], is the maximum deviation value of the absolute difference between measured and simulated isotopic composition:

$$OF_2(P) = max\left[|\delta_{meas} - \delta_{sim}(P)|\right] \tag{9.8}$$

These two indicators allowed estimating whether the anomaly in the isotopic profile was correctly represented and discriminating a null model (i.e., no change in the isotopic profile). Soil parameters obtained from infiltration measurements (Rothfuss et al. 2012) and root segment conductivity functions of wheat plant (Couvreur et al. 2014b) were used as initial guess for the soil and root hydraulic parameters, respectively. Figure 9.3-B presents the two-step optimization scheme that was used. First, a global optimization with the root-rhizosphere model was carried out using soil parameters obtained from infiltration measurements (Rothfuss et al., 2012) and root segment conductivity functions of wheat (Couvreur et al. 2014b) as initial parameter estimates. Subsequently, the optimized parameters from the first optimization were used as initial parameters for the local optimization and the transient model R-SWMS.

The root-rhizosphere model globally optimized the soil and root hydraulic parameters without considering any bulk soil water movement, which makes the model fast. R-SWMS was then used with the optimized parameter set to take into account the water flow and solute transport in the bulk soil requiring additional information about soil and solute. The first parameter set guess for R-SWMS was the optimal parameter set provided by the Root-rhizosphere model. Both models used a root system architecture generated by RootTyp and both optimizations used the objective function OF_1 and OF_2 for assessing the simulation fitness. In order to evaluate the uniqueness of the solution and the sensitivity of the simulations to soil and/or root hydraulic parameters, a local sensitivity analysis (SA) was also performed by varying parameters by more or less 20% around the found global optimum.

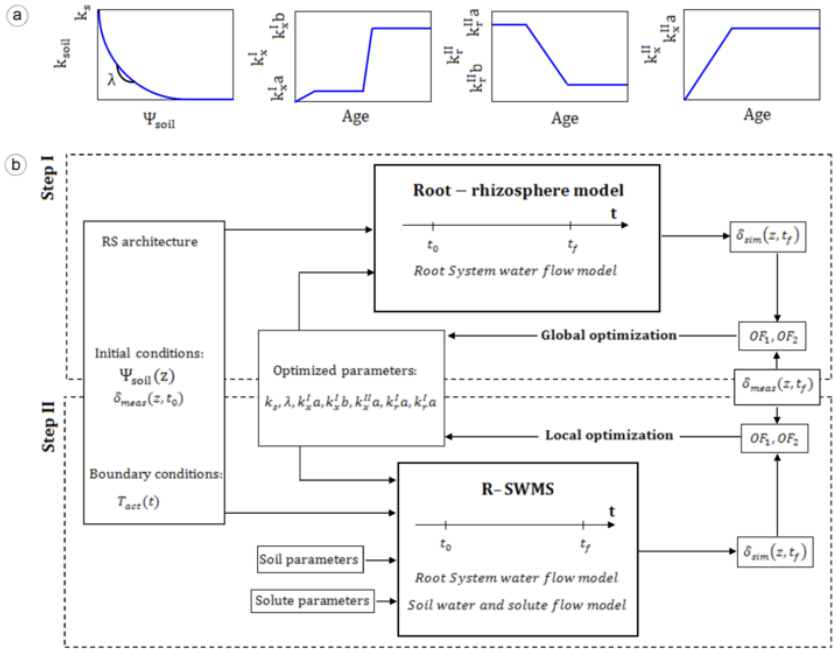


Figure 9.3: Soil and root hydraulic conductivity functions (a) and model optimization scheme (b).

9.3 Results

9.3.1 Experimental results

In Figure 9.4, the experimental soil water retention curve is shown (left) as well as the resulting profile of soil water potential. It can be seen that high gradients exist between top and bottom soil layers at the start of the experiment, which is one of the conditions to observe Hydraulic Lift.

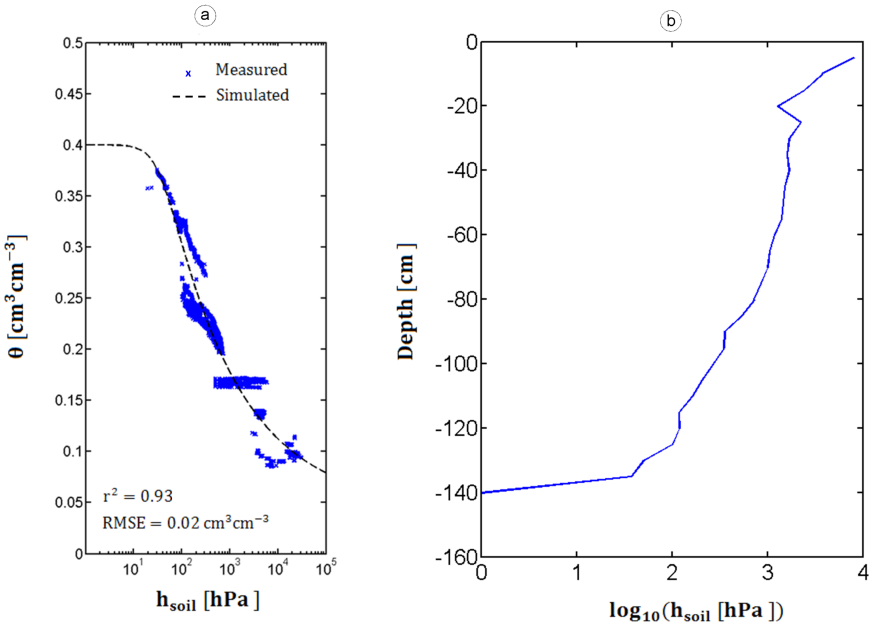


Figure 9.4: Soil water content vs soil water potential as measured by the probes (blue symbols) or as fitted by the van Genuchten parameters given in the first line of Table D.1 (left) and resulting profile of soil water potential in log scale at the beginning of the experiment (right)

Other experimental results are summarized in Figure 9.5. The first subplot represents the water content profile as measured by the reflectometers at the beginning and at the end of the experiment. The upper 80 cm are highlighted in the frame. The development of the vegetation

and the observed surface volumetric water content ($\theta < 0.125$ cm^{3}cm^{-3} corresponding to low soil potential led to assume that the rhizobox water losses were due to transpiration flux solely (i.e. evapotranspiration = transpiration). On DaS 116, a strong water potential gradient existed between the soil surface ($h_{soil} \simeq 10^5$ cm) and bottom ($h_{soil} \simeq 10^2$ cm) of the rhizobox soil. In the topsoil, the changes in water content were absent (15 and 20 cm depth), slightly negative (30 and 35 cm depth, max -0.2%) or slightly positive (10 and 25 cm depth, max. +0.8%).

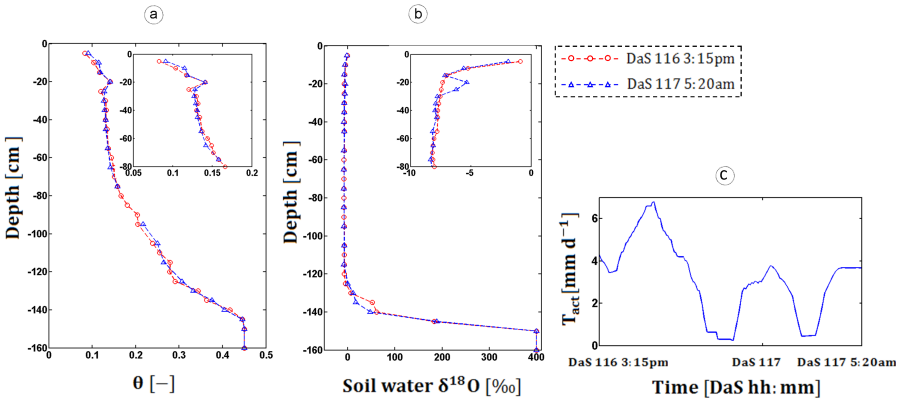


Figure 9.5: Experimental results. Initial (DaS 116 3:15pm, red circles) and final (DaS 117 5:20 am, blue triangles) soil volumetric water content (a) and isotopic composition profiles (b). In the frame, the isotopic anomaly is highlighted while no significant water content change could be observed. (c) Actual transpiration as measured by weight losses during the experiment.

Figure 9.5-B represents the measured isotopic profiles. The observed surface isotopic enrichment was mainly obtained before seeding when the soil was bare and soil water content was still high, and thus soil was actively evaporating. As the vegetation layer progressively covered the soil and surface water content decreased, water losses were then mainly due to non-fractionating root water uptake. As a consequence, the differences observed between the two isotopic profiles following labeling of the reservoir water could only be due to the spatial heterogeneity of soil water potentials entailing water redistribution through capillary flow and HL. Measured soil water δ^{18}O spanned between -8.3

and 182.5 ‰ on DaS 116 and between –8.2 and 188.6‰ on DaS 117 (the two lowest points in the profiles represents the $\delta^{18}O$ values of the labeled water in the reservoir). δ_{meas} profiles were comparable with the exception of the depths 20 cm and 25 cm where enrichments of 2.0 and 1.3‰ were observed on DaS 117 with respect to the values measured at the same depths on DaS 116 (see details frame of Figure 9.5-B). These differences were more than or about ten times larger than the isotopic measurements' precision (i.e., 0.2‰). At around 1.35 m depth significant differences between both measured δ profiles were also observed, due to the bottom supply of isotopic labelled water under pressure (the gravimetric water content measurements show significant differences of around 4% at these depths). Figure 9.5-C finally presents the actual transpiration rate of the rhizotron as measured by the weigh losses by the scale during the beginning and the end of the experiment. The transpiration (even at night) was relatively high except for two short episodes of almost null-transpiration. Consequently, during this experiment we covered a wide range of plant actual transpiration rates.

The highest root length density was measured at the soil surface (38.40 $cm.cm^{-3}$) and decreased exponentially to the bottom of the soil profiles (0.02 $cm.cm^{-3}$) with a mean value of 3.5 $cm.cm^{-3}$ as shown in Figure 9.5-A. The RLD profile could be fit well ($r^2 = 0.92$, RMSE = 0.68 cm cm^{-3}) with ryegrass root system architecture generated by RootTyp. The optimal root system architecture is represented in Figure 9.5-B in its periodic domain (roots crossing x or y borders reappear at the opposite side). It is the same root system as in Figure 9.1-B in a shrunk (continuous, see section 9.2.4) domain. This root system architecture was used in both models (Root-rhizosphere model and R-SWMS).

9.3.2 Modeling results

In Figure 9.7-A simulation results obtained by running the R-SWMS model with the locally optimized plant and soil parameters are compared with data of DaS 116 3:15pm and DaS 117 5:20 am. The soil water $\delta^{18}O$ anomalies observed at 20 cm (-5.3‰) and 25 cm (-6.2‰) were well reproduced by the model (i.e., -5.5‰ and -6.3‰, respectively). The RMSE is comparable to the precision of the isotopic measurements (OF_1

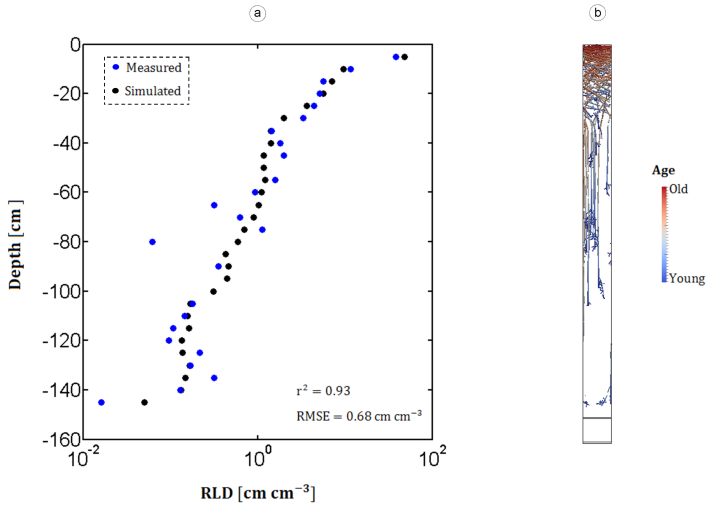


Figure 9.6: Measured (blue dots) and simulated (black dots) root length density (RLD) (a) and optimized root system architecture in the periodic soil domain (b).

= 0.21‰) and corresponded to a correlation coefficient of 0.98. These good results are the consequence of the good calibration procedure. For both of the impacted layers, a change in θ from 0 to 0.02 cm^3.cm^{-3} was modeled, in agreement with the observations made in situ by the water reflectometers, taking into account their measurement's accuracy and representative measuring soil volume. The simulated volume of water involved in the HL process corresponded to 19% of the transpiration of the next day, i.e. to 0.45 mm of water. The second subplot of Figure 9.7 details the radial water flow entering (positive) or leaving (negative) the root as a function of the vertical position of the segment during a low transpiration episode. The root system is taking up water in the middle and deep soil layers and releasing it in shallow layers but not at the very topsoil. The difference between the uptake and the release corresponds to the plant actual transpiration.

Figure 9.8 summarizes the sensitivity analysis results. Each single subplot represents the OF_1 obtained when modifying two plant and/or soil parameters concomitantly around their optimal values. The white crosses indicate where the optimal parameters are in each subplot. In

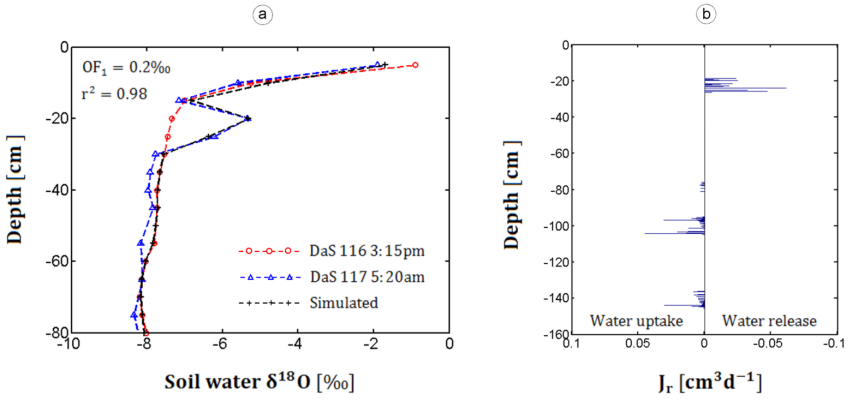


Figure 9.7: Best fit soil water isotopic composition profile (dark symbol) as compared to initial (red symbols) and final profiles (a): root radial flow profile during the first low transpiration rate episode (b).

this contour plot, blue corresponds to low values of the OF (or a good model-to-data fit, i.e., OF_1 close to its minimal value of 0.2‰) while red zones are made of high OF values (bad model-to-data fit, i.e. misrepresented peak of HL). When no HL was simulated, the OF reached a value of 0.5‰. When either the location or the intensity of the HL was misrepresented the OF took values above 0.2‰ and could exceed 0.5‰. It was observed that the simulation was insensitive to the young xylem conductivity of the primaries, in other words, the OF was not impacted by a change of value. This was due to the age of the total root system: as the experiment was conducted four months after plants were sown, the percentage of young primary roots among the root system was very low. Moreover, we assumed (see section 9.2.4) that these primary root segments had a zero radial conductance and did not take part in the uptake or release of water. However, as the axial conductivity of these young laterals were low and systematically lower than the primary axial conductivity in the simulations (i.e.,), the young primary axial conductivities never limited water flow. In the bottom-right subplot, a strong correlation between k_S and λ was observed, illustrating the antithetical effects of the saturated conductivity and the shape parameters in the

(Brooks and Corey 1966) conductivity curve formulation. A larger k_S makes the unsaturated conductivity increase over the whole range of matric potentials, whereas a larger λ makes the conductivity decrease with decreasing potentials or water contents. Note that the two last columns show opposite plots due to the contradictory effect of these two soil parameters. Finally the root axial conductivity of the old segments (primary and laterals) as well as the root radial conductivity of the old laterals controlled the water volumes flowing from the bottom to the top soil layers through the root system, and thus the $\delta^{18}O$ anomaly. In this four months old root system, water mostly entered in the deep soil layers and exited the root system in the upper layers through lateral old segments and was transported by the vessels of primaries and laterals. If one of the respective conductances was too low, the isotopic anomaly could not be reproduced in terms of absolute values because not enough $^1H_2{}^{18}O$ were brought to the top layers. To the contrary, if these conductances were too high the root system would have released too much water and $^1H_2{}^{18}O$ to the topsoil.

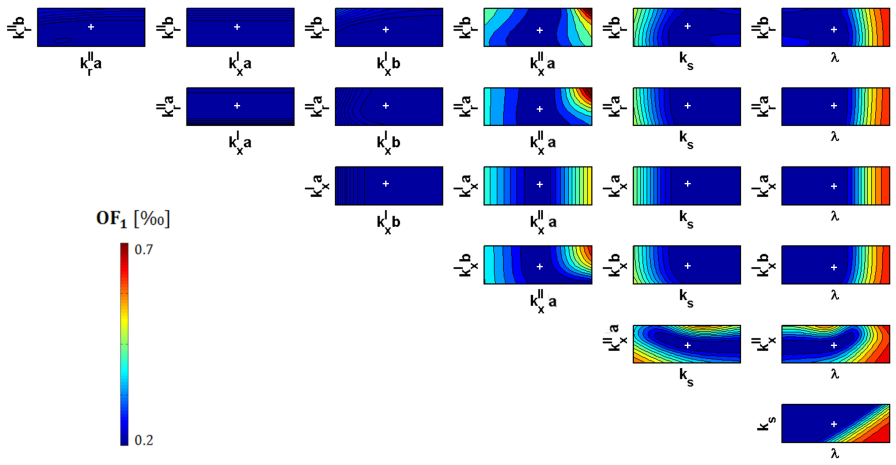


Figure 9.8: Root-rhizosphere model sensitivity analysis of the soil and root hydraulic conductivity functions. The optimal parameter set is shown by the white dot crosses.

Figure 9.9 shows a comparison between measurements and best fit simulation (solid line, Root-rhizosphere model) of the xylem sap water

isotopic composition in the tiller, δ_{Ti} (-, expressed in ‰), for the late simulation period. The general downward trend could satisfactorily be reproduced by the model (RMSE= 15.4‰) without any optimization of model parameters to fit tiller water isotopic composition data, which was remarkable. However the model was not able to capture the variations exhibited by the observed data. Incidentally, it is likely that no other model parameterization would be able to reproduce such variations, as there was no model input variables that exhibited such a high dynamics. These variations could well be due to the measurement protocol, not coming from isotopic analytical precision but rather from the spatial variability of root length density and uptake between plants. In particular with the doped skewed soil isotopic composition profile, it could be expected that little changes in the root hydraulic architecture could generate big changes in terms of tiller concentration. The light (resp. dark) envelope contains 95% (resp. 50%) of the thousand simulation runs with a modified parameter dataset. The parameters were always kept in such a range that it lead to satisfactory OF_1 values for the simulated vs modeled soil water isotopic profiles (lower than 0.3‰).

Figure 9.10-A shows the relation between the actual transpiration rate and the actual release rate by the plant roots as simulated by R-SWMS: the absolute value of the instantaneous water release was negatively correlated with the transpiration rate with a high correlation coefficient: $r^2 = 0.92$. Indeed the second environmental condition to observe Hydraulic Lift is to have a relatively small (but not necessarily null) transpiration rate. As illustrated in this subplot, for small demand, because of the high gradients between top and bottom soil layers, there was still water release in the dry regions of the soil domain. A comparison of the local uptake normalized by the total uptake with and without soil resistance shows the main differences to occur in the topsoil (Fig. 9.10-B) with the soil resistance considerably reducing the release. The normalized uptake of all other segments naturally increases because of the normalization.

In preliminary simulations, the soil resistance between the bulk soil and the soil-root interface was not taken into account, which led to an overestimation of the water release in the topsoil. Soil resistance between the bulk soil and the soil-root interface was indeed underestimated when considering the soil conductivity equal to the bulk soil conductivity

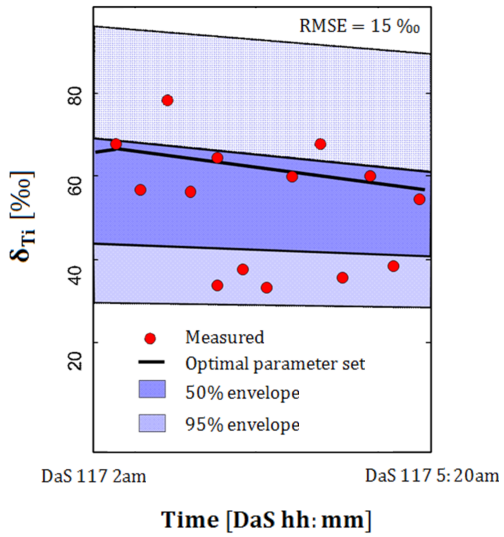


Figure 9.9: Best fit equivalent isotopic composition and uncertainties(the light and dark blue envelopes contain 95% resp. 50% of the simulations run with a set of parameters whose value lead to good fit of the delta isotopic profile) as compared to measured tiller water isotopic composition (red circles).

between those two points. Incorporating the soil resistance allowed the model to better fit the isotopic composition profiles with less or no release in the first soil centimeters.

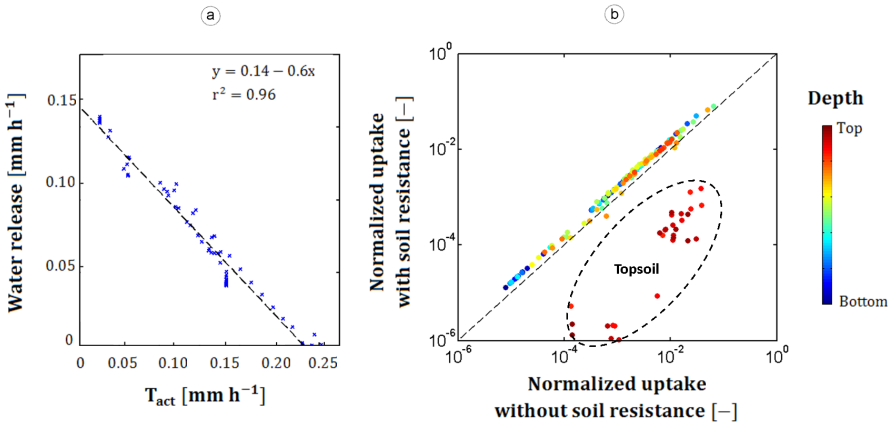


Figure 9.10: Water release rate as a function of the actual transpiration rate (T_{act}) during the experiment (a) and change of the standard uptake fraction when incorporating a soil resistance as a function of soil depth.

9.4 Discussion

The three-dimensional soil-root model used in this study was perfectly able to reproduce the peak observed in the isotopic composition profile. The optimized parameters needed to obtain this result are in the range of observed values in the literature and HL as modelled in this manuscript is consequently a likely mechanism explaining the experimental results. As mentioned in the introduction section, we did not consider any change in root hydraulic conductivity for in- and outflow but the root properties change according to the root type and age.

The estimated volume of water moved upward during the HL episode represented 19% of the transpiration of the next day (according to the RWU model). This is in agreement with results of other studies from the literature (Neumann and Cardon 2012). For instance, Couvreur et al. (2014b) found that HL contributed to between 11% and 20% of the daily transpired water for a maize plant in a simulation study. Caldwell and Richards (1989) and Brooksbank et al. (2011) found also similar proportions for sage brush and Eucalyptus (i.e., 34% and 27%, respectively). These 19% were however observed in the particular conditions of the

greenhouse experiment we conducted. As mentioned in the introduction of this Chapter, two environmental conditions may favour Hydraulic Lift and its magnitude: high soil water potential gradients between two soil regions explored by plant roots and a low transpiration rate. Huge soil water potential gradients existed between the topsoil and bottom soil layers at the beginning of the experiment as highlighted by the z-profile of pF plotted in Fig.9.4. A short period of very low transpiration was also observed at night even though it did not last for long. So the water volume implied by Hydraulic Lift could be temperated as optimal soil conditions were met.

It is worth noting that the water efflux could not be observed trough the water sensors because the HL fluxes were lower than the probe precision level while far from being negligible.

High values of transpiration at night (e.g., DAS 116 11pm – DAS 117 1am) illustrated the particular atmospheric conditions prevailing in the glasshouse during the period of soil and plant sampling. Night transpiration has been shown as an important mechanism (for a complete discussion, see (Caird et al. 2006)). Relative humidity reached only on a few occasions saturation (e.g., DAS 117 1am – 4am, data not shown), as air temperature was still high (e.g., higher than 15°C until DAS 117 1am, data not shown), which did not prevent night transpiration to occur.

Stable water isotopes are powerful tools for partitioning raw fluxes (e.g., transpiration) into net fluxes (e.g., RWU profile). However, the methodology employed to measure the isotopic composition of plant and soil water suffers from major drawbacks which ultimately limits its potential. The present study illustrates some of these limitations: while θ and h_{soil} profiles could be measured in a non-destructive manner at high temporal resolution, soil water $\delta^{18}O$ profile could only be determined destructively on two occasions during the experiment. Even though this was partly due to limited soil availability inside the rhizobox (many soil profiles could have been sampled under field conditions where soil is not limiting), soil water $\delta^{18}O$ profiles could not provide insights into the HL temporal dynamics. New methods (unavailable at the time when the experiment was designed and performed) for monitoring soil water isotopic compositions have been published in the recent years which propose to overcome these limitations (Gaj et al. 2016; Rothfuss et

al. 2013; Volkmann and Weiler 2014). They open avenues towards a dynamic disentangling of ecosystem fluxes and identification of water sources and sinks in the soil-plant-atmosphere continuum system (Gangi et al. 2015; Rothfuss et al. 2015; Volkmann et al. 2016).

Another limitation of this study is the relative poor knowledge of the three dimensional hydraulic architecture of the root system used in the R-SWMS model. We fitted a root architectural model (RootTyp; (Pagès et al. 2004)) to the measured RLD profile. However, different RootTyp parameters could have equally well fitted the RLD profiles and led to distinct hydraulic architectures. The optimized soil and plant hydraulic parameters accurately reproduced the experiment but the solution is not unique. A root system with more laterals in the topsoil (offset by shorter primary length) would fit the RLD profile as well and the optimization would lead to a reduced radial hydraulic conductivity for these segments.

The soil water potential was very low in the top soil (the soil there was very dry, see shallow layers of Figure 9.2), consequently the soil hydraulic conductivity was small and became the main resistance against water flow between the root xylem and the soil. Adding a soil resistance to the root architecture of the root system had consequently an important effect on the water uptake and release vertical location. The low soil water content also explains why the experiment is sensitive to soil hydraulic properties. If k_S is too low or λ too high, the soil resistance is too large in the top soil (there the soil conductivity is highly limiting the flow) and HL could not be simulated in the top layers. Since this upper soil layer was hardly conductive, HL appeared deeper in the soil profile where soil resistances became lower. Two main reasons explained why the HL occurs around 20 centimeters. First the soil resistance was lower there than in the very top soil while the gradient between root xylem potential and bulk soil was still high. Secondly numerous lateral roots could be found in the soil layers while below (especially between 30 and 60 centimeters) the root density was drastically reduced.

9.5 Conclusion

Debate about magnitude of HL is still on-going while it has important impacts for plant nutrient and water uptake, among others. We designed an experimental setup to monitor HL fluxes during a short time period in a planted soil column using a $^{1}H_{2}^{18}O$ labelling method. An isotopic enrichment of the soil water sampled at 20 cm and 25 cm depth was observed after one night experiment while the soil water content at the same depths did not change dramatically. This result led to the conclusion that HL process was observed: isotopically enriched water from the labeled reservoir located at the bottom of the rhizobox and from the rhizobox labeled bottom layers was released by the root system into the shallow layers.

Combining these experimental results with a root water uptake model, we could:

- Confirm that hydraulic lift was a likely mechanism to explain the peak of isotopic enriched water observed around 20 cm depth, as root and soil parameters optimized via inverse modeling ($r^2 = 0.98$ and RMSE = 0.21‰, equivalent to the accuracy of the isotopic measurements) are in the range of magnitude of expected values.
- Quantify the water efflux and demonstrate that although no change of soil moisture could be directly measured by soil water probes, the water efflux was not negligible but lower than the probe precision level.
- Explain which root (root radial conductivity) and soil (soil hydraulic conductivity) factors control the magnitude of the efflux.
- Show that such experiments can provide valuable estimates of hardy measurable variables (like water fluxes) and root-soil hydraulic properties.

It is therefore suggested that further quantitative investigation of hydraulic lift should focus on the hydraulic resistances of the soil plant system and particularly at the soil root interface. The need for additional information about both soil system and hydraulic architecture also

clearly appeared from this modelling exercise. If such an experiment is used to retrieve plant hydraulic properties, (i) a good knowledge of the hydraulic conductivity curve of the soil medium (especially under dry conditions) as well as (ii) regular observations of root system growth for measuring the age distribution of the roots would be mandatory. If these measurements are included in the methodology it is expected that the estimate of plant hydraulic conductivities will be more accurate.

9.6 Appendices

Appendix A: Hydraulic lift in a simple root water uptake model

The model of Couvreur et al. (2012) describes the water flow in a root system hydraulic architecture under a non-limiting xylem hypothesis. It provides an appropriate framework to understand the root water flow in heterogeneous soil conditions (such as the ones imposed to the plants in the presented experiment). Couvreur et al. (2012) demonstrated analytically that the water uptake of a root segment in heterogeneous soil conditions can be written as the sum of two terms: the "standard uptake" or water uptake under uniform soil water potential conditions and the "compensatory uptake" that occurs only under heterogeneous soil water potential distribution. They correspond, respectively, to the two terms of the right-hand side of equation A.1

$$J_{r,i} = T_{act}.SUF_i + K_{comp}\left(\Psi_{sr,i} - \Psi_{seq}\right) SUF_i \tag{A.1}$$

with $J_{r,i}$ [L^3T^{-1}] the water uptake of the root system ith segment (defined positive towards the root), T_{act} [L^3T^{-1}] the actual transpiration rate, SUF_i [-] the standard uptake fraction (defined as the fraction of water taken up by the root segment i under uniform soil water potentials and consequently comprised between 0 and 1), K_{comp} [$L^3P^{-1}T^{-1}$] the root system compensatory water uptake conductance, $\Psi_{sr,i}$ [P] the potential at the soil-root interface and Ψ_{seq} [P] the equivalent soil water potential "felt" by the plant defined as a SUF-weighted soil-root interface potential. In equation A.1, T_{act} and $\Psi_{sr,i}$ depend on environmental conditions that can be measured in-situ while K_{comp} and SUF_i are intrinsic root system properties that can be calculated from root system architecture and root hydraulic properties. HL occurs when $J_{r,i}$ takes negative values. Equation A.1 yields:

$$J_{r,i} \leftrightarrow T_{act} < K_{comp}\left(\sum_j SUF_j \Psi_{sr,j} - \Psi_{sr,i}\right) \tag{A.2}$$

It can be observed that two environmental factors promote HL: a low transpiration rate (i.e., small T_{act}) and large variations of soil water

potential with depth (i.e. $\Psi_{sr,i}$ very different from Ψ_{seq}, e.g., for low water content in the topsoil and high water content in the layers where the deepest roots are located). To observe HL, the root system must also have a large K_{comp} and active root segments (i.e. $SUF_i > 0$) in both dry and wet soil regions, i.e., the soil and root radial conductivity must be high enough to enable root water efflux. Note that we can still observe HL even when the actual transpiration is not zero: then simply the product of the left-hand side of equation A.2 must be larger than the actual transpiration rate.

Appendix B: Radial flow from or to a root through a soil resistance

The mass balance under steady state imposed that the radial flow from root surface to xylem $J_{r,i}$ can be equalized with the water flow from bulk soil to root surface J_{soil} [L^3T^{-1}] given by axisymmetrical Darcy law (Schroeder et al. 2008):

$$J_{r,i} = J_{soil} \leftrightarrow k_{r,i}S_{r,i}\left(\Psi_{sr,i} - \Psi_{x,i}\right) = k_{soil}2\pi l_i B\left(\Psi_{soil} - \Psi_{sr,i}\right) \quad \text{(B.1)}$$

with B [-] is a geometric parameter that depends on the distance between the soil node and the soil-root interface fixed to the mean distance between roots in the simulations (de Jong van Lier et al. 2008) and Ψ_{soil} the potential of the bulk soil linked to the root segment. Note that the products $k_{soil}2\pi l_i B$ and $k_{r,i}S_{r,i}$ have the dimensions of a conductance [$L^3P^{-1}T^{-1}$] and are designed by K_{soil} and $K_{r,i}$ respectively. Under flux and water potential type boundary conditions at the inner (r_i, the root radius) and outer edges (r_{bulk}) representing the bulk soil, and under steady-rate behavior, i.e., ($\frac{\partial\theta}{\partial t}$ null, the general solution for the radial flux [LT^{-1}] without the assumption of uniform K(h) is given by Schroeder et al. (2008):

$$q_{r,i} = \frac{k_{soil}B}{r_i}\left(\Psi_{soil} - \Psi_{sr,i}\right) + B\chi_1 + \chi_2 \quad \text{(B.2)}$$

where

$$k_{soil} = \frac{\int_{h_{soil}}^{h_{sr,i}} k(h)dh}{h_{soil} - h_{sr,i}}$$

$$B = \frac{2(1-\rho)(1+\rho)}{2\rho^2 ln\rho - \rho^2 + 1}$$

$$\rho = \frac{r_{bulk}}{r_i}$$

$$\chi_1 = q_{bulk}\rho ln\frac{1}{\rho}$$

$$\chi_2 = q_{bulk}\rho$$

when it is explained in terms of flow, J_r [L^3T^{-1}], we have:

$$J_{r,i} = \left(\frac{k_{soil}B}{r_i} \left(\Psi_{soil} - \Psi_{sr,i} \right) + B\chi_1 + \chi_2 \right) 2\pi r_i l_i$$

When the outer flux q_{bulk} is 0, it writes:

$$J_{r,i} = 2\pi l_i k_{soil} B \left(\Psi_{soil} - \Psi_{sr,i} \right) = K_{soil} \left(\Psi_{soil} - \Psi_{sr,i} \right)$$

where the conductance term K_{soil} is in [$L^3P^{-1}T^{-1}$]. When this soil conductance is associated in series with a root radial resistance, the equivalent resistance yields:

$$K_{i,eq} = \frac{k_{r,i} k_{soil} 2\pi l_i r_i B}{B k_{soil} + r_i k_{r,i}}$$

Two limit cases can be analysed. First if the soil resistance is much higher than the root resistance, the equivalent conductance yields:

$$K_{i,eq} \approx 2\pi l_i B k_{soil}$$

If it is the root resistance that much limits the flow then the equivalent resistance is close to the root resistance:

$$K_{i,eq} \approx 2\pi l_i r_i k_{r,i}$$

and is independent of the soil resistance.

PART IV

ANALYZING THE PLANT IN ITS SURROUNDING ENVIRONMENT

In the fourth section of this manuscript, we set up a functional-structural model that can physically simulate the water flow in three-dimensions in the soil-plant-atmosphere continuum over a full crop cycle with reasonable simulation times. It will be the basic tool for eco-ideotype generation, i.e. plant root systems perfectly adapted to their surrounding heterogeneous and chaning environment.

*

A tree with strong roots laughts at storms

Malay proverb

IMPACT OF CONTRASTED HYDRAULIC AND ARCHITECTURAL TRAITS ON DROUGHT STRESS TOLERANCE

10

This chapter is a modified version of a paper published as:

> Leitner D., Meunier F., Bodner G., Javaux M. and Schnepf A. Impact of contrasted maize root traits at flowering on water stress tolerance - A simulation study. Fields Crop Research. 2014, 125, 125-137.

Abstract

Water stress is among the dominant yield limiting factors in global crop production. Better drought resistance is therefore a key challenge for breeding and crop management. Avoidance of water stress by effective root water uptake is considered a promising approach to yield stability in water limiting environments. Water uptake efficiency is the result of multiple plant root traits that dynamically interact with site hydrology. Root models are therefore an essential tool to identify key root traits for water efficient crops in a certain target cropping environment.

We present a novel combination of a dynamic root architecture model (Rootbox) with a functional model of root xylem hydraulic properties and soil water flow (R-SWMS). This model integrates structural and functional root traits to simulate water uptake under variable hydrological conditions. Application of the model is exemplified for three different maize root phenotypes to evaluate the role of root architectural

and functional traits to deal with water stress under two contrasted hydrological conditions (deep water storage vs. moist upper profile layer in silt loam). The phenotypes include a reference phenotype (P1), one phenotype with steeper main roots (P2), and one with steep main roots and with longer lateral roots (P3). We showed that those phenotypes whose root axes matched with available water distribution were able to transpire more. This synchronization is a result of root architecture (structural root traits). The temporal dynamics of water depletion on the contrary were essentially determined by root hydraulic properties. We showed that lower gross root conductance is essentially related to a water saving behaviour of the plant, while high root conductance contributes to a water spending type with high initial transpiration that decreases quickly over time.

Our results confirmed that functional-structural root models are appropriate to better understand the role of roots in whole plant adaptation to different drought scenarios and their contribution to distinct drought response types. The newly developed model contains all basic components to further refine complex root processes such as architectural plasticity, dynamic root conductance (xylem vulnerability, composite radial transport) and root exudation. These results could feed into cropping system models to see the effect of these processes on crop yield.

10.1 Introduction

Root system is the key plant organ for more efficient use of available resources (Lynch 2007), particularly under stress conditions (Waines and Ehdaie 2007). Crops have increasing competitive advantage from optimized root systems in resource limited environments due to improved water and nutrient uptake efficiency (Hinsinger et al. 2011; Lynch 2007; Smith and de Smet 2012).

According to Passioura (1977), yield formation under water limited conditions is determined by total water uptake (WU), water use efficiency (WUE) and harvest index (HI). Within this framework, Blum (2009) points to water uptake maximization as a focus for breeding

because of its general compatibility with high yield. Using a model to explain historic yield trends in US maize, Hammer et al. (2009) found that changes in root architecture associated with higher water uptake to be the main reason for better abiotic stress tolerance. For systematic crop improvement it is therefore imperative to understand which root architecture would best contribute to maximize water acquisition under the prevalent drought stress conditions. Different authors have thus discussed the optimal root architecture traits needed to improve plant drought tolerance (Leitner et al. 2010). For rainfed wheat production with high importance of stored subsoil moisture, Wasson et al. (2012) showed that maximum rooting depth and shifting of rooting density to deeper layers were most relevant root traits for yield. Vadez et al. (2008) on the other hand did not find a strong correlation between root length density distribution and water uptake for groundnut in a breeding programme for a tropical residual moisture environment. They suggested to consider root functionality via water uptake and to only subsequently characterize root morphological differences between genotypes. Some authors defined root traits of apparently broad relevance for better crop growth under drought stress, such as steep, deep and metabolically cheap roots (Lynch 2013) or root systems with fine root dominance (Comas et al. 2013). Root plasticity itself has been proposed as a beneficial trait especially when there are trade-offs between different traits (Trachsel et al. 2011; Zhang et al. 2011).

Beyond the architecture itself, different authors have also investigated the question of ideal axial and radial conductance in roots. Richards and Passioura (1989) showed that reduced axial conductance of seminal roots allows water saving during vegetative growth and help to alleviate stress during the generative stage of yield formation Other distributions of root hydraulic properties that favour water uptake are: greater axial and radial conductivities in deep roots in order to increase the uptake and transport capacity of water from deep soil layers (according to (Wasson et al. 2012)) and, decrease of axial conductance in order to save water for the end of the crop cycle (according to (Comas et al. 2013)). Draye et al. (2010) pointed out the importance of the root hydraulic architecture for root water uptake, i.e. not only the architecture per se but also the distribution of the root hydraulic properties between root segments within a given architecture. Mathematical

modelling is highly suitable to analyse the effect of axial and radial conductivities, especially the ratio between axial and radial conductivity proofed useful for classification, since this number determines if root uptake is uniformly, or preferentially from topsoil (Doussan et al. 2006; Draye et al. 2010).

However the above cited studies demonstrated that not always genotypes with apparently better rooting ability provided better water uptake and/or yield improvement. A precondition to obtain better water stress tolerance via the root system is a precise definition of the target trait(s) for a clearly defined environment. In this sense root systems do not differ from what Tardieu (2012) stated for abiotic stress tolerance in general: "Any trait can confer drought tolerance, just design the right drought scenario". Facing this complex root trait-target environment interaction and the inherent adaptive plasticity of root systems, Draye et al. (2010) suggested to develop in-silico experiments to test how root traits may increase drought stress tolerance. To be able to investigate the impact of root architecture on water stress tolerance, models with root growth, soil and root water flow and water uptake modules are thus required. The most sophisticated approach is to describe water movement in soil and roots simultaneously, considering the 3-dimensional root architecture, heterogeneous water distribution in the rooting zone and water potential gradients between soil and roots (Javaux et al. 2013). Root water uptake is then driven by the water potential gradients between root surface and soil.

Maize is a crop growing in a wide range of target environments from temperate to tropical climates, but Meisey and Edmeades (1998) estimated that one-quarter of the global maize area is affected by drought in any given year. Tollenaar and Lee (2002) demonstrated that main yield gains in maize did not come from higher yield potential or heterosis per se, but mainly from better stress tolerance. It has been shown that maize is most susceptible to stress at flowering. Shaw (1977) showed that stress in the period from about 7 days before to 15 days after anthesis reduces maize grain yield two to three times more than at other growth stages. Indeed drought stress during this period increases the period between male and female flowering, widening the anthesis-silking interval (ASI) (Campos et al. 2004). Yield under stress has been showed to be strongly dependent to kernel number per plant, barrenness and

ASI in tropical maize (Bolanos and Edmeades 1996). Our assumption in this simulation study is that stress occurring during this period will have a major impact on the final grain yield.

The objective of this study is to use a mathematical model to quantitatively compare how contrasting root systems of Zea mays affect root water uptake pattern and soil water dynamics. We focus on the flowering period by comparing how three types of maize root architecture (called phenotypes) with different traits will suffer from stress under contrasted water conditions in a silt loam: (a) when most of the water is located at the top of the profile (SWtop) and (b) when the water content is increased in depth (SWbot). A reference phenotype (P1) is compared with two contrasted root system architectures having the same volume (proxy of the amount of invested carbon): a second type (P2) with steeper main roots and a third one (P3) based on P2 with longer lateral roots at depth.

10.2 Material and Methods

In the following we outline the mathematical model in detail, including all parameters and units. For the numerical implementation of the model we refer to the corresponding software packages that we have used, R-SWMS (Javaux et al. 2008) and RootBox (Leitner et al. 2010).

10.2.1 Root architecture modelling

The root growth used in this study is rootbox that is entirely described in Chapter 3. We used the L-System implementation of RootBox (Leitner et al. 2010) to simulate the root growth model in Matlab. The dynamic growth of root systems was simulated until root systems reached a given volume. Those root systems were then used as input for simulating soil and root water flow.

10.2.2 Root water uptake and soil water flow modelling

To describe water uptake by the root system we follow the approach of Javaux et al. (2008), who combined the model of water movement in soil of Somma et al. (1998) with the model describing water flow inside

a root branching structure of Doussan et al. (1998a). In plants, it is common to express water potential as energy per unit volume (yielding pressure units) while it is common to describe the status of water in soils as energy per unit weight (head units). For model coupling, we chose to consistently express water potential in both systems on a volume basis.

Modelling soil water flow

Water movement in the soil is calculated with the Richards equation:

$$\frac{\partial \theta}{\partial t} = \nabla . \left(\frac{K}{\rho . g} \left(\nabla \Psi_m - \rho g e_z \right) \right) - S \tag{10.1}$$

where $\theta := \theta(\mathrm{x}, \mathrm{t})$ is the volumetric water content [$\mathrm{L}^3\mathrm{L}^{-3}$], t is time [T], x is the spatial coordinate [L], $\mathrm{K} := \mathrm{K}(\theta)$ is the hydraulic conductivity tensor [LT^{-1}], Ψ_m is the matric potential [$\mathrm{ML}^{-1}\mathrm{T}^{-2}$], ρ is the fluid density [ML^{-3}], g is the gravitational acceleration [LT^{-2}], $\mathrm{e_z}$ is the unit vector pointing in z direction [-], and S is a volumetric sink term representing water depletion due to root water uptake per volume of soil [$\mathrm{L}^3\mathrm{L}^{-3}\mathrm{T}^{-1}$]. At the top and the bottom of the domain we choose a no-flux boundary condition. At the sides, we assume periodic boundary conditions. As initial condition, we predefine a water content distribution .

The solution for the Richards equation Eq. 10.1 is based on the SWMS 3D algorithm (Simunek et al. 1995). The finite mesh for soil is made of cubic voxels which are automatically subdivided into 6 tetrahedral elements. A Galerkin finite element approach is applied that uses tetrahedral elements for its spatial discretization. The time component is incorporated using an implicit backward finite difference method. A solver based on a conjugate gradient method is integrated and the solution Ψ_m(x,t) is obtained from a Picard iterative numerical scheme. Additional measures are taken to improve solution efficiency in transient problems, including automatic time step adjustment.

Equation 10.1 together with the initial condition and the boundary conditions allow us to simulate soil water flow, if the volumetric sink term S is known. In the following, we describe how we calculate the sink term S, taking the soil water potential, as well as the water potential distribution inside the root system into account.

Water potential distribution within the xylem network

We describe the root water pressure $\Psi_{\mathrm{p}}(\mathrm{t}, \xi)$ in the xylem tubes, where ξ is the arc length of the centreline of a single root segment with $\xi = 0$ at the base of each root segment. For each ξ, the corresponding position in Cartesian space is given by its parameterisation $\mathrm{x}_{\mathrm{roots}}(\xi)$. For a single root segment, we adapt the equation for the axial xylem water flow $\mathrm{J_a}$ ((Javaux et al. 2008), Eq. 2b):

$$J_a = -K_a \left(\frac{\partial \Psi_p}{\partial \xi} - \rho g \mid \frac{\partial x_{root}}{\partial \xi} \mid_z \right) \tag{10.2}$$

where $\mathrm{J_a}$ describes the rate of axial xylem water flow [$\mathrm{L^3T^{-1}}$], $\mathrm{K_a}$ is the axial root hydraulic conductance [$\mathrm{M^{-1}L^5T}$], Ψ_{p} is the pressure potential in the root xylem [$\mathrm{ML^{-1}T^{-2}}$], where ξ is the distance from the root base [L], and $\mid \frac{\partial \mathrm{x_{root}}}{\partial \xi} \mid_{\mathrm{z}}$ is the absolute value of the z-component of the unit tangent vector at position ξ [-]. The total water potential in the xylem (neglecting the osmotic potential) is $\Psi_{\mathrm{total}} = \Psi_{\mathrm{p}} - \rho.\mathrm{g}$.

Following Landsberg and Fowkes (1978) the radial water flux, which enters radially into root segments is described by

$$q_r = 2.\pi.a.k_r(\Psi_m - \Psi_p) \tag{10.3}$$

where $\mathrm{q_r}$ is the rate of water flow into the root per root length [$\mathrm{L^3L^{-1}T^{-1}}$], a is the root radius [L], $\mathrm{k_r}$ is the root radial hydraulic conductivity [$\mathrm{M^{-1}L^2T}$], and Ψ_{m} is the matric potential at the soil root interface [$\mathrm{ML^{-1}T^{-2}}$].

When no water storage is considered, the conservation of water within the root yields

$$\frac{\partial J_a}{\partial \xi} = q_r \tag{10.4}$$

This 1-dimensional partial differential equation describes the water potential in a single root section in dependence on the soil matric potential at the soil root interface.

To describe the flux distribution in a root system we stitch together multiple 1-dimensional root sections. At the nodes between the sections (i.e. the branching points) we apply Kirchhoff's law stating that the water volume flowing into the node is equal to the water volume flowing

out of the node. The remaining boundaries are located at the root collar, and at the root tips. At the root collar we apply flux boundary condition under non-stressed conditions (Neumann boundary condition, $J_{a,c} = T_{pot}$, where T_{pot} is the potential transpiration), changing to a fixed water pressure potential when stress appears (Dirichlet boundary condition, $\Psi_{total,c} = 1.5$MPa). At the remaining boundaries we apply a no-flux boundary condition. It results in a system of $n_n = n_s + 1$ equations (n_n and n_s being respectively the number of root nodes and root segments), which writes in matrix notation (Doussan et al. 1998a).

$$C.\Psi_{total} = Q \tag{10.5}$$

where C (dimensions n_p x n_p) is called the "conductance matrix" which contains the root hydraulics characteristics, Q (dimensions n_p x 1) contains the terms related to soil and $\Psi_t$otal (dimensions n_p x 1) is the unknown xylem water pressure vector (Doussan et al. 1998a). Due to the large size of the system, these matrices are stored under a sparse format to reduce memory consumption. A biconjugate gradient method is used to solve this asymmetric linear system (Press et al. 2012).

Implementation

The coupling between soil and root and the root water uptake was implemented by Javaux et al. (2008) and the software is called R-SWMS. The sink term is calculated by summing up the radial uptake qr of the root sections located within a soil voxel V [L]:

$$S(t,V) = \frac{1}{\mid V \mid} \int_V \delta_2(\chi_{roots}(x) q_r(t,x)) dx \tag{10.6}$$

where | V | is the volume of V [L^3], χ_{roots}(x) is a characteristic function, which we define to be 0 if the Cartesian point lies on the centreline of the root system, and else 1, δ_2 is the 2-dimensional Dirac delta function [L^{-2}], and q_r is the volumetric water flow per root length if x is on the root system, else 0 [$L^3L^{-1}T^{-1}$].

For coupling the water flow in both soil and root system, an implicit iterative scheme is used. First the root water flow equations given by Eq. 10.5 are solved given an initial estimate of the pressure head distribution

in the soil. This generates a first estimate of the xylem potential Ψ_{total} and water flow distribution (Eqs. 10.2 and 10.3). A 3-dimensional sink term distribution can thus be calculated from Eq. 10.6, which allows the numerical solution of the Richards equation (Eq. 10.1). We simultaneously solve these equations for root and soil pressure head using fix point iteration. Note that solving Eqs. 10.3 and 10.5 requires the assessment of the soil water potential in the vicinity of each root node Ψ_{m}, defined as the average of the soil water potential of the 8 nodes of the cuboid around the root node weighted by the inverse distance between root and soil nodes.

10.2.3 Simulation scenarios

Root water uptake scenarios were run for a 7 day or a 10 -day periods (for the high K_{rs} cases, see hereafter) under sinusoidal potential transpiration conditions (daily T_{pot}= 5.33 mm), corresponding to typical Mediterranean climatic conditions in June-July. Simulation scenarios were built from (i) three different root system architectures (P1, P2, and P3), (ii) two distinct values for root axial conductance and radial conductivities of the root segments (indicated by the subscripts R and H), and (iii) two hydrological situations (SWtop and SWbot). This allowed studying the interactions of root system properties with the pedo-climatic environment. Given the fact that the root architecture parameters are associated with random variation (cf. 2.1), each scenario was run in five replicates of root architecture. Each of these replicates share the same parameter sets but differ in the precise location of each root segment. Thus a total number of 60 simulations were run (3 root system architectures x 5 replicates x 2 root segment hydraulic properties x 2 soil moisture conditions).

Root architecture

Three different types of root architectures were used and are referred to as phenotypes P1, P2 and P3 in the following text. We simulated root architectures of approximately 60 days old plants, corresponding to the flowering stage, however ensuring that root volumes were equal between phenotypes. For sake of simplicity, we modelled root systems

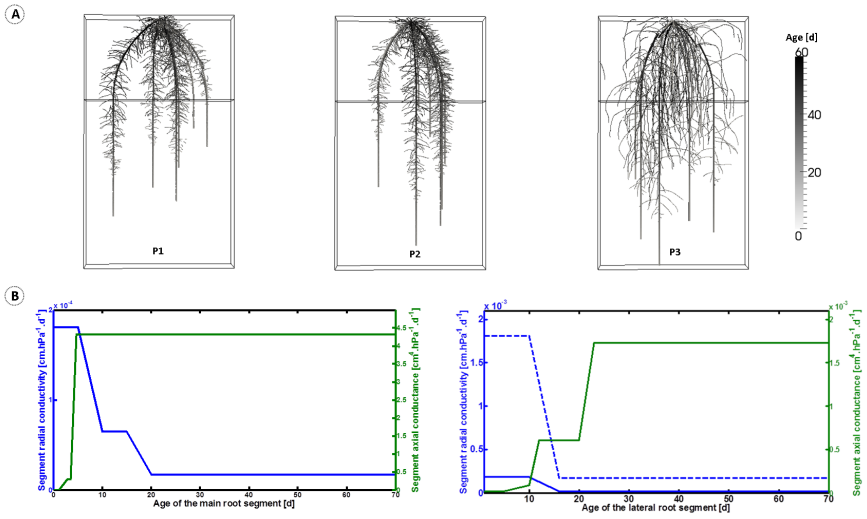


Figure 10.1: (A). Architecture and the age distribution of the root segments for a realization of each phenotype (P1, P2 and P3, respectively) and the separation line for the initial water content. (B). Age dependent root radial conductivity and axial conductance of primary (left) and lateral roots (right). In subplot B, solid and dashed lines stand for reference and increased conductivities, respectively.

only based on first (main roots) and secondary root orders (laterals). In these simulations thus, all main axes (seminal, crown and brace) are mixed together even though we noticed in previous Chapters that they can have different branching, geometric and hydraulic properties. The first P1 is considered as a standard phenotype. The second one (P2) had steeper and deeper principal roots (as suggested by Lynch (2013)), while P3 was created based on the root system architecture of P2 but was changed to have another beneficial trait for drought resistance, i.e., fewer but longer lateral roots at depth (Wasson et al. 2012). Fig. 10.1-A shows one realisation of the architectural model for each phenotype P1, P2 and P3.

The 15 root systems (3 phenotypes x 5 replicates) were generated using the root growth model described in section 10.2.1 based on the parameters presented at Table 10.1. The parameterisation of P1 corresponded to the standard parameter set for maize according to Pages et al. (1989). Two parameters of the main root axes were changed to form

Table 10.1: Root architectural parameters for the phenotypes 1-3

Symbol (Unit)	Meaning	Parameters (Primaries)	Parameters (laterals)
la (cm)	Length of apical zone	18.1(P1*), 24.2(P2), 21.3(P3)	10(P1), 10(P2), 100(P3)
lb (cm)	Length of basal zone	0.5(P1),0.5(P2),2(P3)	0
ln (cm)	Length of branch inter-space	0.5(P1),0.5(P2),2(P3)	1.2
nob (-)	Maximal number of branches	324(P1), 432(P2),109(P3)	0
r (cmd^{-1})	Initial root elongation	2.94(P1), 3.9(P2), 3.55(P3)	0.75(P1), 0.75(P2), 1.5(P3)
theta (rad)	Insertion angle	1.4(P1),1.06(P2),1.06(P3)	1.5
a (cm)	Root radius	0.13	0.05
sigma (cm^{-1})	Standard deviation of the root tip heading	0.1	0.1
N(-)	Number of trials	2	2
type (-)	Tropism type	geotropism	exotropism

the parameter set describing P2: initial growth rate of the main axes was increased while their growth angle was decreased. The magnitude of these parameter changes was evaluated based on available data of the DROPS project (http://www.dropsproject.eu/) where maize genotypes were screened for yield and root system traits. One hundred maize genotypes were screened in aeroponics (De Dorlodot et al. 2005) and the extent of growth rate and insertion angle was estimated from image analysis.

Table 10.2 summarizes the averaged root characteristics of the three phenotypes. As P2 has a higher initial growth rate of main axis, its root system is younger than that of P1 when it reaches the same volume. As P3 has longer laterals with the same root radius, the number of roots is smaller in P3 than in P2. In this way we simulate the same amount of carbon investment in different kinds of root architectures. Their effect on soil water dynamics and root water uptake during one week was simulated and in this time the root system was taken to be static.

When needed, the root length density was calculated by summing up the root length per 5cm-deep soil compartments, considering the soil surface of 75 cm x 15 cm.

Table 10.2: Averaged root statistics

Symbol (Unit)	Meaning	Mean Values
L_0 (cm)	Total root length	6468(P1) 6426(P2) 7002(P3)
L_{comp} (cm)	Total root length by compartment	5104(P1) 4606 (P2) 4348(P3) (top) 1364(P1) 1820(P2) 2654(P3) (bottom)
L_{ord} (cm)	Total root length by order	618(P1) 664 (P2) 759(P3) (primary) 5850(P1) 5762(P2) 6243(P3) (secondary)
r_{Vol} (-)	Relative volume of the root system	1(P1) 1.02(P2) 1.01(P3)
K_{rs} ($cm^3hPa^{-1}d^{-1}$)	Equivalent conductance of the root system	0.06(P1r) 0.062(P2r) 0.051(P3r) 0.17(P1h) 0.166 (P2h) 0.091(P3h)
Age (d)	Age at the beginning of the simulation	64(P1) 60 (P2) 62(P3)

Root hydraulic properties

In order to investigate the role of the plant root hydraulic properties on root water uptake and stress onset, two cases were analysed for each phenotype: a reference scenario with hydraulic properties similar to Doussan et al. (1998a) and another scenario with increased root radial conductivity. They will be referred to by the subscripts R and H: for instance, P3H refers to phenotype 3 with higher conductivity values.

The local conductivity and conductance of the root segment for the reference scenario are taken from Doussan et al. (1998a) with modifications according to Couvreur et al. (2012). Fig. 10.1-B shows the reference (R scenario) radial conductivity and axial conductance of main and lateral roots, respectively in function to segment age. The H-scenario is based on the same values except the radial conductivity of the laterals, which is increased by a factor 10 (dotted line in Fig. 10.1-B, right subplot) as these segments appear to be the most resistive part to water transfer. This factor ten is in the range of variations observed in experimental studies (Draye et al. 2010).

By considering a root system as a network of resistances as in an electrical circuit, the plant root equivalent conductance (K_{rs}; cf. Table 10.2 for values of the three phenotypes) can be estimated using the Thevenin theorem (Couvreur et al. 2012). The actual transpiration (T_{act} [L^3T^{-1}]) of the plant can then be defined as Javaux et al. (2013).

$$T_{act} = K_{rs}\,(\Psi_L - \Psi_{t,eq}) \tag{10.7}$$

where Ψ_L is the water potential at the root collar and $\Psi_{t,eq}$ is an equivalent total soil water potential, which is defined as the effective soil water potential at the soil root-interface (Couvreur et al. 2012). The equivalent root soil water potential is the mean soil water potential of soil-root interfaces, weighted by the relative local extraction rate of the root segments in a homogeneous soil (see Eq. 17 in Couvreur et al. (2012)). It is a physically sound way to define a root-sensed water potential in a heterogeneous soil. The higher $\Psi_{t,eq}$ the less energy is required to extract water from the soil. For a given amount of extracted water (represented by the cumulative transpiration), a plant with a higher (less negative) $\Psi_{t,eq}$ undergoes a less negative suction, and thus is in more favourable conditions of survival or for extracting soil water.

The evaluation of phenotype performance is done based on different indicators: (i) the equivalent soil water potential at the soil-root interface, (ii) the instantaneous stress fraction being defined as the ratio between water uptake (i.e. actual transpiration) and potential transpiration, and (iii) the cumulative water uptake as an indicator of the carbon acquired for the period.

Soil hydraulic properties

The soil was defined as a silt loam with soil hydraulic parameters from Carsel and Parrish (1988) (see Table 10.3). Its water retention curve, which relates the soil matric head ($h = \frac{\Psi_m}{\rho.g}$) to the volumetric soil water content θ, and the functional form of the hydraulic conductivity tensor K(h) are shown in Fig. 10.2. They were modelled using the van Genuchten-Mualem functions (Mualem 1976; van Genuchten 1980) using six parameters: saturated water content θ_s [L^3L^{-3}], residual water content θ_r [L^3L^{-3}], the saturated hydraulic conductivity K_{sat} [LT^{-1}] and the parameters α_{vg} [L^{-1}], n_{vg} [-],and λ_{vg} [-], which describe the curvature of the function.

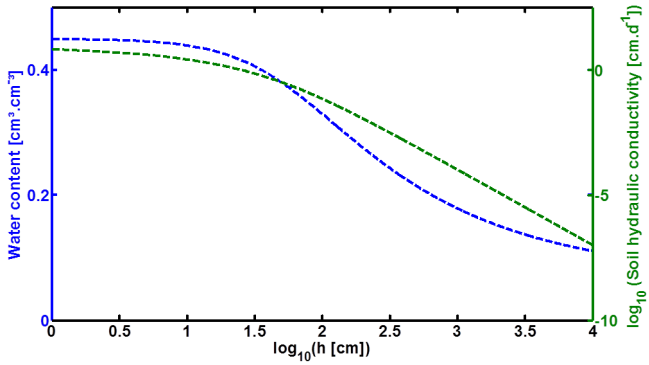


Figure 10.2: (A). Water retention and hydraulic conductivity curves of the soil used for the simulation.

Table 10.3: Parameter values for Mualem-Van Genuchten

Symbol (Unit)	Meaning	Parameters values
K_{sat} ($cm.d^{-1}$)	Saturated hydraulic conductivity	10.8
θ_s ($cm^3.cm^{-3}$)	Saturation water content	0.45
θ_r ($cm^3.cm^{-3}$)	Residual water content	0.067
α_{vg} (cm^{-1})	Shape parameter	0.02
n_{vg} (-)	Shape parameter	1.41
λ_{vg} (-)	Shape parameter	0.5

Hydrological regimes

To account for different climatic conditions in a very simple way, we consider two possible conditions for the initial water content $\theta_0(x)$. In the first case (called SWbot), most of the water is located at the bottom of the profile. This hydrological condition is representative for summer dry climates with high importance of subsoil water, e.g. a Mediterranean climate or an oceanic climate during a summer dry spell. The separation between the wet soil ($\Psi_{m,bot}$= -100 hPa) and the dry one ($\Psi_{m,top}$= -3000 hPa) was set at the first third of the soil depth (42 cm). In the second scenario (SWtop), the boundary is in the same location but the water content is higher close to the soil surface ($\Psi_{m,top}$= -100 hPa and $\Psi_{m,bot}$= -3000 hPa). This second case mimics a climatic situation with dominant role of regular rainfall input for plant water supply and low subsoil water reserves. Such conditions are found particularly for climates with dominant in-season rainfall during the vegetation period (e.g. semi-arid continental climates in the temperate zone), semi-arid tropical conditions before refilling of deep soil profile layers during the rainy season and for irrigation during a dry season.

10.3 Results

We will first present the impact of different types of root traits (phenotypes) using the reference hydraulic properties, while in the second part we will compare the impact of increased root radial conductivity. For sake of clarity, the three phenotypes will be associated with a unique colour code in the subsequent plots: P1 will be in red, P2, in green and P3 in blue.

10.3.1 Influence of root system architecture

Figure 10.3 shows the distribution of the water content for the scenario SWbot after 6.,5 d for one given replicate of each phenotype. Video S1 (supplementary material) shows the evolution of the water content distribution for 7 days for the same scenario. We observe that the impact of the initial water distribution remains visible over the whole period, and that the high hydraulic pressure gradient between the two soil layers generates an upward water flux. The effect of the root water uptake is also clearly visible, and we can distinguish through the water depletion pattern the main features of the root architectures of the three phenotypes. In the videos, the day-night dynamics is visible through the redistribution of the water content during night.

To better investigate the difference between phenotype behaviours, we can look at the transpiration dynamics of the three phenotypes under the two opposite hydrological regimes. In Fig. 10.4, the averaged transpiration of the five replicates is shown for each phenotype and for the SWbot case (Fig. 10.4-A) and for the SWtop case (Fig. 10.4-B). As standard deviations between replicates are small (always smaller than 3% of the mean value), they are not shown on the plots. For all phenotypes and cases, a water stress (i.e. a decrease of the actual transpiration as compared to the potential demand) is observed after the beginning of the first day of simulation and its magnitude increases with time. If we compare both scenarios, we can see that generally these three phenotypes transpire more when the upper layer is wetter: all the phenotypes transpire more than 25 mm after 7 days for SWtop conditions (Fig. 10.4-B), while none of them could reach 25 mm for SWbot (Fig. 10.4-A). When we compare the change of total transpiration between

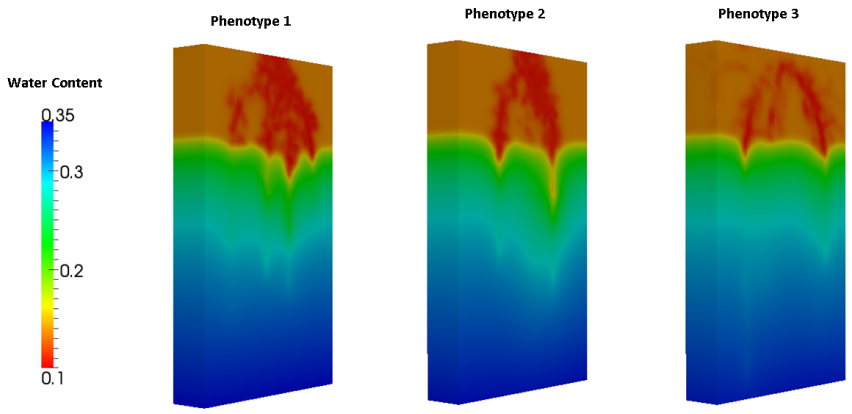


Figure 10.3: (A). 3-dimensional visualisation of soil water content as influenced by reference hydraulic architecture of the three phenotypes after 6.5 days for the SWtop scenario. See corresponding videos in supplementary material S1 and S2 for reference and increased hydraulic properties, respectively.

SWbot and SWtop, we observe differences between phenotypes. For P3, the change of cumulative transpiration is very small (21.5mm), for P2 of about 5 mm and for P1 of about 8mm, demonstrating a different sensitivity to climatic conditions.

In the SWbot scenario (Fig. 10.4-A), the ranking between the three phenotype transpiration rates evolves with time. While P1 and P2 have the highest transpiration rate at the beginning of the period, transpiration of P3 is highest at the end. The phenotypes with deeper root system allocation behaved similarly, with the phenotype P3 having a similar behaviour between days of the whole simulation period.

In the scenario with wetter top soil layer (SWtop, Fig. 10.4-B), it is observed that the two phenotypes P1 and P2 behave similarly while the phenotype P3 suffers from a more drastic transpiration decrease.

Figure 10.5 shows the change of the equivalent soil water potential $\Psi_{t,eq}$ with increasing water extraction from soil between the beginning and the end of the period, expressing the global moisture deficit that builds up at the root-soil interface. Logically, we see that $\Psi_{t,eq}$ has a decreasing trend with time and cumulated uptake. During the night however, $\Psi_{t,eq}$ gets less negative, as the system relaxes: water potential

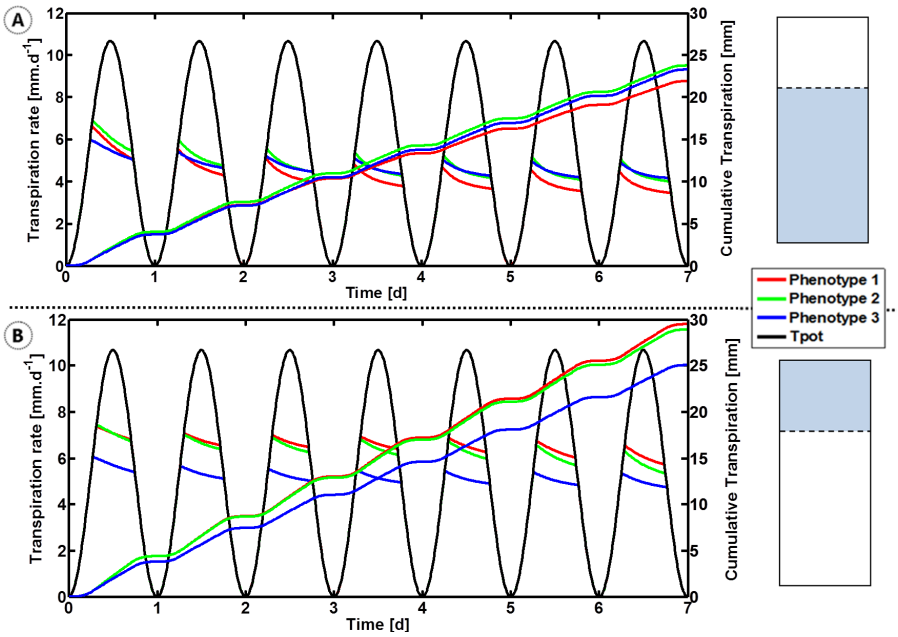


Figure 10.4: Average actual and cumulative transpiration of the three phenotypes in SWbot (A) and SWtop (B) scenarios. Red: Phenotype 1; green: Phenotype 2 and Blue: Phenotype 3. The potential transpiration is represented by the black solid line.

gradients built up during day around the root segments decreases as the uptake is reduced and soil water redistribution occurs.

In the SWbot case (continuous lines), all phenotypes experience a lower soil water potential (and a lower total transpiration) than in the SWtop scenario. However, in SWbot the phenotype P3 is most efficient, as it transpires almost the same amount of water as P2 and experiences higher (less negative) soil water potential. Thus, it could be expected that P3 would be able to sustain a higher transpiration compared to P2 over a longer period of stress as it can access water more easily at depth. In the case where the water is in the upper layer (dashed lines), P1 has always a higher (less negative) total equivalent water potential than P2 and P3 for a similar given amount of cumulated transpiration. As can be expected, the deep rooted phenotype P3 (continuous blue line) not only transpires less (i.e. experiences a more severe stress) but also undergoes a lower (more negative) total equivalent water potential.

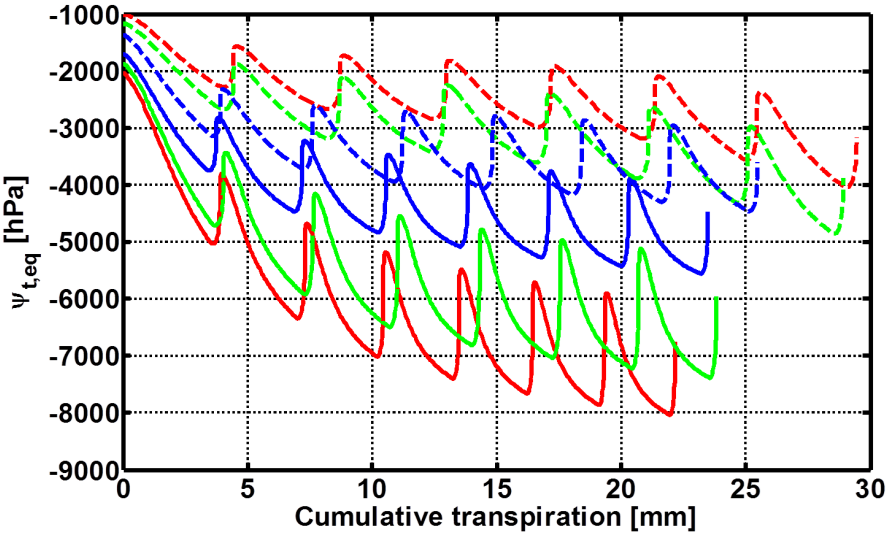


Figure 10.5: Equivalent total soil water pressure as a function of the cumulative transpiration for SWbot (solid lines) and SWtop (dashed lines). Red: P1, Green: P2 and Blue: P3.

However, as already observed for the transpiration dynamics, P3 has a relatively similar behaviour between SWbot and SWtop cases.

Figure 10.6-A and 10.6-B show the averaged sink term profiles of the three phenotypes at two different times (t=0.5 and 6.5 d) and under variable hydrological conditions. Fig. 10.6-D shows the root length density profile of the three phenotypes: P1 has more roots at the top, P3 deeper rooting distribution and P2 an intermediate distribution. When the water is in the bottom layer (SWbot scenario, Fig. 10.6-A), all plant phenotypes decrease their water uptake in the upper layer after 6.5 d while remaining stable in the bottom layer (Fig. 10.6-A: dashed and continuous lines overlap in the bottom layer). Although the water content in the upper layer is low in this scenario, the three phenotypes are able to extract it at the beginning of the period, as they have a lot of roots there. The phenotype P3 has more ability to extract the soil water from deeper layer below 80 cm from the beginning of the period on. On the opposite, phenotype P1 extracts soil water less deep and

suffers from stronger stress (see Fig. 10.5).

When water is located in the upper layer, P1 and P2 are able to take up more water from that horizon as compared to P3 (Fig. 10.6-B). As P3 cannot compensate this lower uptake in the upper horizon by a much higher uptake in the drier bottom horizon, it suffers from earlier stress.

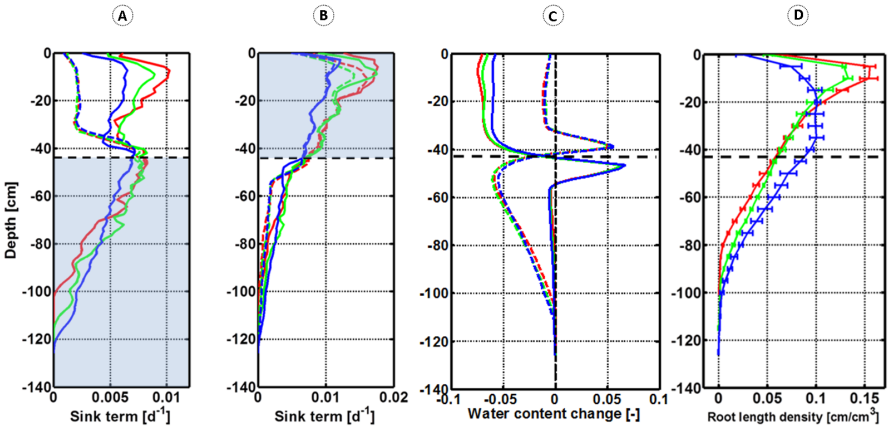


Figure 10.6: 1D Sink term profile under scenario SWbot (A) and SWtop (B) after 0.5 (solid lines) and 6.5 (dashed lines) days and corresponding water changes (C) and root length densities (D). Red: P1, Green: P2 and Blue: P3.

Figure 10.6-C shows the water changes over the whole simulation period for case SWbot (continuous lines) and SWtop (dashed lines). Although the sink terms are very different between phenotypes, this is not reflected in the soil water content changes. Indeed water content changes not only in function of the sink term S but also due to the water pressure distribution in the soil which generate water flow. This is particularly clear near the interface between the wet and dry zones, where water changes occur due to water and thus matric potential differences.

When we compare the sink to the root length density profiles (Fig. 10.6-D), we hardly see any direct correspondences for any phenotypes. This is due to the fact that water is preferentially extracted where the water is available. In addition, the root length density profile only partially reflects the distribution of the root ability to extract water.

The hydraulic architecture i.e. how the root ability to extract water is distributed into the soil, combined with the water availability control the uptake (Javaux et al. 2013).

To summarize, we observed that (1) P1 which has more roots in the upper layer is very efficient in the SWtop case, but has low ability to deal with a drier upper layer; (2) P3, which has more deeper roots outperforms for SWbot; (3) P2 transpires as much as P1 for SWtop and as much as P3 for SWtop. However, its equivalent soil water potential is always more negative than the two other phenotypes.

10.3.2 Influence of root hydraulic properties

It was shown in section 10.3.1. that root architecture determines the extraction pattern. In this section, we investigate how distinct root hydraulic properties influence water extraction and stress onset. By increasing the radial local conductance of the laterals (H case) and comparing the performance of the 3 genotypes as compared to their initial conductance values (R case), we can assess the impact of the hydraulic properties on root water uptake.

The root equivalent conductance K_{rs} (see Eq. 10.7) is a key parameter which characterizes the hydraulic architecture, i.e the impact of the root system architecture and of the distribution of the root segment hydraulic properties. As the local hydraulic properties depend to the root order (main or lateral) and to the age of the root segments (see Table 10.2 and Fig. 10.2-D), each phenotype has a different K_{rs} . Values of the mean plant equivalent conductance K_{rs} for the six cases are given in Table 10.2. Phenotypes P1 and P2 typically have a relatively similar K_{rs}, as they have a similar proportion of root segment age and order. We observe the following ranking: K_{rs} (P3R) < K_{rs} (P1R) < K_{rs} (P2R) < K_{rs} (P3H) < K_{rs} (P2H) < K_{rs} (P1H). Multiplying the radial conductivity of the laterals by 10 increases the K_{rs} by a factor 2.8, 2.7 and 1.8 for P1, P2 and P3, respectively.

The change of water content is visualized in the supplementary material Video S2 for the higher conductance (P1H, P2H and P3H) and the SWBot scenario. As compared to P1R, P2R and P3R (see video S1), the extraction patterns are reinforced. Table 10.4 shows the amount of transpiration after 7 days for the two hydrological regimes, the three

phenotypes and the two K_{rs}. Higher K_{rs} always increases the amount of extracted water. Under the SWtop scenario, we do not observe any stress (100% of the Tpot is extracted) for P1H and P2H, while P3H suffers from a slight stress. For SWtop, the different root system architectures generate a difference actual transpiration difference of 12% between phenotypes. By increasing the conductance of the laterals, there is almost no more impact of the root system architecture. For SWBot, stress still occurs for all phenotypes with higher K_{rs}. However, differences between root architecture generate only 5 to 8% difference of actual transpiration while a difference in K_{rs} increases the actual transpiration by 20 to 30%.

Table 10.4: Cumulative transpiration [mm] (percentage of the total potential transpiration) effectively transpired after seven days for each scenario.

	P1		P2		P3	
	R	H	R	H	R	H
SWtop	29.5(79.1)	37.3(100)	28.9(77.5)	37.3(100)	25.2(67.5)	36(96.5)
SWbot	21.9(58.7)	32.5(87.1)	23.8(63.8)	34.6(92.7)	23.3(62.5)	29.7(79.6)

In the following, we focus on the scenario with predominant subsoil water dependence SWbot, and on the two root phenotypes P2 and P3 with adapted root distribution for such hydrological conditions.

Figure 10.7 compares the transpiration dynamics of P2 and P3 with reference and increased root radial conductivities for a 10 days period. When the local radial conductivity of a plant root is increased, its capacity to extract water is improved (i.e. K_{rs} increases and roots pose less resistance to water uptake and movement inside the root system), and thus transpiration is higher for a given potential difference between soil and root (see Eq. 10.7). We observe that the ranking of cumulative transpiration over 10 days follows the ranking of the K_{rs} explained here before.

While the two phenotypes behave rather similar in the SWbot scenario when the reference hydraulic properties are used (denoted a P2R and P3R), there is a more distinct differentiation when considering an increased K_{rs} (denoted as P2H and P3H). Indeed, P2H is superior in transpiration compared to P3H over the 10 days of simulation. Still P2H also shows a stronger decrease in transpiration rate compared to

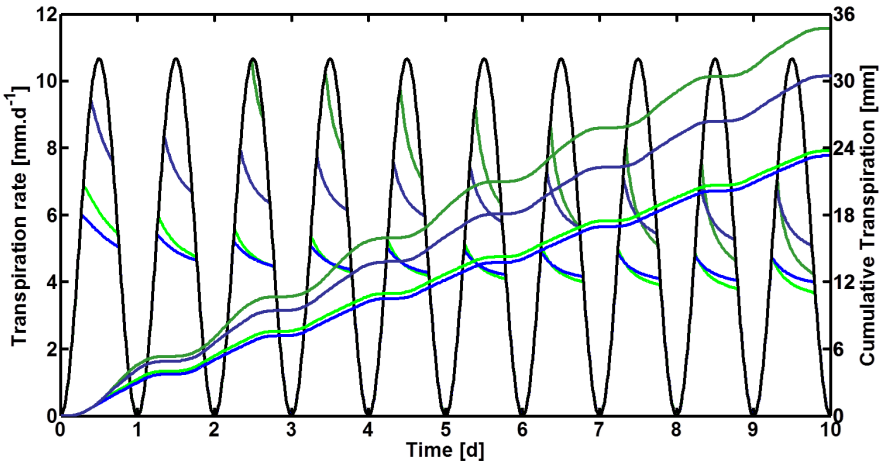


Figure 10.7: Actual and cumulative transpiration changes for P2 with reference (light green, P2R) and increased (dark green, P2H) root radial conductivity and P3 with reference (light blue, P3R) and increased (dark blue, P3H) root radial conductivity for the SWbot scenario. The black solid line is the potential transpiration.

P3H, which would result in higher stress over prolonged dry periods. Indeed, after 10 days, P3H gets a higher daily transpiration rate than P2H. In general, whatever its K_{rs} , P3 remains more stable over the simulation period, and always has a higher transpiration rate than P2 at the end of the simulation period.

Figure 10.8 gives another perspective on the comparison between both phenotypes. It shows the instantaneous stress fraction (T_{act}/T_{pot}) as a function of the fraction of the water extracted from the soil (called hereafter soil water depletion D) defined as:

$$D(t) = 100\frac{\theta_{ini} - \theta(t)}{\theta_{ini} - \theta_r} \tag{10.8}$$

With θ_{ini} , θ_r, $\theta(t)$, the initial, residual and at time t water content of the soil, respectively. The instantaneous stress fraction reflects the reduction in transpiration and thus, the stomatal closure at a given momenttime t. A plant with higher stress fraction keeps its stomata open so that carbon acquisition is not decreased and thus suffers less from water shortage. In Fig. 10.8, we observe that the water depletion

is higher for phenotypes with higher root conductance K_{rs}. We also see that for a given amount of extracted water, the high K_{rs} phenotypes (P2H and P3H) experience less stress. It clearly illustrates that the water availability for plants is not only a question of soil type but also of root conductance. P2H for instance is able to extract the potential transpiration rate at the beginning of the period without reduction, due to its high K_{rs}. If we compare this with Fig. 10.7, we see that P2H is able to extract more water over first part of the simulation period and thus has a stronger trend to deplete available water. P3H on the contrary has a sustained water extraction over longer times. At the end of the periods P3 phenotypes have always higher cumulated water extracted with a higher water potential than P2 phenotypes, i.e. a better resistance to prolonged drought period.

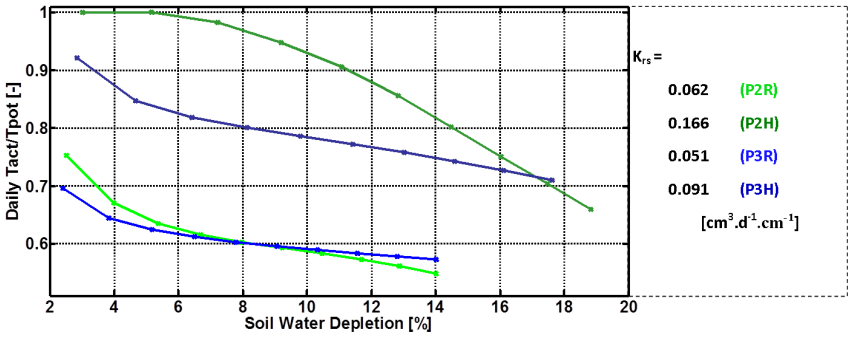


Figure 10.8: Reduction of the actual to potential transpiration ratio for a ten days long simulation as a function of the soil water depletion in the soil (in %). Blues lines are for P3 and green lines for P2. Dark colours stand for root systems with an increased radial conductivity and light colours for reference lateral conductivities, both are for the SWtop scenario. The initial classification of the root systems is determined by the value of the root equivalent conductance (recalled on the right).

This corresponds to two different strategies for the considered period: P2H takes as much water as possible at the beginning but reduces more strongly its transpiration stream, while P3H has a more conservative behaviour, keeping a constant transpiration rate with time.

10.4 Discussion

Agriculture has to achieve a more efficient use of water to cope with future needs of food production and competition between different fresh water users (FAO 2009). This can be achieved by reducing losses via soil management change (e.g. mulch coverage) and more efficient water acquisition by improved crops (e.g. (Passioura 1977)). Root architecture and functioning are key crop traits in rain-fed cropping systems where yield depends on optimum use of site-specific water availability during the growing season.

Strategies for optimizing agricultural water management first of all depend on the site specific hydrology. Yield levels in rain-fed cropping system from Mediterranean and semi-arid tropical climates largely rely on stored soil water from off-season rainfalls (e.g. (French and Schultz 1984)). In these cropping environments part of the later (generative) development stages coincide with the onset of the dry season. Thus stress sensitive processes such as flowering and grain filling are strongly related to the use of previously stored subsoil water (Kirkegaard et al. 2007). In most crops water shortage during the reproductive stage, particularly when flowering, is most detrimental for yield (Farooq et al. 2009).

Effective drought resistance strategies of crops differ between seasonal and intermittent water stress. Seasonal drought during (late) reproductive growth is most effectively mitigated by drought escape (early maturity; e.g. (Thomson and Siddique 1997)) as well as water saving during the vegetative stages to improve water availability (Mori and Inagaki 2012). Richards and Passioura (1989) demonstrated that reducing seminal root axial conductions conserves deep water resources for grain filling. This is in agreement with our simulation results showing reduced axial conductance provides a sustained water uptake over longer periods. However the precondition for successful water saving is an effective later uptake to avoid unutilized deep water after harvest. Kirkegaard et al. (2007) and Lilley and Kirkegaard (2011) quantified the value of available soil water in the subsoil for yield (i.e. additional yield per mm subsoil water use) and showed that its efficiency depends on management strategies that defer water use from early in the season to late in the season so that the crop uses subsoil water during grain

filling.

Historic advance in breeding has largely optimized the aboveground stature of crop plants as well as their radiation use (Araus et al. 2008). It is recognized that superior root water uptake can be a crucial trait explaining superior yield of drought resistant cultivars, e.g. contributing to (flag) leave duration, optimum pollination and grain filling (e.g. (Borrell et al. 2001)). Taking into account the existing variability in root traits in different crops (e.g. chickpea, rice, durum wheat), it can be expected that improvement of root water uptake is a feasible agronomic option. Manschadi et al. (2008) demonstrated diversity of wheat seedling root architecture. Based on field evidence and simulations studies using APSIM, they suggested that selection for growth angle and number of seminal roots may help to identify genotypes with a root system that is better adapted to drought conditions. In climates where crops depend on stored subsoil soil water, narrow growth angle and larger numbers of seminal roots are beneficial, in climates with regular in-season rainfall, less narrow growth angles with shallower root system provide better adaptation.

Two main challenges to breeding for efficient root systems so far are (i) selection of an appropriate root target trait, and (ii) ensuring that this trait effectively conveys improved crop water supply. Vadez et al. (2008) demonstrated that structural knowledge of root systems alone is not sufficient to understand different water uptake capacity among chickpea cultivars. Our study clearly sustains this empirical observation: Although although there is a relation between the distribution of water availability and root axes allocation in the soil profile, root functionality as expressed by xylem conductance appeared as key variable to infer superior water uptake of a given phenotype. A main finding of our study is that root length density distribution alone is not sufficient to describe root water uptake from soil. We demonstrate this based on the root systems of three different phenotypes of maize. Root systems consist of dynamic populations of roots of different types and age, with age dependent root axial conductances and radial conductivities (Draye et al. 2010). As in Doussan et al. (1998a) our model is based on combining root architectural, root system hydraulic and soil hydraulic properties including the possibility of compensation and redistribution. Our results also clearly demonstrate that root architectural traits stricto sensu are

not sufficient to explain water uptake from soil by plant roots, but root architecture and related age distribution of root segments is important for overall conductance. While Doussan et al. (2006) where interested in the water uptake front in a short-term experiment of 11.5 hours, our aim was to quantify the water stress tolerance of different maize phenotypes during a one-week period of stress at anthesis.

Within the dehydration avoidance type of drought resistance strategies, Levitt et al. (1972) distinguished between water savers and water spenders. Our study showed that root traits can confer both, water saving and water spending. The P3 root phenotype was a water saver. Concerning root system architecture (distribution) P3 had comparatively highest allocation of the sink to deeper layers and comparatively less sink strength in upper layers (Fig. 10.6). Whenever upper layers contributed essentially to water supply, P3 thus had lowest transpiration. However with increasing depletion P3 could sustain uptake from deeper parts of the profile over longer times (Figs. 10.7 and 10.8). The prolonged uptake from the deeper layer is related to the lower sink strength leading to a less intense depletion. The other phenotypes had a more water spending behaviour with quick initial depletion and stronger decrease of transpiration over time. For overall crop performance the importance of high short term water extraction vs. low sustained uptake depends on the drought scenario. If only intermittent dry spells have to be buffered, a water spending "depletion root phenotype" is more efficient as such a behaviour will keep stomata more open. In case of longer dry periods however a root phenotype conferring water saving will improve crop water supply. Here we do not consider potential competitive effects between plant water uptake and transpiration losses from upper layers. Generally water saving is only effective for stored soil moisture in deeper layers not prone to evaporation losses.

Traditionally, water uptake simulation mainly considered root distribution, with more recent architecture models giving a better insight into the 3D structure of root systems (Draye et al. 2010). More recently a focus was on integrating root functionality into architecture models. While some cropping system models like APSIM (Keating et al. 2003) used an empirical parameter for functionality, more mechanistic approaches strive to consider root hydraulic architecture as such (e.g. (Sperry et al. 1998)). Our results showed that differentiation between

phenotypes P2 and P3 became more evident when considering root conductance. Under a high conductance scenario, P2 showed a substantial increase in initial water uptake with values near the potential transpiration, followed by a quick decrease. Thus the water spending behaviour was accentuated. For P3 there was also an increase in the transpiration level, still the extent was less compared to P2 and this rooting phenotype maintained a more stable transpiration level even at higher root hydraulic conductance. The stronger differentiation between P2 and P3 in the high conductance scenario was due to the age dependence of this root functional trait. As P3 contained younger root segments in deeper layers with still lower axial conductance, the bulk increase in root conductance (K_{rs} cf. Table 10.2) is less important. This is in line with the findings on the role of root conductance for transpiration resumed by Comas et al. (2013) who stated that generally highly conductive large diameter xylem vessels are related to high levels of (unstressed) transpiration, while lower diameter vessels induce water saving.

The differentiation between P2 and P3 at the high conductance scenario also indicates that still there was significant uptake capacity from the upper soil compartment. The substantially higher initial transpiration of P2 was mainly a result of enhanced uptake for upper layer. As revealed by the sink distribution (Fig. 10.6), the higher root length density in the upper compartment resulted in substantial proportion of water extracted for the upper part of the profile particularly during the first days. The sink distribution reveals that with the advance of depletion over time, upper layer extraction was increasingly "source limited", while towards lower layers sink strength was limited by the lower rooting density, i.e. it was more "sink limited". The sink strength in the upper compartment was further increased in the high conductance scenario, leading to an efficient and quick exploitation of extractable water resources (not shown). In the lower layers sink strength was not only limited by root distribution but further decreased in proportion to the upper layer by the lower conductance of young segments. Following Fitter's terminology (Fitter et al. 1991), root system architecture thus determines the overall exploration capacity of the soil profile via synchronization of water availability and depth distribution of root segments (source-sink synchronization), while root functionality (conductance) is essential for the exploitation dynamics in a given layer, supporting the

spending vs. saving behaviour.

In order to sustain yield under drought conditions, breeders need to blend together all knowledge on drought tolerance-related traits and their phenotypic expression (Cattivelli et al. 2008). It remains difficult to assess the overall effect of traits contributing to drought tolerance, because several traits can play roles, and these traits are likely to interact with one another and with the environment. These effects can be integrated in cropping system models such as APSIM. There are several simulation studies that quantify the effect of modified root traits on crop yield (Manschadi et al. 2006). Using APSIM-Wheat Lilley and Kirkegaard (2011) showed that in simulations across 109 years, 5 soils, 6 management options and 6 combinations of (virtual) wheat root modifications of root system traits could result in more yield gain in dryland cropping regions. The root traits that were modified were: rate of downward root penetration, efficiency of water extraction from the subsoil, an APSIM parameter for the effects of root length density, soil diffusivity and root-soil contact on the rate of water extraction. In our simulations we investigate a smaller part of the system in more details: the soil and root architecture hydraulic system.

10.5 Conclusion

We simulated two contrasting hydraulic regimes to analyse the performance of root phenotypes with surface near root allocation (P1) vs. steeper root allocation (P2 and P3), where P2 and P3 correspond to "deep and steep" phenotypes with high lateral growth for P3. As expected, superiority of a given root architecture was dependent on the water regime. For the soil conditions used here, our simulations showed that a deep and steep phenotype is beneficial only in situations where crop water supply depends on subsoil moisture while surface-near allocation of roots is more preferential when crops can rely on high in-season rainfall. This corresponds to findings from vegetation ecology and ecohydrology (e.g. (Schenk and Jackson 2002)). Although the root systems of the three virtual phenotypes considered in this study have the same volume, they behave quite differently in terms of water uptake from soil. In general, the same amount of carbon spent can create different root

system architectures with different hydraulic properties that will affect overall water uptake behaviour.

In particular, the root length density profile is not sufficient to characterize root system water uptake efficiency. In this simulation case study we kept the overall amount of carbon spent constant and compared the effect when the carbon was spent into more or less "deep and steep" root system architectures. This results however in the fact that we did not model the "cheap" aspect of the ideotype of Lynch (2013), which could also affect the conclusions of this study regarding root system water uptake efficiency.

Regarding the hydrological conditions, phenotype P3 that had fewer and longer laterals was better in a situation that can be found in climates with a dry summer and high importance of subsoil water: it has a more conservative behaviour on a longer term. For plants with comparable rooting depth, the overall root system conductance K_{rs} is a key parameter to explain transpiration dynamics. The plant root systems we created were generic. We demonstrated how root architecture and hydraulic properties can induce different behaviour, also as a function of the environment considered, and thus one should be careful while designing an ideotype based on root architectural traits alone. Beyond the root architecture itself, the age distribution and related root hydraulic properties need to be considered.

USE OF MARSHAL TO DEFINE NOVEL MAIZE ROOT SYSTEM ECO-IDEOTYPES

11

This chapter is a modified version of a conference paper published as:

> • Meunier F., Couvreur V., Draye X., Vanderborght J. and Javaux M. A new model for optimizing the water acquisition of root hydraulic architectures over full crop cycles, Proceedings of the FSPMA conference 2016

Abstract

The concept of ideotypes (plant with ideal traits that is expected to yield a greater quantity or quality of product when developed as a cultivar) opens new avenues for breeding as shown by the results of plant model simulations. However currently root system ideotypes lack quantitative traits and moreover cannot perform optimally in every single environment. We present here a physically-based model of the water flow in the soil-plant-atmosphere continuum working at the plant scale capable of efficiently simulating the root water uptake of growing crops over full crop cycles as well as other environmental flow (rain, irrigation, evapotranspiration). It is adapted to discriminate genotypes/ideotypes performance in any environment. It was first validated using field trials: cumulative transpirations predicted by the models were correlated with observed yield in contrasted pedo-climatic situations.

In a simulation study we analyze the ability of maize root systems to maintain their transpiration under different management practices and in different environments. We showed that local root traits reveal contrasted impacts on flowering transpiration while plant-scale parameters were efficient indicators of plant performances.

11.1 Introduction

Several organ, tissue and cellular level traits have been associated with increased productivity under drought. Xylem conductance, root length or root diameter have been proposed as target traits for breeders (Wasson et al. 2012). All these RS traits have in common that they will either impact the root system structure (root length, root angle) or the root hydraulic function (aquaporin activity, apoplastic barriers). In this context many authors (see for example Lynch (2013) for maize or Wasson et al. (2012) for wheat) suggested root system ideotypes. An ideotype was first defined by Donald as a plant model expected to yield a greater quantity or quality of product when developed as a cultivar (Donald 1968). Yet, the concept of ideotype itself is critized for several reasons. First, it is recognized that a root system ideotype can not perform optimally under all environmental conditions (Tardieu 2012). Ideotypes should also be defined as dynamic property. In addtion how to define "plant ability to extract water" and how root phene states impact is currently impossible.

Therefore the concept of ideotype needs to be revisited and there is an urgent need to define what plant ability to extract water means. Here we propose to define differently plant behavior in a given environment, plant strategies, plant parameters and group of root phene states. We propose to call a strategy a idealized plant hydraulic and foreage behavior. Basically different strategies can be defined : dispensive *vs* water saving, deep *vs* shallow or spread *vs* narrow root systems. Most ideotypes have been defined to be dispensive and deep (Lynch 2013; Wasson et al. 2012). However other strategies might be optimal under different environments. The plant-scale parameters (alternatively called macroscopic) are macroscopic variables arising from the integration of the root system hydraulic architecture. They can be purely architectural (root system volume or convex hull) or combine hydraulics and architecture (root system conductances and depth of standard uptake fraction). At any time, the macroscopic parameters are determined by an ensemble of phene states or local root (hydraulic and architectural) properties such as root radial conductivity distribution or elongation rate.

Establishing relations between root local properties and plant per-

formance would allow breeders to quantify how local properties may improve plant scale uptake potentials or physiologists to define quantitative (and not only qualitative) optimal plant root traits for given environmental conditions. To be able to link specific combinations of plant phene states to eco-ideotypes, several methodological and theoretical gaps need to be overcome: (1) the link between structural and functional properties is not always known at the local scale; (2) functional and structural traits are hard to characterize in real conditions and (3) a general framework to combine structural and functional traits at the plant scale is still missing.

Recently, Couvreur et al. (2012) developed a physically-based plant-scale model for characterizing plant ability to extract water (Tardieu 2012). In this approach, RS hydraulic architecture is characterized via two macroscopic parameters: the global hydraulic conductance of the root system and the relative distribution of water uptake under uniform soil water potential. These two plant-scale parameters define how easily water flows through a root system and the spatial extent of the uptake, and could be used as structural-functional hydraulic RS. Moreover, Meunier et al. (2017) have developed process-based analytical solutions to predict these macroscopic parameters from local phene states (see Chapter 4 and 5). Yet, these characteristics do not assess whether a given RS is optimal under a certain environment, which can only be evaluated taking into account the environmental constraints (evaporative demand, rainfall, soil properties, etc.) and the crop management practices (irrigation volume and time, sowing date, etc.).

The objective of this paper is to provide a novel methodology to develop eco-ideotypes. We first present a series of modelling tools that we intend to validate against real data. In a second stage we use the validated model to investigate the links between local phenes, strategies and behaviors under contrasted pedoclimatic conditions. Through this paper we thus investigate *in silico* how root structural and/or hydraulic phene states impact plant stress or improve their ability to maximize transpiration with a process-based model, after validation of the latter with field trials. Best root water uptake strategies adapted to environment should arise from such an analysis.

Hereafter we define a phenotype as a combination of architectural and hydraulic local root phene states and a species as a specific set of

such possible combinations. Among a species thus, there is a genetic variation of a series of local traits which leads to different macroscopic parameters, behaviors and performances. We identify potentially useful traits and generate virtual phenotypes of the considered species. In a preliminary stage, we compare the phenotypes macroscopic parameters and their field performances with 3D simulations of water flow in the soil-plant-atmosphere continuum considering root growth and development under different management practices, soil and climate conditions. This procedure takes us one step forward in disentangling the relation between drought traits, environment, and crop performances.

This paper is divided in four sections: the model description, the simulation study details used to illustrate the model potential and validation, a presentation of the main outputs of the model simulations and a discussion of the simulation study results and the model.

11.2 Water flow model

The soil water flow in a vegetated soil can be described using the Richards equation (Couvreur et al. 2012) including a three-dimensional volumetric sink term S [$L^3L^{-3}T^{-1}$] for root water uptake:

$$\frac{\partial \theta}{\partial t} = \nabla . (K \nabla \Psi) - S \tag{11.1}$$

where θ [L^3L^{-3}] is the volumetric water content, t [T] is time, K [$L^2P^{-1}T^{-1}$] is the unsaturated hydraulic conductivity tensor, and Ψ [P] is the total soil water potential. To describe the sink term of this equation, we follow the process-based model of Couvreur et al. for isohydric plants (Couvreur et al. 2012, 2014a). At the root segment scale, it has been demonstrated that root water uptake is the sum of two processes: the water uptake in homogeneous conditions and the compensatory uptake due to heterogeneous soil water potential:

$$J_{r,i} = (T_{act} + K_{rs} (\Psi_{sr,i} - \Psi_{rs,eq})) SUF_i \tag{11.2}$$

where $J_{r,i}$ [L^3T^{-1}] is the radial water flow entering (if positive) or leaving (if negative) the root segment i, T_{act} [L^3LT^{-1}] the actual transpiration rate, K_{rs} [$L^3P^{-1}T^{-1}$] the root system conductance (= first macroscopic parameter), SUF_i [-] the Standard Uptake Fraction of segment i (= second macroscopic parameter), $\Psi_{sr,i}$ [P] the potential at the root-soil interface of this segment and a weighted root-soil interface potential. The first macroscopic parameter is defined as the transpiration rate of a root system per unit of water potential difference between the root collar and the soil potential in homogeneous conditions. The second macroscopic parameter is the fraction of the transpiration taken up by the considered segment in homogeneous soil conditions. It is also an intrinsic property of the phenotype and does not depend on the environment (the soil-type for example). This Standard Uptake Fraction is also used to weight the root-soil interface potentials and define the equivalent soil water potential sensed by the plant:

$$\Psi_{rs,eq} = \sum_i SUF_j \Psi_{rs,j}$$

It is worth noting that Equation 11.2 is Equation 7 in Couvreur et al. (2012) where we assumed $K_{comp} = K_{rs}$ with K_{comp} [$L^3P^{-1}T^{-1}$] the root system compensatory water uptake conductance, which is a reasonable hypothesis according to Couvreur et al. (2014b). Just as in Couvreur et al. (2014a), the actual transpiration is the minimum value between the water demand (set by the atmospheric conditions and the leaf area) and water supply (maximum flow rate made available by the soil-root system), see (Denmead and Shaw 1962). The former is calculated using a Penman-Monteith-like equation under the form of a potential transpiration T_{pot} [L^3T^{-1}] and the latter is the maximal water flow brought to the leaves by the root system without exceeding (in absolute value) a minimal collar potential Ψ_{lim} [P] (as we assume a isohydric behavior). The actual transpiration is then given by:

$$T_{act} = min\left(T_{pot}, K_{rs}\left(\Psi_{rs,eq} - \Psi_{lim}\right)\right) \tag{11.3}$$

This transpiration rate is inserted in the stress function of Couvreur et al. to obtain the root collar potential Ψ_{collar} [P] (Couvreur et al. 2012):

$$\Psi_{collar} = \Psi_{rs,eq} - \frac{T_{act}}{K_{rs}} \tag{11.4}$$

Combining 11.2 and 11.3, we obtain the local water flow under water stress condition ($\Psi_{collar} = \Psi_{lim}$) or when no stress is felt by the plant ($\Psi_{collar} \geqslant \Psi_{lim}$):

$$J_{r,i} = \begin{cases} K_{rs}\left(\Psi_{rs,i} - \Psi_{collar}\right) SUF_i, & \Psi_{collar} = \Psi_{lim} \\ \left(T_{pot} + K_{rs}\left(\Psi_{sr,i} - \Psi_{rs,eq}\right)\right) SUF_i, & \Psi_{collar} \geqslant \Psi_{lim} \end{cases} \tag{11.5}$$

Equations 11.5 allow calculation of the water flow in the whole root system and consequently deriving the sink term in the k^{th} soil element S_k [$L^3L^{-3}T^{-1}$]:

$$S_k = \frac{1}{V_k} \sum_i \epsilon_{ik} J_{r,i} \tag{11.6}$$

where V_k [L^3] is the volume of this element and ϵ_{ik} [-] is a factor which is 1 when the k^{th} soil element contains the i^{th} root segment and else 0. The sum is over all root segments i. These equations are encoded in

R-SWMS (Root-Soil Water Movement and Solute transfer, (Javaux et al. 2008)) where they are solved numerically using an iterative scheme between the soil and the root modules for each time step. The root-soil water interface potential is defined as the mean potential of the soil node potential surrounding the root. The macroscopic parameters SUF_i and K_{rs} depend on the root system hydraulic architecture and the hydraulic properties of the root segments (root radial and axial hydraulic conductivities). The root architecture and the hydraulic properties and hence the macroscopic root parameters vary with time as the root grows and develops. The macroscopic parameters are calculated using the hydraulic-tree approach of Doussan et al. (1998a).

Water stress impact on root growth is modelled using a constant water use efficiency coefficient, the cumulative water transpiration, the root system volume and the root carbon cost (Drouet and Pagès 2003). To do so, the actual root growth decreases (as compared to the potential one) everywhere in the root system when the plant is experiencing stress due to limited carbon assimilation.

11.3 Material and Methods

11.3.1 Plant water uptake and performance

To understand the plant water uptake location and performance, we propose several indices reflecting its behavior. We define the actual mean depth of the root water uptake z_{Sink} [L] as the sink-weighted depth:

$$z_{Sink} = \frac{\sum_k S_k z_k}{\sum_k S_k} \tag{11.7}$$

where z_k [L] is the mean z-position of the soil element k and the sum is over all soil elements. It is worth noting that z_{Sink} differs from z_{SUF} because of soil heterogeneity.

The Δt-averaged average potential sensed by the plant $\Psi_{rs,eq}$ [P] is

the temporal mean of the equivalent potential over Δt [T]:

$$\overline{\Psi}_{rs,eq}(t) = \frac{1}{\Delta t} \int_{t-\frac{\Delta t}{2}}^{t+\frac{\Delta t}{2}} \Psi_{rs,eq}(t')dt' \tag{11.8}$$

It can be used to understand what is the mean root-soil water potential felt by the plant during the last 24 hours for example when the period is fixed to one day. The cumulative transpiration T_{cum} [L^3] is simply the integral of the instantaneous transpiration:

$$T_{cum}(t) = \int_0^t T_{act}(t')dt' \tag{11.9}$$

which is strongly correlated to plant yield (Leitner et al. 2014).

Finally, the Δt-averaged transpiration $\overline{T}_{\Delta t}$ [L^3] is defined as the integral value of the actual transpiration over Δt around time t:

$$\overline{T}_{\Delta t}(t) = \frac{1}{\Delta t} \int_{t-\frac{\Delta t}{2}}^{t+\frac{\Delta t}{2}} T_{act}(t')dt' \tag{11.10}$$

The root system volume V_{rs} [L^3], used as a proxy of the carbon spent in the root system, is calculated by summing up all the root volumes, mathematically:

$$V_{rs}(t) = \sum_{i=1}^{N_{order}} \sum_{j=1}^{N_i} \pi r_i^2 l_{ij}(t)$$

where N_{order} [$-$] is the number of root orders, N_i [$-$] is the number of roots of order i, r_i [L] is the root order i radius and l_{ij} [L] is the length of root j of order i. The soil volume explored by the root is calculated through the convex hull of the root system applied to the root tip locations.

11.3.2 Defining groups of phene states

Two sensitivity analyzes are used to investigate how root system properties are linked to plant-scale behavior. The first one focuses on root system local phenes, the second on plant-scale parameters. In order to take into account potential genotype by environment interaction,

we always took in consideration four conditions: two contrasted locations (France, Italy) and two treatments (drought, well-watered) for a reference year (2012).

Local phenes

Each phenotype is considered as a combination of local hydraulic and architectural phene states chosen in a range of natural inner-species variation. All important local phenes described in Chapter 5 were increased by 5% as compared to reference scenario (generated with MARSHAL) and the resulting root systems were modelled in four situations: well-watered and drought scenario in France and Italy fields over the full crop cycle until flowering.

3D Root system architectures were generated using MARSHAL parameterized for maize. The hydraulic macroscopic parameters of each phenotype were calculated using similar (in shape) local hydraulic conductivity functions to the ones obtained by Doussan et al. (1998b) for maize. The structural parameters which were varied were: the inter-branch distance d_{inter}, the radius r, initial elongation rate v_0, maximal length of lateral roots L_{max} and insertion angles θ of all root types. Considered root types were: primary and seminal, short and long laterals, crown and brace roots, as defined in Chapter 3.

The hydraulic parameters considered for genetic variations were the axial and the radial conductivity values of all root types as well as the transient ages for these properties. The hydraulic properties of root segments were considered to vary stepwise with root age (Doussan et al. 2006).

Macroscopic parameters

In an exploratory virtual experiment, 100 000 maize root systems were generated with randomly chosen parameters in ranges typically observed in the literature for the structural traits while one order of magnitude was chosen as limit for the hydraulic property values. As explained in Chapter 7, several orders of magnitude separate minimal and maximal conductivity values of all root orders and ages taken together (typically 3-4 orders of magnitude). But as mentioned by Draye et al. (2010) and

already discussed several times in this manuscript, the root conductivity values are also expected to vary around the mean observed value and one order of magnitude around the mean appears to be a reasonable choice according to measurements on different plant genotypes. This choice was thus dictated by typical variabilities observed in the hydraulic properties (Draye et al. 2010; Leitner et al. 2014). To limit the computational expense and for sake of clarity, the 100 000 root system were then grouped into categories according to their final macroscopic parameters: root system conductance (K_{rs}), root system volume V_{rs} [L^3], exploration volume (computed from the convex hull) of the root system $V_{convexhull}$ [L^3] and normalized depth of the water uptake in standard conditions (z_{SUF} [L]) defined as:

$$z_{SUF} = \sum_i SUF_i z_i \tag{11.11}$$

where z_i [L] is the z-position of the root segment i. The partition of root systems into categories was achieved using k-means algorithm and considering two levels for each macroscopic parameter (i.e. low and high). Sixteen groups resulted from the analysis. In each category a root system representative of the group was selected on the basis of its minimal distance to the center of mass $dist_{i,j}$, calculated as:

$$dist_{i,j} = \sqrt{\sum_{x=1}^{N} (x_i - x_j)^2} \tag{11.12}$$

where i and j designates two realizations and x the relative position in each macroscopic axis. Here, N = 4.

These four macroscopic parameters were chosen because they are key for describing root system water uptake. The root system conductance at any time represent the root system ability to sustain a particular transpiration under a given water potential between the soil and the leaves. It describes the water supply from the root system. Water-spending plant *vs* water saving plant can be discriminated based on this criterion. The depth of standard uptake describes how deep the root preferentially takes up its water under homogeneous soil conditions. Shallow *vs* deep preferential uptakes arise from the analysis of this

Table 11.1: Weather statistical data for the European sites. std = standard deviation

	$\mathbf{ET_0}$ [$\mathbf{mm\,d^{-1}}$]		**Precipitation [mm]**		**Irrigation [mm]**	
	mean	std	Total	std	Total	std
Nerac, France	2.7	1.9	145	51	170	65
Bologna, Italy	2.2	1.4	91	20	94	80
Martonvazar, Hungary	2.4	1.5	185	107	123	37

paramater. The convex hull characterizes the soil exploration by the root system and the potential water available by the root system. Finally the root system volume is chosen as proxy for the carbon spent in the roots and therefore represents the cost of such a root system. Together they form a macroscopic parametric space that is likely to represent plant water uptake strategy.

Environmental modelling

Field trials of a maize reference genotype (B73) in three contrasted locations (Italy, France and Hungary), for two water treatments (well-watered and drought) and for three consecutive years were used for environmental modelling. The weather conditions (air temperature, humidity, wind velocity) were monitored continuously from the sowing date until the plant harvesting for the three years and at the three different locations. Mean statistical data for the three sites are given in Table 11.1 for the duration of the simulation.

The soil properties were derived from undisturbed samples taken locally. The soil hydraulic parameters of the water retention curve were derived from simultaneous measurements of water potential and water content on undisturbed samples of 100 cm^3 sampled at three differents depths. The soil hydraulic conductivity curve parameters were fitted for each soil horizon using results of a MultiStep Outflow experiment on undisturbed soil samples of 1000 cm^3 at the same three differents depths. The soil hydraulic properties are summarized by soil horizon in Table 11.2. Limits of soil horizons were fixed at -30cm and -55cm in Nerac and Bologna and -25cm and -65cm in Martonvazar.

We used MARSHAL (see Chapter 5) to generate realistic maize root system hydraulic architectures. Three replicates were simulated in the contrasted pedo-climatic conditions with reference architectural

Table 11.2: Soil hydraulic properties by horizon for the European sites. Units are centimers and days:α [cm$^-$1] and k_S [cm.d^{-1}]

	Nerac, France					**Bologna, Italy**					**Martonvazar, Hungary**				
	θ_r	θ_s	α	n	k_S	θ_r	θ_s	α	n	k_S	θ_r	θ_s	α	n	k_S
Horizon 1	0.083	0.48	0.009	1.52	30	0.07	0.435	0.005	1.64	15.	0.0	0.4548	0.031	1.18	35
Horizon 2	0.082	0.47	0.009	1.52	25	0.07	0.437	0.005	1.64	14.7	0.02	0.40	0.029	1.21	45
Horizon 3	0.082	0.48	0.012	1.46	27	0.075	0.44	0.006	1.59	13	0.01	0.44	0.031	1.18	50

and hydraulic parameters.

Each category of plant was again subject to four combinations of management and environmental conditions. The environment was defined as a combination of evaporative demand and soil properties and the management practices by the sowing date and the irrigation treatment. Two environments and two management practices were considered in the simulation study. They correspond to two experimental fields of the DROPS project located in Nerac, France and in Bologna, Italy in well-watered conditions (= wet conditions) and under drought stress (= dry conditions). The potential evaporative demand was calculated according to Penmanth-Montheith equation based on temperature, wind velocity and relative humidity measurements. The simulated management practices (sowing date, irrigation timing and volumes) correspond to the actual ones performed on these fields.

The simulation duration was fixed to 80 days after sowing with uniform total potential as initial condition. We use free drainage bottom boundary conditions for a soil domain whose dimensions are: 75cm x 15cm x 126cm. A periodic domain was set to mimic crop field comportment and limit the computational requirements.

11.4 Results

11.4.1 Defining groups of phene states

In this section, we present the results of the sensitivity analyzes.

Local phenes

From the reference root system used for model validation in previous sections, all principal functional and structural parameters were increased by 5% and resulting cumulative transpiration changes are shown in Figure 11.1. The parameters are ranked according to their impact on the cumulative transpiration: the subscripts 1 to 5 refer to seminal (and primary), short lateral, long lateral, crown and brace roots, respectively. The color scale indicates the sign of the slope of the correlation between phene state and difference of transpiration, considering two sites (France and italy) in a drought scenario: dark red when the impact of increasing the parameters is consistently negative on cumulative transpiration, red when it is negative in one situation and neutral in the other, green when it is positive in one situation and neutral in the other and orange when the effect is contradictory in both conditions. Neutral is defined by a not-significant effect on the plant transpiration.

Only the parameters with a significant impact (e.g. significantly different from no transpiration change at $p = 0.05$) are plotted in Figure 11.1.

Defining eco-ideotypes

Out of the 100 000 generated root systems, sixteen different categories (= representative phenotypes) were finally selected on the basis of their different K_{rs}, z_{SUF}, V_{RS} and $V_{convexhull}$ using k-means partition. The final values of the macroscopic parameters of all generated root systems are presented in Fig. 11.2 coloured according to the category it belongs to. The figure presents two-dimensional cross-sections in the four-dimensional macroscopic parametric space. Similarly Table 11.3 summarizes the macroscopic parameters of the sixteen categories 60 days after sowing.

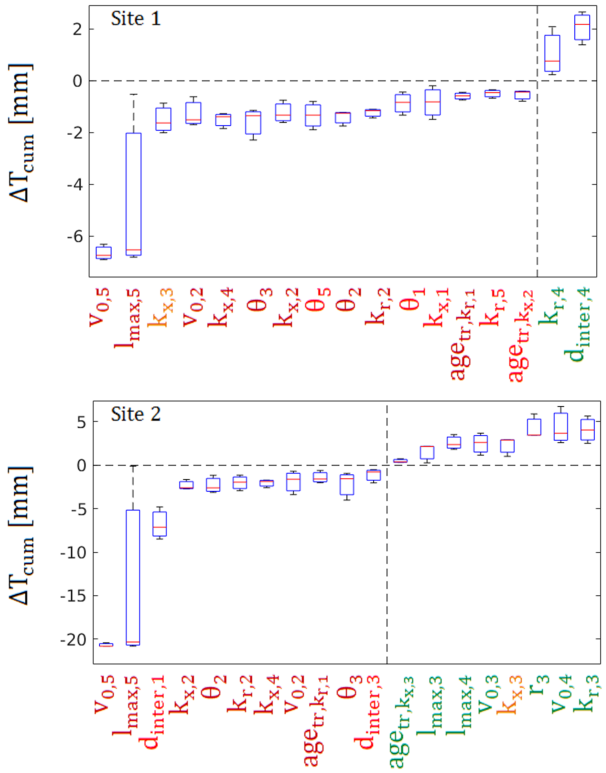


Figure 11.1: Local root phenes impact on the cumulative plant transpiration in two contrasted sites (drought scenario). Only significant phenes are shown. Colours correspond to the sign of correlation amongst the two sites between simulations: green = positive or neutral, red = negative or neutral, dark red = always negative, orange = positive or negative.

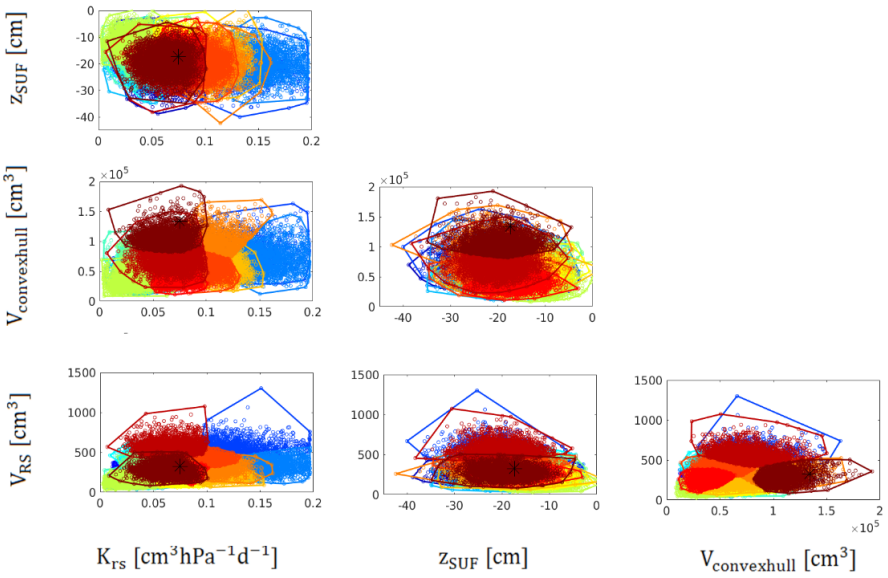


Figure 11.2: Macroscopic root system parameter parametric space and k-means partition of 100 000 simulated root systems. The black star is the reference root systtem hydraulic architecture generated by MARSHAL.

If we consider that the root system volume (= the sum of root volumes) is a proxy for the carbon spent in the roots, it can be directly seen from Fig. 11.2 that some root systems are much more efficient to increase their ability to take up water per gram of carbon invested in the root systems (the yellow dots for example).

Fig. 11.3 shows the cumulative transpiration24h around at any time and for the eleven phenotypes as calculated by 11.10 (normalized by the soil surface) with a period of one day for the two sites and the two treatments. The colors represent the same phenotypes as the ones used in the previous figures. The black lines are the day-averaged potential transpirations of the last day at any time and for each scenario: it is consequently the maximal potential transpiration.

In general, three stages can be highlighted in each case: the initial phase during which the root system cannot provide the water requested by the leaves due to the limited size of the root system, an intermediate stage when the demand is successfully met and the final stage where

Table 11.3: Macroscopic parameters of the different categories

Category	K_{rs} [$cm^3 hPa^{-1} d^{-1}$]	z_{SUF} [cm]	$V_{convexhull}$ [$10^4\,cm^3$]	V_{rs} [cm^3]	Color
1	0.06	-23	6.4	264	Dark blue
2	0.04	-14	4.6	288	⋮
3	0.13	-21	8.3	535	
4	0.15	-20	7.5	334	
5	0.05	-20	4.5	183	
6	0.05	-19	4.8	432	
7	0.04	-12	7.4	202	
8	0.06	-13	7.5	360	
9	0.04	-12	3.9	156	
10	0.07	-15	6.6	197	
11	0.11	-18	5.6	238	
12	0.11	-20	9.3	328	
13	0.09	-16	5.7	392	
14	0.07	-15	4.1	267	
15	0.07	-20	7.6	540	⋮
16	0.06	-20	10.3	283	Dark red

a drought potentially appears. The final stress appearance concerns all phenotypes for the drought conditions (top line) while only few reach this state under wet conditions (bottom line). When comparing treatments for the same site it clearly appears that the performance ranking greatly depends on the management practices. For example at the end of the simulation the cyan phenotype performs the best for the first site in dry conditions while it is the one to experience the water stress the most intense under irrigation treatment. This highlights the fact that a phenotype cannot perform ideally in all situations. Here again we demonstrate that the root phenotype greatly affects the plant performances under water limited conditions while the results are much more uniform when there is no water scarcity.

It is worth noting that the best phenotypes in terms of averaged transpiration after 80 days of simulation under dry conditions have surprisingly small root system conductance over the full crop cycles. On the contrary, the phenotypes with high conductances over the season perform the worst under these conditions. The former save water at the beginning of the crop season that will remain available in case of severe stress later. The latter consume all the available water at any time and rely on new inflow of water from rainfall events or irrigation to keep transpiring. Two strategies clearly appear here: water saving *vs* water spending. There is no a-priori better strategy: it always depends on the

genotype by environment by management interaction. In some cases there is no way to discriminate a better strategy: they perform equally well such as in well-watered conditions in the second site after day 40. But we can find situations where the water savers experience less (end of simulation in dry conditions) or more (beginning of the simulation in any scenario, end of simulations in well-watered conditions for site 1) severe stress than the water spenders.

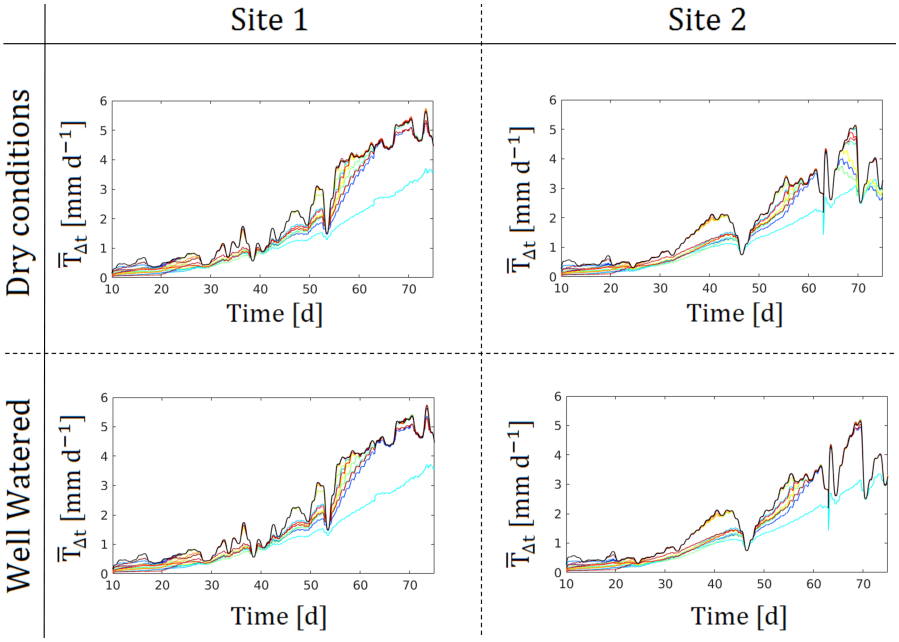


Figure 11.3: Cumulative transpiration of the 24h around any time as calculated using (11.10) with $\Delta t = 1d$ for the eleven selected phenotypes in dry (top panels) and wet (bottom panels) conditions for the two simulated sites (corresponding columns). The black solid lines represent the potential instantaneous cumulative transpiration of the last day.

Fig. 11.4 illustrates the z-profiles of the water content for each scenario and each single root system after 80 days of simulations. Obviously the water content is higher in well-watered conditions than in water-limited conditions. As stated before the water content in wet conditions is generally higher in the topsoil layers thanks to the rains and/or irrigation while the opposite is observed in dry scenarios. Interestingly the

water content profiles are rather similar between phenotypes for many scenarios with only differences of few percent making them probably hard to discriminate if measured in the fields. The biggest differences appear in the topsoil layers of the wet soils with almost 15% of volumetric water content.

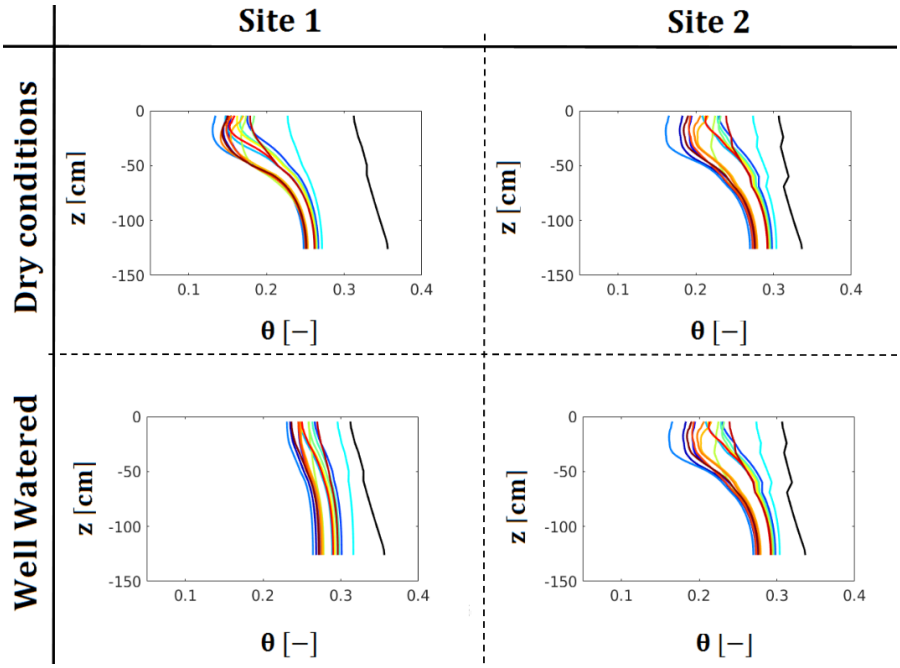


Figure 11.4: Water content z-profiles 70 days after sowing: for all the considered root systems in dry (top panels) and wet (bottom panels) conditions and for the two environments (corresponding columns). The black lines are the initial water content.

In order to investigate the relevance of the sixteen subgroups, we analyzed intra and inter-variations of macroscopic parameters. To do so, one randomly picked up root system hydraulic architecture of each of the sixteen categories was simulated with R-SWMS in the four considered pedo-climatic situations. In Fig. 11.5, we show the plot we obtain when we correlate the cumulative transpiration after 1 month of simulation of two plants that are either the closest (left) or the farthest (right) in the four-dimensional parametric space. The results are plotted for two sites (Nerac and Bologna), two treatments (well-watered and drought),

one year (2012) and sixteen couples of plants (one couple per category).

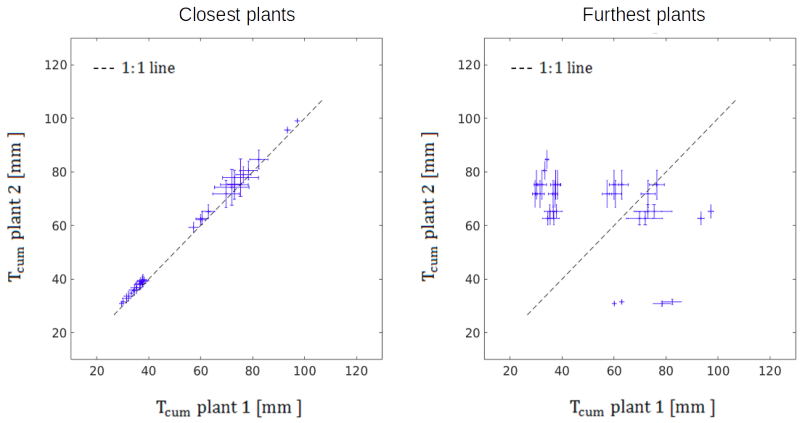


Figure 11.5: Correlation between plant-plant cumulative transpiration in case of close (left) or distant (right) (in the macroscopic parametric space) plants for the two different sites, two treatments and sixteen couples of plants.

Interestingly, in some case contrasted plant strategies lead to similar transpiration (right subplot) but in most cases, we observed a significant mismatch between transpiration when comparing plants with different macroscopic parameters. On the contrary, when plants are relatively close in the macroscopic parametric space, they obtain similar performances in term of plant transpiration (left subplot).

Solving the Richards equation allows obtaining the soil water potential distribution everywhere in the domain which enables to calculate the water flux and potential distributions over the whole soil-plant system. This is illustrated in Fig. 11.6 where the soil pF generated by the uptake of two phenotypes (dark blue (left) and cyan (right)) are represented for the site of Nerac and the two treatments (well-watered condition and drought stress) after 80 days of simulation. Under dry conditions different water distributions appear between both root systems. The root system 1 has always the highest conductance leading to the minimal water content in the soil domain. The root system 2 illustrated here has always one of the lowest conductance. This leads to much higher water content at the end of the simulation which could then play a major role for water availability later on if there is no rainfall

and no scheduled irrigation. On the contrary under irrigation, no clear differences exist between the two phenotypes. The figure also suggests that the root hydraulic architecture is playing a role essentially in dry conditions as we will make it even clearer in the next illustrations. From Fig. 11.6, it is also clear that the irrigation makes the water content higher everywhere in the soil domain, especially in the topsoil layers as compared to dry conditions (bottom line vs top line).

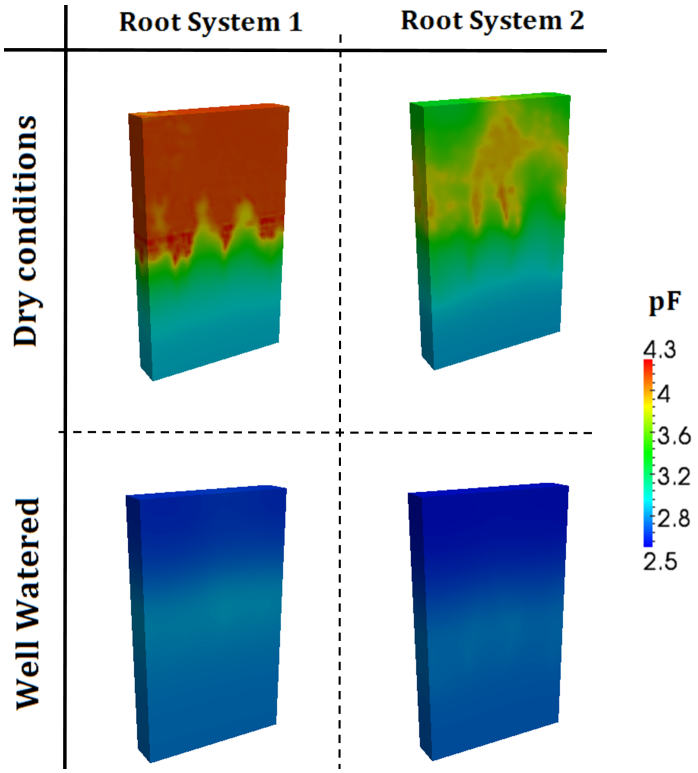


Figure 11.6: Example of three-dimensional simulation results: soil pF distribution for two phenotypes after 80 days of water uptake. The two root systems (columns) have been selected because of their different behaviors. The lines depict the treatment: the irrigation mangement is the bottom line while the dry condition is represented in the top line. No clear differences of water content distribution appears in wet soils unlike in drought conditions.

11.5 Discussion

First it must be pointed out that with a very simple notion of species (set of common architectural and hydraulic rules) and phenotypes (variability of traits), this model enables generating different behaviors in terms of both water uptake location and volume. In the simulation study presented above, the selected sixteen phenotypes offer a range of behaviors. Their performance varies between environments (water demand, soil hydraulic properties) and treatments (irrigation volume and timing) highlighting the genotypes x environment x management interactions. This model makes clear that no perfect ideotypes exist that perform ideally in any situation. On the contrary quantitative traits that make phenotypes more adapted to their location and farming practices exist and can be selected for. We showed that the macroscopic parameters of Couvreur et al. seem to well explain their behavior.

The model is physically-based and describes the main processes of the water flow at the plant scale in three dimensions but remains relatively fast: most of the scenarios presented here ran in less than 12 hours CPU time for 80 days of simulation. Taking advantage of computer clusters makes possible its use for testing specific root traits or root phenotype performance in a really large set of changing environments. It makes this model also suitable to optimize management practices (sowing date, irrigation volume and time) on the long-term.

The phenotypes generated in these simulations are virtual. In next studies however, specific root traits characterizing phenotypes will be implemented and tested in order to compare the measured *vs* simulated field performances (as it was done for one reference genotype). Combining yield observations and local water content measurements or plant transpiration would also allow us to validate the model. However the first trial of model validation led to satisfactory results when correlating predicted transpiration and observed yield in contrasted pedo-climatic conditions for one specific genotype. This experiment should be repated with contrasted genotypes, knowing their main differences in terms of hydraulic or architectural properties.

In this study we assume that all phenotypes had the same aboveground properties (stomatal behavior, canopy development). In further studies these properties will be included in the analysis and different

stomatal regulation strategies will be implemented to represent a larger range of plant behavior (Tardieu and Simonneau 1998). Similarly, further studies will focus on analytic relations between local traits and the macroscopic parameters. Such relations would allow breeders to develop quantitative ideotypes and physiologists to quantify traits beneficial for the plant in specific conditions and to link local traits and field performance through such a kind of simulation study. Even without considering between root traits different water strategies appear. In the future we could also link given root parameters.

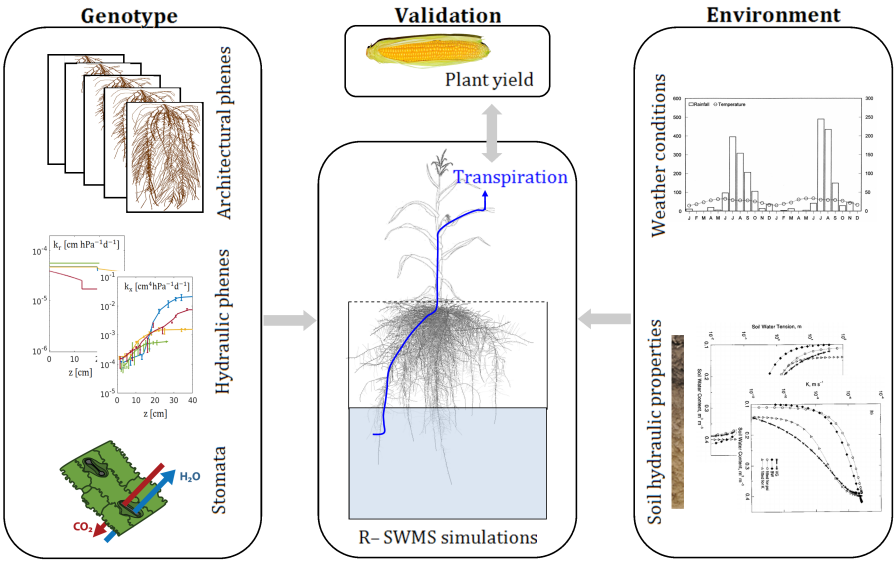


Figure 11.7: Perspective of validation using R-SWMS and the model input parameters.

11.6 Conclusion

We presented a new model able to optimize the water acquisition over full crop growth and development cycles. This model simulates the water flow in the soil-plant-atmosphere continuum through solving the Richards equation in 3D with a physically-based sink term. In a simulation study using this modeling approach we illustrate its potentiality for

quantitative breeding by linking local root traits and field performances through simulation over the full crop season. Different strategies - water saving and water spending - appear and no ideal strategy exist but we were able to pick the best phenotype for water uptake in each specific management and environment interaction situation.

Furthermore, we proposed a new definition of plant water uptake strategy by describing root system macroscopic parameter trajectories with time. These plant-scale parameters (root system volume, conductance, depth of standard uptake and soil exploration volume) are defined by ensembles of phene states and alone define plant performance: plant close in the macroscopic parametric space behaved similarly while it was not necessarly the case when they were distant.

PART V

CONCLUSION AND OUTLOOKS

In this final section, we discuss the principal advances, limitations and perspectives linked to each objective of the thesis.

If we knew what we were doing, it would not be called research, would it?

Albert Einstein

Science never solves a problem without creating ten more.

Georges Bernard Shaw

CONCLUSION AND OUTLOOKS 12

12.1 General conclusion

THE concept of crop ideotypes emerged in the sixties and was initially defined as "a plant model, which is expected to yield a greater quantity or quality of grain when developed as a cultivar" (Donald 1968). Such plant model is characterized by an ensemble of properties (alternatively called phene states) that are responsible for its improved performance, such as root structural (e.g. root length, elongation rates) and functional (e.g. radial or axial hydraulic conductivity) properties.

Even though recent suggestions of plant ideotypes such as the "deep, steep and cheap" maize of Lynch (2013) are of potential help as target for breeders, they are limited in terms of interest for at least four reasons. First they usually do not consider the timing of growth and development of the plant root system while they play a critical role for root water uptake. In many circumstances, colocation and coincidence of root foraging and soil water distribution must be fulfilled to supply the required water amount to plant leaves. Second current root system ideotypes do usually not include root hydraulic properties that though determine the root water uptake capacity distribution within the root system and its ability to convey the water sap towards the root collar and above. A third problem with the current definition of crop ideotypes is that root system phenes (including architectural ones) are described with general statements that are more qualitative than quantitative. Finally, they are never associated to specific environments: when Lynch (2013) or Wasson et al. (2012) present their ideotypes for improving root water uptake of maize and wheat, respectively, they do not specify the drying scenario while Tardieu (2012) insisted on the importance of explicitly associating traits for tolerance to drought scenario.

Furthermore, there is a conceptual problem with the notion of ideotype itself as an ensemble of phenes as there is no unique link between an ensemble of phene states and a plant behavior in terms of water uptake. Two very contrasted root system hydraulic architectures could absolutely behave similarly. Examples are easily imaginable: two roots in a same soil volume or a single one that is more conductive could lead to the same water depletion; no root presence in bottom soil layers is equivalent to deep root systems with no possible uptake of the water that is present in this region due to xylem limitation. Therefore, defining crop root system ideotypes as a combination of local phenes is only part of the solution: other ensembles of phene states could constitute other plant models with identical yields.

To overcome these difficulties, it was proposed to define from now on quantitative crop eco-ideotypes for root water uptake, i.e. ideal root systems that avoid water stress over their crop cycle or, at least, at critical stages such as flowering. Such plant models display optimal water uptake and growth strategies that are determined by macroscopic parameter trajectories in times. In turn, these trajectories and their changes are entirely explained by ensemble of phene states. As no plant can perform ideally in all situations, the ideotypes should systematically be associated to specific pedo-climatic situation.

In this PhD thesis, it was first analyzed how ensembles of phene states define macroscopic parameters and their changes with time. In Chapters 3 to 5, analytical solutions of root system macroscopic parameters were derived based on local root hydraulic and architectural phene states. They were further used to highlight the sensitivity of the calculated plant-scale parameters to local root properties. Then, it was checked how combinations of macroscopic parameters and their changes with time define water uptake strategies such as water spending *vs* water saving or deep *vs* shallow root water uptake. This was done at the single root scale (Chapter 4) and at the root system scale (Chapters 10 and 11). Doing so, progress toward optimal water uptake and growth strategy definitions was achieved but several novel tools and methodologies were needed to (i) generate contrasted root system hydraulic architectures (ii) have accurate root hydraulic properties of the plant roots (iii) combine local root phenes, macroscopic parameters and environmental data to assess plant performance.

In the first part of the very last chapter of this thesis, it is tried to summarize the work in this Ph.D. by going through the three general objectives and the eight specific methodological developments presented in the introduction in order to establish how they were achieved and to give more details and insights of main findings included in this document. In the second part of the present Chapter, several ways to progress one (or several) steps forward are proposed. To do so, remaining open questions and proposals to go towards crop plants of the future generation are listed.

12.2 Thesis summary

12.2.1 General objectives

GO.1: Linking local architectural and hydraulic root phenes and global plant-scale parameters

Focus was put on water flow in root system hydraulic architecture in the second part of this manuscript. The current numerical resolution method of the water flow equation was first improved by integrating the analytical solution of Landsberg and Fowkes (1978) valid at the segment scale in the hydraulic tree model of Doussan et al. (1998a). The resulting hybrid model was shown to be more accurate and even faster than current resolution methods (Chapter 3). The macroscopic parameters of Couvreur et al. 2012's model K_{rs} and **SUF** were also shown to be analytically calculable based on the Thevenin theorem. The newly developped resolution method for the water flow equation highlighted the numerical errors generated by previous approaches when long segments or high radial to axial conductivity ratio are present in the root system hydraulic architecture.

In Chapter 4, novel analytical solutions of water flow equation in roots with varying hydraulic property profiles were proposed, more versatile than current analytical solution only valid for homogeneous root properties. There new solutions are of interest as they create a direct link between local root phenes (elongation rates, changes of radial conductivity along the root axis) and macroscopic parameters (conductance, distribution of root water uptake), giving rise to sensitivity of

the latter parameters to local phenes. As a side effect, they also allow one to verify numerical resolution methods for idealized cases. These solutions were then integrated in a purely analytical model of the root system hydraulic architecture (Chapter 5). Root strategies of uptake (water-saving *vs* water-spending, water uptake location in proximal or distal regions) clearly arise from parametric space sensitivty analysis at the single root scale (Chapter 4) and at root system scale (Chapter 5 and 11).

Finally, an online flexible software, MARSHAL, was elaborated and designed to easily generate constrasted root system hydraulic architecture of maize crop. Gathering existing and novel architectural and hydraulic parameter measurements, it is able to give birth to maize architectural root systems exportable in common root system formats. MARSHAL also solves the water flow equation problem under homogeneous and heterogeneous soil conditions and calculates plant-scale parameters. It is finally coupled to sensitivity and optimization algortihms so that it can be then used to find an optimal set of parameters that minimizes an error function (for example to reproduce a measured root length density profile) or to highlight sensitive input parameters to a given objective function. It clearly allows one to bridge the gap between local root phenes and macroscopic parameters by answering questions such as "which hydraulic or architectural parameters affect the most mature root system conductance" or "are the functional and/or structural plant parameters unique when measuring a certain information in the field".

Chapter 3 | Chapter 4 | Chapter 5

GO.2: Quantifying root hydraulic phenes

The third section of this PhD was dedicated to the hydraulic property quantification of maize, ryegrass and lupine root system using a combination of local or global measurements of proxies of water uptake and inverse modelling based on the developed analytical solutions. In all cases, good correspondences between measurements and simulations were obtained, as well as uncertainty of the fitted parameters.

Local root water uptake combined with plant transpiration and collar

potential was first used to retrieve local radial and axial conductivities of primary and lateral roots of a lupine root system grown in a rhizotron (Chapter 6). Succesive measurement of total and axial conductances of maize and lupine single roots of different lengths served then as observations in an objective function to optimize the local hydraulic profiles along these roots that best reproduce the observed water flow (Chapter 7). In these two experiments, soil was not taken into account because it was either wet and homogeneous or removed and the roots were then immersed in a water solution.

In the next two Chapters, however, soil hydraulic properties and status played an important role on the water movement in the soil-plant system and could therefore not be neglected anymore. First, water content distribution maps obtained during a drought episode by light transmission imaging were used to parametrize a model of the water flow in soil and root systems (Chapter 7). Two-dimensional water content changes were shown to be sensisitive to soil and root hydraulic properties, leading to most likely distribution of radial and axial maize root properties. Second, a macro-rhiztron experiment was designed to accurately track heavy-water redistribution by ryegrass root systems. Hydraulic lift was the only mechanism explaining the enrichment of the top-soil layers in water isotopes and the simulations of the experiment allowed us to define optimal set of soil and root hydraulic properties as well as their uncertainty to best match the measured isotope profiles.

Absolute values of root radial and axial conductivities of different root regions and root types were obtained through these different experiments. It was also shown that high variations of hydraulic conductivities could be observed between species, root types and root regions. This leads to a complete and accurate description of hydraulic distribution in different crop species and predicted root uptake regions. Interestingly orders of magnitudes of the observations were compatible with the existing literature. Mature maize root were also shown to display similar root hydraulic conductance independently of the root order. Maize root-shoot connections are finally expected to deeply impact the water uptake distribution within the root system (Chapter 7).

GO.3: Elaborating a novel definition of root water uptake optimal strategy: crop quantitative eco-ideotypes for root water uptake

With the novel analytical relationships between local root phene states and macroscopic parameters, contrasted root hydraulic architectures could easily be generated. To do so, the parametric space given in the literature was explored and the sensitivity of hydraulic and architectural plant-scale parameters (root system volume, convex hull, root system conductance and depth of standard uptake) to local phene states was analyzed. These macroscopic parameters, together with their changes with time, define the plant strategy for water uptake that can be adapted to certain pedo-climatic conditions and lead to improved performances.

In order to see if the variability of possible behavior was captured, MARSHAL was used to generate maize root system hydraulic architectures. It exports its outputs in common formats suitable in functional-structural models, such as R-SWMS. Contrasted hydraulic architectures were then tested in various pedo-climatic conditions with long-term simulations. In order to do so, weather data records and generic or measured soil hydraulic properties were used as inputs to define the environmental development context in which root systems grow and develop. Two stategies were explored to look for best G x E interaction. Either reference root systems whose cumulative transpiration was correlated to observed yield observation in different locations and for different treatments were modified in a one by one analysis in order to highlight the impact of isolated local phenes (Chapter 10 and chapter 11). It was then shown that single local traits could induce significant positive, neutral or negative impacts on plant cumulative transpiration. Some parameters even reveal opposite effects when simulated in different pedoclimatic conditions, as suggested by Tardieu (2012). Several strategies arised from such simulations such as water-spending and water-saving plants. No strategy was best in all situations, but the plant performance ranking highly depended on G x E x M interaction.

Then contrasted phenotypes were selected based on their hydraulic and architectural macroscopic parameter and simulated in different conditions (Chapter 11). Root systems close in the macroscopic parametric space behaved similarly while cumulative transpiration could be similar or radically different when comparing distant plants. This suggests that

macroscopic parameter trajectories should be used rather than local root phenes when looking for best plant and environment interactions. Indeed, if different trajectories could lead, by chance, to similar behaviors, similar trajectories begets always comparative performances in terms of water uptake.

So a new validated methodology to predict quantitative ideotypes adapted to their environment was elaborated based on environmental characterization, contrasted macroscopic trajectory testing and comparisons of simulated cumulative transpirations. This new procedure, successfully applied locally could now be extended to bigger temporal or spatial scales.

Chapter 10 | Chapter 11

12.2.2 Methodological developments

MD1: The accuracy of current numerical solutions of the water flow equations in roots is too low to make numerical simulations useful tools to compare plant root water uptake

As shown in Chapter 3, water flow equations in current models (such as R-SWMS) are typically solved using a numerical solution (Doussan et al. (1998a)'s algorithm). It predicts the water uptake distribution within root system hydraulic architecture of any complexity by dividing the root system into small pieces, called segments, characterized by hydraulic properties that are order and age dependent. Doing so, water flow equations are linearized and using a matrix connection to describe the root system topology, water potential is found everywhere within the architecture, which *in fine* leads to water flow at any root system position.

As illustrated in the same Chapter 3, the numerical solution of Doussan et al. (1998a) is segment size-dependent and under particular circumstances (high radial to axial conductivity ratio or long root segment), the solution does not accurately predict the water flow in the root system. Inside each root segment, the water potential is supposed to be uniform, which is not a valid assumption with big or higly radially conductive root segments. An elegant solution to overcome this issue was presented in Chapter 3 of this PhD. It consists in combining the hydraulic tree approach of Doussan et al. (1998a) with analytical solutions valid at the segment scale (developed in Chapter 4). The resulting algorithm solution is no more discretization size dependent, is therefore more valid than existing solutions and is even shown faster than current approaches.

MD2: Clear, direct relations between local root phenes and plant-scale parameters do not currently exist

Analytic relationships between local phenes such as root hydraulic property changes along root axis and macroscopic parameters were demonstrated to exist at root scale (Chapter 4) and root system scale (Chapters 4 and 5). At the single root scale, analytical solutions of the water flow

equation were found (Chapter 4) and provide a new tool to verify numerical models, among other applications. These analytical solutions as they are faster (and more valid) than numerical solutions, may replace the latter in any use of the current water flow models. Derivatives of resulting relationships also define the sensitivity of Couvreur et al. (2012)'s model parameters to any explanatory variable. When these analytical solutions are combined for multiple root branches, they provide estimates of root system macroscopic property evolution with time and space, thereby allowing a direct link between ensemble of phene states and plant-scale parameters. In other words, these relations allow one to quantify the impact of phene state values on the plant behavior in space and time. In addition, these novel relations do not only account for growth but also consider root maturations, i.e. the evolution of root hydraulic properties at a given location due to anatomical and biological changes.

At the root system scale, when the distribution and maturation laws governing root hydraulic properties are known, the upscaled model provide accurate estimates of macroscopic plant scale properties (Chapter 5), releasing constraining assumptions needed so far such as the homogeneous root conductivities assumed by Biondini (2008).

In both cases, clear, direct links between root hydraulic and architectural properties (such as root radius, elongation rate and radial conductivity) and plant-scale parameters that are suitable in crop or functional-structural plant models are within reach.

MD3: The link between diversity of local phene observations and diversity of macroscopic parameters observations is currently missing

In the literature, in general, experiments determine either local root properties (elongation rates, radial conductivity etc.) or plant-scale parameters (especially root system total conductance) but to the current knowledge, experiments measuring both were not conducted so far. However, comparison of the variabilities of both can be performed using the developed algorithms. Indeed, ranges of variation of local properties can be inserted in combined model of the root system architecture and the water flow to check wether they match the range of macroscopic parameters observed independently. This trial was successfully performed in

Chapter 5 for the maize root system conductance variability with root system age.

Unfortunately, no many observations of complete water uptake distribution in root systems were achieved so far due to technological limitations, which prevented us to repeat the exercice for the second macroscopic parameter, the Standard Uptake Fraction. But novel techniques such as neutron radiography (Tötzke et al. 2017) will allow us to do so in the near future by quantifying everywhere the water entering the root system in homogeneous soil conditions. However, architectural macroscopic properties (such as root length density profiles) were shown to be accurately reproduced for both maize and ryegrass using reference root growth parameters and dynamics of root length observations (Chapter 5 and 9) but at this stage they do not include hydraulic functions of the roots yet.

MD4: Accurate knowledge of hydraulic property distribution (mean and variation) within a root system is scarce

Several experiments were presented in details in the second and third part of this manuscript. They describe how local or global measurements may be used to retrieve local hydraulic property distributions along the root axes of different species.

These novel experiments combine new or ancient materials to measure proxies of root water uptake and inverse modelling to look for the most likely distirbution of the root hydraulic properties, having a more or less good knowledge of the root system architecture. In these analyzes, the biggest unknown is always the hydraulic behavior of the considering roots that is retrieved alongside with its uncertainty using optimization algorithm coupled with water flow model. In all cases, realistic (or observed) root architectures were used to feed the water flow model with.

In Chapter 6, root water uptake rates measured using neutron radiography were used to obtain the radial and axial conductivities of lupine roots grown in a rhizotron. Chapter 4 and 7 describes how successive measurements of single root conductances can help to retrieve root conductivity profiles. Chapters 8 and 9 include the soil hydraulic properties to get maize and lupine hydraulic functions from water content maps

or z-profiles of heavy water, respectively. In all cases, sensisivity of the solutions to key parameters was shown as well, which indicated that the sensitivite parameters are not always the same. Therefore, the mathematical analysis of the experiments provided us a good idea of some of the hydraulic parameters of maize and lupine while other remain uncertain. Fortunately, *in silico* experiments could be easily imagined with the tools developped in the thesis to design an experiment where the remaining unknown properties are highlighted and can be retrieved.

MD5: Current three-dimensional physically-based models of the water flow in the soil-plant-atmosphere continuum are too slow to be used at field scale over full crop cycles

All the pieces of the puzzle to compute efficiently and accurately the water flow in the soil-plant-atmosphere continuum preceded this PhD thesis. However they needed to be glued together to simulate in routines contrasted root system hydraulic architectures in contrasted pedo-climatic conditions. Crootbox, a root growth model written in C was coupled with the water flow model of Doussan et al. (1998a) in its new version developed in Chapter 4 of this thesis, and the macroscopic parameter calculation method of Couvreur et al. (2012).

Hydraulic and architectural parameters of maize crop were gathered in an online tool, named MARSHAL, together with the coupled here-above explicited model. It allows the user to generate root system hydraulic architectures and to export them in common formats that may serve as inputs in functional-structural models.

Examples of use of MARSHAL were illustrated in Chapter 10 and 11. Taking advantage of the local root phenes observed in nature, contrasted root system hydraulic architectures were generated using this tool and simulated in contrasted pedo-climatic conditions and revealed different performances in terms of cumulative water uptake for root systems sharing the same volume (Chapter 10) or with contrasted macroscopic parameters (Chapter 11).

MD6: The functional-structural model of the water flow R-SWMS has not been validated yet with field observations

MD7: Do different water uptake strategies emerge from combinations of individual root traits in contrasted drying scenarios?

In the two last chapters of this thesis, simulations of the water movement in the soil-plant-atmosphere continuum were achieved using a coupled model of static (Chapter 10) or dynamic (Chapter 11) root system hydraulic architectures and soil Richards equation. It was shown that local root phenes were predicted to have positive, negative or neutral effect according to the pedo-climatic situation through G x E x M interactions. As a consequence, the generated root systems that were defined by a set of local root phenes revealed high differences in terms of water uptake dynamics. Therefore both cumulative transpiration and actual transpiration at critical developmental stages of the simulated phenotypes could be distinguished.

Besides while it was shown that different sets of local root phenes could lead to similar root water uptake performances, it was mainly demonstrated that plants with similar macroscopic properties, i.e. root conductances, depth of standard uptake, root system volume and exploration volume, behave the same when put in the same environement. These plant-scale macroscopic parameters are the true key for defining eco-ideotypes: instead of defining set of local root phenes, it would be better to fix trajectories of macroscopic parameters with time and test them. Best performance selection would lead to best macro-parameter functions that could be obtained by different combinations of local root phenes.

MD8: Best quantitative root phenes specific to contrasted pedo-climatic conditions, defining ideal strategies and root systems ideotypes are currently not known.

Such optimal combinations of local root phenes were shown to exist in Chapter 10 and 11 of the present manuscript but also to depend on the

pedo-climatic conditions defining the field location. Water-saving strategy displays favorable results when water stress occurs at the end of the growing season while it does not make sense when rainfalls (and/or irrigation) are intense and refilled sufficiently the soil domain. At the opposite, water-spending behavior is risky when water resources are scare, especially at the end of the crop cycle but reveal increased transpiration rates under well-watered conditions.

Similarly, depth of uptake is key but highly depends on the weather dynamics and the soil hydraulic properties as well as on the soil depth. Top-standard water uptake is good for maize whose root systems are spread in surface but is inefficient if the root system is steep and deep. An ideotype such as the one proposed by Lynch (steep, deep and cheap) makes sense only if water resources are only available at the bottom of the soil when the root system is mature.

12.3 Perspectives

In the previous sections, was identified the contribution of this Ph.D. to the current state of the art of root water upake modelling and understanding of the mechanisms determining or regulating crop transpiration. If progress was achieved, open questions remain and the developed models, experimental results and analysis open new questions and perspectives that disserve to be asked. In the following, are presented some original ideas that are not yet fully explored in the current literature and that would benefit from the present developments.

Root system hydraulic architectures

In this study, the above parts of plants were reduced to their simplest expression: a big transpiring leaf that reduces actual transpiration as compared to potential one when the plant is experiencing stress. Although this has been shown to be a relatively good assumption in general, the physiological behavior of leaves is expected to be more complex. Tardieu et al. (2015) describes the stomatal aperture as regulated by atmospheric demand (vapore pressure deficit, incoming light) and water supply by the root system. An equilibrium must be found between demand and supply according to regulation mechanisms. In such model, hydraulic conductances are regulated according to past transpiration, circadian clock and soil water potential. In addition, a capacitance, included in the system to sustain the early transpiration, is emptying in the morning and filling in late afternoon.

Since soil-root system and stomatal model all use the same Ohm law analogy to describe the water flow, the coupling between those is straightforward. The plant from the root system to the leaves can thus be represented as a network of hydraulic resistances (and capacitances) and water flows passively from the bulk soil to the atmosphere along the water potential gradient between these compartments. A realistic model of the plant regulated hydraulic architecture that can reproduce experimental observations of leaf and soil properties and have a predictive power about plant's ability to take up water should arise from such a coupling.

First steps to do so were already achieved during this thesis taking

advantage of the simplifying assumptions of Couvreur et al. (2012)'s model. The resulting model of the entire plant could successfully reproduce stomatal behavior and leaf potential dynamics (see Figure 12.1) of pot experiments (no impact of the root system architecture).

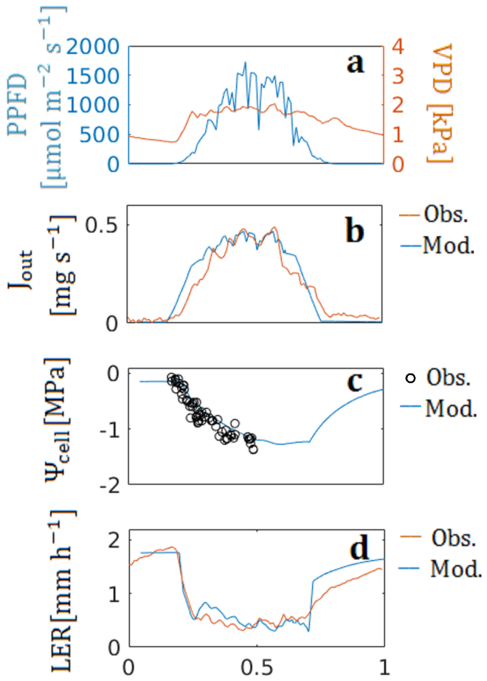


Figure 12.1: Coupled model of Tardieu et al. (2015) for the stomata and Javaux et al. (2008) for the root system lead to good predictions of the stomatal aperture, water potential dynamics in pot experiments. LER = leaf elongation rate, PPFD = photosynthetic photon flux density, VPD = vapour pressure deficit. The other variables were explained in previous chapters.

The coupled model should now be tested in contrasted pedo-climatic conditions with different root system architectures to assess the impact of the latter on plant transpiration. Combination of optimal architectural properties and conductance regulation mechanisms are likely to vary according to the evaporative demand and soil properties.

As soon as stomatal aperture is simulated, carbon assimilation pro-

cess can be computed as well (Schymanski et al. 2013). Depending on the incident light and the stomatal aperture, carbon can be fixed and sent to the different organs for respiration and growth which could be explicitely simulated as well. In a climate change context, CO_2 concentration is expected to increase in next decades with unpredictable consequences on plant yield (see Figure 12.2). On one hand, the water use efficiency should increase because of the abundance of dioxide carbon molecules, on the other hand impact of climate change on the precipitation and temperature can be dramatic for plant performance. Once assimilation models will be coupled to a water flow model, one should be in a position to assess the effect of CO_2 concentration change together with its consequence on the weather (Medlyn and McMurtrie 2005).

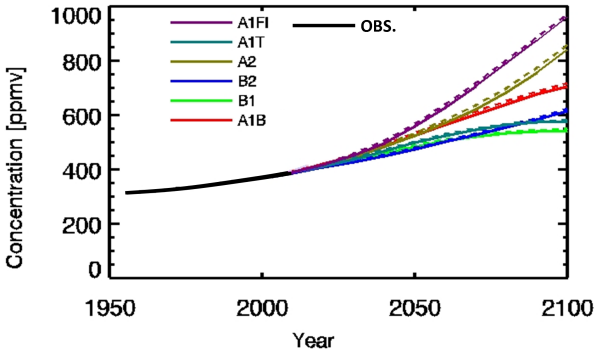


Figure 12.2: Scenarios of CO_2 concentration changes in the atmosphere as proposed by IPCC. Reproduced from IPCC data.

Environment

It would be worth investigating impact of soil complex structure on root performance over full crop cycle. Indeed the soils that are considered here were rather simple, homogeneous, or for the most sophisticated ones, horizontally layered. But in reality, soils are complex, heterogeneous media where preferential flow occurs and physical properties change according to different spatial scales.

The literature is quite abundant to take into account soil hydraulic property variation made by soil physical structures. Hydraulic parameters may be changed, for example, using scaling factors to account for such a spatial variability while keeping mean values unchanged (Warrick et al. 1977). Such soil properties would definitely impact plant performance and so the ideal macroscopic parameter trajectories according to the environmental context.

In Figure 12.3, are illustrated such scaling factors for the unsaturated soil conductivity (top line). α parameter of the retention curve was modified as well in the simulation using the approach of Zhu and Mohanty (2006). In all scenarios (columns of Figure 12.3), the domain mean conductivity is the same but the distribution changes between simulations. It is plotted as possible illustration randomly distributed properties (right), soil correlated properties (left) and correlation between the root foraging presence and high soil conductivities (center). After 7 days of root water uptake, the changes of water content (bottom line) are significantly different and correspond to the scaling factor distribution. The plant water status and cumulative transpiration are contrasted as well (data not shown), suggesting critical impact of soil hydraulic property distribution on plant water stress that should be further investigated.

Similarly, impact of mucilage and more generally rhizosphere processes were always neglected in this study although their potential influence on water movement is crucial Carminati et al. 2010. While a running version of R-SWMS including non-equilibrium water dynamics exists (Schwartz et al. 2016), it was not used in the exploratory simulations for three reasons: it dramatically slows down the solution computation, it is not perfectly parametrized for all soil types and right now it can only be used for single roots. Long term simulations includ-

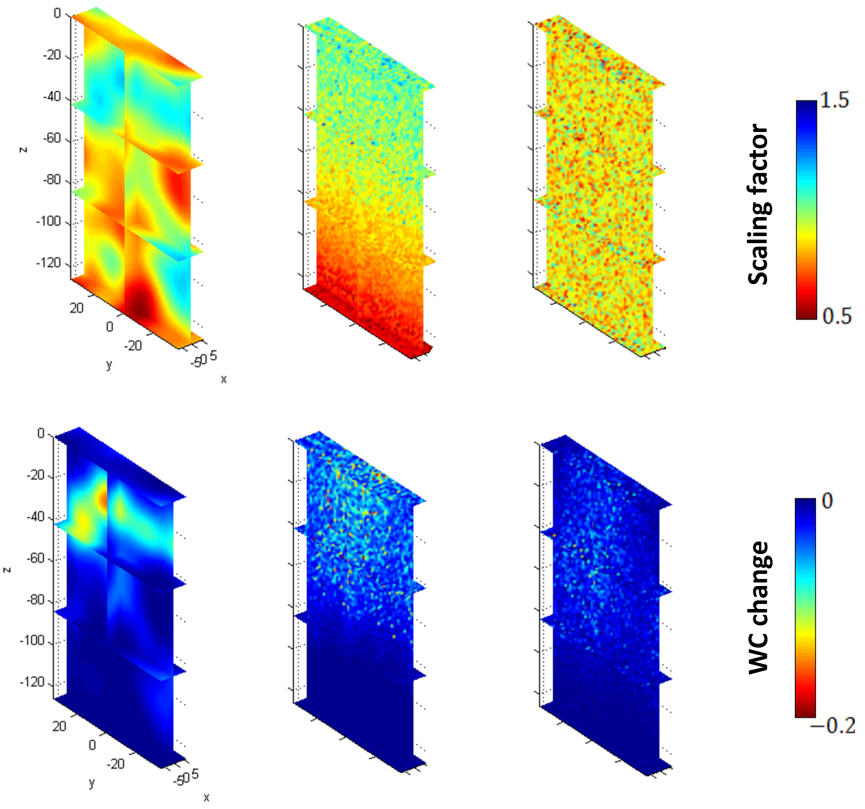


Figure 12.3: Water change distribution in soils after 7 days of water uptake when soil hydraulic property distribution changes.

ing rhizosphere dynamics constitutes a big challenge that should be tackled in further work.

Management practices

Another aspect almost completely neglected in this study (on purpose) is the anthropogenic influence on plant yield. Management practices are a key factor for yield determination and can take different forms: from the soil fertility management to farming works scheduling. Some of these aspects are discussed here below.

Irrigation scheduling

In Chapter 11, two treatements were considered for sensitivity analysis: well-watered and drought conditions. Irrigation was applied several times in the former case as variable flux for top soil boundary condition. The timing was fixed and corresponded to what happened on field trials. However it can be easily imagined that moments of applications, volumes and irrigation type (surface irrigation, drip irrigation) will dramatically impact the plant water stress.

Therefore, optimization of irrigation scheduling could be designed to avoid water stress and minimize water losses by deep drainage in long term simulations. Efficiency of different kinds of irrigations (varying the timing, volume and location of application) could be assessed in contrasted pedo-climatic regions towards "more crop per drop" systems.

Plant interactions

Many suggestions have been made so far to increase or to maintain yields under unsecure environments. For example, crop mixing using different species or cultivars of the same species may be used to save water and nutrients while attenuating the effects of climatic changes on crop production.

In the simulations it was systematically assumed that all the plants behaved similarly in the field, i.e. plant neighbors are exactly the same as the central simulated one. To do so, a periodic soil domain was always used: roots crossing x or y borders systematically reappear at the opposite side of the soil domain. It is a simple way to efficiently

simulate impact of the plant neighbors but it was then assumed that all plants in the field have the same root system hydraulic architecture. This assumption is useful when interest is in understanding the added benefits of local root phene change or macroscopic parameter modification. However it is unrealistic in the sense that all plants in the field, even when they belong to the same cultivar, are unique, although they share somme common properties. In the simulations, by the way, generated plants look different between them because each architectural (and hydraulic) parameter is also characterized by its uncertainty.

In further study, it would be definitely interesting to look at plant-plant interactions. Neighbor plant with too similar hydraulic architectures could compete for resources if not sown remote enough. At the opposite, root growth and development of two different plants characterized by the same mean and higher standard deviation parameters could lead to contrasted hydraulic architectures and, as a consequence, commensalism or mutualism for natural resources through biological mechanisms such as hydraulic redistribution.

If it is worth looking at plant-plant interactions of two identical genotypes, it is a fortiori worth doing it when considering mixing of different plant cultivars or intercropping. Thanks to recent developments, R-SWMS is now able to simulate different plants within the same field, their growth and development, their unique boundary conditions (i.e. the plant transpiration is also function of its corresponding leaf surface) and potential interaction (competition for water uptake can occur in voxels where are located roots of the two plants or a shallow root system could benefit from hydraulic redistribution of a deep root system) using the Couvreur et al. (2012)'s model. To illustrate this last point, was simulated the water uptake from two contrasted plant species and their association in a intercropping system: a shallow one (plant A, Fig. 12.4) and a deep one (plant B, FIg. 12.4). As it can be seen from the central subplot, their contrasted hydraulic architectures allow these plants to take up in the upper or lower layer of the soil profile, respectively. In case of intercropping though, the standard uptake is more spread all over the soil-depth.

When it is looked at the corresponding plant transpiration rates (bottom right subplot), it can be realized that, under high transpiration demand and with a low conductive soil, the intercropping system

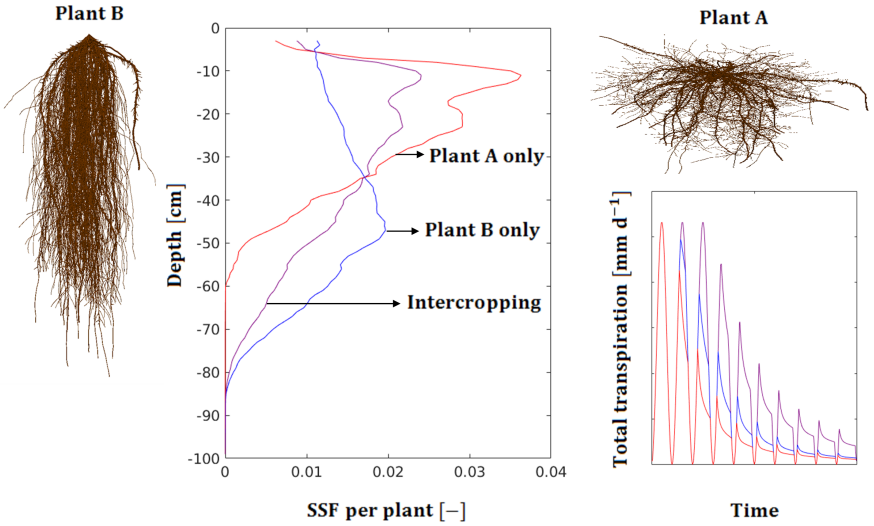


Figure 12.4: Intercropping positive impact on total transpiration as compared to reduced sole plant transpiration.

outperforms any sole plant system. Rapidly the latter experience water stress as water is taken up from the same regions.

G x E x M Interactions

As the long term simulations are no longer too time-consuming and depend on G x E interaction, the model could be run on large spatial scale, typically country or continent-scale as soon as the different environments are correctly described. Even though the perspectives of use of the present developments are numerous, this one drew the attention for two reasons. First because all the pieces were already gathered together for the European continent and that simulations can already run massively in routines on parallel cluster. Secondly because it would be very informative to understand best genotypes-environment associations and which local phenes can be benefitial in a particular environment or as suggested in this PhD, what macroscopic parameter trajectory is the best one for given pedo-climatic situation.

The procedure to follow is schematically represented in Fig. 12.5.

Grey boxes stand for inputs of the large-scale simulation model, white boxes indicate the processes that need to be fed with these input data.

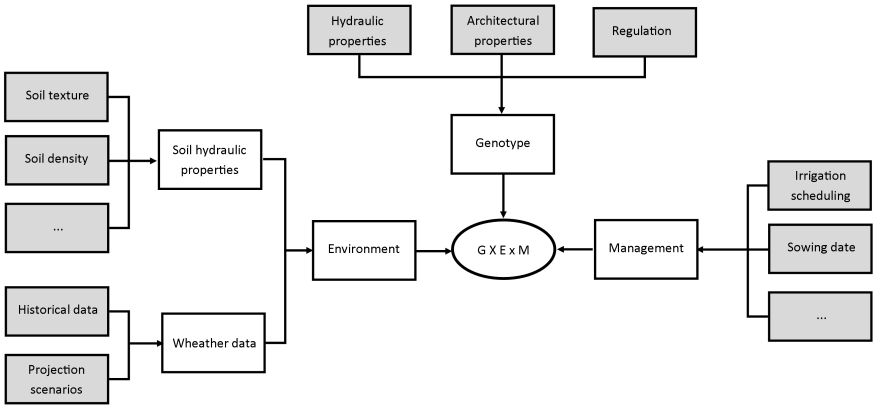


Figure 12.5: Flowchart of a large-scale performance forecast model with input parameters (gray boxes) and important processes (white boxes) innteraction.

Basically, the performance is affected by the interaction of the plant genotype, the environment and the management practices, as it was mentionned earlier in this manuscript. To run large-scale simulations for one specific genotype whose architectural and hydraulic properties are known as well as its regulation properties, the two latter must be characterized at the considered spatial scales.

The soil properties can be derived from soil databases available in the soil science community. In particular, the Harmonized World Soil Database provides a world map of soil types, soil depths and properties (texture, bulkd density and organic carbon content) of the different soil horizons (Nachtergaele et al. 2009). Taking advantage of existing pedo-transfer functions, these soil properties can be converted into hydraulic functions used as inputs for soil definition in R-SWMS. Distribution of silts and clay separate fractions in Europe are illustrated in Fig. 12.6 where are plotted the properties of the dominating soil at each location, only.

Historical weather data also exist in Europe such as the one developed by the European Climate Assessment & Dataset that give in open access records of temperatures, wind velocities, rainfalls and sea

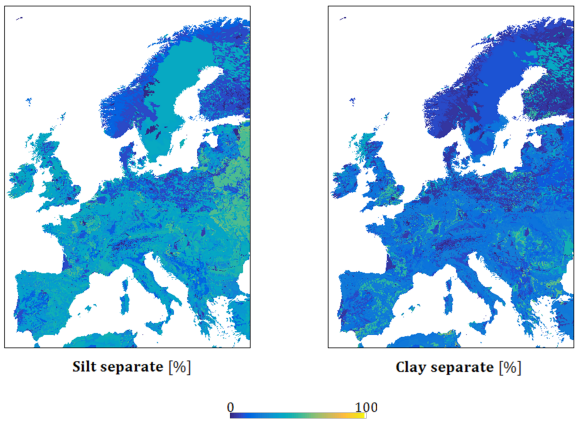


Figure 12.6: European soil map of silt and clay separate fractions of the dominating soil in each pixel.

level pressure in all member weather stations collected by 68 participant organizations in 63 countries (Van Den Besselaar et al. 2015), freely downloadable on http://www.ecad.eu. The dataset contains 43227 series of daily observations at 10584 meteorological stations throughout Europe and the Mediterranean. These datasets were used to generate daily gridded observational dataset for precipitation, temperature and sea level pressure in Europe. The full dataset covers the period 1950-01-01 until 2016-12-31.

As illustration, potential evapotranspiration derived from Hargreaves formula (Hargreaves 1974) and the dasasets and precipitation records were mapped and plotted in Figures 12.7 and 12.8 for a particular day of June 2014, chosen randomly. These figures also show historical (in blue) records of evaotranspiration dynamics and cumulative precipitation at a specific location in Spain, calculated based on the statistical times series of the closest station. In these plots, the blue dark line is the daily mean of 30 years of observations while the blue enveloppes encompass more or less one standard deviation over these 30 years.

Interestingly, the observations can also serve as inputs for weather generator sofwares and algorithms such as LARS-WG (Semenov et al. 2002) that produce new weather data timeseries according to chosen climatic scenario. Temperatures and precipitation dynamics are indeed

likely to evolve in the future because of climate change. Historical data and this weather generator were used to forecast the future evapotranspiration and precipitation of the same location in Spain according to scenario A2 of IPCC at the end of the century. The resulting curves are the red distribution shown in Figures 12.7 and 12.8.

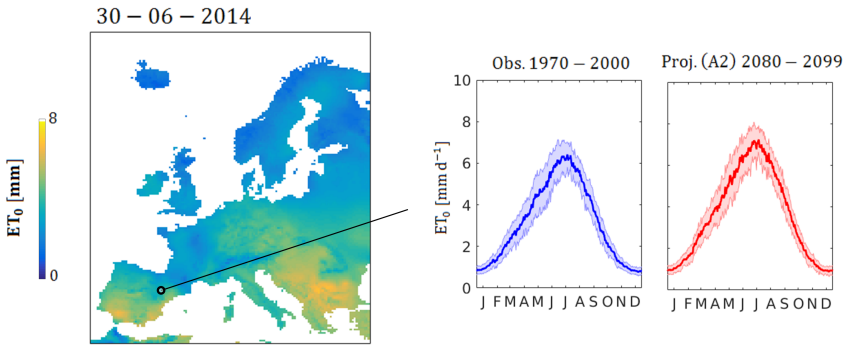


Figure 12.7: Potential evapotranspiration in Europe and scenario of evolution at a specific location in Spain.

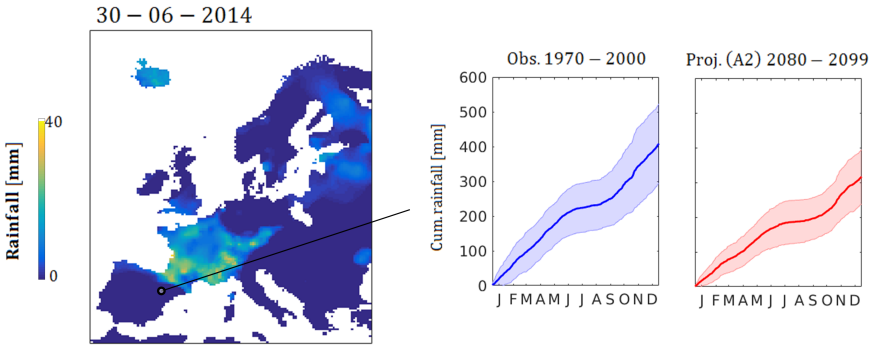


Figure 12.8: Precipitation in Europe and scenario of evolution of cumulative rainfall at a specific location in Spain.

As a consequence of the climate change, the maximal potential evapotranspiration is expected to increase and the total cumulative precipitation to decrease before the end of this century with potential

dramatic consequences on agricultural productions under unchanged agricultural practices. Maintaining the yield under such extreme conditions would be a big challenge that the present work could help to fulfill by testing new varieties or management strategies.

Finally, long term simulations could also help to understand pesticides or nutrient fate when applied to the field. Their transport into and within root systems may already be simulated in R-SMWS but such simulations are still time-consuming. If they are maybe too computationnally heavy right now to be run at large scale, contrasted pedo-climatic conditions and root system hdyraulic architectures could be already tested over full crop cycles in order to assess the nutrient losses or uptake efficiency and the final destiny of applied pesticides.

GENERAL BIBLIOGRAPHY

(1) Ahmed, M. A., Kroener, E., Holz, M., Zarebanadkouki, M. and Carminati, A. (2014). Mucilage exudation facilitates root water uptake in dry soils., en *Functional Plant Biology 41*, 1129, DOI: 10.1071/FP13330 (cit. on p. 178).

(2) Alm, D. M., Cavelier, J. and Nobel, P. S. (1992). A Finite-element Model of Radial and Axial Conductivities for Individual Roots: Development and Validation for Two Desert Succulents. *Annals of Botany 69*, 87–92 (cit. on pp. 43, 80, 205).

(3) Amenu, G. G. and Kumar, P. (Jan. 2008). A model for hydraulic redistribution incorporating coupled soil-root moisture transport., en *Hydrology and Earth System Sciences 12*, 55–74, DOI: 10.5194/hess-12-55-2008 (cit. on p. 46).

(4) Araguás-Araguás, L., Rozanski, K., Gonfiantini, R. and Louvat, D. (June 1995). Isotope effects accompanying vacuum extraction of soil water for stable isotope analyses., en *Journal of Hydrology 168*, 159–171, DOI: 10.1016/0022-1694(94)02636-P (cit. on p. 233).

(5) Araus, J. L., Slafer, G. A., Royo, C. and Serret, M. D. (2008). Breeding for yield potential and stress adaptation in cereals. *Critical Reviews in Plant Science 27*, 377–412 (cit. on p. 287).

(6) Ariyaratna, R. An extension to the Landsberg and Fowkes' Model., Ph.D. Thesis, Texas Tech University, 1990 (cit. on pp. 80, 86).

(7) Armengaud, P. (Feb. 2009). EZ-Rhizo software: The gateway to root architecture analysis. *Plant Signaling and Behavior 4*, 139 (cit. on p. 22).

(8) Asbjornsen, H., Mora, G. and Helmers, M. J. (Aug. 2007). Variation in water uptake dynamics among contrasting agricultural and native plant communities in the Midwestern U.S., en *Agriculture, Ecosystems & Environment 121*, 343–356, DOI: 10.1016/j.agee.2006.11.009 (cit. on p. 229).

(9) Bechmann, M., Schneider, C., Carminati, A., Vetterlein, D., Attinger, S. and Hildebrandt, A. (Oct. 2014). Effect of parameter choice in root water uptake models: the arrangement of root hydraulic properties within the root architecture affects dynamics and efficiency of root water uptake., en *Hydrology and Earth System Sciences 18*, 4189–4206, DOI: 10.5194/hess-18-4189-2014 (cit. on p. 80).

(10) Bengough, A. G., McKenzie, B., Hallett, P. and Valentine, T. (2011). Root elongation, water stress, and mechanical impedance: a review of limiting stresses and beneficial root tip traits. *Journal of Experimental Botany 62*, 59–68 (cit. on p. 12).

(11) Bengough, A. G., Bransby, M. F., Hans, J., McKenna, S. J., Roberts, T. J. and Valentine, T. A. (2006). Root responses to soil physical conditions; growth dynamics from field to cell. *Journal of Experimental Botany 57*, 437–447, DOI: 10.1093/jxb/erj003 (cit. on p. 178).

(12) Biondini, M. (Mar. 2008). Allometric scaling laws for water uptake by plant roots., en *Journal of Theoretical Biology 251*, 35–59, DOI: 10.1016/j.jtbi.2007.11.018 (cit. on pp. 43, 79, 96, 106, 110, 159, 329).

(13) Blum, A (2005). Drought resistance, water-use efficiency, and yield potential—are they compatible, dissonant, or mutually exclusive? *Australian Journal of Agricultural Research 56*, 1159–1168 (cit. on p. 6).

(14) Blum, A (2009). Effective use of water (EUW) and not water-use efficiency (WUE) is the target of crop yield improvement under drought stress. *Field Crops Research* (cit. on p. 264).

(15) Bolanos, J and Edmeades, G. (1996). The importance of the anthesis-silking interval in breeding for drought tolerance in tropical maize. *Field Crops Research 48*, 65–80 (cit. on p. 267).

(16) Borrell, A., Hammer, G. and Oosterom, E. (2001). Stay-green: A consequence of the balance between supply and demand for nitrogen during grain filling? *Annals of Applied Biology 138*, 91–95 (cit. on p. 287).

(17) Boursiac, Y., Boudet, J., Postaire, O., Luu, D.-T., Tournaire-Roux, C. and Maurel, C. (Oct. 2008). Stimulus-induced down-regulation of root water transport involves reactive oxygen species-activated cell signalling and plasma membrane intrinsic protein internalization. *The Plant Journal 56*, 207–218 (cit. on p. 10).

(18) Bramley, H, Turner, D. W., Tyerman, S. D. and Turner, N. C. (2007). Water Flow in the Roots of Crop Species: The Influence of Root Structure, Aquaporin Activity, and Waterlogging. *Advances in Agronomy 96* (cit. on pp. 22, 23, 48).

(19) Bramley, H., Turner, N. C., Turner, D. W. and Tyerman, S. D. (July 2007). Comparison between gradient-dependent hydraulic conductivities of roots using the root pressure probe: the role of pressure propagations and implications for the relative roles of parallel radial pathways., en *Plant, Cell & Environment 30*, 861–874, DOI: 10.1111/j.1365-3040.2007.01678.x (cit. on p. 79).

(20) Bramley, H., Turner, N., Turner, D. and Tyerman, S. D. (May 2009). Roles of Morphology, Anatomy, and Aquaporins in Determining Contrasting Hydraulic Behavior of Roots. *Plant Physiology 150*, 348–364 (cit. on pp. 9, 10, 239).

(21) Braud, I., Bariac, T., Gaudet, J. and Vauclin, M. (July 2005). SiSPAT-Isotope, a coupled heat, water and stable isotope (HDO and H218O) transport model for bare soil. Part I. Model description and first verifications., en *Journal of Hydrology 309*, 277–300, DOI: 10.1016/j.jhydrol.2004.12.013 (cit. on p. 236).

(22) Brodersen, C. R. and McElrone, A. J. (2013). Maintenance of xylem network transport capacity: a review of embolism repair in vascular plants. *Frontiers in plant science 4* (cit. on p. 11).

(23) Brooks, J. R., Meinzer, F. C., Coulombe, R. and Gregg, J. (Nov. 2002). Hydraulic redistribution of soil water during summer drought in two contrasting Pacific Northwest coniferous forests.,

en *Tree Physiology 22*, 1107–1117, DOI: 10.1093/treephys/22.15-16.1107 (cit. on p. 229).

(24) Brooks, J. R. (2015). Water, bound and mobile. *Science 349*, 138–139, DOI: 10.1126/science.aac4742 (cit. on p. 208).

(25) Brooks, R. H. and Corey, A. T. (1966). Properties of porous media affecting fluid flow. *Journal of the Irrigation and Drainage Division 92*, 61–90 (cit. on pp. 239, 247).

(26) Brooksbank, K., White, D. A., Veneklaas, E. J. and Carter, J. L. (Aug. 2011). Hydraulic redistribution in Eucalyptus kochii subsp. borealis with variable access to fresh groundwater., en *Trees 25*, 735–744, DOI: 10.1007/s00468-011-0551-0 (cit. on p. 250).

(27) Burdine, N. et al. (1953). Relative permeability calculations from pore size distribution data. *Journal of Petroleum Technology 5*, 71–78 (cit. on p. 238).

(28) Burgess, S. S. O. (Apr. 2011). Can hydraulic redistribution put bread on our table?, en *Plant and Soil 341*, 25–29, DOI: 10.1007/s11104-010-0638-1 (cit. on p. 228).

(29) Burgess, S. S. O., Adams, M. A., Turner, N. C. and Ong, C. K. (July 1998). The redistribution of soil water by tree root systems. *Oecologia 115*, 306–311, DOI: 10.1007/s004420050521 (cit. on p. 228).

(30) Burton, A. L., Williams, M, Lynch, J. P. and Brown, K. M. (2012). RootScan: Software for high-throughput analysis of root anatomical traits. *Plant and Soil* (cit. on p. 22).

(31) Burton, A. L., Brown, K. M. and Lynch, J. P. (2013). Phenotypic Diversity of Root Anatomical and Architectural Traits in Species., en *Crop Science 53*, 1042, DOI: 10.2135/cropsci2012.07.0440 (cit. on p. 11).

(32) Caird, M. A., Richards, J. H. and Donovan, L. A. (Nov. 2006). Nighttime Stomatal Conductance and Transpiration in C3 and C4 Plants., en *PLANT PHYSIOLOGY 143*, 4–10, DOI: 10.1104/pp.106.092940 (cit. on p. 251).

(33) Caldeira, C. F., Bosio, M., Parent, B., Jeanguenin, L., Chaumont, F. and Tardieu, F. (Apr. 2014). A Hydraulic Model Is Compatible with Rapid Changes in Leaf Elongation under Fluctuating Evaporative Demand and Soil Water Status., en *Plant physiology 164*, 1718–1730, DOI: 10.1104/pp.113.228379 (cit. on p. 160).

(34) Caldwell, M. M. and Richards, J. H. (Apr. 1989). Hydraulic lift: water efflux from upper roots improves effectiveness of water uptake by deep roots., en *Oecologia 79*, 1–5, DOI: 10.1007/BF00378231 (cit. on pp. 229, 250).

(35) Campos, H., Cooper, M., Habben, J., Edmeades, G. and Schussler, J. (Nov. 2004). Improving drought tolerance in maize: a view from industry. *Field Crops Research 90*, 19–34, DOI: 10.1016/j.fcr.2004.07.003 (cit. on pp. 78, 266).

(36) Canal, N., Calvet, J.-C., Decharme, B., Carrer, D., Lafont, S. and Pigeon, G. (2014). Evaluation of root water uptake in the ISBA-A-gs land surface model using agricultural yield statistics over France. *Hydrology and Earth System Sciences 18*, 4979–4999 (cit. on p. 208).

(37) Cannavó, F. (July 2012). Sensitivity analysis for volcanic source modeling quality assessment and model selection. *Computers & Geosciences 44*, 52–59, DOI: 10.1016/j.cageo.2012.03.008 (cit. on p. 141).

(38) Carminati, A. (2012). A model of root water uptake coupled with rhizosphere dynamics. *Vadose Zone Journal 11* (cit. on p. 178).

(39) Carminati, A. and Vetterlein, D. (2012). Plasticity of rhizosphere hydraulic properties as a key for efficient utilization of scarce resources. *Annals of Botany*, DOI: 10.1093/aob/mcs262 (cit. on p. 19).

(40) Carminati, A, Moradi, A. B., Vetteriein, D, Vontobel, P, Lehmann, E. H., Weller, U, Vogel, H and Oswald, S. E. (2010). Dynamics of soil water content in the rhizosphere. *Plant and Soil 332*, 163–176 (cit. on pp. 178, 337).

(41) Carminati, A, Schneider, C. L., Moradi, A. B., Zarebanadkouki, M., Vetterlein, D., Vogel, H., Hildebrandt, A., Weller, U., Schueler, L. and Oswald, S. E. (2011). How the Rhizosphere May Favor Water Availability to Roots. *Vadose Zone Journal 10*, 988–998 (cit. on p. 19).

(42) Carminati, A. (2013). Rhizosphere wettability decreases with root age: a problem or a strategy to increase water uptake of young roots? *Frontiers in Plant Science 4*, DOI: 10.3389/fpls.2013.00298 (cit. on p. 178).

(43) Carsel, R. F. and Parrish, R. S. (1988). Developing joint probability distributions of soil water retention characteristics. *Water Resources Research 24*, 755–769 (cit. on p. 275).

(44) Cattivelli, L., Rizza, F., Badeck, F.-W., Mazzucotelli, E., Mastrangelo, A. M., Francia, E., Marè, C., Tondelli, A. and Stanca, A. M. (Jan. 2008). Drought tolerance improvement in crop plants: An integrated view from breeding to genomics. *Field Crops Research 105*, 1–14, DOI: 10.1016/j.fcr.2007.07.004 (cit. on pp. 6, 78, 127, 290).

(45) Chapman, S. C. (2008). Use of crop models to understand genotype by environment interactions for drought in real-world and simulated plant breeding trials. *Euphytica 161*, 195–208 (cit. on p. 127).

(46) Chaumont, F. and Tyerman, S. D. (Apr. 2014). Aquaporins: Highly Regulated Channels Controlling Plant Water Relations., en *Plant physiology 164*, 1600–1618, DOI: 10.1104/pp.113.233791 (cit. on pp. 79, 222).

(47) Chaves, M. and Davies, B. (2010). Drought effects and water use efficiency: improving crop production in dry environments. *Functional Plant Biology 37*, iii–vi (cit. on p. 127).

(48) Clark, R. T., MacCurdy, R. B., Jung, J. K., Shaff, J. E., McCouch, S. R., Aneshansley, D. J. and Kochian, L. V. (2011). Three-dimensional root phenotyping with a novel imaging and software platform. *Plant physiology 156*, 455–465 (cit. on p. 22).

(49) Clausnitzer, V and Hopmans, J. W. (July 1994). Simultaneous modeling of transient three-dimensional root growth and soil water flow. *Plant and Soil 164*, 299–314 (cit. on p. 209).

(50) Cochard, H, Venisse, J.-S., Barigah, T. S., Brunel, N., Herbette, S., Guilliot, A., TYREE, M. T. and Sakr, S. (2007). Putative role of aquaporins in variable hydraulic conductance of leaves in response to light. *Plant Physiology 143*, 122–133 (cit. on p. 10).

(51) Cochard, H., Barigah, S. T., Kleinhentz, M. and Eshel, A. (2008). Is xylem cavitation resistance a relevant criterion for screening drought resistance among Prunus species? *Journal of plant physiology 165*, 976–982 (cit. on p. 11).

(52) Comas, L. H., Becker, S. R., Cruz, V. M. V., Byrne, P. F. and Dierig, D. A. (2013). Root traits contributing to plant productivity under drought., eng *Frontiers in Plant Science 4*, 442, DOI: 10.3389/fpls.2013.00442 (cit. on pp. 12, 17, 127, 183, 265, 289).

(53) Couvreur, V., Vanderborght, J. and Javaux, M. (Aug. 2012). A simple three-dimensional macroscopic root water uptake model based on the hydraulic architecture approach., en *Hydrology and Earth System Sciences 16*, 2957–2971, DOI: 10.5194/hess-16-2957-2012 (cit. on pp. 14, 15, 21, 30, 44, 45, 48, 55, 58, 60, 80, 84, 94, 111, 125, 128, 129, 137, 140, 177, 229, 239, 255, 274, 295, 297, 298, 323, 329, 331, 335, 340).

(54) Couvreur, V., Vanderborght, J., Draye, X. and Javaux, M. (Nov. 2014). Dynamic aspects of soil water availability for isohydric plants: Focus on root hydraulic resistances., en *Water Resources Research 50*, 8891–8906, DOI: 10.1002/2014WR015608 (cit. on pp. 97, 297, 298).

(55) Couvreur, V., Vanderborght, J., Beff, L. and Javaux, M. (May 2014). Horizontal soil water potential heterogeneity: simplifying approaches for crop water dynamics models., en *Hydrology and Earth System Sciences 18*, 1723–1743, DOI: 10.5194/hess-18-1723-2014 (cit. on pp. 48, 95, 210, 240, 250, 298).

(56) Couvreur, V., *Emergent properties of plant hydraulic architecture: a modelling study*; Presses universitaires de Louvain: 2013 (cit. on pp. 14, 164, 211).

(57) Dai, X., Wang, Y., Yang, A. and Zhang, W.-H. (2012). OsMYB2P-1, an R2R3 MYB transcription factor, is involved in the regulation of phosphate-starvation responses and root architecture in rice. *Plant Physiology 159*, 169–183 (cit. on p. 13).

(58) Daily, G. et al. (1998). Food Production, Population Growth, and the Environment., en *Science 281*, 1291–1292, DOI: 10.1126/science.281.5381.1291 (cit. on p. 5).

(59) Dara, A., Moradi, B. A., Vontobel, P. and Oswald, S. E. (2015). Mapping compensating root water uptake in heterogeneous soil conditions via neutron radiography. *Plant and soil 397*, 273–287 (cit. on pp. 171, 175, 177).

(60) Dawson, T. E. (Oct. 1993). Hydraulic lift and water use by plants: implications for water balance, performance and plant-plant interactions., en *Oecologia 95*, 565–574, DOI: 10.1007/BF00317442 (cit. on p. 229).

(61) Dawson, T. E. and Ehleringer, J. R. (Mar. 1991). Streamside trees that do not use stream water., en *Nature 350*, 335–337, DOI: 10.1038/350335a0 (cit. on p. 229).

(62) De Dorlodot, S, Bertin, P, Baret, P and Draye, X (2005). Scaling up quantitative phenotyping of root system architecture using a combination of aeroponics and image analysis. *Asp Appl Biol 73*, 41–54 (cit. on p. 273).

(63) de Jong van Lier, Q., van Dam, J. C., Metselaar, K., de Jong, R. and Duijnisveld, W. H. M. (2008). Macroscopic Root Water Uptake Distribution Using a Matric Flux Potential Approach., en *Vadose Zone Journal 7*, 1065, DOI: 10.2136/vzj2007.0083 (cit. on pp. 235, 257).

(64) Delzon, S, Douthe, C, Sala, A and Cochard, H (Nov. 2010). Mechanism of water-stress induced cavitation in conifers: bordered pit structure and function support the hypothesis of seal

capillary-seeding. *Plant, Cell and Environment 33*, 2101–2111 (cit. on p. 11).

(65) Denmead, O. and Shaw, R. H. (1962). Availability of soil water to plants as affected by soil moisture content and meteorological conditions. *Agronomy journal 54*, 385–390 (cit. on p. 298).

(66) Döll, P. and Siebert, S. (2002). Global modeling of irrigation water requirements. *Water Resources Research 38* (cit. on p. 6).

(67) Domec, J.-C., Scholz, F. G., Bucci, S. J., Meinzer, F. C., Goldstein, G. and Villalobos-Vega, R. (Jan. 2006). Diurnal and seasonal variation in root xylem embolism in neotropical savanna woody species: impact on stomatal control of plant water status., en *Plant, Cell & Environment 29*, 26–35, DOI: 10.1111/j.1365-3040.2005.01397.x (cit. on p. 10).

(68) Domec, J.-C., King, J. S., Noormets, A., Treasure, E., Gavazzi, M. J., Sun, G. and McNulty, S. G. (July 2010). Hydraulic redistribution of soil water by roots affects whole-stand evapotranspiration and net ecosystem carbon exchange., en *New Phytologist 187*, 171–183, DOI: 10.1111/j.1469-8137.2010.03245.x (cit. on p. 228).

(69) Donald, C. M. (1968). The breeding of crop ideotypes., en *Euphytica 17*, 385–403, DOI: 10.1007/BF00056241 (cit. on pp. 127, 294, 321).

(70) Doussan, C., Vercambre, G. and Pagès, L. (Feb. 1998). Modelling of the Hydraulic Architecture of Root Systems: An Integrated Approach to Water Absorption—Model Description. *Annals of Botany 81*, 213–223, DOI: 10.1006/anbo.1997.0540 (cit. on pp. 9, 20, 32, 43, 44, 47, 68, 69, 79, 80, 83, 93, 97, 99, 101, 102, 124, 125, 129, 136, 160, 161, 163–165, 168, 171, 175, 178, 182, 197, 205, 216, 234, 268, 270, 274, 287, 299, 323, 328, 331).

(71) Doussan, C, Vercambre, G and Pagès, L (Jan. 1998). Modelling of the hydraulic architecture of root systems: and integrated approach to water absorption - Distribution of axial and radial conductances in maize. *Annals of Botany 81*, 225–232 (cit. on pp. 137, 140, 301).

(72) Doussan, C., Pierret, A., Garrigues, E. and Pagès, L. (2006). Water uptake by plant roots: II–Modelling of water transfer in the soil root-system with explicit account of flow within the root system–Comparison with experiments. *Plant and soil 283*, 99–117 (cit. on pp. 7, 12, 14, 20, 160, 177, 210, 213, 266, 288, 301).

(73) Draye, X., Kim, Y., Lobet, G. and Javaux, M. (2010). Model-assisted integration of physiological and environmental constraints affecting the dynamic and spatial patterns of root water uptake from soils. *Journal of Experimental Botany 61*, 2145–2155 (cit. on pp. 12, 13, 19, 20, 165, 177, 199, 265, 266, 274, 287, 288, 301, 302).

(74) Drouet, J.-L. and Pagès, L (June 2003). GRAAL: a model of GRowth, Architecture and carbon ALlocation during the vegetative phase of the whole maize plant. Model description and parametrisation. *Ecological Modelling 165*, 143–173 (cit. on p. 299).

(75) Dunbabin, V. M., Postma, J. A., Schnepf, A., Pagès, L., Javaux, M., Wu, L., Leitner, D., Chen, Y. L., Rengel, Z. and Diggle, A. J. (2013). Modelling root–soil interactions using three–dimensional models of root growth, architecture and function. *Plant and soil 372*, 93–124 (cit. on pp. 20, 128, 210).

(76) Durand, J., Bariac, T., Ghesquière, M., Biron, P., Richard, P., Humphreys, M. and Zwierzykovski, Z. (May 2007). Ranking of the depth of water extraction by individual grass plants, using natural 18O isotope abundance., en *Environmental and Experimental Botany 60*, 137–144, DOI: 10.1016/j.envexpbot.2006.09.004 (cit. on p. 232).

(77) Ehlert, C., Maurel, C., Tardieu, F. and Simonneau, T. (2009). Aquaporin-mediated reduction in maize root hydraulic conductivity impacts cell turgor and leaf elongation even without changing transpiration. *Plant Physiology 150*, 1093–1104 (cit. on p. 199).

(78) Enstone, D. E., Peterson, C. A. and Ma, F. (Dec. 2002). Root Endodermis and Exodermis: Structure, Function, and Responses to the Environment., en *Journal of Plant Growth Regulation 21*,

335–351, DOI: 10.1007/s00344-003-0002-2 (cit. on pp. 9, 79, 160, 175).

(79) Esser, H. G., Carminati, A, Vontobel, P, Lehmann, E. H. and Oswald, S. E. (May 2010). Neutron radiography and tomography of water distribution in the root zone. *Journal of Plant Nutrition and Soil Science 173*, 757–764 (cit. on p. 23).

(80) Fan, M., Bai, R., Zhao, X. and Zhang, J. (2007). Aerenchyma formed under phosphorus deficiency contributes to the reduced root hydraulic conductivity in maize roots. *Journal of Integrative Plant Biology 49*, 598–604 (cit. on pp. 12, 198).

(81) *Strengthening the enabling environment for food security and nutrition*, eng; FAO, Ed.; The state of food insecurity in the world 2014, OCLC: 931799626; FAO: Rome, 2014 (cit. on p. 5).

(82) FAO, *The state of food insecurity in the world*, English; FAO: Rome, 2009 (cit. on pp. 5, 286).

(83) Farooq, M., Wahid, A., Kobayashi, N., Fujita, D. and Basra, S. M. A. (Mar. 2009). Plant drought stress: effects, mechanisms and management., en *Agronomy for Sustainable Development 29*, 185–212, DOI: 10.1051/agro:2008021 (cit. on pp. 6, 286).

(84) Feddes, R. and Raats, P. (2004). Parameterizing the soil–water–plant root system. *Unsaturated-zone Modeling: Progress, Challenges, Applications 6*, 95–141 (cit. on p. 209).

(85) Feddes, R. and Zaradny, H. (May 1978). Model for simulating soil-water content considering evapotranspiration — Comments. *Journal of Hydrology 37*, 393–397, DOI: 10.1016/0022-1694(78)90030-6 (cit. on pp. 160, 209).

(86) Fischer, G., van Velthuizen, H. T. and Nachtergaele, F. O. (2000). Global agro-ecological zones assessment: methodology and results. (cit. on p. 5).

(87) Fiscus, E. L. (Oct. 1977). Determination of Hydraulic and Osmotic Properties of Soybean Root Systems. *Plant Physiology 59*, 1013–1020 (cit. on p. 43).

(88) Fitter, A. H., Stickland, T. R., Harvey, M. L. and Wilson, G. W. (1991). Architectural analysis of plant root systems 1. Architectural correlates of exploitation efficiency. *New Phytologist 118*, 375–382 (cit. on p. 289).

(89) Flavel, R. J., Guppy, C. N., Tighe, M., Watt, M., McNeill, A. and Young, I. M. (Apr. 2012). Non-destructive quantification of cereal roots in soil using high-resolution X-ray tomography., en *Journal of Experimental Botany 63*, 2503–2511, DOI: 10.1093/jxb/err421 (cit. on p. 48).

(90) French, R. and Schultz, J. (1984). Water use efficiency of wheat in a Mediterranean-type environment. I. The relation between yield, water use and climate. *Australian Journal of Agricultural Research 35*, 743–764 (cit. on p. 286).

(91) Frensch, J. and Steudle, E. (1989). Axial and radial hydraulic resistance to roots of maize (Zea mays L.) *Plant Physiology 91*, 719–726 (cit. on pp. 48, 79, 93, 159, 172, 185, 204).

(92) Frensch, J., Hsiao, T. C. and Steudle, E. (1996). Water and solute transport along developing maize roots., en *Planta 198*, 348–355, DOI: 10.1007/BF00620050 (cit. on pp. 79, 198).

(93) Gaj, M., Beyer, M., Koeniger, P., Wanke, H., Hamutoko, J. and Himmelsbach, T. (Feb. 2016). In situ unsaturated zone water stable isotope (^{2}H and ^{18}O) measurements in semi-arid environments: a soil water balance., en *Hydrology and Earth System Sciences 20*, 715–731, DOI: 10.5194/hess-20-715-2016 (cit. on p. 251).

(94) Galvan-Ampudia, C. S., Julkowska, M. M., Darwish, E., Gandullo, J., Korver, R. A., Brunoud, G., Haring, M. A., Munnik, T., Vernoux, T. and Testerink, C. (2013). Halotropism is a response of plant roots to avoid a saline environment. *Current Biology 23*, 2044–2050 (cit. on p. 14).

(95) Gangi, L., Rothfuss, Y., Ogée, J., Wingate, L., Vereecken, H. and Brüggemann, N. (2015). A New Method for In Situ Measurements of Oxygen Isotopologues of Soil Water and Carbon Dioxide with High Time Resolution., en *Vadose Zone Journal 14*, 0, DOI: 10.2136/vzj2014.11.0169 (cit. on p. 252).

(96) Gao, Y., Duan, A., Qiu, X., Liu, Z., Sun, J., Zhang, J. and Wang, H. (2010). Distribution of roots and root length density in a maize/soybean strip intercropping system. *Agricultural water management 98*, 199–212 (cit. on pp. 140, 144).

(97) Gardner, W. R. (1960). Dynamic aspects of water availability to plants. *Soil science 89*, 63–73 (cit. on p. 209).

(98) Garrigues, E., Doussan, C. and Pierret, A. (2006). Water uptake by plant roots: I–Formation and propagation of a water extraction front in mature root systems as evidenced by 2D light transmission imaging. *Plant and soil 283*, 83–98 (cit. on pp. 23, 177, 213).

(99) Gebauer, R. and Volařík, D. (June 2013). Root hydraulic conductivity and vessel structure modification with increasing soil depth of two oak species: Quercus pubescens and Quercus robur., en *Trees 27*, 523–531, DOI: 10.1007/s00468-012-0805-5 (cit. on p. 11).

(100) Godfray, H. C. J., Beddington, J. R., Crute, I. R., Haddad, L., Lawrence, D., Muir, J. F., Pretty, J., Robinson, S., Thomas, S. M. and Toulmin, C. (2010). Food Security: The Challenge of Feeding 9 Billion People. *Science 327*, 812–818, DOI: 10.1126/science.1185383 (cit. on p. 5).

(101) Gonfiantini, R. (Feb. 1978). Standards for stable isotope measurements in natural compounds. *Nature 271*, 534–536, DOI: 10.1038/271534a0 (cit. on p. 229).

(102) Gonzalez-Dugo, V., Durand, J.-L., Gastal, F. and Picon-Cochard, C. (2005). Short-term response of the nitrogen nutrition status of tall fescue and Italian ryegrass swards under water deficit., en *Australian Journal of Agricultural Research 56*, 1269, DOI: 10.1071/AR05064 (cit. on p. 233).

(103) Green, S. R., Kirkham, M. and Clothier, B. E. (2006). Root uptake and transpiration: From measurements and models to sustainable irrigation. *Agricultural Water Management 86*, 165–176 (cit. on p. 208).

(104) Gregory, P. J., Ingram, J. S. I. and Brklacich, M (Nov. 2005). Climate change and food security. *Philosophical Transactions of the Royal Society B: Biological Sciences 360*, 2139–2148 (cit. on p. 6).

(105) Gruber, B. D., Giehl, R. F., Friedel, S. and von Wirén, N. (2013). Plasticity of the Arabidopsis root system under nutrient deficiencies. *Plant Physiology 163*, 161–179 (cit. on p. 13).

(106) Guswa, A. J. (2012). Canopy vs. Roots: Production and Destruction of Variability in Soil Moisture and Hydrologic Fluxes., en *Vadose Zone Journal 11*, 0, DOI: 10.2136/vzj2011.0159 (cit. on p. 229).

(107) Haber-Pohlmeier, S, Vanderborght, J and Pohlmeier, A Quantitative mapping of solute accumulation in a soil-root system by Magnetic Resonance imaging. *Water Resources Research* (cit. on p. 23).

(108) Hachez, C., Moshelion, M., Zelazny, E., Cavez, D. and Chaumont, F. (Sept. 2006). Localization and Quantification of Plasma Membrane Aquaporin Expression in Maize Primary Root: A Clue to Understanding their Role as Cellular Plumbers., en *Plant Molecular Biology 62*, 305–323, DOI: 10.1007/s11103-006-9022-1 (cit. on pp. 9, 10, 79).

(109) Hachez, C., Veselov, D., Ye, Q., Reinhardt, H., Knipfer, T., Fricke, W. and Chaumont, F. (Jan. 2012). Short-term control of maize cell and root water permeability through plasma membrane aquaporin isoforms: Maize root plasma membrane aquaporins., en *Plant, Cell & Environment 35*, 185–198, DOI: 10.1111/j.1365-3040.2011.02429.x (cit. on pp. 10, 51, 199).

(110) Haile, M. G., Wossen, T., Tesfaye, K. and von Braun, J. (2017). Impact of Climate Change, Weather Extremes, and Price Risk on Global Food Supply. *Economics of Disasters and Climate Change*, 1–21 (cit. on p. 5).

(111) Hall, A., Lemcoff, J. and Trapani, N. (1971). Water stress before and during flowering in maize and its effects on yield, its components, and their determinants. *Maydica (Italy)* (cit. on p. 6).

(112) Hammer, G., Dong, Z., Mclean, G., Doherty, A., Messina, C., Schussler, J., Zinselmeier, C., Paszkiewicz, S. and Cooper, M. (Jan. 2009). Can Changes in Canopy and/or Root System Architecture Explain Historical Maize Yield Trends in the U.S. Corn Belt? *Crop Science 49*, 299–312 (cit. on pp. 17, 127, 265).

(113) Hamza, M. and Aylmore, L. (1992). Soil solute concentration and water uptake by single lupin and radish plant roots. *Plant and soil 145*, 197–205 (cit. on pp. 176, 210).

(114) Hargreaves, G. H. (1974). Estimation of potential and crop evapotranspiration. *Transactions of the ASAE 17*, 701–0704 (cit. on p. 343).

(115) Hauck, A. L., Novais, J., Grift, T. E. and Bohn, M. O. (2015). Characterization of mature maize (Zea mays L.) root system architecture and complexity in a diverse set of Ex-PVP inbreds and hybrids. *SpringerPlus 4*, 424 (cit. on p. 126).

(116) Herkelrath, W., Miller, E. and Gardner, W. (1977). Water uptake by plants: II. The root contact model. *Soil Science Society of America Journal 41*, 1039–1043 (cit. on p. 209).

(117) Hinsinger, P., Brauman, A., Devau, N., Gérard, F., Jourdan, C., Laclau, J.-P., Cadre, E., Jaillard, B. and Plassard, C. (July 2011). Acquisition of phosphorus and other poorly mobile nutrients by roots. Where do plant nutrition models fail? *Plant and Soil 348*, 29–61 (cit. on p. 264).

(118) Hochholdinger, F., Woll, K., Sauer, M. and Dembinsky, D. (2004). Genetic dissection of root formation in maize (Zea mays) reveals root-type specific developmental programmes. *Annals of Botany 93*, 359–368 (cit. on pp. 126, 183).

(119) Huber, K., Vanderborght, J., Javaux, M., Schröder, N., Dodd, I. C. and Vereecken, H. (2014). Modelling the impact of heterogeneous rootzone water distribution on the regulation of transpiration by hormone transport and/or hydraulic pressures. *Plant and soil 384*, 93–112 (cit. on p. 210).

(120) Huber, K., Vanderborght, J., Javaux, M. and Vereecken, H. (2015). Simulating transpiration and leaf water relations in response to heterogeneous soil moisture and different stomatal control mechanisms. *Plant and soil 394*, 109–126 (cit. on pp. 127, 210).

(121) Hund, A, Trachsel, S and Stamp, P (2009). Growth of axile and lateral roots of maize: I development of a phenotying platform. *Plant and Soil 325*, 335–349 (cit. on p. 22).

(122) Hupet, F. and Vanclooster, M. (Mar. 2005). Micro-variability of hydrological processes at the maize row scale: implications for soil water content measurements and evapotranspiration estimates., en *Journal of Hydrology 303*, 247–270, DOI: 10.1016/j.jhydrol.2004.07.017 (cit. on p. 42).

(123) IPCC (2007). Synthesis Report. *Climate Change : Fourth Assessment* (cit. on p. 19).

(124) Iwata, S., Miyazawa, Y., Fujii, N. and Takahashi, H. (2013). MIZ1-regulated hydrotropism functions in the growth and survival of Arabidopsis thaliana under natural conditions. *Annals of botany 112*, 103–114 (cit. on p. 14).

(125) Iyer-Pascuzzi, A., Symonova, O., Mileyko, Y., Hao, Y., Belcher, H., Harer, J., Weitz, J. and Benfey, P. N. (Mar. 2010). Imaging and Analysis Platform for Automatic Phenotyping and Trait Ranking of Plant Root Systems. *Plant Physiology 152*, 1148–1157 (cit. on p. 22).

(126) Jackson, R. B., Sperry, J. S. and Dawson, T. E. (2000). Root water uptake and transport: using physiological processes in global predictions. *Trends in Plant Science 5*, 482–488 (cit. on p. 228).

(127) Jahnke, S., Menzel, M. I., van Dusschoten, D., Roeb, G. W., Bühler, J., Minwuyelet, S., Blümler, P., Temperton, V. M., Hombach, T., Streun, M., Beer, S., Khodaverdi, M., Ziemons, K., Coenen, H. H. and Schurr, U. (Aug. 2009). Combined MRI-PET dissects dynamic changes in plant structures and functions. *The Plant Journal 59*, 634–644 (cit. on p. 22).

(128) Jarvis, P. G. (Feb. 1976). The Interpretation of the Variations in Leaf Water Potential and Stomatal Conductance Found in Canopies in the Field. *Philosophical Transactions of the Royal Society B: Biological Sciences 273*, 593–610 (cit. on pp. 15, 209).

(129) Javaux, M., Schröder, T., Vanderborght, J. and Vereecken, H. (2008). Use of a three-dimensional detailed modeling approach for predicting root water uptake. *Vadose Zone Journal 7*, 1079–1088 (cit. on pp. 18, 20, 23, 43, 46, 56, 64, 80, 111, 128, 159, 160, 184, 210, 229, 230, 233, 235, 267, 269, 270, 299).

(130) Javaux, M., Rothfuss, Y., Vanderborght, J., Vereecken, H. and Brüggemann, N. (Aug. 2016). Isotopic composition of plant water sources. *Nature 536*, E1–E3, DOI: 10.1038/nature18946 (cit. on p. 229).

(131) Javaux, M., Couvreur, V., Vanderborght, J. and Vereecken, H. (2013). Root Water Uptake: From Three-Dimensional Biophysical Processes to Macroscopic Modeling Approaches., en *Vadose Zone Journal 12*, 0, DOI: 10.2136/vzj2013.02.0042 (cit. on pp. 14, 21, 42, 209, 230, 234, 266, 274, 282).

(132) Javot, H, Lauvergeat, V, Santoni, V, Martin-Laurent, F, Guclu, J, Vinh, J, Heyes, J, Franck, K. I., Schaffner, A. R., Bouchez, D and Maurel, C (2003). Role of a Single Aquaporin Isoform in Root Water Uptake. *Plant Cell 15*, 509–522. (Cit. on pp. 10, 108).

(133) Jensen, M. E. (1968). Water consumption by agricultural plants (Chapter 1). (cit. on p. 6).

(134) Johnson, D. M., McCulloh, K. A., Woodruff, D. R. and Meinzer, F. C. (2012). Evidence for xylem embolism as a primary factor in dehydration-induced declines in leaf hydraulic conductance. *Plant, Cell and Environment 35*, 760–769 (cit. on p. 11).

(135) Katul, G. G. and Siqueira, M. B. (July 2010). Biotic and abiotic factors act in coordination to amplify hydraulic redistribution and lift: Commentary., en *New Phytologist 187*, 3–6, DOI: 10.1111/j.1469-8137.2010.03306.x (cit. on p. 228).

(136) Keating, B. A. et al. (2003). An overview of APSIM, a model designed for farming systems simulation. *European Journal of Agronomy 18*, 267–288 (cit. on p. 288).

(137) Kellermeier, F., Chardon, F. and Amtmann, A. (2013). Natural variation of Arabidopsis root architecture reveals complementing adaptive strategies to potassium starvation. *Plant Physiology 161*, 1421–1432 (cit. on p. 13).

(138) Kirkegaard, J., Lilley, J., Howe, G. and Graham, J. (2007). Impact of subsoil water use on wheat yield. *Australian Journal of Agricultural Research 58*, 303–315 (cit. on p. 286).

(139) Knipfer, T, Besse, M., Verdeil, J.-L. and Fricke, W (Feb. 2011). Aquaporin-facilitated water uptake in barley (Hordeum vulgare L.) roots. *Journal of Experimental Botany 62*, 4115–4126. (Cit. on pp. 9, 160).

(140) Koebernick, N., Huber, K., Kerkhofs, E., Vanderborght, J., Javaux, M., Vereecken, H. and Vetterlein, D. (2015). Unraveling the hydrodynamics of split root water uptake experiments using CT scanned root architectures and three dimensional flow simulations. *Frontiers in plant science 6* (cit. on pp. 210, 211).

(141) Kuchenbuch, R. O., Gerke, H. H. and Buczko, U. (2009). Spatial distribution of maize roots by complete 3D soil monolith sampling. *Plant and soil 315*, 297–314 (cit. on p. 209).

(142) Lambot, S., Binley, A., Slob, E. and Hubbard, S. (Feb. 2008). Ground Penetrating Radar in Hydrogeophysics. *Vadose Zone Journal 7*, 137 (cit. on p. 23).

(143) Lambot, S., Javaux, M., Hupet, F. and Vanclooster, M. (2002). A global multilevel coordinate search procedure for estimating the unsaturated soil hydraulic properties. *Water Resources Research 38* (cit. on p. 168).

(144) Lamy, J.-B., Delzon, S., Bouche, P. S., Alia, R., Vendramin, G. G., Cochard, H. and Plomion, C. (2014). Limited genetic variability and phenotypic plasticity detected for cavitation resistance in a Mediterranean pine. *New Phytologist 201*, 874–886 (cit. on p. 11).

(145) Landsberg, J. J. and Fowkes, N. D. (May 1978). Water Movement Through Plant Roots., en *Annals of Botany 42*, 493–508, DOI: 10.1093/oxfordjournals.aob.a085488 (cit. on pp. 43, 45, 51, 68, 71, 75, 79–82, 86, 90, 94, 110, 112, 129, 176, 190, 204, 269, 323).

(146) Lawlor, D and Cornic, G (2002). Photosynthetic carbon assimilation and associated metabolism in relation to water deficits in higher plants. *Plant, cell & environment 25*, 275–294 (cit. on p. 6).

(147) Leitner, D, Klepsch, S, Ptashnyk, M, Marchant, A, Kirk, G., Schnepf, A and Roose, T (2010). A dynamic model of nutrient uptake by root hairs. *New Phytologist 185*, 792–802 (cit. on pp. 265, 267).

(148) Leitner, D., Meunier, F., Bodner, G., Javaux, M. and Schnepf, A. (June 2014). Impact of contrasted maize root traits at flowering on water stress tolerance – A simulation study., en *Field Crops Research*, DOI: 10.1016/j.fcr.2014.05.009 (cit. on pp. 78, 109, 127, 159, 178, 182, 211, 213, 300, 302).

(149) Levin, A., Shaviv, A. and Indelman, P. (Oct. 2007). Influence of root resistivity on plant water uptake mechanism, part I: numerical solution., en *Transport in Porous Media 70*, 63–79, DOI: 10.1007/s11242-006-9084-1 (cit. on p. 12).

(150) Levitt, J. et al. (1972). Response of plants to environmental stresses. *Water, radiation, Salt and other stresses 2* (cit. on p. 288).

(151) Lhomme, J.-P. (1998). Formulation of root water uptake in a multi-layer soil-plant model: does van den Honert's equation hold?, en *Hydrology and Earth System Sciences 2*, 31–39, DOI: 10.5194/hess-2-31-1998 (cit. on p. 46).

(152) Li, X, Wang, X, Yang, Y, Li, R, He, Q, Fang, X, Luu, D. T., Maurel, C and Lin, J (2011). Single-Molecule Analysis of PIP2;1 Dynamics and Partitioning Reveals Multiple Modes of Arabidopsis Plasma Membrane Aquaporin Regulation. *Plant Cell 23*, 3780–3797 (cit. on p. 10).

(153) Li, Y, Sperry, J. S. and Shao, M (2009). Hydraulic conductance and vulnerability to cavitation in corn (Zea mays L.) hybrids of differing drought resistance. *Environmental and Experimental Botany 66*, 341–346 (cit. on p. 11).

(154) Lilley, J. and Kirkegaard, J. (2011). Benefits of increased soil exploration by wheat roots. *Field Crops Research 122*, 118–130 (cit. on pp. 286, 290).

(155) Lobet, G., Couvreur, V., Meunier, F., Javaux, M. and Draye, X. (Feb. 2014). Plant Water Uptake in Drying Soils., en *Plant Physiology*, DOI: 10.1104/pp.113.233486 (cit. on pp. 78, 160, 182, 208).

(156) Lobet, G. Regulation of water flow in the soil-root domain. New tools and methods., Ph.D. Thesis, Université catholique de Louvain, 2012 (cit. on p. 214).

(157) Lobet, G. and Draye, X. (2013). Novel scanning procedure enabling the vectorization of entire rhizotron-grown root systems. *Plant Methods 9*, 1 (cit. on pp. 22, 48, 210).

(158) Lobet, G., Pagès, L. and Draye, X. (Sept. 2011). A Novel Image-Analysis Toolbox Enabling Quantitative Analysis of Root System Architecture. *Plant Physiology 157*, 29–39 (cit. on pp. 22, 48, 214).

(159) Lobet, G., Draye, X. and Périlleux, C. (2013). An online database for plant image analysis software tools. *Plant methods 9*, 38 (cit. on p. 22).

(160) Lobet, G., Pound, M. P., Diener, J., Pradal, C., Draye, X., Godin, C., Javaux, M., Leitner, D., Meunier, F., Nacry, P., Pridmore, T. P. and Schnepf, A. (Mar. 2015). Root System Markup Language: Toward a Unified Root Architecture Description Language., en *Plant Physiology 167*, 617–627, DOI: 10.1104/pp.114.253625 (cit. on p. 48).

(161) Lobet, G., Pound, M. P., Diener, J., Pradal, C., Draye, X., Godin, C., Javaux, M., Leitner, D., Meunier, F., Nacry, P., Pridmore, T. P. and Schnepf, A. (Mar. 2015). Root System Markup Language: Toward a Unified Root Architecture Description Language., en

Plant Physiology 167, 617–627, DOI: 10.1104/pp.114.253625 (cit. on p. 125).

(162) Ludwig, F., Dawson, T. E., de Kroon, H., Berendse, F. and Prins, H. H. T. (Feb. 2003). Hydraulic lift in Acacia tortilis trees on an East African savanna., en *Oecologia 134*, 293–300, DOI: 10.1007/s00442-002-1119-x (cit. on p. 229).

(163) Lynch, J. P. (2007). Roots of the second green revolution. *Australian Journal of Botany 55*, 493–512 (cit. on p. 264).

(164) Lynch, J. P. (2013). Steep, cheap and deep: an ideotype to optimize water and N acquisition by maize root systems. *Annals of Botany*, DOI: 10.1093/aob/mcs293 (cit. on pp. 12, 17, 127, 136, 140, 178, 183, 265, 272, 291, 294, 321).

(165) Lynch, J. P. and Brown, K. M. (Apr. 2012). New roots for agriculture: exploiting the root phenome. *Philosophical Transactions of the Royal Society B: Biological Sciences 367*, 1598–1604 (cit. on pp. 13, 183).

(166) Lynch, J. P., Nielsen, K. L., Davis, R. D. and Jablokow, A. G. (1997). SimRoot: Modelling and visualization of root systems. *Plant and Soil 188*, 139–151 (cit. on p. 68).

(167) Mach, K. In *2017 AAAS Annual Meeting (February 16-20, 2017)*, 2017 (cit. on p. 5).

(168) Mairhofer, S., Zappala, S., Tracy, S. R., Sturrock, C., Bennett, M., Mooney, S. J. and Pridomore, T. (2012). RooTrak: Automated Recovery of Three-Dimensional Plant Root Architecture in Soil from X-Ray Microcomputed Tomography Images Using Visual Tracking. *Plant Physiology 158*, 561–569 (cit. on p. 22).

(169) Manschadi, A. M., Hammer, G. L., Christopher, J. T. and deVoil, P (2008). Genotypic variation in seedling root architectural traits and implications for drought adaptation in wheat (Triticum aestivum L.) *Plant and Soil 303*, 115–129 (cit. on p. 287).

(170) Manschadi, A. M., Christopher, J., Hammer, G. L., et al. (2006). The role of root architectural traits in adaptation of wheat to water-limited environments. *Functional plant biology 33*, 823–837 (cit. on p. 290).

(171) Manschadi, A., Christopher, J., Hammer, G. and Devoil, P (2010). Experimental and modelling studies of drought-adaptive root architectural traits in wheat (Triticum aestivum L.) *Plant Biosystems 144*, 458–462 (cit. on p. 17).

(172) Martre, P, Cochard, H and Durand, J.-L. (2001). Hydraulic architecture and water flow in growing grass tillers (Festuca arundinacea Schreb.) *Plant, Cell and Environment 24*, 65–76 (cit. on pp. 158, 182).

(173) Maurel, C and Chrispeels, M. J. (2001). Aquaporins. A Molecular Entry into Plant Water Relations. *Plant Physiology 125*, 135–138. (Cit. on p. 10).

(174) McCole, A. A. and Stern, L. A. (Sept. 2007). Seasonal water use patterns of Juniperus ashei on the Edwards Plateau, Texas, based on stable isotopes in water., en *Journal of Hydrology 342*, 238–248, DOI: 10.1016/j.jhydrol.2007.05.024 (cit. on p. 229).

(175) McCulloh, K., Sperry, J. S., Lachenbruch, B., Meinzer, F. C., Reich, P. B. and Voelker, S. (2010). Moving water well: comparing hydraulic efficiency in twigs and trunks of coniferous, ring-porous, and diffuse-porous saplings from temperate and tropical forests. *New Phytologist 186*, 439–450 (cit. on p. 11).

(176) McCully, M. E. and Canny, M. J. (1988). Pathways and processes of water and nutrient movement in roots. *Plant and Soil 111*, 159–170, DOI: 10.1007/BF02139932 (cit. on p. 79).

(177) McElrone, A. J., Choat, B., Gambetta, G. A. and Brodersen, C. R. (2013). Water Uptake and Transport in Vascular Plants. *Nature Education Knowledge 5*, 6 (cit. on p. 78).

(178) McLean, E. H., Ludwig, M. and Grierson, P. F. (2011). Root hydraulic conductance and aquaporin abundance respond rapidly to partial root-zone drying events in a riparian Melaleuca species. *New Phytologist 192* (cit. on p. 160).

(179) McMichael, B. and Lascano, R. J. (2010). Evaluation of hydraulic lift in cotton (Gossypium hirsutum L.) germplasm. *Environmental and experimental botany 68*, 26–30 (cit. on p. 18).

(180) Medlyn, B. E. and McMurtrie, R. E. In *A History of Atmospheric CO2 and Its Effects on Plants, Animals, and Ecosystems*; Springer: 2005, pp 441–467 (cit. on p. 336).

(181) Meinzer, F. C., Brooks, J. R., Bucci, S., Goldstein, G., Scholz, F. G. and Warren, J. M. (Aug. 2004). Converging patterns of uptake and hydraulic redistribution of soil water in contrasting woody vegetation types., en *Tree Physiology 24*, 919–928, DOI: 10.1093/treephys/24.8.919 (cit. on p. 228).

(182) Meisey, P and Edmeades, G Maize production in drought-stressed environments: Technical options and research resource allocation., tech. rep., CIMMYT, México, DF (México)., 1998 (cit. on p. 266).

(183) Meunier, F., Couvreur, V., Draye, X., Vanderborght, J. and Javaux, M. (2016). Water movement through plant roots: Exact solutions of the water flow equation in roots with varying hydraulic properties. *Hydrology and Earth System Sciences Discussions 2016*, 1–35, DOI: 10.5194/hess-2016-633 (cit. on pp. 186, 190, 205).

(184) Meunier, F., Javaux, M., Couvreur, V., Draye, X. and Vanderborght, J. In *Functional-Structural Plant Growth Modeling, Simulation, Visualization and Applications (FSPMA), International Conference on*, 2016, pp 140–149 (cit. on pp. 56, 95).

(185) Meunier, F., Couvreur, V., Draye, X., Vanderborght, J and Javaux, M. (2017). Towards quantitative root hydraulic phenotyping: novel mathematical functions to calculate plant-scale hydraulic parameters from root system functional and structural traits. *Journal of Mathematical Biology*, 1–38 (cit. on pp. 43, 45, 79, 84, 90, 95, 133, 184, 199, 295).

(186) Mir, R. R., Zaman-Allah, M., Sreenivasulu, N., Trethowan, R. and Varshney, R. K. (2012). Integrated genomics, physiology and breeding approaches for improving drought tolerance in

crops. *Theoretical and Applied Genetics 125*, 625–645, DOI: 10.1007/s00122-012-1904-9 (cit. on p. 127).

(187) Molz, F. J. and Remson, I. (1970). Extraction term models of soil moisture use by transpiring plants. *Water Resources Research 6*, 1346–1356 (cit. on p. 209).

(188) Mooney, S. J., Pridmore, T. P., Helliwell, J. and Bennett, M. J. (Nov. 2011). Developing X-ray Computed Tomography to non-invasively image 3-D root systems architecture in soil. *Plant and Soil 352*, 1–22 (cit. on pp. 22, 209).

(189) Moore, G. and Ryder, C. (2015). The Use of Ground-Penetrating Radar to Locate Tree Roots. *Arboriculture & Urban Forestry 41* (cit. on p. 23).

(190) Moradi, A. B., Carminati, A., Vetterlein, D., Vontobel, P., Lehmann, E., Weller, U., Hopmans, J. W., Vogel, H.-J. and Oswald, S. E. Three-dimensional visualization and quantification of water content in the rhizosphere. *New Phytologist 192*, 653–663 (cit. on p. 178).

(191) Mori, M and Inagaki, M (2012). Root development and water-uptake under water deficit stress in drought-adaptive wheat genotypes. *Cereal Research Communications 40*, 44–52 (cit. on p. 286).

(192) Mualem, Y. (1976). A new model for predicting the hydraulic conductivity of unsaturated porous media. *Water resources research 12*, 513–522 (cit. on p. 275).

(193) Musters, P. A. D. and Bouten, W. (2000). A method for identifying optimum strategies of measuring soil water contents for calibrating a root water uptake model. *Journal of hydrology 227*, 273–286 (cit. on p. 42).

(194) Nachtergaele, F., van Velthuizen, H., Verelst, L., Batjes, N., Dijkshoorn, K., van Engelen, V., Fischer, G., Jones, A., Montanarella, L., Petri, M., et al. (2009). Harmonized world soil database. *Wageningen: ISRIC* (cit. on p. 342).

(195) Nadezhdina, N. and Čermák, J. (2003). Instrumental methods for studies of structure and function of root systems of large trees. *Journal of Experimental Botany 54*, 1511–1521 (cit. on p. 23).

(196) Neumann, R. B. and Cardon, Z. G. (Apr. 2012). The magnitude of hydraulic redistribution by plant roots: a review and synthesis of empirical and modeling studies: Tansley review., en *New Phytologist 194*, 337–352, DOI: 10.1111/j.1469-8137.2012.04088.x (cit. on pp. 228, 250).

(197) Nimah, M. N. and Hanks, R. J. (1973). Model for Estimating Soil Water, Plant, and Atmospheric Interrelations: I. Description and Sensitivity1., en *Soil Science Society of America Journal 37*, 522, DOI: 10.2136/sssaj1973.03615995003700040018x (cit. on p. 46).

(198) North, G. B. and Nobel, P. S. (July 1991). Changes in Hydraulic Conductivity and Anatomy Caused by Drying and Rewetting Roots of Agave deserti (Agavaceae). *American Journal of Botany 78*, 906–915, DOI: 10.2307/2445169 (cit. on pp. 42, 43, 108, 160).

(199) Oki, T. and Kanae, S. (Aug. 2006). Global Hydrological Cycles and World Water Resources. *Science 313*, 1068–1072, DOI: 10.1126/science.1128845 (cit. on p. 6).

(200) *Climate change 2014: synthesis report*, eng; Pachauri, R. K., Mayer, L. and Intergovernmental Panel on Climate Change, Eds., OCLC: 914851124; Intergovernmental Panel on Climate Change: Geneva, Switzerland, 2015 (cit. on p. 6).

(201) Pagès, L, Serra, V., Draye, X., Doussan, C and Pierret, A (July 2010). Estimating root elongation rates from morphological measurements of the root tip. *Plant and Soil 328*, 35–44 (cit. on p. 12).

(202) Pages, L., Jordan, M.-O. and Picard, D. (1989). A simulation model of the three-dimensional architecture of the maize root system. *Plant and Soil 119*, 147–154 (cit. on p. 272).

(203) Pagès, L., Vercambre, G., Drouet, J. L., Lecompte, F., Collet, C. and Le Bot, J. (2004). Root Typ: a generic model to depict and analyse the root system architecture. *Plant and Soil 258*, 103–119 (cit. on pp. 48, 55, 56, 89, 97, 122, 128, 131, 209, 237, 252).

(204) Passioura, J. B. (2012). Phenotyping for drought tolerance in grain crops: when is it useful to breeders?, en *Functional Plant Biology 39*, 851, DOI: 10.1071/FP12079 (cit. on p. 13).

(205) Passioura, J. B. (1980). The transport of water from soil to shoot in wheat seedlings. *Journal of Experimental Botany 31*, 333–345 (cit. on pp. 78, 182).

(206) Passioura, J. B. (1988). Water Transport in and to Roots. *Annual Review of Plant Physiology and Plant Molecular Biology 39*, 245–265 (cit. on pp. 158, 177).

(207) Passioura, J. (1977). Grain yield, harvest index, and water use of wheat. *Journal of the Australian Institute of Agricultural Science* (cit. on pp. 264, 286).

(208) Passioura, J. (Jan. 1984). Hydraulic Resistance of Plants. I. Constant or Variable? *Functional Plant Biology 11*, 333–339 (cit. on pp. 16, 42).

(209) Peterson, C., Murrmann, M. and Steudle, E. (May 1993). Location of the major barriers to water and ion movement in young roots of Zea mays L., en *Planta 190*, DOI: 10.1007/BF00195684 (cit. on p. 7).

(210) Pinheiro, H. A., DaMatta, F., Chaves, A. R. M., Loureiro, M. E. and Ducatti, C (Apr. 2005). Drought Tolerance is Associated with Rooting Depth and Stomatal Control of Water Use in Clones of Coffea canephora. *Annals of Botany 96*, 101–108 (cit. on p. 17).

(211) Pound, M. P., French, A. P., Atkinson, J. A., Wells, D. M., Bennett, M. J. and Pridmore, T. (2013). RootNav: navigating images of complex root architectures. *Plant Physiology 162*, 1802–1814 (cit. on p. 22).

(212) Press, W. H. et al. Numerical recipes in Fortran 90: the art of parallel scientific computing., 2012 (cit. on p. 270).

(213) Prieto, I., Armas, C. and Pugnaire, F. I. (2012). Water release through plant roots: new insights into its consequences at the plant and ecosystem level., en *New Phytologist 193*, 830–841, DOI: 10.1111/j.1469-8137.2011.04039.x (cit. on p. 229).

(214) Purushothaman, R., Zaman-Allah, M., Mallikarjuna, N., Pannirselvam, R., Krishnamurthy, L. and Gowda, C. L. L. (2013). Root anatomical traits and their possible contribution to drought tolerance in grain legumes. *Plant Production Science 16*, 1–8 (cit. on p. 11).

(215) Richards, J. H. and Caldwell, M. M. (Oct. 1987). Hydraulic lift: Substantial nocturnal water transport between soil layers by Artemisia tridentata roots., en *Oecologia 73*, 486–489, DOI: 10.1007/BF00379405 (cit. on p. 228).

(216) Richards, L. A (1931). Capillary conduction of liquids through porous mediums. *Physics-a Journal of General and Applied Physics 1*, 318–333 (cit. on pp. 58, 208).

(217) Richards, R. and Passioura, J. (1989). A breeding program to reduce the diameter of the major xylem vessel in the seminal roots of wheat and its effect on grain yield in rain-fed environments. *Australian Journal of Agricultural Research 40*, 943–950 (cit. on pp. 11, 265, 286).

(218) Richardson, L. F., *Weather prediction by numerical process*; Cambridge University Press: 2007 (cit. on p. 235).

(219) Rieger, M. and Litvin, P. (1999). Root system hydraulic conductivity in species with contrasting root anatomy. *Journal of Experimental Botany 50*, 201–209 (cit. on p. 199).

(220) Robinson, D. A., Jones, S. B., Wraith, J. M., Or, D and Friedman, S. P. (Nov. 2003). A Review of Advances in Dielectric and Electrical Conductivity Measurement in Soils Using Time Domain Reflectometry. *Vadose Zone Journal 2*, 444–475 (cit. on p. 23).

(221) Roose, T. and Fowler, A. (May 2004). A model for water uptake by plant roots., en *Journal of Theoretical Biology 228*, 155–171, DOI: 10.1016/j.jtbi.2003.12.012 (cit. on pp. 43, 160, 177).

(222) Roose, T. and Schnepf, A. (2008). Mathematical models of plant–soil interaction. *Philosophical Transactions of the Royal Society A: Mathematical, Physical and Engineering Sciences 366*, 4597–4611 (cit. on pp. 79, 106).

(223) Rothfuss, Y., Merz, S., Vanderborght, J., Hermes, N., Weuthen, A., Pohlmeier, A., Vereecken, H. and Brüggemann, N. (Oct. 2015). Long-term and high-frequency non-destructive monitoring of water stable isotope profiles in an evaporating soil column., en *Hydrology and Earth System Sciences 19*, 4067–4080, DOI: 10.5194/hess-19-4067-2015 (cit. on p. 252).

(224) Rothfuss, Y. and Javaux, M. (May 2017). Reviews and syntheses: Isotopic approaches to quantify root water uptake: a review and comparison of methods., en *Biogeosciences 14*, 2199–2224, DOI: 10.5194/bg-14-2199-2017 (cit. on p. 229).

(225) Rothfuss, Y., Braud, I., Le Moine, N., Biron, P., Durand, J.-L., Vauclin, M. and Bariac, T. (June 2012). Factors controlling the isotopic partitioning between soil evaporation and plant transpiration: Assessment using a multi-objective calibration of SiSPAT-Isotope under controlled conditions., en *Journal of Hydrology 442-443*, 75–88, DOI: 10.1016/j.jhydrol.2012.03.041 (cit. on p. 240).

(226) Rothfuss, Y., Vereecken, H. and Brüggemann, N. (June 2013). Monitoring water stable isotopic composition in soils using gas-permeable tubing and infrared laser absorption spectroscopy: Monitoring Water Stable Isotopic Composition in Soils., en *Water Resources Research 49*, 3747–3755, DOI: 10.1002/wrcr.20311 (cit. on p. 251).

(227) Rothfuss, Y., Biron, P., Braud, I., Canale, L., Durand, J.-L., Gaudet, J.-P., Richard, P., Vauclin, M. and Bariac, T. (June 2010). Partitioning evapotranspiration fluxes into soil evaporation and plant transpiration using water stable isotopes under

controlled conditions., en *Hydrological Processes 24*, 3177–3194, DOI: 10.1002/hyp.7743 (cit. on p. 231).

(228) Sanderson, J. (1983). Water Uptake by Different Regions of the Barley Root. Pathways of Radial Flow in Relation to Development of the Endodermis., en *Journal of Experimental Botany 34*, 240–253, DOI: 10.1093/jxb/34.3.240 (cit. on p. 79).

(229) Sanderson, J., Whitbread, F. C. and Clarkson, D. T. (1988). Persistent xylem cross-walls reduce the axial hydraulic conductivity in the apical 20 cm of barley seminal root axes: implications for the driving force for water movement. *Plant, Cell & Environment 11*, 247–256 (cit. on p. 48).

(230) Schenk, H. J. and Jackson, R. B. (2002). Rooting depths, lateral root spreads and below-ground/above-ground allometries of plants in water-limited ecosystems. *Journal of Ecology 90*, 480–494 (cit. on p. 290).

(231) Schneider, C., Attinger, S, Delfs, J.-O. and Hildebrandt, A (2010). Implementing small scale processes at the soil-plant interface–the role of root architectures for calculating root water uptake profiles. *Hydrology and Earth System Sciences 14*, 279–289 (cit. on p. 210).

(232) Schnepf, A., Leitner, D., Landl, M., Lobet, G., Mai, T. H., Morandage, S., Sheng, C., Zoerner, M., Vanderborght, J. and Vereecken, H. (2017). CRootBox: A Structural-Functional Modelling Framework For Root Systems. *bioRxiv*, 139980 (cit. on pp. 128, 129, 134, 183).

(233) Scholander, P. F., Hammel, H. T., Bradstreet, E. D. and Hemmingsen, E. A. (1965). Sap Pressure in Vascular Plants. *Science 148*, 339–346 (cit. on p. 161).

(234) Scholz, F. G., Bucci, S. J., Hoffmann, W. A., Meinzer, F. C. and Goldstein, G. (Apr. 2010). Hydraulic lift in a Neotropical savanna: Experimental manipulation and model simulations., en *Agricultural and Forest Meteorology 150*, 629–639, DOI: 10.1016/j.agrformet.2010.02.001 (cit. on p. 228).

(235) Schoppach, R. and Sadok, W. (2012). Differential sensitivities of transpiration to evaporative demand and soil water deficit among wheat elite cultivars indicate different strategies for drought tolerance., English *Environmental and Experimental Botany 84*, 1–10, DOI: 10.1016/j.envexpbot.2012.04.016 (cit. on p. 19).

(236) Schoppach, R., Wauthelet, D., Jeanguenin, L. and Sadok, W. (2014). Conservative water use under high evaporative demand associated with smaller root metaxylem and limited trans-membrane water transport in wheat., en *Functional Plant Biology 41*, 257, DOI: 10.1071/FP13211 (cit. on pp. 17, 184).

(237) Schröder, T, Tang, L, Javaux, M, Vanderborght, J, Körfgen, B and Vereecken, H (2009). A grid refinement approach for a three-dimensional soil-root water transfer model. *Water Resour. Res. 45*, W10412 (cit. on p. 43).

(238) Schroeder, T., Javaux, M., Vanderborght, J, Koerfgen, B. and Vereecken, H (2008). Effect of local soil hydraulic conductivity drop using a three-dimensional root water uptake model. *Vadose Zone Journal 7*, 1089–1098 (cit. on pp. 18, 20, 257).

(239) Schröder, N., Javaux, M., Vanderborght, J., Steffen, B. and Vereecken, H. (2012). Effect of root water and solute uptake on apparent soil dispersivity: A simulation study. *Vadose Zone Journal 11* (cit. on pp. 20, 210, 236).

(240) Schröder, N., Lazarovitch, N., Vanderborght, J., Vereecken, H. and Javaux, M. (Apr. 2014). Linking transpiration reduction to rhizosphere salinity using a 3D coupled soil-plant model., en *Plant and Soil 377*, 277–293, DOI: 10.1007/s11104-013-1990-8 (cit. on p. 210).

(241) Schwartz, N., Carminati, A. and Javaux, M. (Jan. 2016). The impact of mucilage on root water uptake-A numerical study: Rhizo-RSWMS., en *Water Resources Research 52*, 264–277, DOI: 10.1002/2015WR018150 (cit. on pp. 177, 337).

(242) Schymanski, S. J., Or, D. and Zwieniecki, M. (2013). Stomatal control and leaf thermal and hydraulic capacitances under rapid environmental fluctuations. *PloS one 8*, e54231 (cit. on p. 336).

(243) Semenov, M. A., Barrow, E. M. and Lars-Wg, A (2002). A stochastic weather generator for use in climate impact studies. *User Man Herts UK* (cit. on p. 343).

(244) Shane, M., McCully, M. E. and Canny, M. (2000). Architecture of branch-root junctions in maize: structure of the connecting xylem and the porosity of pit membranes. *Annals of Botany 85*, 613–624 (cit. on p. 198).

(245) Shaw, R. (1977). Water use and requirements of maize-a review. *Agrometeorology of the maize (corn) crop 480*, 119–134 (cit. on p. 266).

(246) Simunek, J., Huang, K. and Van Genuchten, M. T. (1995). The SWMS_3D code for simulating water flow and solute transport in three-dimensional variably-saturated media. *Rep 139* (cit. on p. 268).

(247) Smith, S and de Smet, I (Apr. 2012). Root system architecture: insights from Arabidopsis and cereal crops. *Philosophical Transactions of the Royal Society B: Biological Sciences 367*, 1441–1452 (cit. on p. 264).

(248) Somma, F., Hopmans, J. W. and Clausnitzer, V. (1998). Transient three-dimensional modeling of soil water and solute transport with simultaneous root growth, root water and nutrient uptake. *Plant and Soil 202*, 281–293 (cit. on pp. 48, 209, 267).

(249) Sperry, J. S., Adler, F. R., Campbell, G. S. and Comstock, J. P. (1998). Limitation of plant water use by rhizosphere and xylem conductance: results from a model. *Plant, Cell and Environment 21*, 347–359 (cit. on p. 288).

(250) Sperry, J. S. and Tyree, M. T. (1988). Mechanism of water stress-induced xylem embolism. *Plant Physiology 88*, 581–587 (cit. on p. 198).

(251) Sposito, G. (2013). Green Water and Global Food Security. *Vadose Zone Journal 12*, DOI: 10.2136/vzj2013.02.0041 (cit. on p. 6).

(252) St. Aubin, G, Canny, M. and McCully, M. (1986). Living vessel elements in the late metaxylem of sheathed maize roots. *Annals of Botany 58*, 577–588 (cit. on p. 197).

(253) Steele, K. A., Price, A. H., Witcombe, J. R., Shrestha, R., Singh, B. N., Gibbons, J. M. and Virk, D. S. (Sept. 2012). QTLs associated with root traits increase yield in upland rice when transferred through marker-assisted selection. *TAG Theoretical and Applied Genetics* (cit. on p. 17).

(254) Steudle, E (2001). The cohesion-tension mechanism and the acquisition of water by plant roots. *Annual Review of Plant Physiology and Plant Molecular Biology 53*, 847–875 (cit. on p. 7).

(255) Steudle, E (Jan. 2000). Water uptake by plant roots: an integration of views. *Plant and Soil 226*, 45–56 (cit. on pp. 11, 182).

(256) Steudle, E and Boyer, J. (1985). Hydraulic resistance to radial water flow in growing hypocotyl of soybean measured by a new pressure-perfusion technique. *Planta 164*, 189–200 (cit. on p. 198).

(257) Steudle, E. (Sept. 2000). Water uptake by roots: effects of water deficit., en *Journal of Experimental Botany 51*, 1531–1542, DOI: 10.1093/jexbot/51.350.1531 (cit. on p. 79).

(258) Steudle, E. and Peterson, C. A. (May 1998). How does water get through roots?, en *Journal of Experimental Botany 49*, 775–788, DOI: 10.1093/jxb/49.322.775 (cit. on pp. 22, 79, 81, 158, 175, 208).

(259) Stingaciu, L. R., Weihermüller, L., Pohlmeier, A., Stapf, S. and Vereecken, H. In *AIP Conference Proceedings*, 2011; Vol. 1330, p 77 (cit. on p. 209).

(260) Stingaciu, L., Schulz, H., Pohlmeier, A., Behnke, S., Zilken, H., Javaux, M. and Vereecken, H. (2013). In Situ Root System Architecture Extraction from Magnetic Resonance Imaging for Water Uptake Modeling., en *Vadose Zone Journal 0*, 0, DOI: 10.2136/vzj2012.0019 (cit. on pp. 22, 48).

(261) Sutka, M, Li, G, Boudet, J, Boursiac, Y, Doumas, P and Maurel, C (2011). Natural variation of root hydraulics in Arabidopsis grown in normal and salt-stressed conditions. *Plant Physiology 155*, 1264–1276 (cit. on p. 9).

(262) Tang, J., Riley, W. J. and Niu, J. (2015). Incorporating root hydraulic redistribution in CLM4. 5: Effects on predicted site and global evapotranspiration, soil moisture, and water storage. *Journal of Advances in Modeling Earth Systems 7*, 1828–1848 (cit. on p. 208).

(263) Tardieu, F. (2012). Any trait or trait-related allele can confer drought tolerance: just design the right drought scenario. *Journal of experimental botany 63*, 25–31 (cit. on pp. 13, 127, 266, 294, 295, 321, 326).

(264) Tardieu, F. and Simonneau, T. (1998). Variability among species of stomatal control under fluctuating soil water status and evaporative demand: modelling isohydric and anisohydric behaviours. *Journal of Experimental Botany 49*, 419–432 (cit. on p. 314).

(265) Tardieu, F., Simonneau, T. and Parent, B. (Apr. 2015). Modelling the coordination of the controls of stomatal aperture, transpiration, leaf growth, and abscisic acid: update and extension of the Tardieu-Davies model., eng *Journal of Experimental Botany 66*, 2227–2237, DOI: 10.1093/jxb/erv039 (cit. on pp. 107, 158, 179, 184, 334).

(266) Tazawa, M., Ohkuma, E., Shibasaka, M. and Nakashima, S. (1997). Mercurial-sensitive water transport in barley roots. *Journal of Plant Research 110*, 435–442 (cit. on p. 48).

(267) Thomson, B. and Siddique, K. (1997). Grain legume species in low rainfall Mediterranean-type environments II. Canopy development, radiation interception, and dry-matter production. *Field Crops Research 54*, 189–199 (cit. on p. 286).

(268) Thévenin, L. (1883). Extension of Ohm's law to complex electromotive circuits. *Annales télégraphiques 10*, 222–224 (cit. on pp. 14, 51).

(269) Tollenaar, M and Lee, E. (2002). Yield potential, yield stability and stress tolerance in maize. *Field Crops Research 75*, 161–169 (cit. on p. 266).

(270) Tötzke, C., Kardjilov, N., Manke, I. and Oswald, S. E. (2017). Capturing 3D Water Flow in Rooted Soil by Ultra-fast Neutron Tomography. *Scientific reports 7*, 6192 (cit. on p. 330).

(271) Tournier, P.-H., Hecht, F. and Comte, M. (2015). Finite element model of soil water and nutrient transport with root uptake: explicit geometry and unstructured adaptive meshing. *Transport in Porous Media 106*, 487–504 (cit. on p. 210).

(272) Trachsel, S., Kaeppler, S. M., Brown, K. M. and Lynch, J. P. (2011). Shovelomics: high throughput phenotyping of maize (Zea mays L.) root architecture in the field. *Plant and Soil 341*, 75–87 (cit. on p. 265).

(273) Trillo, N. and Fernández, R. J. (Dec. 2005). Wheat plant hydraulic properties under Prolonged exp. Drought: stronger decline in root-system conductance than in leaf area., en *Plant and Soil 277*, 277–284, DOI: 10.1007/s11104-005-7493-5 (cit. on p. 51).

(274) Tsuda, M. and Tyree, M. T. (Apr. 2000). Plant hydraulic conductance measured by the high pressure flow meter in crop plants., eng *Journal of Experimental Botany 51*, 823–828 (cit. on p. 159).

(275) Tylová, E., Pecková, E., Blascheová, Z. and Soukup, A. (2017). Casparian bands and suberin lamellae in exodermis of lateral roots: an important trait of roots system response to abiotic stress factors. *Annals of Botany* (cit. on p. 198).

(276) Tyree, M. T., Yang, S., Cruiziat, P. and Sinclair, B. (1994). Novel methods of measuring hydraulic conductivity of tree root systems and interpretation using AMAIZED (A maize-root dynamic model for water and solute transport). *Plant Physiology 104*, 189–199 (cit. on p. 159).

(277) Uga, Y., Sugimoto, K., Ogawa, S., Rane, J., Ishitani, M., Hara, N., Kitomi, Y., Inukai, Y., Ono, K., Kanno, N., et al. (2013). Control of root system architecture by DEEPER ROOTING 1 increases rice yield under drought conditions. *Nature genetics 45*, 1097–1102 (cit. on pp. 11, 12).

(278) Vadez, V, Soltani, A and Sinclair, T. R. (Oct. 2012). Modelling possible benefits of root related traits to enhance terminal drought adaptation of chickpea. *Field Crops Research 137*, 108–115 (cit. on p. 17).

(279) Vadez, V, Rao, S, Kholova, J, Krishnamurthy, L, Kashiwagi, J, Ratnakumar, P, Sharma, K., Bhatnagar-Mathur, P and Basu, P. (2008). Root research for drought tolerance in legumes: quo vadis. *Journal of Food legumes 21*, 77–85 (cit. on pp. 265, 287).

(280) Vadez, V. (Apr. 2014). Root hydraulics: The forgotten side of roots in drought adaptation., en *Field Crops Research*, DOI: 10.1016/j.fcr.2014.03.017 (cit. on pp. 103, 159, 184).

(281) van Genuchten, M. (1980). A closed-form equation for predicting the hydraulic conductivity of unsaturated soils. *Soil Science Society of America Journal 44*, 891–898 (cit. on p. 275).

(282) Van Alfen, N. K., McMillan, B. D., Turner, V. and Hess, W. M. (1983). Role of pit membranes in macromolecule-induced wilt of plants. *Plant Physiology 73*, 1020–1023 (cit. on p. 198).

(283) Van Dam, J., Stricker, J. and Droogers, P (1994). Inverse method to determine soil hydraulic functions from multistep outflow experiments. *Soil science society of America journal 58*, 647–652 (cit. on p. 216).

(284) van den Honert, T. H. (1948). Water transport in plants as a catenary process., en *Discussions of the Faraday Society 3*, 146, DOI: 10.1039/df9480300146 (cit. on p. 46).

(285) Van Den Besselaar, E. J., Klein Tank, A. M., Van Der Schrier, G., Abass, M. S., Baddour, O., Van Engelen, A. F., Freire, A., Hechler, P., Laksono, B. I., Jilderda, R., et al. (2015). International climate assessment & dataset: climate services across

borders. *Bulletin of the American Meteorological Society 96*, 16–21 (cit. on p. 343).

(286) Vandeleur, R. K., Mayo, G, Shelden, M. C., Gilliham, M, Kaiser, B. N. and Tyerman, S. D. (2009). The role of plasma membrane intrinsic protein aquaporins in water transport through roots: diurnal and drought stress responses reveal different strategies between isohydric and anisohydric cultivars of grapevine. *Plant Physiology 149*, 445–460 (cit. on p. 9).

(287) Vanderborght, J, Kemna, A. and Hardelauf, H. (2005). Potential of electrical resistivity tomography to infer aquifer transport characteristics from tracer studies: A synthetic case study. *Water Resources Research 41* (cit. on p. 23).

(288) Vandoorne, B., Beff, L., Lutts, S. and Javaux, M. (2012). Root Water Uptake Dynamics of var. Under Water-Limited Conditions., en *Vadose Zone Journal 11*, 0, DOI: 10.2136/vzj2012.0005 (cit. on p. 42).

(289) Varney, G. T. and Canny, M. J. (Jan. 1993). Rates of water uptake into the mature root system of maize plants., en *New Phytologist 123*, 775–786, DOI: 10.1111/j.1469-8137.1993.tb03789.x (cit. on pp. 79, 160).

(290) Vercambre, D. (2002). Influence of xylem development on axial hydraulic conductance within Prunus root systems. *16*, 479–487, DOI: 10.1007/s00468-002-0190-6 (cit. on pp. 10, 109).

(291) Volkmann, T. H. M. and Weiler, M. (May 2014). Continual in situ monitoring of pore water stable isotopes in the subsurface., en *Hydrology and Earth System Sciences 18*, 1819–1833, DOI: 10.5194/hess-18-1819-2014 (cit. on p. 252).

(292) Volkmann, T. H. M., Haberer, K., Gessler, A. and Weiler, M. (May 2016). High-resolution isotope measurements resolve rapid ecohydrological dynamics at the soil-plant interface., en *New Phytologist 210*, 839–849, DOI: 10.1111/nph.13868 (cit. on p. 252).

(293) Volpe, V., Marani, M., Albertson, J. and Katul, G. (Oct. 2013). Root controls on water redistribution and carbon uptake in the soil–plant system under current and future climate., en *Advances in Water Resources 60*, 110–120, DOI: 10.1016/j.advwatres.2013.07.008 (cit. on pp. 78, 229, 230).

(294) Vrugt, J., Wijk, M. v., Hopmans, J. W. and Šimunek, J (2001). One-, two-, and three-dimensional root water uptake functions for transient modeling. *Water Resources Research 37*, 2457–2470 (cit. on p. 209).

(295) Waines, J. G. and Ehdaie, B. (2007). Domestication and crop physiology: roots of green-revolution wheat. *Annals of Botany 100*, 991–998 (cit. on p. 264).

(296) Wang, K. and Dickinson, R. E. (2012). A review of global terrestrial evapotranspiration: Observation, modeling, climatology, and climatic variability. *Reviews of Geophysics 50* (cit. on p. 208).

(297) Warren, J., Meinzer, F., Brooks, J. and Domec, J. (May 2005). Vertical stratification of soil water storage and release dynamics in Pacific Northwest coniferous forests., en *Agricultural and Forest Meteorology 130*, 39–58, DOI: 10.1016/j.agrformet.2005.01.004 (cit. on p. 229).

(298) Warrick, A., Mullen, G. and Nielsen, D. (1977). Scaling field-measured soil hydraulic properties using a similar media concept. *Water Resources Research 13*, 355–362 (cit. on p. 337).

(299) Wasson, A. P., Richards, R. A., Chatrath, R., Misra, S. C., Prasad, S. V., Rebetzke, G. J., Kirkegaard, J. A., Christopher, J. and Watt, M. (2012). Traits and selection strategies to improve root systems and water uptake in water-limited wheat crops. *Journal of experimental botany 63*, 3485–3498 (cit. on pp. 12, 17, 127, 265, 272, 294, 321).

(300) Watt, M, Magee, L. J. and McCully, M. E. (2008). Types, structure and potential for axial water flow in the deepest roots of field-grown cereals. *New Phytologist 178*, 135–146 (cit. on p. 11).

(301) Wenzel, C. L., McCully, M. E. and Canny, M. J. (1989). Development of water conducting capacity in the root systems of young plants of corn and some other C4 grasses. *Plant Physiology 89*, 1094–1101 (cit. on p. 197).

(302) Werner, C. et al. (Aug. 2012). Progress and challenges in using stable isotopes to trace plant carbon and water relations across scales., en *Biogeosciences 9*, 3083–3111, DOI: 10.5194/bg-9-3083-2012 (cit. on p. 229).

(303) Wesseling, J. Meerjarige simulatie van grondwaterstroming voor verschillende bodemprofielen, grondwatertrappen en gewassen met het model SWATRE., Dutch, tech. rep., Winand Staring Centre for Integrated Land, Soil and Water Research: Wageningen : DLO-Staring Centrum (Rapport / DLO-Staring Centrum 152), 1991, p 63 (cit. on p. 42).

(304) Wheeler, T. D. and Stroock, A. D. (Sept. 2008). The transpiration of water at negative pressures in a synthetic tree., en *Nature 455*, 208–212, DOI: 10.1038/nature07226 (cit. on p. 158).

(305) Yang, X, Li, Y, Ren, B, Ding, L, Gao, C, Shen, Q and Guo, S (Mar. 2012). Drought-Induced Root Aerenchyma Formation Restricts Water Uptake in Rice Seedlings Supplied with Nitrate. *Plant and Cell Physiology 53*, 495–504 (cit. on p. 9).

(306) Zaman-Allah, M., Jenkinson, D. M. and Vadez, V (2011). Chickpea genotypes contrasting for seed yield under terminal drought stress in the field differ for traits related to the control of water use. *Functional Plant Biology 38*, 270 (cit. on p. 17).

(307) Zarebanadkouki, M., Kim, Y. X., Moradi, A. B., Vogel, H. J., Kaestner, A. and Carminati, A. (2012). Quantification and modeling of local root water uptake using neutron radiography and deuterated water. *Vadose Zone Journal 11* (cit. on pp. 160, 161, 178).

(308) Zarebanadkouki, M., Meunier, F., Couvreur, V., Cesar, J., Javaux, M. and Carminati, A. (Aug. 2016). Estimation of the hydraulic conductivities of lupine roots by inverse modelling of high-resolution measurements of root water uptake., en *Annals of Botany*, mcw154,

DOI: 10.1093/aob/mcw154 (cit. on pp. 43, 48, 57, 79, 183, 189, 197, 198).

(309) Zarebanadkouki, M., Kim, Y. X. and Carminati, A. (Sept. 2013). Where do roots take up water? Neutron radiography of water flow into the roots of transpiring plants growing in soil., eng *The New Phytologist 199*, 1034–1044, DOI: 10.1111/nph.12330 (cit. on pp. 7, 23, 160–162, 165, 166, 168, 175, 176, 208, 213).

(310) Zegada-Lizarazu, W. and Iijima, M. (Jan. 2004). Hydrogen Stable Isotope Analysis of Water Acquisition Ability of Deep Roots and Hydraulic Lift in Sixteen Food Crop Species., en *Plant Production Science 7*, 427–434, DOI: 10.1626/pps.7.427 (cit. on p. 229).

(311) Zhang, H., Huang, Y., Ye, X. and Xu, F. (2011). Genotypic variation in phosphorus acquisition from sparingly soluble P sources is related to root morphology and root exudates in Brassica napus. *Science China Life Sciences 54*, 1134–1142 (cit. on p. 265).

(312) Zhu, J. and Mohanty, B. P. (2006). Effective scaling factor for transient infiltration in heterogeneous soils. *Journal of hydrology 319*, 96–108 (cit. on p. 337).

(313) Zhuang, J., Nakayama, K., Yu, G.-R. and Urushisaki, T. (2001). Estimation of root water uptake of maize: an ecophysiological perspective. *Field Crops Research 69*, 201–213 (cit. on p. 79).

(314) Zimmermann, H. M., Hartmann, K., Schreiber, L. and Steudle, E. (2000). Chemical composition of apoplastic transport barriers in relation to radial hydraulic conductivity of corn roots (Zea mays L.) *Planta 210*, 302–311 (cit. on p. 198).

(315) Zufferey, V., Cochard, H., Ameglio, T., Spring, J.-L. and Viret, O. (2011). Diurnal cycles of embolism formation and repair in petioles of grapevine (Vitis vinifera cv. Chasselas). *Journal of experimental botany 62*, 3885–3894 (cit. on pp. 11, 222).

(316) Zwieniecki, M. A. and Holbrook, N. M. (Oct. 2009). Confronting Maxwell's demon: biophysics of xylem embolism repair. *Trends in Plant Science 14*, 530–534 (cit. on p. 11).

(317) Zwieniecki, M. A. and Secchi, F. In *Plant Aquaporins*; Springer: 2017, pp 237–254 (cit. on p. 11).

(318) Zwieniecki, M. A., Thompson, M. V. and Holbrook, N. M. (Dec. 2002). Understanding the Hydraulics of Porous Pipes: Tradeoffs Between Water Uptake and Root Length Utilization., en *Journal of Plant Growth Regulation 21*, 315–323, DOI: 10.1007/s00344-003-0008-9 (cit. on pp. 79, 159, 239).